604
USNDC-7
EANDC(US)-181"U"
INDC(USA)-56"U"

Reports to...

THE U.S. NUCLEAR DATA COMMITTEE

Meeting at

OAK RIDGE NATIONAL LABORATORY

18-20 JUNE 1973

Compiled by...

H. E. Jackson, Secretary, USNDC
Physics Division

U of C-AUA-USAEC

Argonne National Laboratory

Printed in the United States of America
Available from
National Technical Information Service
U.S. Department of Commerce
5285 Port Royal Road
Springfield, Virginia 22151
Price: Printed Copy $7.60; Microfiche $0.95

USNDC-7
EANDC(US)-181"U"
INDC(USA)-56"U"

Physics--General

REPORTS TO

THE U.S. NUCLEAR DATA COMMITTEE

Meeting at

OAK RIDGE NATIONAL LABORATORY

18-20 JUNE 1973

Compiled by

H. E. Jackson, Secretary
USNDC

ARGONNE NATIONAL LABORATORY
9700 South Cass Avenue
Argonne, Illinois 60439

PREFACE

The reports in this document were submitted to the United States Nuclear Data Committee (USNDC) at the meeting at Oak Ridge National Laboratory, 18-20 June, 1973. The reporting laboratories are those having a substantial effort in the acquisition of nuclear data of general relevance to the U. S. applied nuclear program. The material contained in these reports is to be regarded as comprised of informal statements of recent developments and preliminary data. Appropriate subjects include:

1. Microscopic nuclear cross sections relevant to the applied nuclear program. Inverse reactions where pertinent are included.

2. Standard nuclear cross sections and flux standards which are used in the measurement of other nuclear cross sections.

3. Gamma-ray production, radioactive decay, and theoretical developments in nuclear structure which are applicable to nuclear programs.

4. Values of nuclear parameters necessary in the description and understanding of fission and other nuclear processes of relevance to the applied energy program.

These reports cannot be regarded as a complete summary of the nuclear research efforts of the AEC. A number of laboratories, whose research is less programmatically oriented do not submit reports; neither do the submitted reports reflect all the work related to nuclear cross sections in progress at the submitting laboratory. Budgetary limitations have made it mandatory to follow more strictly the subject guidelines described above and therefore to restrict the size of this document.

Persons wishing to make use of these data should contact the individual experimenter for further details. The data which appear in this document should be quoted only by permission of the contributor and should be referenced as private communication, and not by this document number.

This compilation has been produced almost completely from master copies prepared by the individual contributors listed in the Table of Contents. It is a pleasure to acknowledge their help in the preparation of these reports.

H. E. Jackson
Secretary, USNDC
Argonne National Laboratory
Argonne, Illinois 60439

TABLE OF CONTENTS

Recent Reports submitted to the USNDC or its predecessor, the AEC Nuclear Cross Sections Advisory Committee, include the following:

October 1972 Meeting at National Bureau of Standards	USNDC- 3 EANDC(US)-176U INDC(USA) - 54U
May 1972 Meeting at Los Alamos, New Mexico	USNDC- 1 EANDC(US)-168U INDC(USA) - 43U
November 1971 Meeting at Brookhaven National Laboratory	NCSAC- 42 EANDC(US)-165U INDC(USA) - 36U
May 1971 Meeting at Duke University	NCSAC- 38 EANDC(US)-156U INDC(USA) - 30U
December 1970 Meeting at Lawrence Radiation Laboratory	NCSAC- 33 EANDC(US)-150U INDC(US)- 25U
May 1970 Meeting at Argonne National Laboratory	NCSAC- 31 EANDC(US)-143U INDC(US)- 22U
September 1969 Meeting at Rice University	WASH-1136 EANDC(US)-122U INDC(US)- 14U
April 1969 Meeting at Oak Ridge, Tennessee	WASH-1136 EANDC(US)-120U INDC(US)- 10U
October 1968 Meeting at Columbia University	WASH-1124 EANDC(US)-111U INDC(US)- 9U
April 1968 Meeting at Los Alamos, New Mexico	WASH-1093 EANDC(US)-105U INDC(US)- 2U
October 1967 Meeting at Idaho Falls, Idaho	WASH-1079 EANDC(US)-104U INDC(US)- 12U

The CINDA-type index which follows was prepared by L. T. Whitehead, Nuclear Data Section, Science and Technology Branch, Oak Ridge National Laboratory, Oak Ridge, Tennessee.

ELEMENT S	A	QUANTITY	TYPE	ENERGY MIN	MAX	DOCUMENTATION REF	VOL	PAGE	DATE	LAB	COMMENTS	SERIAL NO.
HE	003	TOTAL XSECT	EXPT-PROG	7.9+6	2.4+7	USNDC-7	131		6/73	LAS	SEAGRAVE+. TABLE. 5 ENERGIES. TBP	65450
HE	003	ELASTIC	EXPT-PROG	7.9+6	2.4+7	USNDC-7	131		6/73	LAS	SEAGRAVE+. TABLE. 5 ENERGIES. TBP	65448
HE	003	DIFF ELASTIC	EXPT-PROG	8.0+6	1.7+7	USNDC-7	228		6/73	DKE	LISOWSKI+.POL ANG DIST MEASD.NO DATA	65605
HE	003	POLARIZATION	EXPT-PROG	8.0+6	1.7+7	USNDC-7	228		6/73	DKE	LISOWSKI+.POL ANG DIST MEASD.NO DATA	65606
HE	003	NONELASTIC	EXPT-PROG	1.4+7	2.4+7	USNDC-7	131		6/73	LAS	SEAGRAVE+. TABLE. 3 ENERGIES. TBP	65449
HE	003	N2N REACTION	EXPT-PROG	1.4+7	2.4+7	USNDC-7	131		6/73	LAS	SEAGRAVE+.TABLE.3ES.(N,PN)+(N,2N)	65454
HE	003	N,GAMMA	EXPT-PROG	THR		USNDC-7	21		6/73	ANL	BOLLINGER+.NAI(TL) DET.PRELIM SIG	65354
HE	003	N,PROTON	EXPT-PROG	7.9+6	2.4+7	USNDC-7	131		6/73	LAS	SEAGRAVE+. TABLE. 5ES.(N,P)+(N,D).	65451
HE	003	N,DEUTERON	EXPT-PROG	7.9+6	2.4+7	USNDC-7	131		6/73	LAS	SEAGRAVE+. TABLE. 5ES.(N,P)+(N,D).	65452
HE	003	N,N PROTON	EXPT-PROG	1.4+7	2.4+7	USNDC-7	131		6/73	LAS	SEAGRAVE+.TABLE.3ES.(N,PN)+(N,2N)	65453
HE	004	DIFF ELASTIC	THEO-PROG		1.8+7	USNDC-7	138		6/73	LAS	NISLEY+. R-MATRIX ANALYSIS.NO DATA	65457
HE	004	DIFF ELASTIC	EXPT-PROG	1.4+7	1.7+7	USNDC-7	228		6/73	DKE	LISOWSKIF.POL ANG DIST MEASD.NO DATA	65583
HE	004	POLARIZATION	THEO-PROG		1.8+7	USNDC-7	138		6/73	LAS	NISLEY+. R-MATRIX ANALYSIS.NO DATA	65458
HE	004	POLARIZATION	EXPT-PROG	1.4+7	1.7+7	USNDC-7	228		6/73	DKE	LISOWSKIF.POL ANG DIST MEASD.NJ DATA	65584
LI	006	TOTAL XSECT	EXPT-PROG	1.0+3	4.0+5	USNDC-7	172		6/73	ORL	GOOD+. LINAC. TRANS. NO DATA GIVEN	65527
LI	006	N,ALPHA	EXPT-PROG	1.0+3	1.7+6	USNDC-7	88		6/73	GA	FRIESENHAHN+. TO BE DONE	65397
LI	006	N,ALPHA	EXPT-PROG	9.0 4	1.5 6	USNDC-7	9		6/73	ANL	POENITZ. SIG AT PEAK(246KEV) GIVEN	65349
BE	009	DIFF ELASTIC	EXPT-PROG	1.5+6	4.0+6	USNDC-7	275		6/73	YAL	FIRK+. DIFF POLARIZATN.ANAL TBC. NDG	65621
BE	009	DIFF ELASTIC	EXPT-PROG	7.6+6		USNDC-7	271		6/73	ABD	BUCHER+. THETA#2.67-14.09DEG.NO DATA	65610
BE	009	POLARIZATION	EXPT-PROG	1.5+6	4.0+6	USNDC-7	275		6/73	YAL	FIRK+. DIFF POLARIZATN.ANAL TBC. NDG	65622
B	010	DIFF ELASTIC	EXPT-PROG	1.5+6	4.4+6	USNDC-7	193		6/73	OHO	HAUSLADEN+.TOF.50-KEV STEPS. CURVES	65551
B	010	N,ALPHA	THEO-PROG		1.0+6	USNDC-7	138		6/73	LAS	HALE+. R-MATRIX ANAL. TBC. NO DATA	65459
B	010	N,ALPHA	EXPT-PROG	8.0+5		USNDC-7	148		6/73	NBS	LAMAZE+.VDG. PROP DET.BRANCH RAT.NDG	65472
B	011	DIFF ELASTIC	EXPT-PROG	2.2+6	4.5+6	USNDC-7	193		6/73	OHO	NELSON+.TOF.45 ES.CURVS LEG COEFFS	65550
C	012	TOTAL XSECT	EXPT-PROG		4.0 6	USNDC-7	9		6/73	ANL	SMITH+. ANAL TBC. NO DATA GIVEN.	65340
C	012	DIFF ELASTIC	EXPT-PROG		4.0 6	USNDC-7	9		6/73	ANL	SMITH+. ANAL TBC. NO DATA GIVEN.	65341
C	012	DIFF ELASTIC	EXPT-PROG	1.0+6	2.0+7	USNDC-7	166		6/73	ORL	MORGAN+.LINAC.THICK TARG.3ANGS. NDG	65483
C	012	DIFF ELASTIC	EXPT-PROG	1.0+7	1.4+7	USNDC-7	271		6/73	ABD	BUCHER+.SMALL-ANGLE SCAT.TBC.NO DATA	65607
C	012	DIFF ELASTIC	EXPT-PROG	1.2+7		USNDC-7	197		6/73	OHO	CARLSON+. CURV ANG DIST. 70-145 DEG.	65552
C	012	DIFF ELASTIC	EXPT-PROG	7.6+6		USNDC-7	271		6/73	ABD	BUCHER+. THETA#2.67-14.09DEG.NO DATA	65611
C	012	SCATTERING	EXPT-PROG	+6		USNDC-7	89		6/73	GA	HARRIS+.INTEGRAL EXPT.NO DATA GIVEN	65405
C	012	NONEL GAMMAS	EXPT-PROG	+6		USNDC-7	89		6/73	GA	HARRIS+. INTEGRAL EXPT. NO DATA GIVN	65401
C	012	NONEL GAMMAS	EXPT-PROG	+6	+7	USNDC-7	88		6/73	GA	HOOT+. LINAC. GE(LI) DET. NO DATA	65398
C	012	DIFF INELAST	EXPT-PROG		4.0 6	USNDC-7	9		6/73	ANL	SMITH+. ANAL TBC. NO DATA GIVEN.	65342
C	012	DIFF INELAST	EXPT-PROG	1.2+7		USNDC-7	197		6/73	OHO	CARLSON+. CURV ANG DIST. 70-145 DEG.	65558
N		DIFF ELASTIC	EXPT-PROG	7.9+6	1.4+7	USNDC-7	271		6/73	ABD	BUCHER+.SMALL-ANGLE SCAT.TBC.NO DATA	65608
N		SCATTERING	EXPT-PROG	+6		USNDC-7	89		6/73	GA	HARRIS+.INTEGRAL EXPT.NEUT SPEC GVN	65404
N		NONEL GAMMAS	EXPT-PROG	+6		USNDC-7	89		6/73	GA	HARRIS+. INTEGRAL EXPT. NO DATA GIVN	65400
N	001	N,GAMMA	EXPT-PROG	2.5-2		USNDC-7	78		6/73	COL	COKINOS+. SIG GIVEN. TBP PR	65395
N	012	NONEL GAMMAS	EXPT-PROG	+6	+7	USNDC-7	88		6/73	GA	HOOT+. LINAC. GE(LI) DET. NO DATA	65399
N	014	NONEL GAMMAS	EXPT-PROG	4.2+6	1.5+7	USNDC-7	89		6/73	GA	HARRIS+.GE(LI) DET.LINAC.GAM SPECTRA	65408
N	014	NONEL GAMMAS	EXPT-PROG	2.0+6	2.0+7	USNDC-7	174		6/73	ORL	DICKINS+. ABST OF ORNL-4864. NO DATA	65532
O		DIFF ELASTIC	EXPT-PROG	1.0+7	1.4+7	USNDC-7	271		6/73	ABD	BUCHER+.SMALL-ANGLE SCAT.TBC.NO DATA	65609
O		SCATTERING	EXPT-PROG	+6		USNDC-7	89		6/73	GA	HARRIS+.INTEGRAL EXPT.NO DATA GIVEN	65406
O	012	NONEL GAMMAS	EXPT-PROG	+6		USNDC-7	89		6/73	GA	HARRIS+. INTEGRAL EXPT. NO DATA GIVN	65402
O	016	DIFF ELASTIC	EXPT-PROG	1.0+6	4.0+6	USNDC-7	275		6/73	YAL	FIRK+.20-150DEG.DIFF POLARIZTN.CURVS	65619
O	016	POLARIZATION	EXPT-PROG	1.0+6	4.0+6	USNDC-7	275		6/73	YAL	FIRK+.20-150DEG.DIFF POLARIZTN.CURVS	65620
F	019	RESON PARAMS	EXPT-PROG	2.7+4	1.5+6	USNDC-7	178		6/73	ORL	MACKLIN+.WG,J GIVN FOR 10RESON.	65539

ELEMENT S	A	QUANTITY	TYPE	ENERGY MIN	MAX	DOCUMENTATION REF	VOL	PAGE	DATE	LAB	COMMENTS	SERIAL NO.
MG		EVALUATION	EVAL-PROG	NDG		USNDC-7	92		6/73	GA	DRAKE+.NO DATA GIVEN. TBP SOON.	65409
AL	027	DIFF ELASTIC	EXPT-PROG	1.2+7		USNDC-7	197		6/73	OHO	CARLSON+. CURV ANG DIST. 70-145 DEG.	65553
AL	027	DIFF ELASTIC	EXPT-PROG	7.6+6		USNDC-7	271		6/73	ABD	BUCHER+. THETA#2.67-14.09DEG.NO DATA	65612
AL	027	DIFF INELAST	EXPT-PROG	1.2+7		USNDC-7	197		6/73	OHO	CARLSON+. CURV ANG DIST. 70-145 DEG.	65562
SI		TOTAL XSECT	EXPT-PROG	NDG		USNDC-7	223		6/73	DKE	CLEMENT+. TBP. NO DATA GIVEN.	65580
SI		RESON PARAMS	EXPT-PROG	2.5+3	1.0+6	USNDC-7	171		6/73	ORL	ALLEN+.LINAC. AVERAG WG GIVEN.	65499
SI		N,GAMMA	EXPT-PROG	2.5+3	1.0+6	USNDC-7	171		6/73	ORL	ALLEN+.LINAC.NO DATA GIVEN.	65498
SI	029	TOTAL XSECT	EXPT-PROG	1.0+3	4.0+5	USNDC-7	172		6/73	ORL	GOOD+.TRANS.TABLE OF 8 RESON ES.	65500
SI	029	RESON PARAMS	EXPT-PROG	1.5+4	6.5+5	USNDC-7	172		6/73	ORL	GOOD+.TRANS.TABLE OF 8 RESON ES.	65506
SI	030	TOTAL XSECT	EXPT-PROG	1.0+3	4.0+5	USNDC-7	172		6/73	ORL	GOOD+.TRANS.TABLE OF 10RESON ES.	65501
SI	030	RESON PARAMS	EXPT-PROG	2.2+3	8.5+5	USNDC-7	172		6/73	ORL	GOOD+.TRANS.TABLE OF 10RESON ES	65507
S	033	TOTAL XSECT	EXPT-PROG	1.0+3	4.0+5	USNDC-7	172		6/73	ORL	GOOD+.TRANS.TABLE OF 18RESON ES.	65502
S	033	RESON PARAMS	EXPT-PROG	1.3+4	2.4+5	USNDC-7	172		6/73	ORL	GOOD+.TRANS.TABLE OF 18RESON ES	65508
S	034	TOTAL XSECT	EXPT-PROG	1.0+3	4.0+5	USNDC-7	172		6/73	ORL	GOOD+.TRANS.TABLE OF 27RESON ES.	65503
S	034	RESON PARAMS	EXPT-PROG	3.0+4	1.4+6	USNDC-7	172		6/73	ORL	GOOD+.TRANS.TABLE OF 27RESON ES	65509
CL		TOTAL XSECT	EXPT-PROG	0.0+0	4.5+5	USNDC-7	56		6/73	COL	SINGH+. CURVES. TBP PHYSICAL REVIEW	65388
CL	035	RESON PARAMS	EXPT-PROG	4.0+2	1.9+5	USNDC-7	56		6/73	COL	SINGH+.TABLE L J A*G*WN. TBP PR	65389
CL	037	RESON PARAMS	EXPT-PROG	8.3+3	9.3+4	USNDC-7	56		6/73	COL	SINGH+. TABLE L J A*G*WN. TBP PR	65390
CA	040	TOTAL XSECT	EXPT-PROG	1.0+3	4.0+5	USNDC-7	172		6/73	ORL	GOOD+.LINAC. TRANS. NO DATA GIVEN	65512
CA	040	TOTAL XSECT	EXPT-PROG	6.0+4	1.0+6	USNDC-7	167		6/73	ORL	FOWLER+.LINAC.0.1-1.0KEV RESOL. NDG	65487
CA	042	TOTAL XSECT	EXPT-PROG	1.0+3	4.0+5	USNDC-7	172		6/73	ORL	GOOD+.LINAC. TRANS. NO DATA GIVEN	65513
CA	043	TOTAL XSECT	EXPT-PROG	1.0+3	4.0+5	USNDC-7	172		6/73	ORL	GOOD+.LINAC. TRANS. NO DATA GIVEN	65514
CA	044	TOTAL XSECT	EXPT-PROG	1.0+3	4.0+5	USNDC-7	172		6/73	ORL	GOOD+.LINAC. TRANS. NO DATA GIVEN	65515
TI		DIFF ELASTIC	EXPT-PROG		1.5 6	USNDC-7	8		6/73	ANL	MOLDAUER+. CFD THEORY. NO DATA GIVEN	65330
TI		DIFF INELAST	EXPT-PROG		1.5 6	USNDC-7	8		6/73	ANL	MOLDAUER+. CFD THEORY. NO DATA GIVEN	65331
TI	047	TOTAL XSECT	EXPT-PROG	1.0+3	4.0+5	USNDC-7	172		6/73	ORL	GOOD+.LINAC. TRANS. NO DATA GIVEN	65516
TI	049	TOTAL XSECT	EXPT-PROG	1.0+3	4.0+5	USNDC-7	172		6/73	ORL	GOOD+.LINAC. TRANS. NO DATA GIVEN	65517
V	051	TOTAL XSECT	EXPT-PROG		4.0 6	USNDC-7	9		6/73	ANL	SMITH+. ANAL TBC. NO DATA GIVEN.	65343
V	051	DIFF ELASTIC	EXPT-PROG		4.0 6	USNDC-7	9		6/73	ANL	SMITH+. ANAL TBC. NO DATA GIVEN.	65344
V	051	DIFF INELAST	EXPT-PROG		4.0 6	USNDC-7	9		6/73	ANL	SMITH+. ANAL TBC. NO DATA GIVEN.	65345
MN	055	GAMMA N	EXPT-PROG	TR	3.6+7	USNDC-7	115		6/73	LRL	ALVAREZ+.POSITRON-ELECTRON LINAC.CRV	65434
FE		TOTAL XSECT	EXPT-PROG		4.0 6	USNDC-7	9		6/73	ANL	SMITH+. ANAL TBC. NO DATA GIVEN.	65346
FE		DIFF ELASTIC	EXPT-PROG		4.0 6	USNDC-7	9		6/73	ANL	SMITH+. ANAL TBC. NO DATA GIVEN.	65347
FE		DIFF ELASTIC	EXPT-PROG	1.0+4	6.5+5	USNDC-7	203		6/73	RPI	ZUHR+.1-6 PC ERROR. NO DATA GIVEN	65568
FE		DIFF ELASTIC	EXPT-PROG	1.2+7		USNDC-7	197		6/73	OHO	CARLSON+. CURV ANG DIST. 70-145 DEG.	65554
FE		DIFF ELASTIC	EXPT-PROG	7.6+6		USNDC-7	271		6/73	ABD	BUCHER+. THETA#2.67-14.09DEG.NO DATA	65613
FE		SCATTERING	EXPT-PROG	+6		USNDC-7	89		6/73	GA	HARRIS+.INTEGRAL EXPT.NO DATA GIVEN	65407
FE		NONEL GAMMAS	EXPT-PROG	+6		USNDC-7	89		6/73	GA	HARRIS+. INTEGRAL EXPT. NO DATA GIVN	65403
FE		DIFF INELAST	EXPT-PROG		4.0 6	USNDC-7	9		6/73	ANL	SMITH+. ANAL TBC. NO DATA GIVEN.	65348
FE		DIFF INELAST	EXPT-PROG	1.2+7		USNDC-7	197		6/73	OHO	CARLSON+. CURV ANG DIST. 70-145 DEG.	65561
FE		SPECT NGAMMA	EXPT-PROG	2.4 4		USNDC-7	36		6/73	BNL	WASSON+. GE(LI) DET. NO DATA GIVEN	65369
FE	054	TOTAL XSECT	EXPT-PROG	1.0+3	4.0+5	USNDC-7	172		6/73	ORL	GOOD+.TRANS.TABLE OF 11RESON ES.	65504
FE	054	TOTAL XSECT	EXPT-PROG	1.0+4	2.0+5	USNDC-7	207		6/73	RPI	KNOX+. 9 NSEC RESOL.TRANS.TBC. NDG	65574
FE	054	RESON PARAMS	EXPT-PROG	7.8+3	9.9+4	USNDC-7	172		6/73	ORL	GOOD+.TRANS.TABLE OF 11RESON ES	65510
FE	054	N,GAMMA	EXPT-PROG	1.0+4	2.0+5	USNDC-7	207		6/73	RPI	KNOX+. 9 NSEC RESOL. NO DATA GIVEN	65576
FE	056	NONEL GAMMAS	THEO-PROG	1.4+7		USNDC-7	128		6/73	LAS	DRAKE+.PRELIM SIG 0.85-MEV GAMMA GVN	65443
FE	057	TOTAL XSECT	EXPT-PROG	1.0+3	4.0+5	USNDC-7	172		6/73	ORL	GOOD+.TRANS.TABLE OF 34RESON ES.	65505
FE	057	RESON PARAMS	EXPT-PROG	1.6+3	1.2+5	USNDC-7	172		6/73	ORL	GOOD+.TRANS.TABLE OF 34RESON ES	65511

ELEMENT S A	QUANTITY	TYPE	ENERGY MIN	ENERGY MAX	DOCUMENTATION REF	VOL	PAGE	DATE	LAB	COMMENTS	SERIAL NO.
CO 059	TOTAL XSECT	EXPT-PROG		4.0 6	USNDC-7	9		6/73	ANL	SMITH+. NO DATA GIVEN	65336
CO 059	TOTAL XSECT	EXPT-PROG	1.0+6	1.6+7	USNDC-7	122		6/73	LOK	FISHER+.ALIGNED TARGET. SOME DATA.	65436
CO 059	DIFF ELASTIC	EXPT-PROG		4.0 6	USNDC-7	9		6/73	ANL	SMITH+. NO DATA GIVEN	65335
CO 059	DIFF INELAST	EXPT-PROG		4.0 6	USNDC-7	9		6/73	ANL	SMITH+. NO DATA GIVEN	65337
CO 059	GAMMA N	EXPT-PROG	TR	3.6+7	USNDC-7	115		6/73	LRL	ALVAREZ+.POSITRON-ELECTRON LINAC.CRV	65435
NI	TOTAL XSECT	EXPT-PROG		4.0 6	USNDC-7	9		6/73	ANL	SMITH+. NO DATA GIVEN	65334
NI	DIFF ELASTIC	EXPT-PROG		4.0 6	USNDC-7	9		6/73	ANL	SMITH+. NO DATA GIVEN	65338
NI	DIFF ELASTIC	EXPT-PROG	1.0+4	6.5+5	USNDC-7	203		6/73	RPI	ZUHR+.1-6 PC ERROR. NO DATA GIVEN	65569
NI	DIFF ELASTIC	EXPT-PROG	1.2+7		USNDC-7	197		6/73	OHO	CARLSON+. CURV ANG DIST. 70-145 DEG.	65555
NI	DIFF INELAST	EXPT-PROG		4.0 6	USNDC-7	9		6/73	ANL	SMITH+. NO DATA GIVEN	65339
NI	DIFF INELAST	EXPT-PROG	1.2+7		USNDC-7	197		6/73	OHO	CARLSON+. CURV ANG DIST. 70-145 DEG.	65560
NI	SPECT NGAMMA	EXPT-PROG	2.4 4		USNDC-7	36		6/73	BNL	WASSON+. GE(LI) DET. CURVE.	65366
NI 060	SPECT NGAMMA	EXPT-PROG	2.4+4		USNDC-7	36		6/73	BNL	WASSON+. GE(LI) DET. CURVE	65370
NI 060	SPECT NGAMMA	EXPT-PROG	2.5-2	1.2+4	USNDC-7	203		6/73	RPI	BROWN+.TOF. GAMMA TRANSITION INTENS	65564
NI 061	TOTAL XSECT	EXPT-PROG	1.0+4	2.0+5	USNDC-7	207		6/73	RPI	KNOX+. 9 NSEC RESOL.TRANS.TBC. NDG	65575
NI 061	N,GAMMA	EXPT-PROG	1.0+4	2.0+5	USNDC-7	207		6/73	RPI	KNOX+. 9 NSEC RESOL. NO DATA GIVEN	65577
CU	EVALUATION	EVAL-PROG	NDG		USNDC-7	92		6/73	GA	DRAKE+.NO DATA GIVEN. TBP SOON.	65410
CU	DIFF ELASTIC	EXPT-PROG	7.6+6		USNDC-7	271		6/73	ABO	BUCHER+. THETA#2.67-14.09DEG.NO DATA	65614
CU	NONEL GAMMAS	EXPT-PROG	1.0+6	2.0+7	USNDC-7	174		6/73	ORL	DICKINS+. ABST OF ORNL-4846 NO DATA	65533
CU 063	RESON PARAMS	EXPT-PROG	4.0+2	3.0+4	USNDC-7	56		6/73	COL	RAHN+. TABLE A*G*WN,SOME J AND WN	65386
CU 065	RESON PARAMS	EXPT-PROG	2.3+2	2.7+4	USNDC-7	56		6/73	COL	RAHN+. TABLE A*G*WN,SOME J AND WN	65387
AS 075	STRNTH FNCTN	EXPT-PROG	1.0+3	7.0+5	USNDC-7	147		6/73	NBS	CAMARDA. LINAC. S1 MEASD. NO DATA	65464
RB 087	N,GAMMA	EXPT-PROG	PILE		USNDC-7	1		6/73	AGN	HARKER. CFRMF INTEGRAL MEAST. VALUE	65310
SR 088	RESON PARAMS	EXPT-PROG	2.5+3	4.0+5	USNDC-7	166		6/73	ORL	WINTERS+.LINAC.WG+WN MEASD.CAPT. NDG	65485
SR 088	N,GAMMA	EXPT-PROG	2.5+3	4.0+5	USNDC-7	166		6/73	ORL	WINTERS+.LINAC.SCINT.NO DATA GIVEN	65484
ZR	SPECT NGAMMA	EXPT-PROG	2.4 4		USNDC-7	36		6/73	BNL	WASSON+. GE(LI) DET. NO DATA GIVEN	65367
ZR 090	TOTAL XSECT	EXPT-PROG	1.0+3	4.0+5	USNDC-7	172		6/73	ORL	GOOD+.LINAC. TRANS. NO DATA GIVEN	65522
ZR 091	TOTAL XSECT	EXPT-PROG	1.0+3	4.0+5	USNDC-7	172		6/73	ORL	GOOD+.LINAC. TRANS. NO DATA GIVEN	65523
ZR 092	TOTAL XSECT	EXPT-PROG	1.0+3	4.0+5	USNDC-7	172		6/73	ORL	GOOD+.LINAC. TRANS. NO DATA GIVEN	65524
ZR 094	TOTAL XSECT	EXPT-PROG	1.0+3	4.0+5	USNDC-7	172		6/73	ORL	GOOD+.LINAC. TRANS. NO DATA GIVEN	65525
ZR 096	TOTAL XSECT	EXPT-PROG	1.0+3	4.0+5	USNDC-7	172		6/73	ORL	GOOD+.LINAC. TRANS. NO DATA GIVEN	65526
NB 093	TOTAL XSECT	EXPT-PROG	3.0 5	5.0 6	USNDC-7	7		6/73	ANL	SMITH+. SEE REPORT AP/CTR/TM-4. NDG	65327
NB 093	STRNTH FNCTN	EXPT-PROG	1.0+3	7.0+5	USNDC-7	147		6/73	NBS	CAMARDA. LINAC. S1 MEASD. NO DATA	65465
NB 093	DIFF ELASTIC	EXPT-PROG	1.2+7		USNDC-7	197		6/73	OHO	CARLSON+. CURV ANG DIST. 70-145 DEG.	65556
NB 093	DIFF ELASTIC	EXPT-PROG	3.0 5	5.0 6	USNDC-7	7		6/73	ANL	SMITH+. SEE REPORT AP/CTR/TM-4. NDG	65328
NB 093	DIFF INELAST	EXPT-PROG	1.2+7		USNDC-7	197		6/73	OHO	CARLSON+. CURV ANG DIST. 70-145 DEG.	65559
NB 093	DIFF INELAST	EXPT-PROG	3.0 5	5.0 6	USNDC-7	7		6/73	ANL	SMITH+. SEE REPORT AP/CTR/TM-4. NDG	65329
MO 098	RESON PARAMS	EXPT-PROG		1.0+5	USNDC-7	169		6/73	ORL	COLE+.VALIDITY OF VALENCE MODEL.NDG	65491
MO 098	RESON PARAMS	EXPT-PROG	5.0 2	1.0 4	USNDC-7	27		6/73	BNL	COLE+. P-WAVE WN AND WG GIVEN. TBC	65358
TC 099	N,GAMMA	EXPT-PROG	PILE		USNDC-7	1		6/73	AGN	HARKER. CFRMF INTEGRAL MEAST. VALUE	65311
RU 099	RESON PARAMS	EXPT-PROG	NDG		USNDC-7	33		6/73	BNL	RIMAWI+. REDUCED PARTIAL WG SHOWN.	65360
RU 101	RESON PARAMS	EXPT-PROG	NDG		USNDC-7	33		6/73	BNL	RIMAWI+. REDUCED PARTIAL WG SHOWN.	65361
RU 102	N,GAMMA	EXPT-PROG	PILE		USNDC-7	1		6/73	AGN	HARKER. CFRMF INTEGRAL MEAST. VALUE	65312
RU 104	N,GAMMA	EXPT-PROG	PILE		USNDC-7	1		6/73	AGN	HARKER. CFRMF INTEGRAL MEAST. VALUE	65313
AG	STRNTH FNCTN	EXPT-PROG	1.0+3	7.0+5	USNDC-7	147		6/73	NBS	CAMARDA. LINAC. S1 MEASD. NO DATA	65466
CD 110	RESON PARAMS	EXPT-PROG		1.0+3	USNDC-7	56		6/73	COL	LIOU+. AVERAG D VALUE GIVEN	65378
CD 110	STRNTH FNCTN	EXPT-PROG		1.0+3	USNDC-7	56		6/73	COL	LIOU+. SO AND S1 VALUES GIVEN	65372
CD 111	RESON PARAMS	EXPT-PROG		1.0+3	USNDC-7	56		6/73	COL	LIOU+. AVERAG D VALUE GIVEN	65379

ELEMENT S A	QUANTITY	TYPE	ENERGY MIN	ENERGY MAX	DOCUMENTATION REF VOL PAGE	DATE	LAB	COMMENTS	SERIAL NO.
CD 111	STRNTH FNCTN	EXPT-PROG		1.0+3	USNDC-7 56	6/73	COL	LIOU+. SO AND S1 VALUES GIVEN	65373
CD 112	RESON PARAMS	EXPT-PROG		1.0+3	USNDC-7 56	6/73	COL	LIOU+. AVERAG D VALUE GIVEN	65380
CD 112	STRNTH FNCTN	EXPT-PROG		1.0+3	USNDC-7 56	6/73	COL	LIOU+. SO AND S1 VALUES GIVEN	65374
CD 113	RESON PARAMS	EXPT-PROG		1.0+3	USNDC-7 56	6/73	COL	LIOU+. AVERAG D VALUE GIVEN	65381
CD 113	STRNTH FNCTN	EXPT-PROG		1.0+3	USNDC-7 56	6/73	COL	LIOU+. SO VALUE GIVEN	65375
CD 114	RESON PARAMS	EXPT-PROG		1.0+3	USNDC-7 56	6/73	COL	LIOU+. AVERAG D VALUE GIVEN	65382
CD 114	STRNTH FNCTN	EXPT-PROG		1.0+3	USNDC-7 56	6/73	COL	LIOU+. SO AND 91 VALUES GIVEN	65376
CD 116	RESON PARAMS	EXPT-PROG		1.0+3	USNDC-7 56	6/73	COL	LIOU+. AVERAG D VALUE GIVEN	65383
CD 116	STRNTH FNCTN	EXPT-PROG		1.0+3	USNDC-7 56	6/73	COL	LIOU+. SO VALUE GIVEN	65377
IN	STRNTH FNCTN	EXPT-PROG	1.0+3	7.0+5	USNDC-7 147	6/73	NBS	CAMARDA. LINAC. S1 MEASD. NO DATA	65467
IN	DIFF ELASTIC	EXPT-PROG	1.2+7		USNDC-7 197	6/73	CHO	CARLSON+. CURV ANG DIST. 70-145 DEG.	65557
IN	N,GAMMA	EXPT-PROG	3.0+2	6.0+5	USNDC-7 112	6/73	LRL	CZIRR+. NO DATA GIVEN. TBP.	65432
IN 115	N,GAMMA	EXPT-PROG	PILE		USNDC-7 1	6/73	AGN	HARKER. CFRMF INTEGRAL MEAST. VALUE	65314
SN	DIFF ELASTIC	EXPT-PROG	7.6+6		USNDC-7 271	6/73	ABD	BUCHER+. THETA#2.67-14.09DEG.NO DATA	65615
SB	STRNTH FNCTN	EXPT-PROG	1.0+3	7.0+5	USNDC-7 147	6/73	NBS	CAMARDA. LINAC. S1 MEASD. NO DATA	65468
SB 121	N,GAMMA	EXPT-PROG	PILE		USNDC-7 1	6/73	AGN	HARKER. CFRMF INTEGRAL MEAST. VALUE	65315
SB 123	N,GAMMA	EXPT-PROG	PILE		USNDC-7 1	6/73	AGN	HARKER. CFRMF INTEGRAL MEAST. VALUE	65316
TE	N,GAMMA	EXPT-PROG	5.0-1	7.0+3	USNDC-7 107	6/73	LRL	BROWNE+. CURVES.	65426
TE 128	RESON PARAMS	EXPT-PROG	4.2+2	4.3+3	USNDC-7 107	6/73	LRL	BROWNE+. TABLE G*WN AND G*WG.12RESON	65427
TE 128	N,GAMMA	EXPT-PROG	5.0-1	7.0+3	USNDC-7 107	6/73	LRL	BROWNE+. CURVES.	65424
TE 130	RESON PARAMS	EXPT-PROG	1.1+3	4.4+3	USNDC-7 107	6/73	LRL	BROWNE+. TABLE G*WN AND G*WG.3 RESON	65428
TE 130	N,GAMMA	EXPT-PROG	5.0-1	7.0+3	USNDC-7 107	6/73	LRL	BROWNE+. CURVES.	65425
I 127	STRNTH FNCTN	EXPT-PROG	1.0+3	7.0+5	USNDC-7 147	6/73	NBS	CAMARDA. LINAC. S1 MEASD. NO DATA	65469
I 127	N,GAMMA	EXPT-PROG	PILE		USNDC-7 1	6/73	AGN	HARKER. CFRMF INTEGRAL MEAST. VALUE	65317
XE 132	N,GAMMA	EXPT-PROG	PILE		USNDC-7 1	6/73	AGN	HARKER. CFRMF INTEGRAL MEAST. VALUE	65318
XE 134	N,GAMMA	EXPT-PROG	PILE		USNDC-7 1	6/73	AGN	HARKER. CFRMF INTEGRAL MEAST. VALUE	65319
CS 133	N,GAMMA	EXPT-PROG	PILE		USNDC-7 1	6/73	AGN	HARKER. CFRMF INTEGRAL MEAST. VALUE	65320
BA 135	RESON PARAMS	EXPT-PROG	2.4 1	4.6 2	USNDC-7 25	6/73	BNL	HOLM+.TABLE PARTIAL WG. 10 RESON.	65356
BA 135	SPECT NGAMMA	EXPT-PROG	2.5-2	1.0 2	USNDC-7 25	6/73	BNL	HOLM+.9108KEV TRANSITION. CURVE	65357
CE	TOTAL XSECT	EXPT-PROG	+3	+5	USNDC-7 224	6/73	DKE	PINEO+. AVG SIG CFD OPTMOD.NDG.TBP	65585
CE	STRNTH FNCTN	EXPT-PROG	+3	+5	USNDC-7 224	6/73	DKE	PINEO+.SO,S1,S2.NO DATA GVN.TBP AP.	65596
PR 141	N,GAMMA	EXPT-PROG	PILE		USNDC-7 1	6/73	AGN	HARKER. CFRMF INTEGRAL MEAST. VALUE	65321
ND	TOTAL XSECT	EXPT-PROG	+3	+5	USNDC-7 224	6/73	DKE	PINEO+. AVG SIG CFD OPTMOD.NDG.TBP	65586
ND	STRNTH FNCTN	EXPT-PROG	+3	+5	USNDC-7 224	6/73	DKE	PINEO+.SO,S1,S2.NO DATA GVN.TBP AP.	65597
ND 144	TOTAL XSECT	EXPT-PROG	+3	+5	USNDC-7 224	6/73	DKE	PINEO+. AVG SIG CFD OPTMOD.NDG.TBP	65591
ND 144	STRNTH FNCTN	EXPT-PROG	+3	+5	USNDC-7 224	6/73	DKE	PINEO+.SO,S1,S2.NO DATA GVN.TBP AP.	65602
ND 146	TOTAL XSECT	EXPT-PROG	+3	+5	USNDC-7 224	6/73	DKE	PINEO+. AVG SIG CFD OPTMOD.NDG.TBP	65592
ND 146	STRNTH FNCTN	EXPT-PROG	+3	+5	USNDC-7 224	6/73	DKE	PINEO+.SO,S1,S2.NO DATA GVN.TBP AP.	65603
ND 148	TOTAL XSECT	EXPT-PROG	+3	+5	USNDC-7 224	6/73	DKE	PINEO+. AVG SIG CFD OPTMOD.NDG.TBP	65593
ND 148	STRNTH FNCTN	EXPT-PROG	+3	+5	USNDC-7 224	6/73	DKE	PINEO+.SO,S1,S2.NO DATA GVN.TBP AP.	65604
ND 148	N,GAMMA	EXPT-PROG	PILE		USNDC-7 1	6/73	AGN	HARKER. CFRMF INTEGRAL MEAST. VALUE	65323
ND 150	N,GAMMA	EXPT-PROG	PILE		USNDC-7 1	6/73	AGN	HARKER. CFRMF INTEGRAL MEAST. VALUE	65324
PM 147	N,GAMMA	EXPT-PROG	PILE		USNDC-7 1	6/73	AGN	HARKER. CFRMF INTEGRAL MEAST. VALUE	65322
SM 149	TOTAL XSECT	EXPT-PROG	+3	+5	USNDC-7 224	6/73	DKE	PINEO+. AVG SIG CFD OPTMOD.NDG.TBP	65594
SM 149	STRNTH FNCTN	EXPT-PROG	+3	+5	USNDC-7 224	6/73	DKE	PINEO+. NO DATA GIVEN.S1,2,3.TBP AP	65581
SM 152	TOTAL XSECT	EXPT-PROG	+3	+5	USNDC-7 224	6/73	DKE	PINEO+. AVG SIG CFD OPTMOD.NDG.TBP	65595
SM 152	STRNTH FNCTN	EXPT-PROG	+3	+5	USNDC-7 224	6/73	DKE	PINEO+. NO DATA GIVEN.S1,2,3.TBP AP	65582
SM 152	N,GAMMA	EXPT-PROG	PILE		USNDC-7 1	6/73	AGN	HARKER. CFRMF INTEGRAL MEAST. VALUE	65325

ELEMENT S	A	QUANTITY	TYPE	ENERGY MIN	MAX	DOCUMENTATION REF	VOL	PAGE	DATE	LAB	COMMENTS	SERIAL NO.
SM	154	N,GAMMA	EXPT-PROG	PILE		USNDC-7	1		6/73	AGN	HARKER. CFRMF INTEGRAL MEAST. VALUE	65326
GD		TOTAL XSECT	EXPT-PROG	+3	+5	USNDC-7	224		6/73	DKE	PINEO+. AVG SIG CFD OPTMOD.NDG.TBP	65587
GD		STRNTH FNCTN	EXPT-PROG	+3	+5	USNDC-7	224		6/73	DKE	PINEO+.S0,S1,S2.NO DATA GVN.TBP AP.	65598
GD		SPECT NGAMMA	EXPT-PROG	2.4 4		USNDC-7	36		6/73	BNL	WASSON+. GE(LI) DET. NO DATA GIVEN	65368
TB	159	TOTAL XSECT	EXPT-PROG	+3	+5	USNDC-7	224		6/73	DKE	PINEO+. AVG SIG CFD OPTMOD.NDG.TBP	65588
TB	159	RESON PARAMS	EXPT-PROG	NDG		USNDC-7	32		6/73	BNL	CCLE+.PARTIAL WG CORRELATN. NDG. TBC	65359
TB	159	STRNTH FNCTN	EXPT-PROG	+3	+5	USNDC-7	224		6/73	DKE	PINEO+.S0,S1,S2.NO DATA GVN.TBP AP.	65599
DY		TOTAL XSECT	EXPT-PROG	+3	+5	USNDC-7	224		6/73	DKE	PINEO+. AVG SIG CFD OPTMOD.NDG.TBP	65589
DY		STRNTH FNCTN	EXPT-PROG	+3	+5	USNDC-7	224		6/73	DKE	PINEO+.S0,S1,S2.NO DATA GVN.TBP AP.	65600
DY	162	N,GAMMA	EXPT-PROG	1.0 0		USNDC-7	22		6/73	BNL	CCLE+. DIRECT CAPTURE SIG GIVEN	65355
DY	163	RESON PARAMS	EXPT-PROG	1.7+0	1.0+3	USNDC-7	56		6/73	COL	LIOU. TABLE G*WN AND WG. MANY RESON	65384
DY	163	STRNTH FNCTN	EXPT-PROG	0.0+0	7.5+2	USNDC-7	56		6/73	COL	LIOU. S0 VALUE GIVEN	65385
HO	165	TOTAL XSECT	EXPT-PROG	+3	+5	USNDC-7	224		6/73	DKE	PINEO+. AVG SIG CFD OPTMOD.NDG.TBP	65590
HO	165	STRNTH FNCTN	EXPT-PROG	+3	+5	USNDC-7	224		6/73	DKE	PINEO+.S0,S1,S2.NO DATA GVN.TBP AP.	65601
HO	165	N,GAMMA	EXPT-PROG	1.7+2	6.0+5	USNDC-7	112		6/73	LRL	CZIRR+. ABST. TBP. NO DATA GIVEN	65430
TM	169	RESON PARAMS	EXPT-PROG	3.9+0	1.0+3	USNDC-7	79		6/73	COL	ARBOT.CAPT RESON AREAS. TABLE.	65396
TA	181	TOTAL XSECT	EXPT-PROG	4.0+2	6.0+2	USNDC-7	57		6/73	COL	HACKEN+. TRANSMISSION CURVE ONLY.	65391
TA	181	RESON PARAMS	EXPT-PROG		2.5+2	USNDC-7	57		6/73	COL	HACKEN+. AVERAGE D GIVEN	65392
TA	181	RESON PARAMS	EXPT-PROG	0.0+0	1.8+3	USNDC-7	57		6/73	COL	HACKEN+. EXPTL AND P-T WN DISTR GIVN	65394
TA	181	RESON PARAMS	EXPT-PROG	1.0+4	1.0+5	USNDC-7	204		6/73	RPI	BYOUN+.TABLE AVG D,WG,R PRIME.L#0,1	65570
TA	181	STRNTH FNCTN	EXPT-PROG		1.8+3	USNDC-7	57		6/73	COL	HACKEN+. S0 VALUE GIVEN	65393
TA	181	STRNTH FNCTN	EXPT-PROG	1.0+4	1.0+5	USNDC-7	204		6/73	RPI	BYOUN+. S0 AND S1 VALUES GIVEN.	65572
TA	181	SPECT NGAMMA	EXPT-PROG	2.0+0	5.0+3	USNDC-7	112		6/73	LRL	STELTS+.GE(LI)-NAI 3-XTAL SPEC.CURVS	65429
TA	181	SPECT NGAMMA	EXPT-PROG	2.4 4		USNDC-7	36		6/73	BNL	WASSON+. GE(LI) DET. NO DATA GIVEN	65365
W		ELASTIC	EXPT-PROG	4.3+6	8.6+6	USNDC-7	174		6/73	ORL	KINNEY+. ABST OF ORNL-4803. NO DATA.	65528
W		DIFF ELASTIC	EXPT-PROG	4.3+6	8.6+6	USNDC-7	174		6/73	ORL	KINNEY+. ABST OF ORNL-4803. NO DATA.	65529
W		DIFF ELASTIC	EXPT-PROG	7.6+6		USNDC-7	271		6/73	ABD	BUCHER+. THETA#2.67-14.09DEG.NO DATA	65616
W		NONEL GAMMAS	EXPT-PROG	1.0+6	2.0+7	USNDC-7	174		6/73	ORL	DICKINS+. ABST OF ORNL-4847 NO DATA	65534
W		NONEL GAMMAS	EXPT-PROG	1.4+7		USNDC-7	128		6/73	LAS	DRAKE+. NO DATA GIVEN.TO BE COMPLTD	65440
W		TOT INELASTC	EXPT-PROG	4.3+6	8.6+6	USNDC-7	174		6/73	ORL	KINNEY+. ABST OF ORNL-4803. NO DATA.	65530
W		DIFF INELAST	EXPT-PROG	4.3+6	8.6+6	USNDC-7	174		6/73	ORL	KINNEY+. ABST OF ORNL-4803. NO DATA.	65531
W		N,GAMMA	EVAL-PROG	6.0+3	2.0+7	USNDC-7	139		6/73	LAS	DEVANEY. NO DATA. TBP LA-5221.	65460
W	186	DIFF ELASTIC	EXPT-PROG		3.0 6	USNDC-7	9		6/73	ANL	SMITH+. NUCL DEFORMATN EFFECTS. NDG	65332
W	186	DIFF INELAST	EXPT-PROG		3.0 6	USNDC-7	9		6/73	ANL	SMITH+. NUCL DEFORMATN EFFECTS. NDG	65333
RE	185	RESON PARAMS	EXPT-PROG		3.0+3	USNDC-7	157		6/73	NRL	STOLOVY+. LINAC. CAPT MEAST. NO DATA	65477
RE	185	STRNTH FNCTN	EXPT-PROG		3.0+3	USNDC-7	157		6/73	NRL	STOLOVY+. LINAC. CAPT MEAST. NO DATA	65479
RE	185	SPECT NGAMMA	EXPT-PROG	1.0+2	3.4+3	USNDC-7	157		6/73	NRL	STOLOVY+. TOF SPECT SHOWN. LINAC	65481
RE	187	RESON PARAMS	EXPT-PROG		3.0+3	USNDC-7	157		6/73	NRL	STOLOVY+. LINAC. CAPT MEAST. NO DATA	65478
RE	187	STRNTH FNCTN	EXPT-PROG		3.0+3	USNDC-7	157		6/73	NRL	STOLOVY+. LINAC. CAPT MEAST. NO DATA	65480
RE	187	SPECT NGAMMA	EXPT-PROG	1.0+2	3.4+3	USNDC-7	157		6/73	NRL	STOLOVY+. LINAC. NO DATA GIVEN	65482
PT		SPECT NGAMMA	EXPT-PROG	2.4 4		USNDC-7	36		6/73	BNL	WASSON+. GE(LI) DET. CURVE.	65362
AU	197	STRNTH FNCTN	EXPT-PROG	1.0+3	7.0+5	USNDC-7	147		6/73	NBS	CAMARDA. LINAC. S1 MEASD. NO DATA	65470
AU	197	NONEL GAMMAS	EXPT-PROG	1.4+7		USNDC-7	128		6/73	LAS	DRAKE+. NO DATA GIVEN.TO BE COMPLTD	65441
AU	197	N,GAMMA	EXPT-PROG	1.7+2	6.0+5	USNDC-7	112		6/73	LRL	CZIRR+. ABST. TBP. NO DATA GIVEN	65431
AU	197	SPECT NGAMMA	EXPT-PROG	2.4 4		USNDC-7	36		6/73	BNL	WASSON+. GE(LI) DET. NO DATA GIVEN	65364
PB		DIFF ELASTIC	EXPT-PROG	1.1+7	1.4+7	USNDC-7	271		6/73	ABD	BUCHER+. ALSO 12.5MEV.ANAL TBC. NDG.	65618
PB		DIFF ELASTIC	EXPT-PROG	8.0+6		USNDC-7	271		6/73	ABD	BUCHER+.THETA#1.4 AND 20DEG.NO DATA	65617
PB		NONEL GAMMAS	EXPT-PROG	1.4+7		USNDC-7	128		6/73	LAS	DRAKE+. NO DATA GIVEN.TO BE COMPLTD	65442

ELEMENT S A	QUANTITY	TYPE	ENERGY MIN	ENERGY MAX	DOCUMENTATION REF VOL PAGE DATE	LAB	COMMENTS	SERIAL NO.
PB	SPECT NGAMMA	EXPT-PROG	2.4 4		USNDC-7 36 6/73	BNL	WASSON+. GE(LI) DET. TBL PARTIAL SIG	65363
PB 204	TOTAL XSECT	EXPT-PROG	1.0+3	4.0+5	USNDC-7 172 6/73	ORL	GOOD+.LINAC. TRANS. NO DATA GIVEN	65518
PB 206	TOTAL XSECT	EXPT-PROG	1.0+3	4.0+5	USNDC-7 172 6/73	ORL	GOOD+.LINAC. TRANS. NO DATA GIVEN	65519
PB 207	TOTAL XSECT	EXPT-PROG	1.0+3	4.0+5	USNDC-7 172 6/73	ORL	GOOD+.LINAC. TRANS. NO DATA GIVEN	65520
PB 207	TOTAL XSECT	EXPT-PROG	9.0+1	1.0+6	USNDC-7 107 6/73	LRL	PHILLIPS+.TRANS. R-MATRIX FIT GIVEN	65423
PB 207	SPECT NGAMMA	EXPT-PROG	2.4+4		USNDC-7 36 6/73	BNL	WASSON+. GE(LI) DET. CURVE	65371
PB 208	TOTAL XSECT	EXPT-PROG	1.0+3	4.0+5	USNDC-7 172 6/73	ORL	GOOD+.LINAC. TRANS. NO DATA GIVEN	65521
TH 232	STRNTH FNCTN	EXPT-PROG	1.0+3	7.0+5	USNDC-7 147 6/73	NBS	CAMARDA. LINAC. S1 MEASD. NO DATA	65471
TH 232	PHOTO-FISSN	EXPT-PROG		6.0+6	USNDC-7 92 6/73	GA	GOZANI.PROMPT AND DELAYED NEUTS. CRV	65412
U 233	FISSION	EXPT-PROG	1.5 6	3.0 6	USNDC-7 10 6/73	ANL	MEADOWS.RATIO TO U235. 2 ASSAY METHD	65350
U 233	NU	EXPT-PROG	2.5-2	1.0+2	USNDC-7 202 6/73	RPI	REED+. LINAC NO DATA GIVEN. TOF.	65566
U 233	SPECT FISS G	EXPT-PROG	THR		USNDC-7 170 6/73	ORL	PLEASONTON+. NO DATA GIVEN.	65494
U 235	TOTAL XSECT	EXPT-PROG	5.0+5	1.5+6	USNDC-7 147 6/73	NBS	SCHWARTZ+. LINAC. BAP ABST ONLY. NDG	65461
U 235	RESON PARAMS	EXPT-PROG	2.5-2	3.0+1	USNDC-7 202 6/73	RPI	REED+.J FROM NUBAR MEAST.NO DATA GUN	65567
U 235	FISSION	EXPT-PROG	PILE		USNDC-7 149 6/73	NBS	GRUNDL.SIG RATIOS GVN.FISS RATE MEAS	65474
U 235	FISSION	EXPT-PROG	THR	2.0+6	USNDC-7 105 6/73	LRL	CZIRR+.LINAC.TO BE DONE.	65417
U 235	FISSION	EXPT-PROG	1.0+6	6.0+6	USNDC-7 130 6/73	LAS	SMITH+. ABSOL MEAST. NO DATA GIVEN	65447
U 235	FISSION	EXPT-PROG	1.5 6	3.0 6	USNDC-7 10 6/73	ANL	MEADOWS.RATIO TO U233. 2 ASSAY METHD	65351
U 235	FISSION	EXPT-PROG	2.0+6	2.0+7	USNDC-7 105 6/73	LRL	CZIRR+.LINAC.SIG REL TO U235(N,P)NDG	65416
U 235	FISSION	EXPT-PROG	3.5 4	3.5 6	USNDC-7 11 6/73	ANL	POENITZ.TABLE FINAL RESULTS. TBP NSE	65352
U 235	FISSION	EXPT-PROG	8.0+0	1.0+4	USNDC-7 176 6/73	ORL	PEREZ+.LINAC.ABST OF ORNL-TM-3696.	65536
U 235	ALPHA	EXPT-PROG	8.0+0	1.0+4	USNDC-7 176 6/73	ORL	PEREZ+.LINAC.ABST OF ORNL-TM-3696.	65538
U 235	NU	EXPT-PROG	THR	1.5+7	USNDC-7 105 6/73	LRL	HOWE+. TO BE DONE	65419
U 235	NU	EXPT-PROG	2.5-2	3.0+1	USNDC-7 202 6/73	RPI	REED+. LINAC. TOF. MEAN VALUES GIVEN	65565
U 235	NU	EXPT-PROG	5.0-1	1.0+2	USNDC-7 105 6/73	LRL	HOWE+. TO BE COMPLETED NO DATA	65418
U 235	SPECT FISS N	EXPT-PROG	1.7+6	2.2+7	USNDC-7 127 6/73	LAS	AUCHAMPAUGH+. 6ES. NO DATA GIVEN.TBP	65439
U 235	SPECT FISS G	EXPT-PROG	THR		USNDC-7 170 6/73	ORL	PLEASONTON+. NO DATA GIVEN.	65495
U 235	PHOTO-FISSN	EXPT-PROG		6.0+6	USNDC-7 92 6/73	GA	GOZANI.PROMPT AND DELAYED NEUTS. NDG	65413
U 235	N,GAMMA	EXPT-PROG	8.0+0	1.0+4	USNDC-7 176 6/73	ORL	PEREZ+.LINAC.ABST OF ORNL-TM-3696.	65537
U 238	TOTAL XSECT	EXPT-PROG	5.0+5	1.5+6	USNDC-7 147 6/73	NBS	SCHWARTZ+. LINAC. BAP ABST ONLY. NDG	65462
U 238	RESON PARAMS	EXPT-PROG	1.0+4	1.0+5	USNDC-7 204 6/73	RPI	BYOUN+.TABLE AVG D,WG,R PRIME.L#0,1	65571
U 238	RESON PARAMS	EXPT-PROG	7.2+2	1.2+3	USNDC-7 207 6/73	RPI	BLOCK+. 2 RESON. WF GIVEN	65579
U 238	STRNTH FNCTN	EXPT-PROG	1.0+4	1.0+5	USNDC-7 204 6/73	RPI	BYOUN+. S0 AND S1 VALUES GIVEN.	65573
U 238	FISSION	EXPT-PROG	PILE		USNDC-7 149 6/73	NBS	GRUNDL.SIG RATIOS GVN.FISS RATE MEAS	65473
U 238	FISSION	EXPT-PROG	1.0+4	1.0+5	USNDC-7 207 6/73	RPI	BLOCK+.SUBTHRESHOLD FISS.AVG SIG GVN	65578
U 238	SPECT FISS N	EXPT-PROG	1.3+6	2.2+7	USNDC-7 127 6/73	LAS	AUCHAMPAUGH+. 7ES. NO DATA GIVEN.TBP	65438
U 238	PHOTO-FISSN	EXPT-PROG		6.0+6	USNDC-7 92 6/73	GA	GOZANI.PROMPT AND DELAYED NEUTS.CRVS	65411
U 238	N,GAMMA	EXPT-PROG	5.0+0	1.0+5	USNDC-7 175 6/73	ORL	DE SAUSSURE+.LINAC.TOF.SCINT. NDG	65535
NP 237	TOTAL XSECT	EXPT-PROG	+0	+3	USNDC-7 128 6/73	LAS	KEYWORTH+.POL BEAM AND TARGET. NDG	65445
NP 237	RESON PARAMS	EXPT-PROG	+0	+3	USNDC-7 128 6/73	LAS	KEYWORTH+.POL BEAM AND TARGET. NDG	65446
NP 237	FISSION	EXPT-PROG	+0	+3	USNDC-7 128 6/73	LAS	KEYWORTH+.POL BEAM AND TARGET. NDG	65444
NP 237	FISSION	EXPT-PROG	PILE		USNDC-7 149 6/73	NBS	GRUNDL.SIG RATIOS GVN.FISS RATE MEAS	65476
PU 239	EVALUATION	EVAL-PROG	2.5+4	+7	USNDC-7 136 6/73	LAS	HUNTER+. NO DATA GIVEN.TBP LA-5172	65455
PU 239	TOTAL XSECT	EXPT-PROG	5.0+5	1.5+6	USNDC-7 147 6/73	NBS	SCHWARTZ+. LINAC. BAP ABST ONLY. NDG	65463
PU 239	FISSION	EXPT-PROG	PILE		USNDC-7 149 6/73	NBS	GRUNDL.SIG RATIOS GVN.FISS RATE MEAS	65475
PU 239	FISSION	EXPT-PROG	2.5-2	2.0+4	USNDC-7 179 6/73	ORL	WESTON+. NO DATA GIVEN	65540
PU 239	ALPHA	EXPT-PROG	2.5-2	2.0+5	USNDC-7 179 6/73	ORL	WESTON+. NO DATA GIVEN	65544
PU 239	NU	EXPT-PROG	THR	1.5+7	USNDC-7 105 6/73	LRL	HOWE+. TO BE DONE	65420

ELEMENT S A	QUANTITY	TYPE	ENERGY MIN	ENERGY MAX	DOCUMENTATION REF VOL PAGE DATE	LAB	COMMENTS	SERIAL NO.
PU 239	NU	EXPT-PROG	1.0-2	1.0+2	USNDC-7 202 6/73	RPI	HOCKENBURY+.LINAC. QUALITATIVE DATA	65563
PU 239	SPECT FISS G	EXPT-PROG	THR		USNDC-7 170 6/73	ORL	PLEASONTON+. NO DATA GIVEN.	65496
PU 239	PHOTO-FISSN	EXPT-PROG		6.0+6	USNDC-7 92 6/73	GA	GOZANI.PROMPT AND DELAYED NEUTS. NDG	65414
PU 239	PHOTO-FISSN	EXPT-PROG	5.5 6	6.0 6	USNDC-7 19 6/73	ANL	STUBBINS. TOF. 2ES. LINAC.NEUT SPECT	65353
PU 239	ABSORPTION	EXPT-PROG	2.5-2	2.0+4	USNDC-7 179 6/73	ORL	WESTON+. NO DATA GIVEN.	65546
PU 240	EVALUATION	EVAL-PROG	4.0+4	+7	USNDC-7 136 6/73	LAS	HUNTER+. NO DATA GIVEN.TBP LA-5172	65456
PU 240	FISSION	EXPT-PROG	2.5-2	2.0+4	USNDC-7 179 6/73	ORL	WESTON+. NO DATA GIVEN	65541
PU 240	ABSORPTION	EXPT-PROG	2.5-2	2.0+5	USNDC-7 179 6/73	ORL	WESTON+. NO DATA GIVEN.	65547
PU 241	TOTAL XSECT	EXPT-PROG	5.0-1	8.0+6	USNDC-7 168 6/73	ORL	SIMPSON+.LINAC. TBC. NO DATA GIVEN.	65488
PU 241	FISSION	EXPT-PROG	2.5-2	2.0+4	USNDC-7 179 6/73	ORL	WESTON+. NO DATA GIVEN	65542
PU 241	ALPHA	EXPT-PROG	2.5-2	2.0+5	USNDC-7 179 6/73	ORL	WESTON+. NO DATA GIVEN	65545
PU 241	ABSORPTION	EXPT-PROG	2.5-2	2.0+4	USNDC-7 179 6/73	ORL	WESTON+. NO DATA GIVEN.	65548
AM 241	FISSION	EXPT-PROG	2.5-2	2.0+4	USNDC-7 179 6/73	ORL	WESTON+. NO DATA GIVEN	65543
AM 241	ABSORPTION	EXPT-PROG	2.5-2	2.0+5	USNDC-7 179 6/73	ORL	WESTON+. NO DATA GIVEN.	65549
CM 246	FRAG SPECTRA	EXPT-PROG	SPON		USNDC-7 166 6/73	ORL	PLEASONTON+.SI DET.FRAG MASS+KE DIST	65486
CM 248	TOTAL XSECT	EXPT-PROG	5.0-1	3.0+3	USNDC-7 170 6/73	ORL	BENJAMIN+.TOF.LINAC.40 RESON SEEN.	65492
CM 248	RESON PARAMS	EXPT-PROG	7.2+0	3.0+3	USNDC-7 170 6/73	ORL	BENJAMIN+.LINAC.40RESON. AVG D GIVEN	65493
CF 249	RESON PARAMS	EXPT-PROG	3.0-1	2.0+1	USNDC-7 169 6/73	ORL	DABBS+.LINAC.TOF.11 NEW RESON SEEN	65490
CF 249	FISSION	EXPT-PROG	-1	+2	USNDC-7 169 6/73	ORL	DABBS+.LINAC.TOF.11 NEW RESON SEEN	65489
CF 251	FISSION	EXPT-PROG	THR		USNDC-7 106 6/73	LRL	RAGAINI+. SIG VALUE GIVEN REL U233NF	65421
CF 252	SPECT FISS G	EXPT-PROG	SPON		USNDC-7 170 6/73	ORL	PLEASONTON+. NO DATA GIVEN.	65497
CF 252	FRAG SPECTRA	EXPT-PROG	SPON		USNDC-7 95 6/73	GA	GOZANI.GAM MULTIPLICTY/SPEC CRLN.CRV	65415
FM 255	FISSION	EXPT-PROG	THR		USNDC-7 106 6/73	LRL	RAGAINI+. SIG VALUE GIVEN REL U233NF	65422
FM 257	NU	EXPT-PROG	SPON		USNDC-7 127 6/73	LAS	VEESER+. TO BE COMPLETED.	65437

AEROJET NUCLEAR COMPANY

A. INTEGRAL CROSS SECTION MEASUREMENTS IN THE CFRMF (Y. D. Harker)

The results of integral cross section measurements of 17 fission product isotopes listed in Table A-1 have been submitted to CSEWG for Phase II testing of the fission product date file for ENDF/B Version 4. Along with these data, the tabulation of the CFRMF spectrum (Table A-2) as determined from improved one-dimensional transport calculations has also been submitted. These data, reaction rates and spectrum, have been prepared using the latest cross section and nuclear decay data. More results of not only capture but also reactivity worth measurements will be reported shortly.

Present activities include integral measurements applicable to the present interests in the use of europium oxide as control material for fast reactors. The capture measurements on separated samples of ^{151}Eu and ^{153}Eu have been completed and are being analyzed. Reactivity worth measurements on Eu_2O_3 and B_4C are planned and will be compared with each other and with earlier measurements on enriched samples of elemental boron-10.

TABLE A-1

MEASURED INTEGRAL DATA FOR PHASE II TESTING OF CAPTURE CROSS SECTIONS OF FISSION-PRODUCT ISOTOPES

Reaction	Chemical* Form	Thickness** (mg/cm^2)	$\bar{\sigma}_m$† (barns/target atom)
$^{87}Rb(n,\gamma)^{88}Rb$	RbCl	79.7	0.0132 ± .0018
$^{99}Tc(n,\gamma)^{100}Tc$	Tc powder	126.3	0.294 ± .039
$^{102}Ru(n,\gamma)^{103}Ru$	Ru powder	111.4	0.097 ± .011
$^{104}Ru(n,\gamma)^{105}Ru$	Ru powder	96.00	0.0932 ± .0093
$^{115}In(n,\gamma)^{116m}In$	In foil	81.11	0.288 ± .027
$^{121}Sb(n,\gamma)^{122}Sb$	Sb powder	168.2	0.309 ± .028
$^{123}Sb(n,\gamma)^{124}Sb$	Sb powder	168.2	0.171 ± .024
$^{127}I(n,\gamma)^{128}I$	HIO_3	249.2	0.216 ± .080
$^{132}Xe(n,\gamma)^{133m}Xe$	^{132}Xe	.2868	0.00248 ± .00043
$^{132}Xe(n,\gamma)^{133}Se$	^{132}Xe	.2868	0.0401 ± .0040

TABLE A-1 (Continued)

Reaction	Chemical* Form	Thickness** (mg/cm^2)	$\bar{\sigma}_m$ † (barns/target atom)
$^{134}Xe(n,\alpha)^{135}Xe$	^{134}Xe	.1060	0.0152 ± .0016
$^{133}Cs(n,\gamma)^{134m}Cs$	Cs_2SO_4	88.62	0.0362 ± .0069
$^{133}Cs(n,\gamma)^{134}Cs$	$CsNO_3$	22.94	0.300 ± .026
$^{141}Pr(n,\gamma)^{142}Pr$	Pr powder	101.6	0.080 ± .10
$^{147}Pm(n,\gamma)^{148m}Pm$	$^{147}Pm(NO_3)_3$	13.38	0.379 ± .059
$^{147}Pm(n,\gamma)^{148}Pm$	$^{147}Pm(NO_3)_3$	13.38	0.462 ± .059
$^{148}Nd(n,\gamma)^{149}Nd$	Nd_2O_3	77.44	0.118 ± .015
$^{150}Nd(n,\gamma)^{151}Nd$	Nd_2O_3	77.44	0.107 ± .024
$^{152}Sm(n,\gamma)^{153}Sm$	Sm_2O_3	111.3	0.302 ± .030
$^{154}Sm(n,\gamma)^{155}Sm$	Sm_2O_3	111.3	0.121 ± .012

* Natural abundance elements are used except where the specific isotopes are indicated.

** Mass includes all constituent elements indicated in chemical form. The real thickness for powdered and compound samples is .76 mm and for foils the real thickness can be determined using normal densities.

† $\bar{\sigma}_m$ is determined by dividing the measured reaction rate $\phi_o\sigma_m$ by $\phi_o = 1.205 \times 10^{11}$ $n/cm^2/sec$ (± 8%). ϕ_o is the integral flux as measured using SAND II and the reaction rates measured in the ILRR program. The error assignments are for 67% confidence level and are absolute, i.e. systematic errors have been included.

TABLE A-2

CFRMF Central Fluxes As Calculated by SCAMP

One Dimensional Transport, P1-S6 Approximation, Twenty Region Cell Calculation

SCAMP 73/008

Group Number	Lower Lethargy	Lower Energy (ev)	Real Flux $\phi(u)\Delta u$	Adjoint Flux $\phi^*(u)$
1	0.25	7.79×10^6	0.015915	1.0
2	0.50	6.07	0.047192	0.80420
3	0.75	4.72	0.099282	0.67108
4	1.00	3.68	0.15826	0.65349
5	1.25	2.87	0.22956	0.64363
6	1.50	2.23	0.30044	0.63980
7	1.75	1.74	0.32838	0.62121
8	2.00	1.35	0.37165	0.56690
9	2.25	1.05	0.48196	0.50539
10	2.50	8.21×10^5	0.65123	0.50217
11	2.75	6.39	0.87768	0.50374
12	3.00	4.98	1.00	0.49581
13	3.25	3.88	0.96504	0.47814
14	3.50	3.02	0.97404	0.46437
15	3.75	2.35	0.87086	0.43954
16	4.00	1.83	0.73469	0.41390
17	4.25	1.43	0.59642	0.39230
18	4.50	1.11	0.53875	0.37561
19	4.75	8.65×10^4	0.41965	0.35070
20	5.00	6.74	0.39890	0.33418
21	5.25	5.25	0.27323	0.30970
22	5.50	4.09	0.22890	0.28183
23	5.75	3.18	0.15576	0.25766
24	6.00	2.48	0.15655	0.25298
25	6.25	1.93	0.11410	0.24348
26	6.50	1.50	0.080494	0.22613
27	6.75	1.17	0.077870	0.22072
28	7.00	9.12×10^3	0.065567	0.20962
29	7.25	7.10	0.051764	0.19600
30	7.50	5.53	0.044402	0.18976
31	7.75	4.31	0.042918	0.19116
32	8.00	3.36	0.043315	0.19085
33	8.25	2.61	0.034658	0.18112
34	8.50	2.04	0.031480	0.18596
35	8.75	1.59	0.033850	0.19033

CFRMF Central Fluxes, SCAMP 73/008 (cont'd)

Group Number	Lower Lethargy	Lower Energy (ev)	Real Flux $\phi(u)\Delta u$	Adjoint Flux $\phi^*(u)$
36	9.00	1.23×10^3	0.027442	0.18201
37	9.25	961.1	0.020435	0.16747
38	9.50	748.5	0.020955	0.17505
39	9.75	582.9	0.015951	0.18771
40	10.00	454.0	0.015354	0.20813
41	10.25	353.6	0.010261	0.18331
42	10.50	275.4	8.7379×10^{-3}	0.20582
43	10.75	214.5	6.5036×10^{-3}	0.22284
44	11.00	167.0	4.9708×10^{-3}	0.20369
45	11.25	130.1	4.9375×10^{-3}	0.20523
46	11.50	101.3	1.7187×10^{-3}	0.19667
47	11.75	78.9	2.6564×10^{-3}	0.20079
48	12.00	61.4	1.1628×10^{-3}	0.19713
49	12.25	47.9	1.3074×10^{-3}	0.35037
50	12.50	37.3	5.1720×10^{-4}	0.25078
51	12.75	29.0	3.3158×10^{-4}	0.26508
52	13.00	22.6	2.8618×10^{-4}	0.30092
53	13.25	17.6	4.8196×10^{-5}	0.25178
54	13.50	13.7	1.1940×10^{-4}	0.21980
55	13.75	10.68	5.6173×10^{-5}	0.22511
56	14.00	8.32	1.6846×10^{-5}	0.39369
57	14.25	6.48	1.3368×10^{-6}	0.084526
58	14.50	5.04	8.9927×10^{-7}	0.16826
59	14.75	3.93	9.4233×10^{-7}	0.038638
60	15.00	3.06	2.9062×10^{-7}	0.23203
61	15.25	2.38	8.4601×10^{-8}	0.13119
62	15.50	1.86	1.6601×10^{-8}	0.11921
63	15.75	1.44	2.8681×10^{-9}	0.14434
64	16.00	1.125	3.7852×10^{-10}	0.31297
65	16.25	0.876	7.1949×10^{-11}	0.48998
66	16.50	0.683	3.5829×10^{-11}	0.43869
67	16.75	0.532	2.1580×10^{-12}	0.49489
68	17.00	0.414	1.3690×10^{-13}	0.59395
69	∞	0.0	8.2748×10^{-15}	0.73126

ARGONNE NATIONAL LABORATORY

A. FAST NEUTRON PHYSICS

1. Medical Applications

a. Thick Target Neutron Yields from ^{3}He-Bombardment of ^{9}Be For Neutron Radiaton-Therapy (F. T. Kuchnir,* L. S. Skaggs,* A. J. Elwyn, and F. P. Mooring)

As mentioned in a previous report,[1] we have measured the energy spectra and angular distribution of the neutrons produced by bombarding thick Be targets by 8 and 16 MeV deuterons and 14.8 MeV protons at the ANL tandem. These results are being used in the design of a neutron radiation-therapy facility that involves a 30" medical cyclotron at the Argonne Cancer Research Hospital. To complement these measurements we have more recently studied the neutron spectra and angular distribution in the bombardment of thick Be targets by 20.3 MeV ^{3}He particles by techniques similar to those utilized in the previous measurements. Some of the results are shown in Fig. A-1. Along with ref. 1 these suggest that the neutron yield per incident particle at 0° is approximately the same for 8.3-MeV deuterons and 14.8-MeV protons but less by about a factor of three for the ^{3}He particles. Further, the median neutron energy at 0° is 3.3. MeV, 2.4 MeV, and 6.3 MeV for 8.3-MeV deuterons, 14.8-MeV protons, and 20.3-MeV ^{3}He particles, respectively. On the basis of the measurements it becomes evident that a deuteron beam is the best choice for production of intense fast neutrons for radiotherapy with a 30" medical cyclotron.

---

* Franklin McLean Memorial Research Institute, University of Chicago, Chicago, Illinois

[1] USNDC-3, 24 October 1972

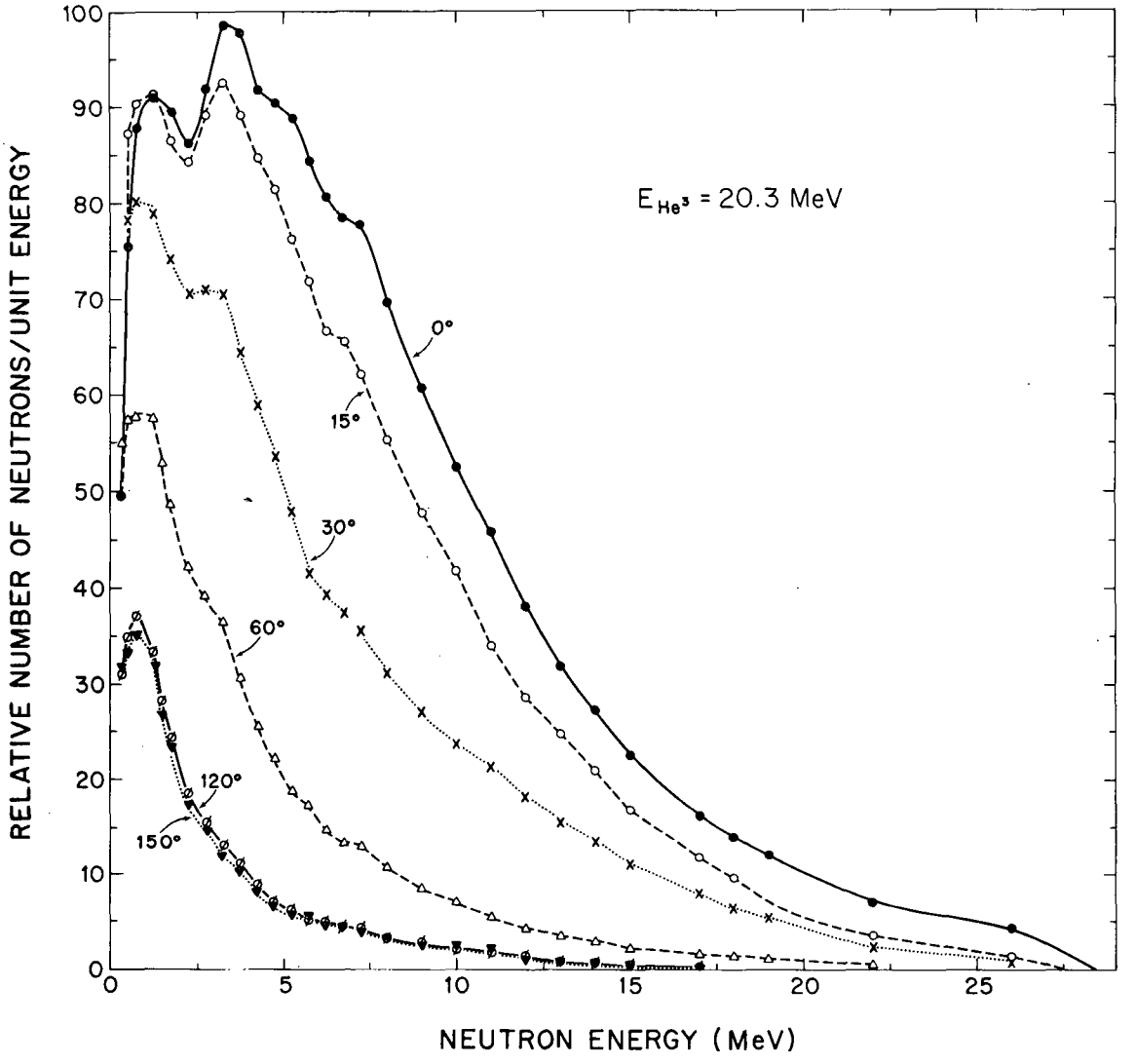
RELATIVE NUMBER OF NEUTRONS/UNIT ENERGY
NEUTRON ENERGY (MeV)
E_{He^3} = 20.3 MeV
0°
15°
30°
60°
120°
150°
0
10
20
30
40
50
60
70
80
90
100
0
5
10
15
20
25

Fig. A-1

b. Collimation of Fast Neutrons for Radiation Therapy (F. T. Kuchnir,* L. S. Skaggs,* K. Kawachi*, A. Smith and J. Whalen)

The design of collimating systems for fast neutron therapy purposes is in progress. A report of this work has been submitted to the annual meeting of The American Association of Physicists in Medicine. The abstract is as follows:

> A polyethylene collimator of simple design has been developed and its performance investigated using Monte Carlo techniques and neutrons of known spectral distribution. In the forward direction, this spectrum has a broad maximum at 3.2 MeV with a median energy of 3.5 MeV. Using these results as a starting point, we constructed a mockup collimator having a straight cylindrical opening into which disc-shaped inserts with circular holes of graduated sizes could be placed. By removal or addition of different discs, several configurations in the collimated beam, as well as on leakage and scattered components, were investigated using a source of monoenergetic 3.5 MeV neutrons and time-of-flight techniques. These results are being used in the design of an optimized collimator for a fast-neutron beam for radiation therapy.

---

* Franklin McLean Memorial Research Institute, University of Chicago, Chicago, Illinois

2. Fast Neutron Total and Scattering Cross Sections

a. Fast Neutron Processes in Niobium—Measurements and Evaluation. (A. Smith, P. Guenther and J. Whalen)

The program of niobium measurements to 5.0 MeV has been completed and a formal report is available (AP/CTR/TM-4). The work is inclusive of: detailed experimental studies, development of a nuclear model applicable to the continuum region and a comprehensive evaluation. The work is summarized in the following abstract:

Neutron total and elastic and inelastic scattering cross sections of niobium are measured in the incident energy interval 0.3 to 5.0 MeV. Differential elastic neutron scattering cross sections are determined at ≈20 scattering angles distributed between 20 and 160 degrees. The cross sections for the inelastic neutron excitation of 11 states with Q-values of ≤ 2520 keV are quantitatively measured and the excitation of an additional 8 states qualitatively observed. The experimental results are compared with previously reported values and provide a foundation from which is deduced an optical potential suitable for the interpolation and extrapolation of the measured values. The experimental results and the associated theoretical model are used to construct an evaluated data file in the ENDF format with particular attention to fast neutron cross sections applicable to the neutronic study of fusion reactor systems.

b. Compound and Direct Effects in Fast Neutron Scattering from Titanium (P. A. Moldauer, A. Smith and P. Guenther).

A program of measurements has provided a detailed base of experimental information to incident neutron energies of 1.5 MeV. These data are compared with theoretical predictions obtained by generating random unitary statistical model cross sections that are consistent with predetermined optical/coupled-channels model parameters. It is found that while both the average and fluctuation statistics of the total cross section could be fitted with the use of (spherical nucleus) single-channel optical model parameters, the statistics of the ^{48}Ti inelastic cross section required the use of (spheroidal nucleus) coupled-channels model parameters. The deduced deformation parameter of $\beta_2 = 0.3$ is consistent with that obtained from some other methods.

The analytical method provides a tool for the statistical construction of resonance cross sections in difficult experimental regions where measurements are either not definitive or are unavailable.

c. Nuclear Deformation in the Scattering of Fast Neutrons ^{186}W (A. Smith and P. Guenther)

Differential elastic and inelastic neutron scattering cross sections of ^{186}W have been measured to incident neutron energies of 3.0 MeV. The scattered neutron resolution is sufficient to well resolve the first rotational (125 keV, 2+) state throughout the measured energy range and to define approximately 15 excited states. The latter appear to be primarily collective excitations, some of them previously unreported. Comparison of the measured values with the results of couple-channel calculations determines β_2 to ± 15% without undue model dependence. The excitation of the first excited state is largely (> 50%) by direct processes at energies of 2—3 MeV. The model developed from the ^{186}W studies is being applied to the analogous scattering processes in ^{238}U where it is not possible to experimentally resolve the similar structures.

d. Neutron Total and Scattering Cross Section of Ni and Co (A. Smith, P. Guenther and J. Whalen)

Measurements of neutron total and scattering cross sections of Ni and Co have been completed to incident energies of 4.0MeV. The results are being utilized in a re-evaluation of the fast neutron cross sections of both elements which will be presented in the ENDF format.

e. Fast Neutron Total and Scattering Cross Sections of C, V, and Fe. (A. Smith and P. Guenther)

The program of measurements for these elements has been completed to incident neutron energies of 4.0MeV. Final analysis and reporting will be initiated shortly.

3. Measurements of the $^{6}Li(n,\alpha)$ Cross Section in the Energy Range from 90 to 1500 keV. (W. P. Poenitz)

Previously reported measurements of this cross section[1] were extended to the energy range above 600 keV. New measurements by two different experimenters resulted in differences up to 70 per cent in the $^{6}Li(n,\alpha)$ cross section at 1.5 MeV. This discrepancy was the main reason for the new measurements; however, some data were also obtained in the 100—200 keV and 300—500 keV range where previously few values have been reported.

Measurements were carried out with a ^{6}Li glass detector and with the "Grey Neutron Detector."[2] In addition, an improved value for the amount of ^{6}Li in the Li-glass was obtained from a transmission experiment at 0.08 eV. The value compares well with the results from chemical and mass-spectroscopic analysis of the material.

The measurements result in a peak (246 keV) -to-valley (95 keV) ratio of 4.76 and an absolute value of about 3 barn in the resonance peak. These values compare well with recent results by Coates et al.[3] and of Fort and Marquette.[4] In the energy range above 500 keV our values support the data by Fort and Marquette.

Though the experimental knowledge of the $^{6}Li(n, \alpha)$ cross section has improved dramatically in the last year, the reaction appears to be difficult to apply as a standard above 100 keV. Large uncertainties may be caused by small variations in the energy scale due to the strong energy dependence of the cross section in the resonance range.

---

[1] W. P. Poenitz, USNDC-3, p. 8 (1972).

[2] W. P. Poenitz, ANL-7915.

[3] M. S. Coates et al., IAEA-Conf. on Standard Reference Data, November, 1972.

[4] E. Fort and J. P. Marquette, EANDC(E) - 148 "U".

4. Fission Cross Sections

a. The ^{233}U to ^{235}U Fission Cross Section Ratio (J. W. Meadows)

Preliminary results from the ^{233}U to ^{235}U fission ratio measurement are now available. The experimental method is similar to the one previously described.[1] The uranium deposits are

---

[1] J. W. Meadows, Nucl. Sci. Eng., 49, 310 (1972)

~60 ug/cm^2 and 2.5 cm in diameter with an isotopic purity of 99.54% ^{233}U. The ^{235}U contains a few percent (<10%) ^{233}U and has a combined ^{235}U—^{233}U content of 99.56%. The mass ratios of the deposits were measured in two ways: 1) alpha counting, 2) comparing the thermal fission ratios in the thermal column of the Argonne Thermal Source Reactor and using the thermal fission cross section and g factor of Hanna et al.[2]. A comparison of three ^{233}U deposits and six ^{235}U deposits including three isotopic mixtures showed that the two methods agreed to within 0.8 ± 0.7%.

Ratio measurements were made with two ^{233}U and four ^{235}U deposits with the following results:

$$\sigma_f(^{233}U)/\sigma_f(^{235}U)$$

E_n, MeV	Assay Method 1	Assay Method 2
1.51	1.582	1.566
2.00	1.566	1.561
2.50	1.577	1.567
3.00	1.590	1.576

The estimated absolute errors are ≤2%. The relative errors in each set is ≤1%. These values are 4—9% higher than the ratios calculated from the ENDF/B-III error reaction set.

---

[2] G. C. Hanna, C. H. Westcott, H. D. Lemmel, B. K. Leonard Jr., J. S. Story, P. M. Atture, "Atomic Energy Review", Vol. VII, No. 4, IAEA, Vienna, 1969.

b. Relative and Absolute Measurements of the Fast Neutron Fission Cross Section of ^{235}U. (W. P. Poenitz)

The present program was completed with additional shape and absolute measurements in the 400—3000 keV range using the "Black Neutron Detector".[1] An average shape result was derived

---

[1] W. P. Poenitz, ANL - 7915

from the three different measurements [Grey Neutron Detector, Black Neutron Detector, and $^{6}Li(n, \alpha)$] and then normalized to the absolute values obtained with three independent techniques. The results for the absolute values are listed in Table A-1. The results for the normalized shape values are given in Table A-2.

A paper has been prepared for publication in Nuclear Science and Engineering.

TABLE A-1. Absolute Values for the Fission Cross Section of ^{235}U

E_n/keV	$\pm\Delta E$/keV	σ/mb	$\Delta\sigma$/mb	Technique
800	27	1134	27	BND, small
3500	80	1198	26	BND, large
448	60	1220	44	Associated ^{51}Cr-Activity
552	60	1116	42	Associated ^{51}Cr-Activity
601	60	1108	41	Associated ^{51}Cr-Activity
644	65	1101	42	Associated ^{51}Cr-Activity
498	30	1151	42	Calibr. Van. Bath

TABLE A-2. Final Results for the Fission Cross Sections of ^{235}U

E_n/keV	$\sigma_{n,f}$/mb	E_n/keV	$\sigma_{n,f}$/mb
35	2006	800	1110
40	1931	840	1120
45	1856	860	1135
50	1818	890	1161
55	1794	920	1185
60	1772	950	1214
70	1710	980	1209
80	1647	1000	1207
90	1588	1200	1204
100	1555	1400	1213
120	1493	1500	1226
140	1437	1800	1279
170	1387	1900	1290
200	1357	2000	1294
250	1307	2100	1292

TABLE A-2 (Cont'd)

E_n/keV	$\sigma_{n,f}$/mb	E_n/keV	$\sigma_{n,f}$/mb
300	1268	2200	1285
350	1228	2400	1266
400	1201	2600	1253
500	1160	3000	1224
600	1125	3500	1192
700	1110		

5. The Fast Neutron Generator. (A. B. Smith)

The ANL Fast Neutron Generator on March 10 completed a full year of 24 hr/dy-6 dy/wk operation with no opening of the pressure vessel. This reliability is very gratifying.

Testing of the new high-intensity ion source has continued on the bench setup. $^-$H beams of greater than 3 ma have been achieved through approximately 1/4 inch apertures and with an emittance reasonably suitable for the FNG. The testing continues with the objective of $^-$H beams of greater than 1 ma through the 1/8 inch aperture required for proper operation of the nsec pulsing system. When this is achieved the source will be installed.

The long flight path is slowly growing having now reached approximately 60 m. Sections are being added in 40 foot increments.

B. CHARGED PARTICLE REACTIONS

1. Reactions Relevant to Controlled Thermonuclear Research (R. E. Segel)

The following reactions which may be of interest both in nuclear astrophysics and in controlled thermonuclear research have been investigated. (1) The ^{7}Li(d, p)^{8}Li reaction. The cross section for this reaction has been measured from 280 keV which is only 30 keV above threshold up to 500 keV. The measurement has been carried out by using plastic track detectors to measure the delayed α particles emitted in the ^{8}Li decay. The cross section rises monotonically,

reaching a value of about 5 mb at 500 keV. The yield curve can be fitted with the direct interaction code DWUCK, and a spectroscopic factor of about 0.45. (2) The cross section for the $^{6}Li(^{3}He, n)^{8}B$ reaction has been measured from threshold (2.97 MeV) up to 7 MeV. The data are still being analyzed, but a preliminary value of 5.4 mb can be quoted for the cross section at a 3.5-MeV bombarding energy.

2. Experimental Study of Spontaneously Fissioning Isomers (K. L. Wolf and J. P. Unik)

Half-lives have been measured for several new fissioning isomers and more accurate values have been determined for many previously identified isomers. Pulsed beam techniques were used at the ANL 152 cm cyclotron to measure delayed fission activities that decayed with half-lives greater than a few ns. Fissioning isomers were produced with charged particle reactions such as (p, xn), (d, xn) and (α, pxn) reactions and the isotopic assignment of each new activity was made by measurement of an excitation function.

A compilation of half-lives is given in Fig. B-1 for nearly all known fissioning isomers. A heavy outline marks the cases that have been studied in this laboratory and those isomers recently discovered at ANL are indicated by cross-hatched areas.

Several features of fission isomerism can be seen from a half-life systematics:

1) There is an unpaired nucleon effect that increases half-lives approximately 10^3 for each unpaired nucleon, analogous to the hindrance effect on ground state spontaneous fission lifetimes.

2) The maximum stability for a given atomic number Z occurs at neutron number N = 147.

3) In the trans-neptunium isomers there is a decrease in half-life with increasing Z.

4) The isomeric fission decay of ^{237}Pu, ^{238}Pu and ^{242}Bk each has two components and appears to be caused by spin-forbidden isomerism in the secondary potential minimum.

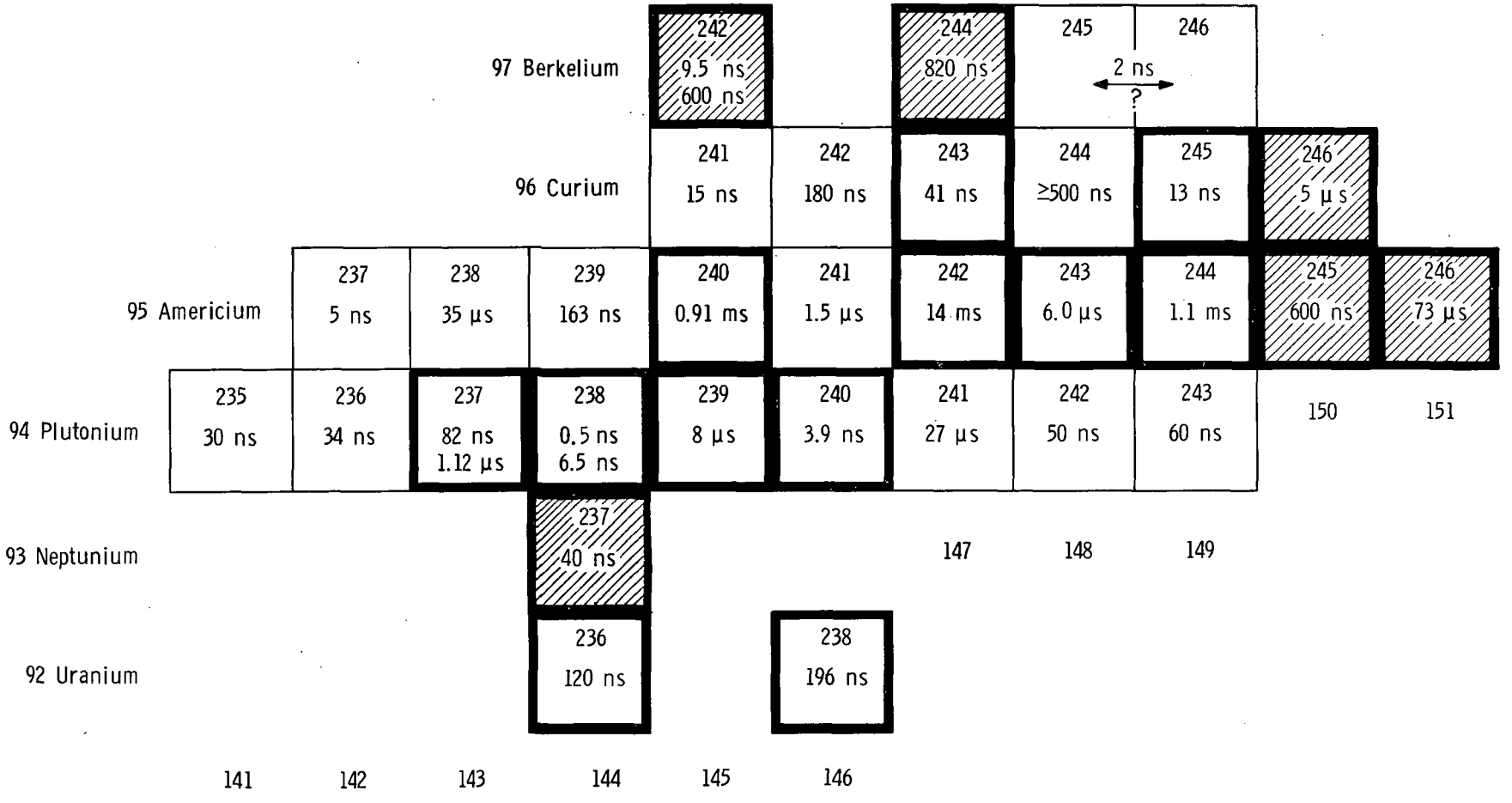
97 Berkelium
242 9.5 ns 600 ns
244 820 ns
245
246
2 ns
?
96 Curium
241 15 ns
242 180 ns
243 41 ns
244 ≥500 ns
245 13 ns
246 5 μs
95 Americium
237 5 ns
238 35 μs
239 163 ns
240 0.91 ms
241 1.5 μs
242 14 ms
243 6.0 μs
244 1.1 ms
245 600 ns
246 73 μs
94 Plutonium
235 30 ns
236 34 ns
237 82 ns 1.12 μs
238 0.5 ns 6.5 ns
239 8 μs
240 3.9 ns
241 27 μs
242 50 ns
243 60 ns
150
151
93 Neptunium
237 40 ns
147
148
149
92 Uranium
236 120 ns
238 196 ns
141
142
143
144
145
146

Fig. B-1

5) Uranium and neptunium fissioning isomers are rarely observed, proabably because some mode of decay other than fission is dominant in the deexcitation of these shape isomers.

3. Polarization and Differential Cross Section in Analog-Resonant (p, n) Reactions (A. J. Elwyn and J. E. Monahan)

Most previous studies of the neutron decay to low-lying residual nucleon states of analog-resonances excited in proton induced reactions have made use of the one-channel formalism proposed by Ronson and his collaborators. We have considered a more general approach to an interpretation of such reactions. The general form of the collision matrix elements that describe the process have been obtained on the basis of an R-matrix formalism. Various approximations to the energy-averaged collision matrix elements have been considered and we find that phase-correlation effects between the background $T_<$ states and other nuclear states may be important in the interpretation of any resonant contributions to neutron polarization in isospin forbidden (p, n) processes. In fact, the experimental study of both the differential cross sections and the polarization of the neutrons in such reactions might be expected to provide evidence about the role of correlated states in such processes. These general considerations are being applied to the case of a non-zero resonant neutron polarization in the $^{51}V(p, n)^{51}Cr$ reaction, that has been measured at proton energies near the 2.335 analog resonance in ^{52}Cr at the Argonne Dynamitron accelerator.

C. PHOTONUCLEAR PHYSICS

1. Giant M1 Resonance in ^{207}Pb (L. R. Medsker and H. E. Jackson)

The ANL threshold photoneutron facility has been used in a high resolution study of the photoneutron spectra from an enriched target of ^{207}Pb. An earlier status report on this experiment together with the photoneutron spectrum was given in USNDC-3. For each resonance the photoneutron angular distribution and resonance yield were measured. The s-wave resonances due to E1 transitions were identified by comparing the results with data on total neutron cross section. An important feature of the data is the intensity of the p-wave resonances excited by M1 transitions. The expected strength of an M1

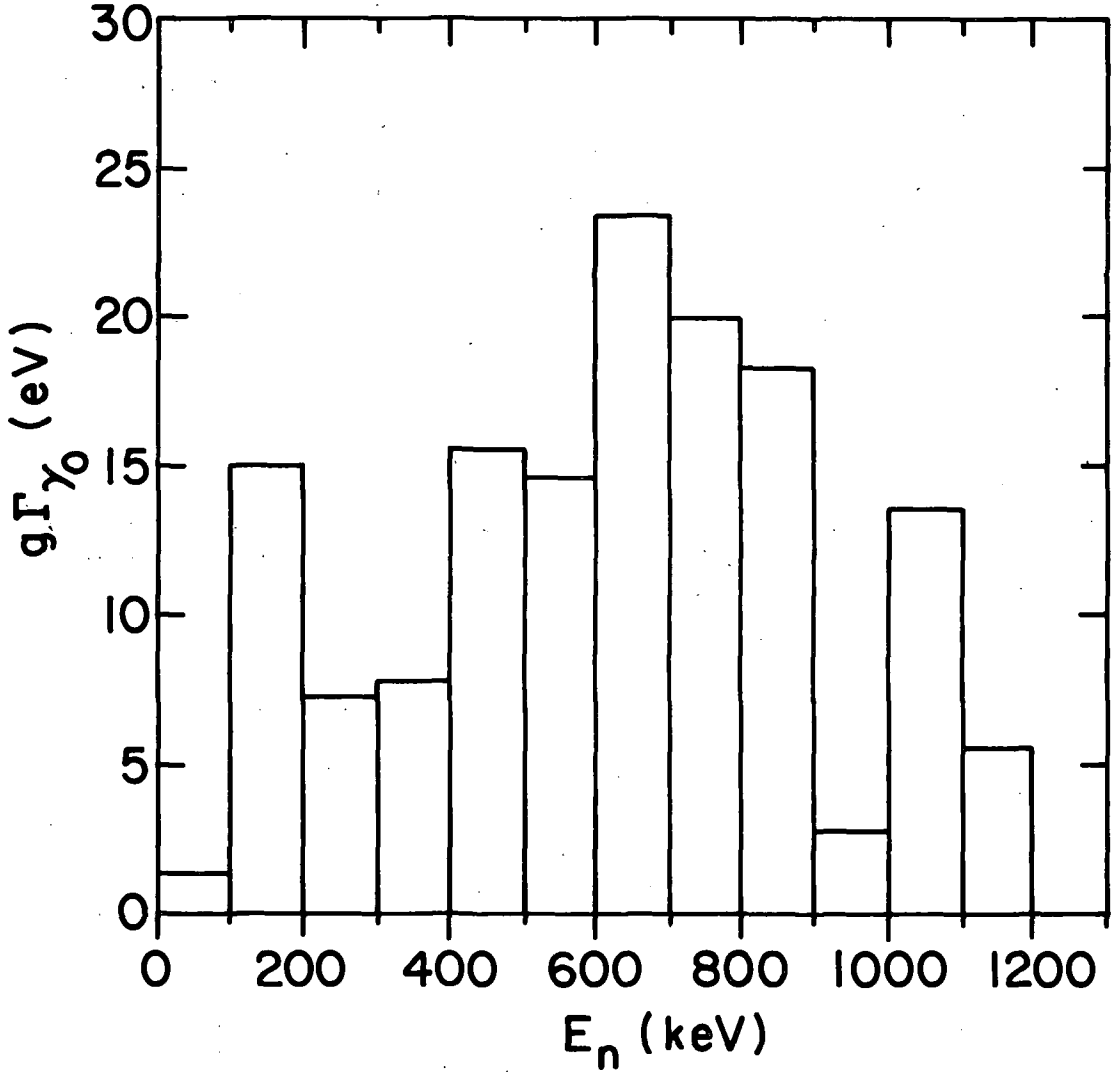

Fig. C-1

Fig. C-1. Histogram of the values of $g\Gamma_{\gamma o}$ for p-wave photoneutron resonances in ^{208}Pb.

giant resonance, calculated in terms of a $\pi(i_{11/2})(i_{13/2})^{-1}$ or $\nu(h_{9/2})(h_{11/2})^{-1}$ particle-hole pair coupled to the ground state of ^{207}Pb is 200 eV. From the present study a lower limit of 125 eV can be placed on the measured integrated strength. Because of M1 + E2 mixing and the absence of total neutron cross-section data for $E_n > 717$ keV, the value of J^{π} for several resonances could not be assigned definitely. However, there is a high probability that the contributions of many of these resonances to the total M1 strength exhaust the strength predicted for the giant M1 resonance. The distribution of radiative strength (see Fig. C-1) suggests a peaking of the M1 strength function near 700 keV.

2. Ground-State Radiative Strength in ^{117}Sn and ^{119}Sn (H. E. Jackson and E. N. Strait)

The following abstract describes the current status of work on Sn isotopes: The spectra of neutrons from photoexcited states in ^{119}Sn and ^{117}Sn near threshold have been observed in time-of-flight measurements. Highly enriched samples were irradiated by bremsstrahlen from the ANL pulsed electron linac. Bremsstrahlung end-point energies were chosen to permit only ground-state photoneutron transitions in the regions of interest. Data for the resolved resonance structure below 20 keV photoneutron energy give no suggestion of unusually strong E1 or M1 strength. The anomalous peak in the (γ, n) cross section reported[1] for ^{117}Sn and ^{119}Sn near 1 MeV are not observed in measurements of the (γ, n) cross section in the energy range 500—2000 MeV. Measurements of photoneutron angular distributions and of their energy dependence suggest that the reaction is dominated by E1 excitation of a mixture of $p_{\frac{1}{2}}$ and $p_{\frac{3}{2}}$ states.

---

[1] E. J. Winhold et al., Phys. Letters 32B, 607 (1970).

3. Valence Component in $^{91}Zr(\gamma, n)^{90}Zr$ (R. E. Toohey and H. E. Jackson)

Ground-state radiation widths ($\Gamma_{\gamma 0}$) for thirty-six $p_{3/2}$ photoneutron resonances in ^{91}Zr have been measured from 5 to 225 keV above threshold at the Argonne National Laboratory threshold photoneutron facility. Reduced neutron widths (γ_n^2) for the same

resonances were obtained at the Oak Ridge Electron Linear Accelerator (ORELA) facility from total-cross-section measurements on ^{90}Zr. A strong correlation ($\rho = +0.59$) is evident from the analysis shown in Fig. C-2. Because of a lack of knowledge of the relative phase of the compound-nucleus and valence amplitudes in the individual resonances, the average valence component cannot be deduced from the correlation analysis. However, one can obtain a mean compound-nucleus contribution by studying those resonances where the valence amplitude is expected to be negligible. By using such a procedure, an average valence component is obtained which is in excellent agreement with the average valence strength calculated from the valence model. The s-wave neutron strength function is found to be $S^0 = 3.9 \pm 0.8 \times 10^{-5}$ and the p-wave strength function is $S^1 = 3.2 \pm 0.8 \times 10^{-4}$. The p-wave value agrees with the predictions of the nuclear optical model, while the value of S^0 is about one order of magnitude smaller than predicted, as is usually the case in this mass region. The reduced photon width for E1 transition is $\bar{k}(E1) = 3.2 \pm 0.6 \times 10^{-3}$, in agreement with the single-particle reduced width derived from the Weisskopf model. Both neutron and photonwidths are observed to follow a Porter-Thomas distribution.

4. Neutron Energy Spectrum in Photofission of ^{239}Pu near Threshold (Warren F. Stubbins†)

The energy spectra of neutrons from photofission of ^{239}Pu with bremsstrahlung end points at 5.5 and 6.0 MeV were measured by time-of-flight at the Argonne National Laboratory electron linear accelerator. 69.05 grams of ^{239}Pu in an aluminum matrix with an aluminum cladding was placed 12.5 cm from a 0.102 cm thick gold converter backed with 5.0 cm of aluminum. Neutrons were detected at 90° approximately 10 meters from the target by a plastic scintillator viewed by two photomultipliers. Two centimeters of bismuth and two inches of lead were in the flight path. The detector efficiency was measured by the $^2H(\gamma, n)^1H$ reaction in a heavy water sample with a bremsstrahlung end point of 9.1 MeV. The neutron energy spectrum fits the Maxwell distribution

$$N(E)\, dE = K\, E^{\frac{1}{2}} \exp(-E/T)\, dE$$

with T = 1.361 MeV which corresponds to the neutron energy spectrum in thermal fission of ^{239}Pu. K is a constant. No evidence of the limited energy in excess of threshold, except small neutron yield, was found in the neutron energy spectra.

† University of Cincinnati

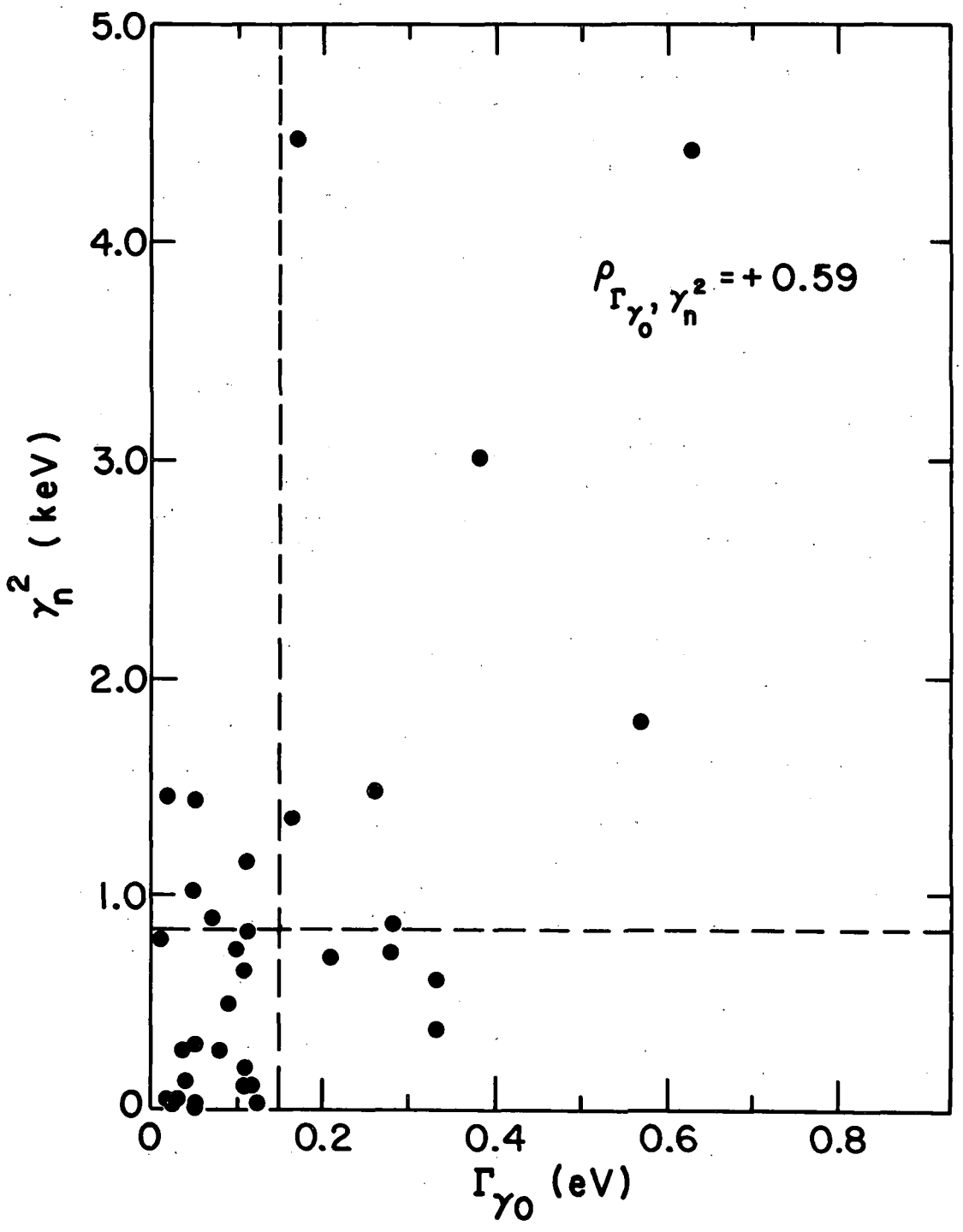

Fig. C-2. Scatter diagram of the ground-state radiation widths and reduced neutron widths for $p_{3/2}$ resonances. The dashed lines give average values.

D. REACTOR NEUTRON PHYSICS

1. Radiative Capture of Thermal Neutrons in ^{3}He (L. M. Bollinger, J. R. Specht, and G. E. Thomas)

Flowers and Mandl[1] have shown from rather general considerations that the ^{3}He(n, γ) ^{4}He cross section for electric dipole and quadrupole radiation approaches zero as the neutron energy approaches zero. Thus, the (n, γ) reaction for thermal neutrons is expected to be dominated by magnetic dipole radiation, which is also very weak and involves matrix elements that are masked in other reactions. Previous efforts to measure the (n, γ) cross section for thermal neutrons have not been successful because of its small size and because σ(n, p) is very large. We have solved the experimental problem by mounting a ^{3}He sample in the high-flux region of the CP-5 reactor and detecting the 20.6-MeV thermal-neutron-capture γ ray with a spectrometer consisting of a large array of NaI(Tl) scintillators. The preliminary result of the measurement is $\sigma(n, \gamma) = 60 \pm 30\,\mu b$, where the error results mainly from uncertainties in the efficiency of the detection system.

---

[1] Flowers and Mandl, Proc. Roy. Soc. (London) A206, 131 (1951).

2. Reconsideration of the Electron-Neutron Scattering Length as Measured by the Scattering of Thermal Neutrons by Noble Gases (V. E. Krohn and G. R. Ringo)

Our value for the electron-neutron scattering length has been corrected on the basis of new measurements of some neutron scattering lengths and now is $-1.30 \pm 0.03 \times 10^{-16}$ cm, which is 3% lower than our original result. (The equivalent figure in the Fermi convention is -3630 ± 70 eV and at $q = 0$, $dG_{En}/dq^2 = 0.0189 \pm 0.0004$ fm^2.) A check on the worrisome possibility of an H_2 impurity in the scattering gases showed that this is quite unlikely to be a significant source of error. The difference between our results and the Munich measurement and also the Foldy calculation thus continues unexplained.

BROOKHAVEN NATIONAL LABORATORY

A. NEUTRON PHYSICS

1. Fast Chopper

a) Direct Capture Studies in Dy-162(n,γ)Dy-163

(G. W. Cole, S. F. Mughabghab* and R. E. Chrien)

The study of radiative neutron capture near the 4-S resonance of the neutron strength function is an important tool in the investigation of departures from the extreme statistical description of neutron resonances. The Dy-162(n,γ) reaction has been studied with particular care at BNL.[1] Table 1 shows the values obtained for σ_D^0, the direct capture cross section at 1 eV. Resonances at 5.43, 70.7 and 267 eV were included in the multilevel fits from which these values were deduced. The observed intensities[2] with which the final states are populated in (d,p) stripping work are shown for comparison. It is of interest to note that the four states exhibiting direct capture also show a positive correlation between the partial radiative widths and the reduced neutron widths of the three resonances considered. The correlation coefficient is 0.56. While the existence of direct capture is expected to imply a positive correlation between the neutron and photon channels,[3] the small statistical sample size limits our ability to draw further conclusions.

The remaining ambiguity in this work is a recent claim by the Columbia University group[4] that both the 5.43 eV and 70.7 eV resonances are in fact doublets. Table 2 shows the resonance parameters used in this work,[5] together with estimates of the doublet

---

* Department of Applied Science, BNL.

1 See the BNL report to the USNDC, October 1972, for more details.

2 O.W.B. Schult et al, Phys. Rev. 154, 1146 (1967).

3 A. M. Lane, Annals of Physics 63, 171 (1971).

4 H. I. Liou, private communication. The values in Table 3 are preliminary results, for which we are grateful to Dr. Liou.

5 S. F. Mughabghab and R. E. Chrien, Phys. Rec. C-1 1850 (1970).

parameters. One of the two members of the proposed 5 eV doublet may belong to another Dy isotope.

A reanalysis of the multilevel fitting shows that the 70 eV doublet, closely spaced as it is, will not materially affect our results. At 5 eV, our resolution should be adequate to observe a sharp resonance-resonance interference pattern arising from the proposed doublet. Such a pattern would be masked in our present data by multiple scattering effects in the thick target used. A thin Dy-162 target ($\sim$0.02 gm-cm^{-2} $(Dy\text{-}162)_2O_3$) will be used in the near future to re-examine the 5 eV region. This data will allow us to verify the accuracy of the previous analysis, and should also allow us to determine whether or not the two resonances near 5 eV do indeed both belong to Dy-162.

TABLE A-1

Direct Capture Results for Dy-162

Transition Energy (keV)	σ_D^o (mb)	I(d,p) (Ref. 2)
5213	50	{38 (unresolved)}
5219	0.7	
5449	1.4	20
5848	40	64
5880	22	12
5919	13.6	142

TABLE A-2

Resonance Parameters for Dy-162

Ref. 5		Ref. 4	
E_{res} (eV)	Γ_n^o (meV)	E_{res} (eV)	Γ_n^o (meV)
5.43	9.1	5.45	9.0
		5.80	2.4
70.7	47.1	70.55	13.1
		72.10	21.2

b) Transition Strengths in Ba-135(n,γ)Ba-136
(J. L. Holm, R. E. Chrien and G. W. Cole)

The apparent existence of anomalously strong M-1 decay of resonant capturing states in the Ba-135(n,γ) reaction has been of interest for some time.[6] In an attempt to resolve or explain this anomaly we have studied resonances up to several hundred eV, using an enriched target containing ~50 grams of Ba-135. The intensities of primary transitions on-resonance and off-resonance have been measured. The normalization was obtained by running a composite sample consisting of the Ba-135 target and a thin boron target of the same area. Comparison with the well-known B-10(n,$\alpha\gamma$) cross section gives a value for the intensity of the 818 keV transition in Ba-136, which is combined with the work of Gelletly et al.[7] at thermal to provide the intensities of primary transitions. Table A-3 lists partial radiative widths obtained in this manner.

In particular, the 9108 keV transition in the 24.5 eV resonance has been considered anomalously large. The partial width obtained in the present work, however, could occur with a 4% probability in a Porter-Thomas distribution of partial widths in the Ba-135(n,γ) reaction; thus it seems reasonable that one such width be observed in our experiment. The other partial widths in Table A-3 are not unusually large; the M-1 photon strength function $k(M\text{-}1) = \bar{\Gamma}_{\gamma i}/E_\gamma^3 D$ derived from 16 observed partial widths is $(22\pm7)\times10^{-9}$ MeV^{-3}, which is consistent with a value of 14×10^{-9} MeV^{-3} to be expected on the basis of observations in many nuclei.[8]

The off-resonance behavior of the 9108 keV transition has also been studied, for two purposes: 1) To ascertain the parity of the resonance. If the 24.5 eV resonance is a p-wave resonance, then the transition would be E-1 rather than M-1 (however, the neutron width would then be anomalously large). 2) To search for an M-1 background amplitude. This would be of interest with respect to the possible existence of an M-1 giant resonance in Ba-135.

---

[6] F. Becvar et al., Czech. J. Phys. B19, 899 (1969).

[7] W. Gelletly, J. A. M. Moragnes, M. A. J. Mariscotti and W. R. Kane, Phys. Rev. 181, 1682 (1969).

[8] L. Bollinger, International Conf. on Photonuclear Reactions and Applications, Asilomar, 1973.

TABLE A-3

^{135}Ba Partial Radiation Widths, meV

Resonances eV	γ-transitions, keV 9106	8288	6574	6063	5677	5601
24.4	8.37± .85	1.88± .19	--	--	.46± .08	1.22± .13
80.9	.16± .03	.65± .08	1.05± .13	2.05± .22	--	.55± .07
86.1	.14± .04	.18± .04	.22± .04	.41± .09	--	.48± .07
104.4	.21± .05	3.15± .32	--	.47± .10	.16± .06	.20± .07
224.1	.93± .15	.81± .15	1.33± .15	.31± .10	--	.47± .12
280.2	.34± .10	.55± .13	1.07± .25	.48± .16	.60± .11	--
315.0	.41± .13	2.00± .31	2.29± .24	.20± .10	.39± .11	.84± .21
376.4	.77± .20	1.36± .33	.57± .16	--	.36± .12	1.33± .25
407.1	.45± .10	.48± .12	.50± .13	--	.50± .12	--
463.4	.63± .14	.66± .15	.27± .23	.47± .18	--	2.04± .27

Figure A-1 shows the results of a multilevel fit for the 9108 keV transition between thermal and the first resonance at 24.5 eV. The solid line is obtained from resonance amplitudes only, while the dashed line includes a "best-fit" background amplitude which is real and constant with neutron energy. In this fit the 24.5 eV resonance was treated as an ℓ=0 level. Since the fit is adequate for ℓ=0, there is no indication that the resonance is p-wave. This provides additional evidence that the 9108 keV transition is indeed M-1. The background amplitude required to produce the dashed curve is ~0.25 mb at 1 eV, which demonstrates that the neutron energy dependence of the transition is essentially accounted for by resonance amplitudes alone. From this, we conclude that there is no need to postulate an M-1 resonance in Ba-135 near 9 MeV. The multilevel fit included an artificially constructed bound level at -300 eV, which is necessary to give the correct magnitude for the total capture cross section; however, this level did not make any contribution to the amplitude for the 9108 keV transition in these fits. Similar fits will be carried out for the other transitions.

c) Validity of the Valence Model in Mo-98 (G. W. Cole, R. E. Chrien, R. C. Byrd,* J. A. Harvey,** and G. G. Slaughter)**

The success of the valence model of Lane and Lynn[9] in the first few p-wave resonances of Mo-98[10] leads naturally to an investigation of the higher energy resonances. In order to test the model over a wider range of energies, both partial radiative widths and neutron widths were measured at ORELA. The capture γ-ray measurements were made using an enriched Mo-98 target, with a flight path of 10m and a nominal resolution of 2.5 nsec-m^{-1}. The neutron widths were obtained from a total cross section measurement using a thick (0.0434 atoms/barn) Mo-98 target, with a flight path of 78.2 m and a nominal resolution of 0.06 nsec-m^{-1}.

---

* BNL Neutron Physics Summer Student

** Oak Ridge National Laboratory, Oak Ridge, Tennessee

[9] J.E.Lynn, "Theory of Neutron Resonance Reactions," Clarendon Press, Oxford (1968).

[10] S. F. Mughabghab, R. E. Chrien, O. A. Wasson, G. W. Cole and M. R. Bhat, Phys. Rev. Lett. 26, 1118 (1971).

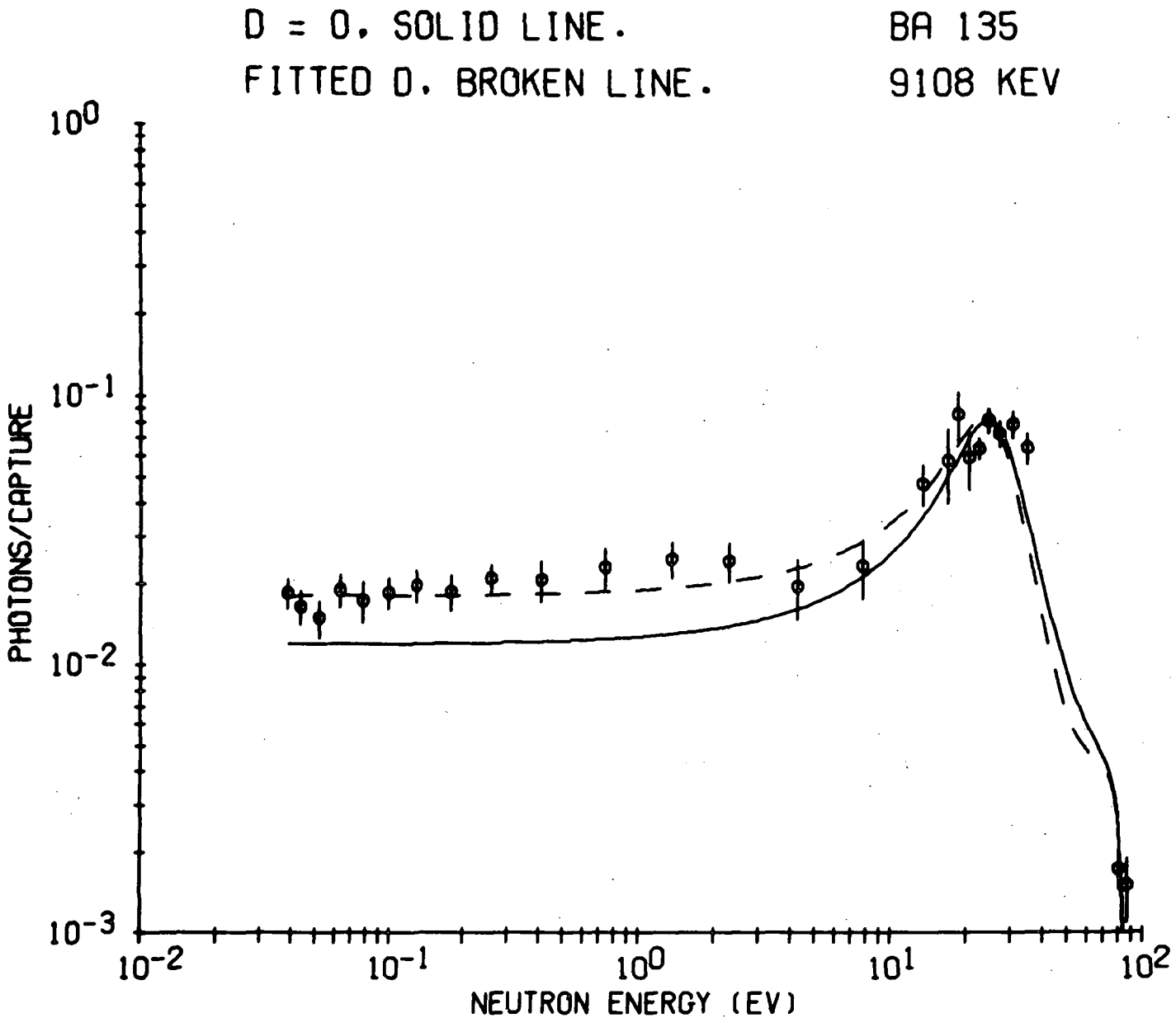
D = 0. SOLID LINE.
FITTED D. BROKEN LINE.
BA 135
9108 KEV
PHOTONS/CAPTURE
NEUTRON ENERGY (EV)
10^0
10^{-1}
10^{-2}
10^{-3}
10^{-2}
10^{-1}
10^0
10^1
10^2

Fig. A-1

The Atta-Harvey area analysis code was modified to accommodate the large data arrays (50,000 time-of-flight channels) used in the total cross section measurement. Neutron widths were obtained for resonances up to 100 keV, although the study of the valence model was extended only to 6 keV, owing to the limited resolution and statistical accuracy of the capture γ-ray measurements. Figure A-2 shows the reduced widths of the p-wave resonances which were included in the present analysis. The quantity plotted is $g\Gamma_n^1$, the p-wave reduced neutron width. Below 1 keV, the results are those of Weigmann,[11] since those widths were the ones actually used in the valence model analysis. The parities of the resonances were deduced by observing s-wave interference minima in the total cross section, and also by inspection of primary transitions appearing in the capture spectra. The ℓ=1 resonances have spin 1/2 or 3/2, and in many cases the resonance spin can also be established by the occurrence of primary transitions to $5/2^+$ final states.

The present analysis includes 18 p-wave resonances. Ten are assigned spin 3/2, two are known to be spin 1/2, and six more are tentatively assigned as p 1/2. Since the reduced neutron widths above 1 keV are significantly smaller than those below 1 keV, valence effects are expected to be less important compared to compound nuclear processes. Indeed, no further cases are found which produce agreement as striking as that obtained below 1 keV. However, the average behavior of the model over the 18 resonances and six final states may also be examined. Figure A-3 shows the average predicted radiative widths for six final states, computed from the 18 measured p-wave widths, compared with the average measured radiative widths. For each of the six final states, the bar on the left is the valence prediction, while the bar on the right is the measured value. Since the sample includes ten p 3/2 resonances and eight p 1/2 resonances, it is unlikely that more than a few of the p 1/2 assignments could be incorrect. Thus, although individual cases might be debated on the basis of spin assignments, the values averaged over all resonances will be little affected by such uncertainties.

For each of the final states, the valence model predicts, on the average, too little strength. This is to be expected because of the presence of compound nuclear contributions to the capture process. The mean correlation coefficient between the reduced neutron widths of the 18 resonances and the radiative widths of the four transitions allowed for both resonance spin states is 0.60, which is significant at the 99% level for this sample size. Similarly,

---

[11] H. Weigmann, G. Rohr and J. Winter, Third Conf. on Neutron Cross Sections and Technology, Knoxville, Tennessee (1971).

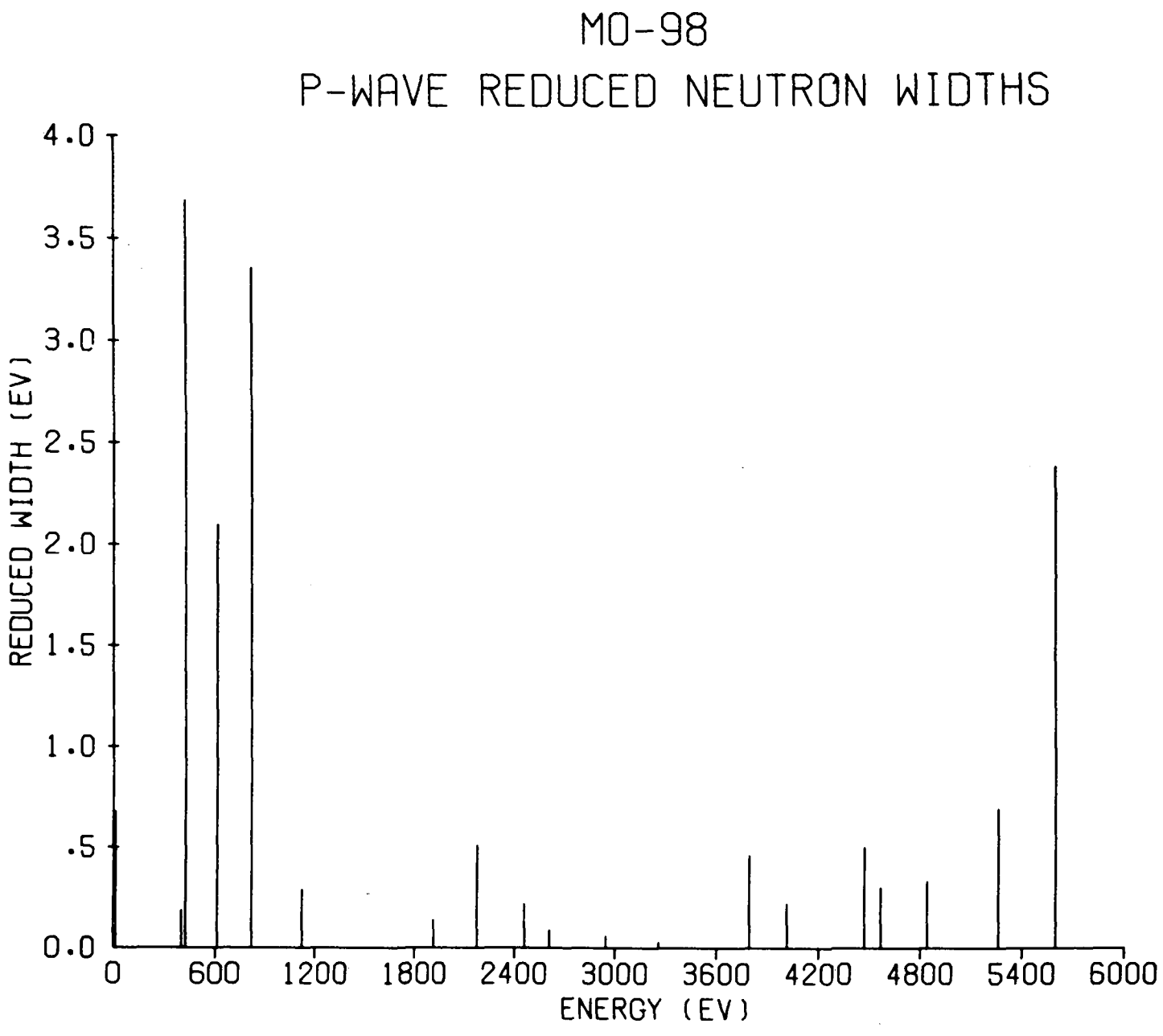
MO-98
P-WAVE REDUCED NEUTRON WIDTHS
REDUCED WIDTH (EV)
4.0
3.5
3.0
2.5
2.0
1.5
1.0
.5
0.0
0
600
1200
1800
2400
3000
3600
4200
4800
5400
6000
ENERGY (EV)

Fig. A-2

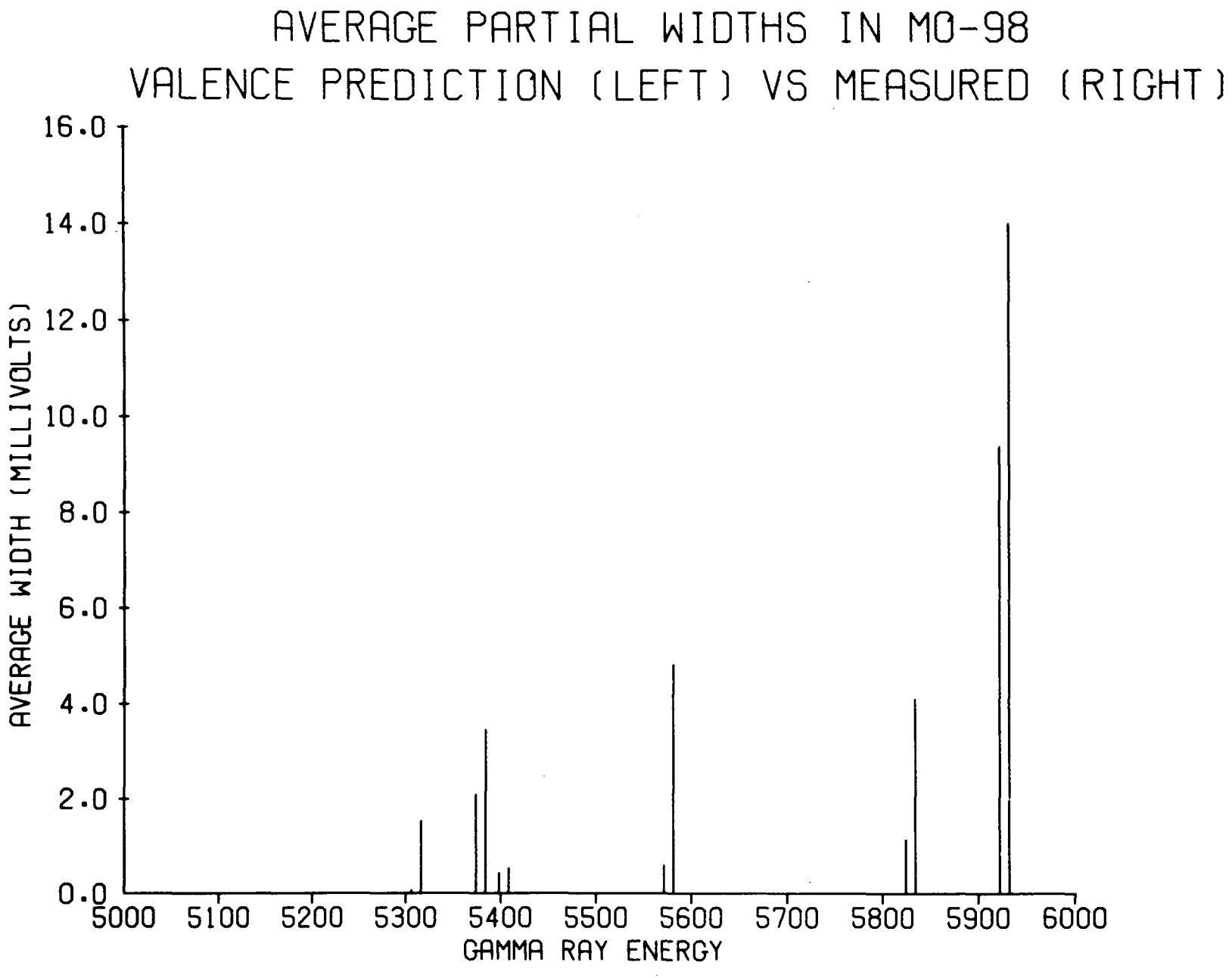
AVERAGE PARTIAL WIDTHS IN MO-98
VALENCE PREDICTION (LEFT) VS MEASURED (RIGHT)
AVERAGE WIDTH (MILLIVOLTS)
16.0
14.0
12.0
10.0
8.0
6.0
4.0
2.0
0.0
5000
5100
5200
5300
5400
5500
5600
5700
5800
5900
6000
GAMMA RAY ENERGY

Fig. A-3

the correlation between the average radiative widths for the four transitions, normalized by $E\gamma^3$, and the final state spectroscopic factors is 0.85, which is significant at the 92% level.

Finally, we may compute the proportion of the capture strength which is contributed by valence processes. The partial radiative width amplitude may be written as a sum of two terms, one of which is the compound nuclear width amplitude and one of which is proportional to the reduced neutron width amplitude. When an average of the partial radiative width over many final states is taken, the usual assumption can be made that the cross-product between the two terms vanishes because of the random choice of signs for the amplitudes. The observed average partial radiative width for the 18 resonances and six final states is 4.75 meV. The valence term contributes 2.29 meV, based on the measured neutron widths. Therefore, 2.46 meV may be ascribed to the compound nucleus contribution. In other words, for these six final states, roughly half of the capture strength is attributable to channel capture.

In the near future, the total cross section measurements will be refined by making additional transmission measurements at ORELA using thinner targets and taking advantage of improved signal-to-background conditions available at ORELA since the original data were obtained.

d) Partial Width Correlation in Tb-159(n,γ)Tb-160
(G. W. Cole and R. E. Chrien)

In a recent study of Tb-159(n,γ), Jain et al.[12] have reported an apparent positive correlation between reduced neutron widths and decay strengths to low-lying final states. Rather than measuring individual transition intensities, Jain uses a NaI detector, and measures a ratio R between the total γ-ray intensity at a high bias (say 5 MeV) and the total intensity at a low bias (say 1.5 MeV). R should be essentially the quantity $\sum_i \Gamma_{\gamma i}/\Gamma_\gamma$, where the sum is over final states which can be reached by γ-rays of energy greater than the high bias level. The correlation coefficient $\rho(R,\Gamma_n^o)$ is found to be 0.96±.04 for the 1^+ levels up to 500 eV in Tb-159, while no such correlation appears for the 2^+ resonances.

As a check on these results, we have performed capture γ-ray measurements using a Ge(Li) detector, and a 150 gm sample of Tb_4O_7. Line analysis is being carried out in the usual fashion.

---

[12] A. P. Jain, B. Cauvin and A. Lottin, private communication.

If the reported correlation is verified, it will be of interest to examine the nature of the final states which exhibit such a correlation, in order to elicit further information concerning the reaction mechanism involved.

e) Resonance Neutron Capture in Ru (K. Rimawi,* R. E. Chrien, G. W. Cole and O. A. Wasson)

Capture γ-ray measurements have been performed using a 150 gm sample of natural Ru at the 48 m flight path of the Fast Chopper facility. The present analysis is concerned with capture in Ru-99 (12.72% abundance, $I^{\pi} = 5/2^{+}$) and Ru-101 (17.07% abundance, $I^{\pi} = 5/2^{+}$). Previous studies of the level structure of Ru-100 and Ru-102 were made using β-decay samples; many new levels have been identified in each isotope above the energy cut-off of the β-decay studies.

Figure A-4 shows the reduced widths $\Gamma_{\gamma i}/E_{\gamma}^{3}$ of primary transitions in Ru-99(n,γ), averaged over resonances and over final states in 500 keV intervals. Near the ground state, all available levels are of positive parity and the transitions are M-1 in nature. The high reduced widths correspond to the onset of E-1 transitions to negative parity states above 2 MeV excitation. However, the peak which is evident near 2 MeV excitation energy is of unknown multipolarity. The error bars represent statistical errors, while the vertical lines give the uncertainty due to averaging of a distribution which is subject to Porter-Thomas fluctuations.

Figure A-5 is a similar plot for Ru-101(n,γ). Again the peak at $\sim$2 MeV excitation is evident; in this case the peak is largely due to an enhanced M-1 transition to the 2262 keV final state.

The M-1 photon strength function $\overline{k}_{M1} = \overline{\Gamma}_{\gamma i}/DE_{\gamma}^{3}$ is computed to be 28×10^{-9} MeV^{-3} for the Ru-99(n,γ) case, based on nine final states known to have positive parity. For the case of Ru-101(n,γ), $\overline{k}_{M1} = 67\times10^{-9}$ MeV^{-3}, based on 12 final states. One transition gives a value of 630×10^{-9} MeV^{-3}. In the mass region A$\approx$100, we expect $\overline{k}_{M1} \approx 4\times10^{-9}$ MeV^{-3}.[8] In addition, for Ru-99(n,γ) the ratio $\langle\Gamma_{\gamma i}(M1)\rangle/\langle\Gamma_{\gamma i}(E1)\rangle \approx 0.5$, whereas a value of 1/7 is expected.[8] Although the value 0.5 is subject to error due to the finite size of the sample, which is subject to Porter-Thomas fluctuations, this error is less than a factor of 2. Thus the ratio $\langle\Gamma_{\gamma i}(M1)\rangle/\langle\Gamma_{\gamma i}(E1)\rangle$ is also inconsistent with expectations in this mass region. This apparent M-1 enhancement may be due to a giant resonance effect associated with the $g_{7/2} \rightarrow g_{9/2}$ transition.

---

* State University of New York, Albany, N. Y.

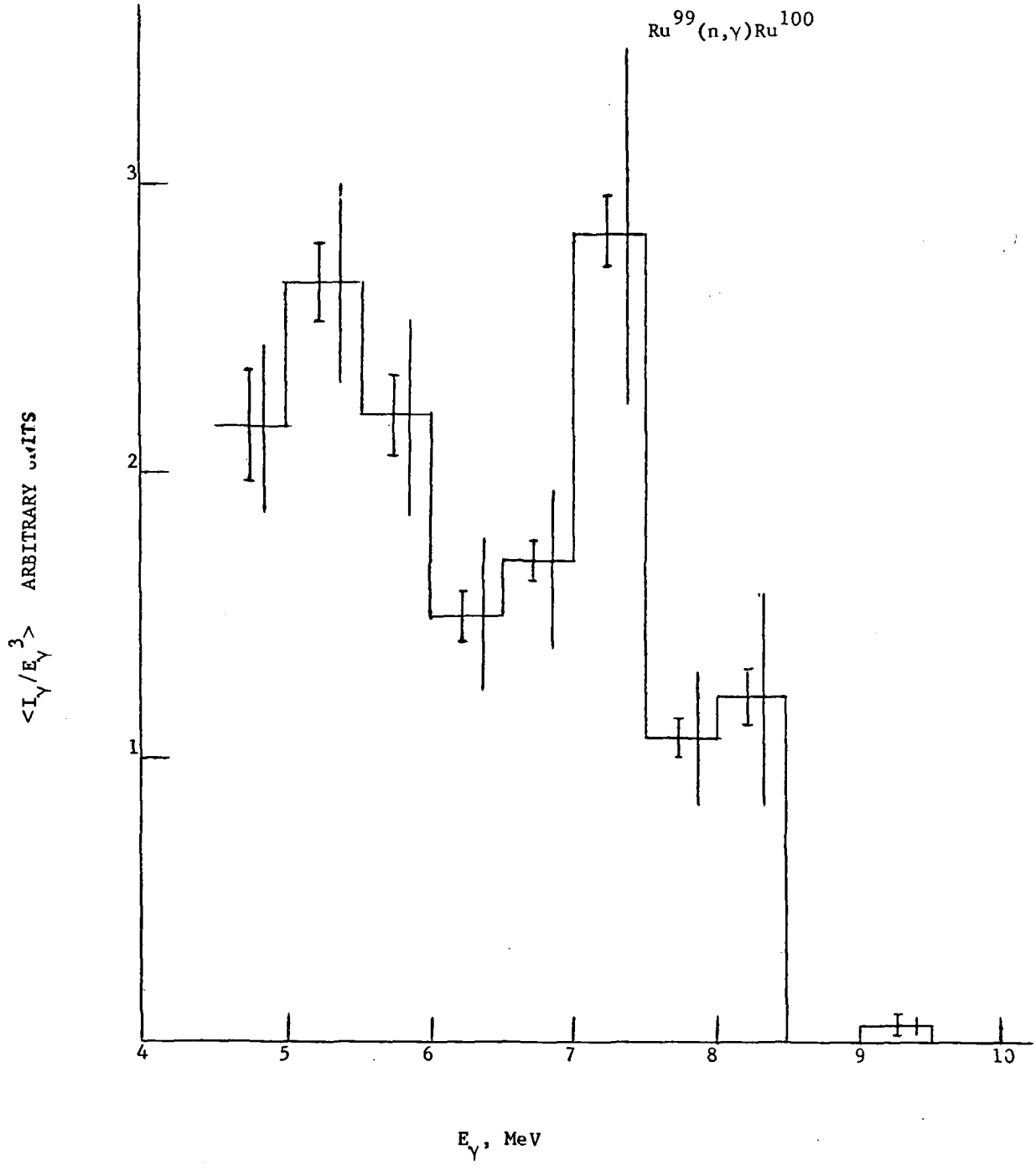
$Ru^{99}(n,\gamma)Ru^{100}$
$\langle I_\gamma/E_\gamma^3 \rangle$ ARBITRARY UNITS
3
2
1
4
5
6
7
8
9
10
E_γ, MeV

Fig. A-4

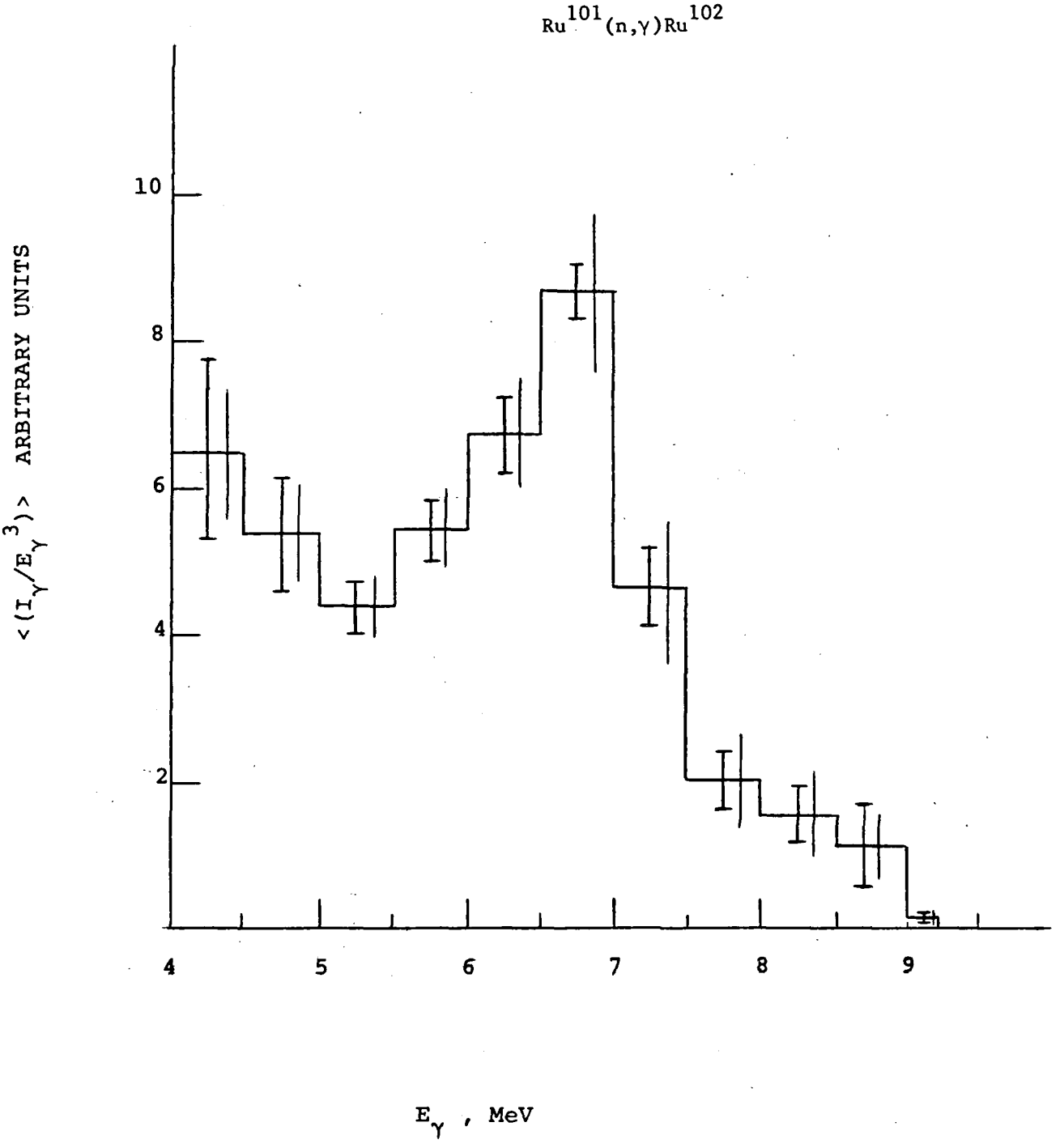
$Ru^{101}(n,\gamma)Ru^{102}$
$<(I_\gamma/E_\gamma^3)>$ ARBITRARY UNITS
10
8
6
4
2
4
5
6
7
8
9
E_γ , MeV

Fig. A-5

2. The 24.3 keV Neutron Beam Facility at the HFBR

(O. A. Wasson, R. E. Chrien and R. C. Greenwood*)

The 24 keV neutron flux has been increased by a factor of three by removing a portion of the narrow angle collimator in the H1B beam port. We now have a 24 keV beam intensity of 1×10^6 n/cm^{2}sec for a filter consisting of 9 inches Fe, 14 inches Al, and 2 inches S. The fluxes listed in the previous report for various filters have been increased by this factor.

A program to measure 24 keV capture γ-ray spectra with a Ge(Li) detector is in progress. Spectra have been recorded for samples of Pt, Pb, Au, Ta, Ni, Zr, Gd, and Fe using the above-mentioned filter which transmits a beam with an energy width of 2 keV (FWHM). As examples of the types of spectra obtained for nuclei with different level densities at the neutron binding energy, we present spectra for Pt, Ni, and Pb.

Figure A-6 shows the spectrum from 24 keV capture in a natural platinum sample. This spectrum results from neutron capture in several hundred resonances and shows that the average γ-ray intensities of the primary γ-rays exhibit little fluctuation, in contrast to the spectrum from capture in individual resonances. Such average measurements are useful for investigations of the γ-ray strength function.

The results from capture in a nickel sample of natural isotopic abundance are shown in Fig.A-7. In the nickel isotopes the capture is dominated by only a few resonances. The top spectrum results from 24 keV neutron capture while the bottom spectrum contains a 0.5% thermal neutron component. The γ rays from thermal capture which are indicated by vertical lines, serve as energy calibrations to determine the energy of the captured neutrons in the 24 keV beam at the top. The double-escape peaks of the four highest energy γ-rays in ^{58}Ni(n,γ)^{59}Ni are indicated.

The four highest energy γ rays from the ^{60}Ni(n,γ)^{61}Ni reaction are shown in an expanded scale in Fig.A-8. Here each γ-ray has several peaks which result from thermal neutron capture as well as capture in an s-wave resonance at 12.5 keV and a p-wave resonance at 23.9 keV. The positions of the known resonances are indicated by vertical lines above the horizontal axis. Again the down pointing vertical line indicates the position of the peak from thermal neutron capture which also determines the energy of the captured neutrons from the 24 keV beam.

---

*Aerojet Nuclear Corporation, Idaho Falls, Idaho

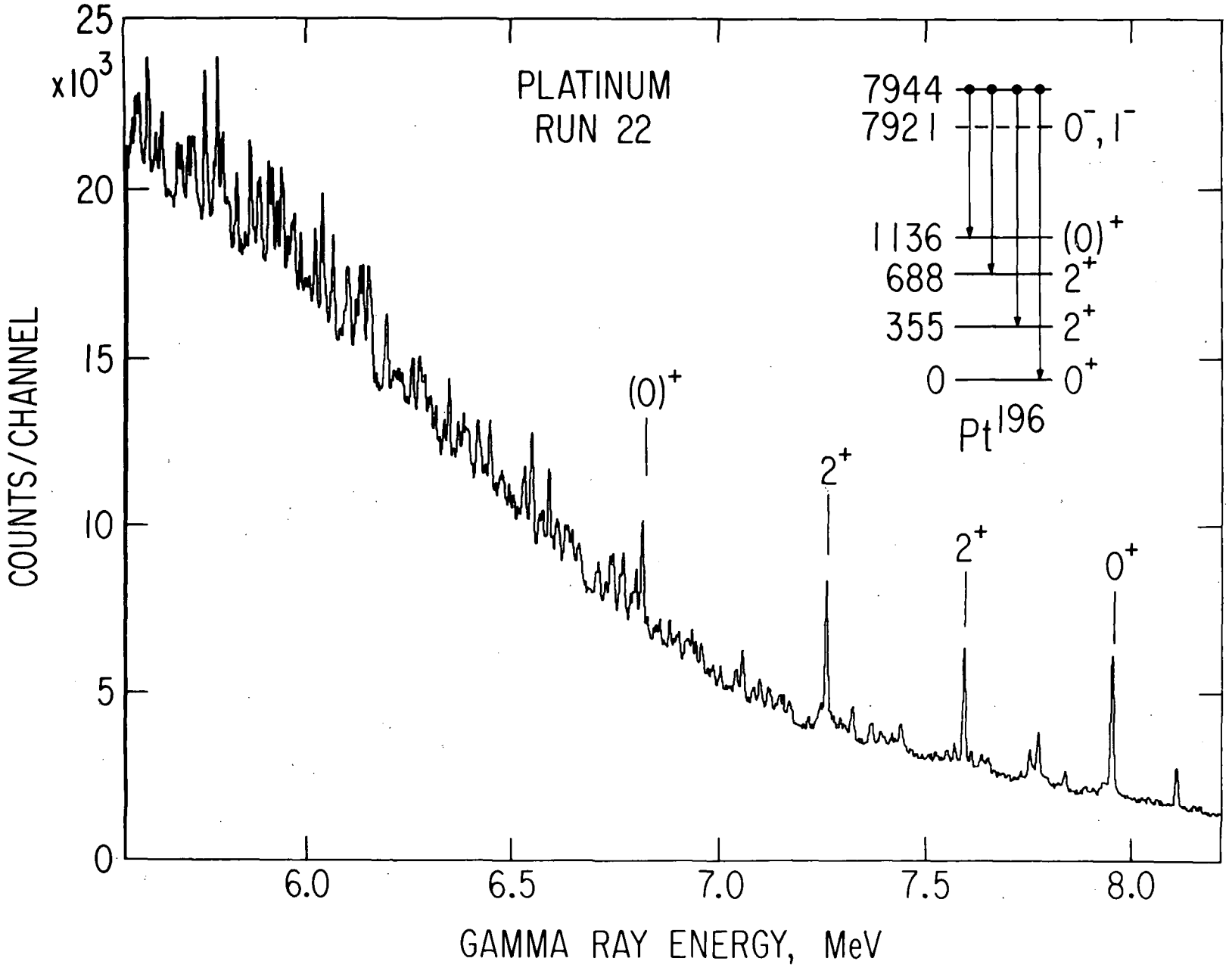
PLATINUM
RUN 22
7944
7921
0⁻, 1⁻
1136
(0)⁺
688
2⁺
355
2⁺
0
0⁺
Pt196
(0)⁺
2⁺
2⁺
0⁺
COUNTS/CHANNEL
x10³
25
20
15
10
5
0
6.0
6.5
7.0
7.5
8.0
GAMMA RAY ENERGY, MeV

Fig. A-6

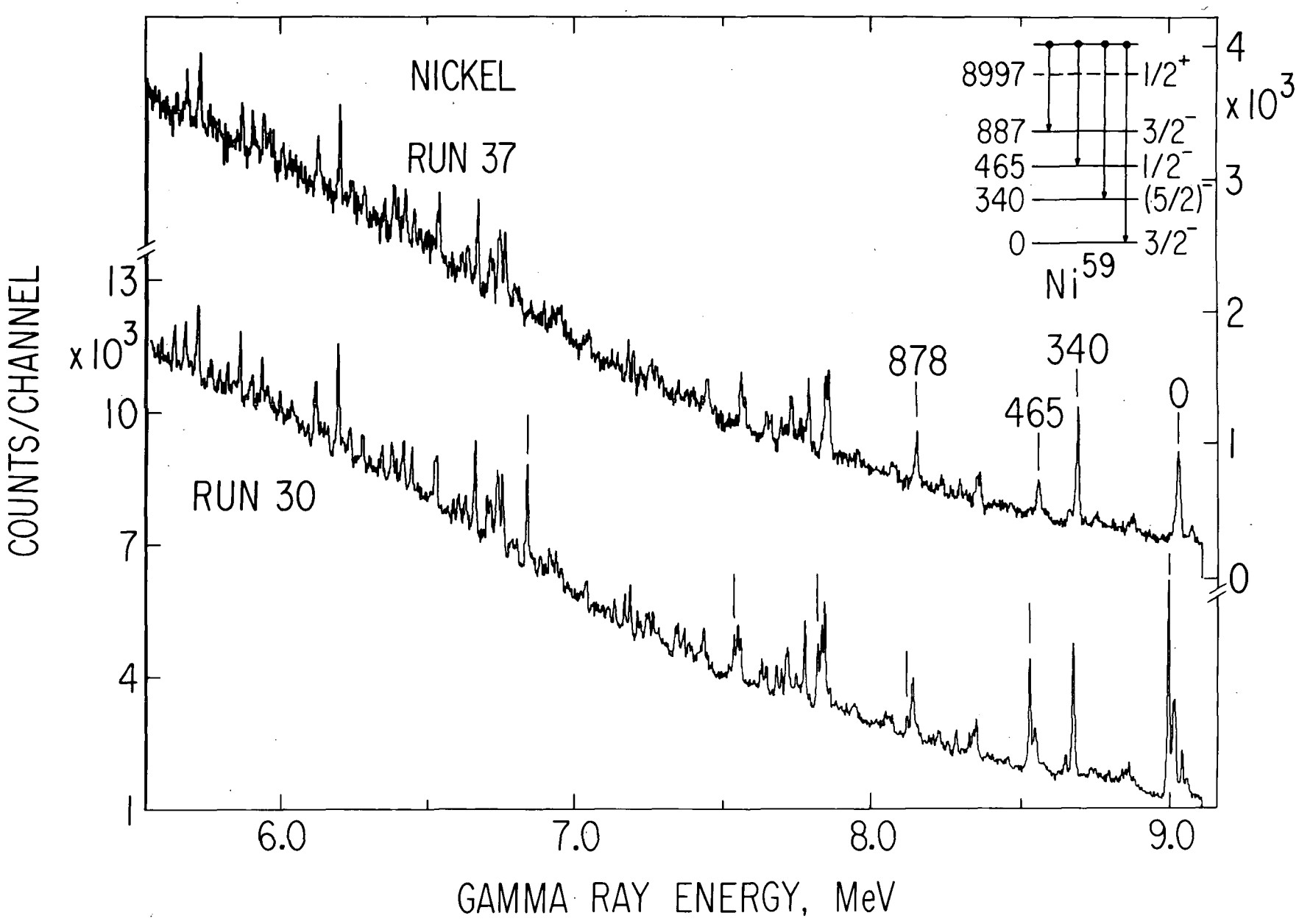
NICKEL
RUN 37
RUN 30
8997
887
465
340
0
1/2+
3/2−
1/2−
(5/2)−
3/2−
Ni59
878
340
465
0
COUNTS/CHANNEL
x10^3
13
10
7
4
1
4
3
2
1
0
6.0
7.0
8.0
9.0
GAMMA RAY ENERGY, MeV

Fig. A-7

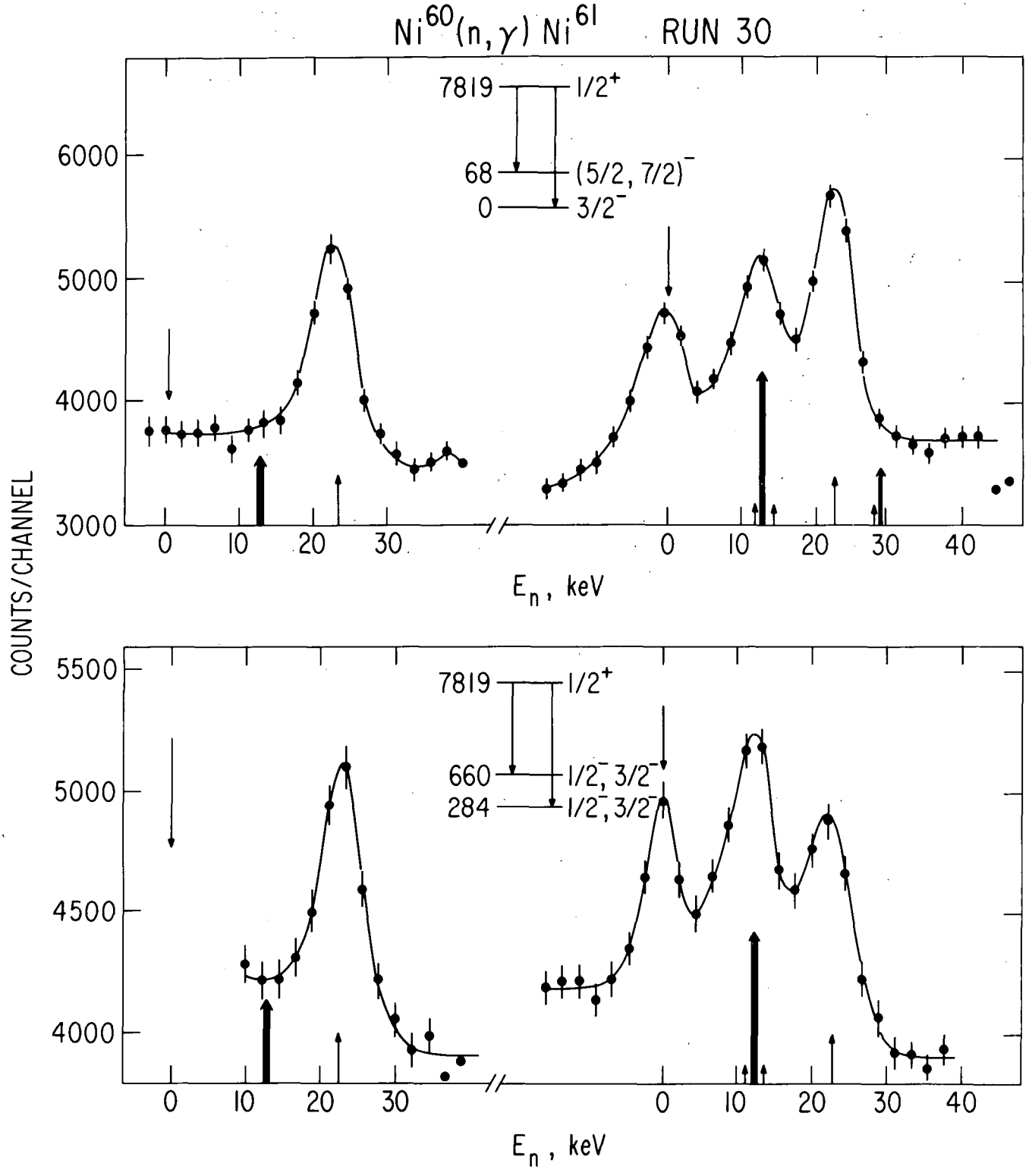
Ni60(n,γ) Ni61 RUN 30
7819
1/2+
68
(5/2, 7/2)−
0
3/2−
6000
5000
4000
3000
0
10
20
30
0
10
20
30
40
En, keV
COUNTS/CHANNEL
7819
1/2+
660
1/2−, 3/2−
284
1/2−, 3/2−
5500
5000
4500
4000
0
10
20
30
0
10
20
30
40
En, keV

Fig. A-8

The observation of only one peak in the γ-ray populating the 68 keV excited state indicates that the spin of the 23.9 keV neutron resonance is 3/2 and that the final state spin is 5/2. Also the constant γ-ray intensity ratio between thermal and the 12.5 keV resonance for the four γ-rays indicates the thermal neutron capture is dominated by the tail at the 12.5 keV resonance.

The final example is capture in ^{207}Pb which occurs in the off-resonant region where the capture cross section is small. A detailed view of the ^{207}Pb(n,γ)^{208}Pb ground state γ-ray obtained with a thermal neutron contaminant in the 24 keV neutron beam is shown in Fig. A-9. The widths and separation of the two peaks indicates that the higher energy peak results from 24 keV neutron capture and that multiple neutron scattering effects are small. Relative to a gold standard cross section of 660 mb at 24 keV we deduce a value of 1.1±0.3 mb for the capture cross section in Pb^{207}. This result along with other previous measurements at thermal and 2 keV are shown in Fig.A-10. The smooth curve results from including the contribution of a non-resonant as well as the tail of the 41 keV resonance to the capture cross section in this energy region. A non-resonant cross section of 0.3±0.1mb evaluated at 41 keV is deduced from this analysis. This result is slightly larger than the upper limit of 0.1 mb deduced by Allen and Macklin[1] from the shape of the 41 keV resonance. This result is much less than the values determined from the various analyses of the shape of the 41 keV resonance observed in the inverse ^{208}Pb(γ,n)^{207}Pb reactions.[2,3]

The 24 keV partial capture cross sections for the γ-rays from a natural lead sample are listed in Table 1.

---

[1] B. J. Allen and R. L. Macklin, Proceedings of Knoxville Conference p. 764 (1971).

[2] C. D. Bowman, R. J. Baglan, and B. L. Berman, Phys. Rev. Letters 23, 796 (1969).

[3] C. M. Shakin and M. S. Weiss, Phys. Rev. C2, 1809 (1970).

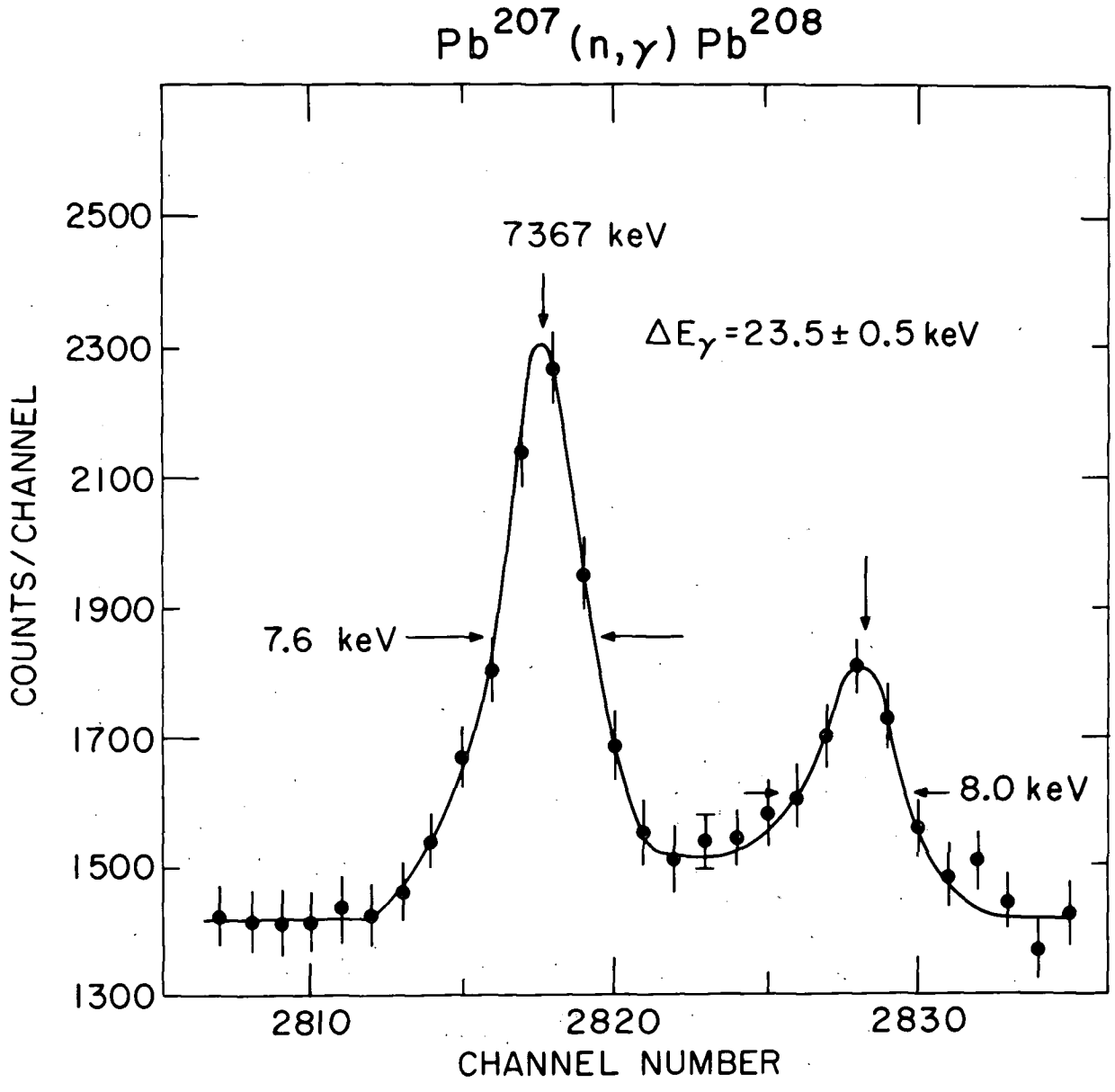
Pb207 (n,γ) Pb208
7367 keV
ΔEγ = 23.5 ± 0.5 keV
7.6 keV
8.0 keV
COUNTS/CHANNEL
2500
2300
2100
1900
1700
1500
1300
2810
2820
2830
CHANNEL NUMBER

Fig. A-9

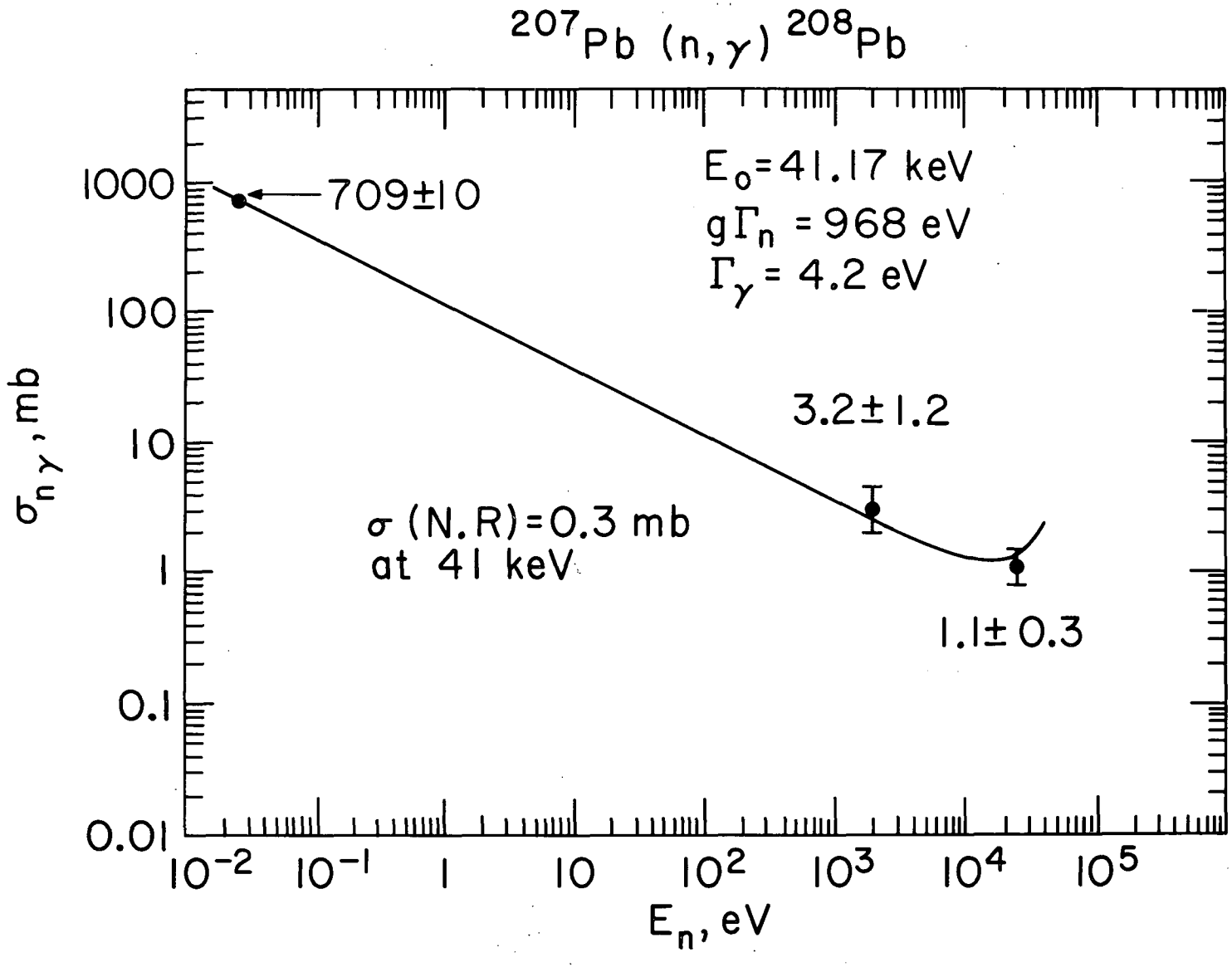
$^{207}Pb\ (n,\gamma)\ ^{208}Pb$
E_o=41.17 keV
$g\Gamma_n$ = 968 eV
Γ_γ = 4.2 eV
709±10
3.2±1.2
1.1± 0.3
σ (N.R)=0.3 mb
at 41 keV
$\sigma_{n\gamma}$, mb
1000
100
10
1
0.1
0.01
10^{-2}
10^{-1}
1
10
10^2
10^3
10^4
10^5
E_n, eV

Fig. A-10

TABLE 4

Partial Capture Cross Sections in Pb Averaged over the Incident 24 keV Neutron Spectrum

E_γ, keV	$\sigma_{n\gamma j}$, mb	Emitting Nucleus
7392	1.1±0.3	208
4228	<0.26	208
2614	<0.26	208
6763	10.3±1.1	207
6190	4.2±0.3	207
5862	<0.4	207
4138	3.0±0.3	207

3. Boron Density Profiles by $B^{10}(n,\alpha)$
(G. W. Cole and J. F. Ziegler*)

The $B^{10}(n,\alpha)$ reaction has proved to be a useful tool for investigating boron density distributions in various substrates.[1] A continuing series of such measurements is being carried out using the B-beam of the H-1 beam port at HFBR. The internal collimation at this beam port has recently been redesigned to increase the available flux for the 25 keV average capture measurements (see section 2). Our most recent boron profiling measurements, which use an unfiltered thermal beam, indicate an increase of ~ 20% in the thermal flux due to this redesign. This increase is smaller than that achieved for the epithermal flux due to the effects of total internal reflection for slow neutrons in the previous collimator.

One series of boron profiling measurements was designed to compare the range of boron ions implanted into amorphous silicon with the range of boron ions implanted into crystalline silicon in a random (i.e. non-channeling) direction.[2] Targets were prepared in three ways:

1) implantation of 50 keV B^{10} ions into crystalline Si in a non-channeling direction;

2) implantation of 50 keV B^{10} ions into crystalline Si in a non-channeling direction, followed by making the surface amorphous by the implantation of 280 keV Si^{28} ions ("post-damage");

3) implantation of 50 keV B^{10} ions into amorphous Si prepared by bombardment of crystalline Si with Si^{28} ions ("pre-damage").

In each case, the B^{10} dose formed a layer of $1 \times 10^{15} cm^{-2}$ atoms, extending to a depth of ~0.4μm. The amorphous layer produced by Si bombardment extended to a depth of ~0.6μm.

The B^{10} profiles in the crystalline sample and the post-damaged sample are identical, which indicates the absence of any radiation damage induced diffusion of the B^{10}. The pre-damaged sample,

---

* Thomas J. Watson Research Center, IBM, Yorktown Heights, N. Y.

1 J. F. Ziegler, G. W. Cole and J. E. E. Baglin, J. Appl. Phys. 43, 3809 (1972).

2 B. L. Crowder, J. F. Ziegler and G. W. Cole, contributed to the Intl. Conf. on Ion Implantation in Semiconductors, Yorktown Heights, N. Y. (1972).

however, exhibits a distribution of B^{10} which is ~25% narrower than the other two cases; this is probably due to the scattering of ions into channels in the crystalline sample, which allows deeper penetration. These effects must be taken into account in theoretical efforts to describe the range of ions in Si.

The effects of annealing on the same series of targets were also studied. For 600°C annealing cycles, the diffusion of the B^{10} is the same for all targets. However, at 900°C, the diffusion of the B^{10} is greatly enhanced in the amorphous samples. The explanation of this effect is unclear at present.

Studies of the diffusion of boron in the presence of arsenic doping are also continuing. Figure A-11 shows the distribution of ion-implanted B^{10} in Si following rather extreme annealing. The initial B^{10} distribution in both samples following implantation would be approximately Gaussian. The distribution plotted with crosses has shown the extreme diffusion broadening which would be expected (no other impurities present). The distribution plotted with squares was obtained by implanting the B^{10} into a Si crystal uniformly doped with As; the diffusion of the B^{10} during annealing is obviously severely retarded.

The mechanism by which the As inhibits the diffusion of boron has not yet been determined. Further experiments to probe this question used Si crystals which had B^{10} and As implanted together. Before annealing, each impurity has an approximately Gaussian distribution (with different depths and widths). In Figure A-12 the B^{10} distribution in such a sample before annealing is plotted with crosses. The B^{10} distribution after annealing (plotted with squares) clearly exhibits different diffusion of the boron in the As doped region of the crystal. The location of the tall, narrow region of this distribution shows that the As has both attracted and "trapped" the boron. The study of the boron-arsenic interaction under varied conditions should elucidate the nature of the process.

"Isoconcentration" studies of the boron diffusion constant are also continuing. In this experiment, we wish to measure the diffusion speed of a boron ion in the midst of a uniform sea of boron ions. A target is prepared by successive ion implantations of B^{11} to produce a uniform distribution of boron having a dip in the concentration at some depth. This dip is then filled in by implanting B^{10}, so that the overall distribution of boron ions is constant with depth. Since the (n,α) reaction indicates the position of only the B^{10}, we can observe the diffusion broadening of the B^{10} implant peak in the presence of the uniform boron ion distribution. Preliminary results indicate an anomalous boron diffusion for this case; investigation is continuing.

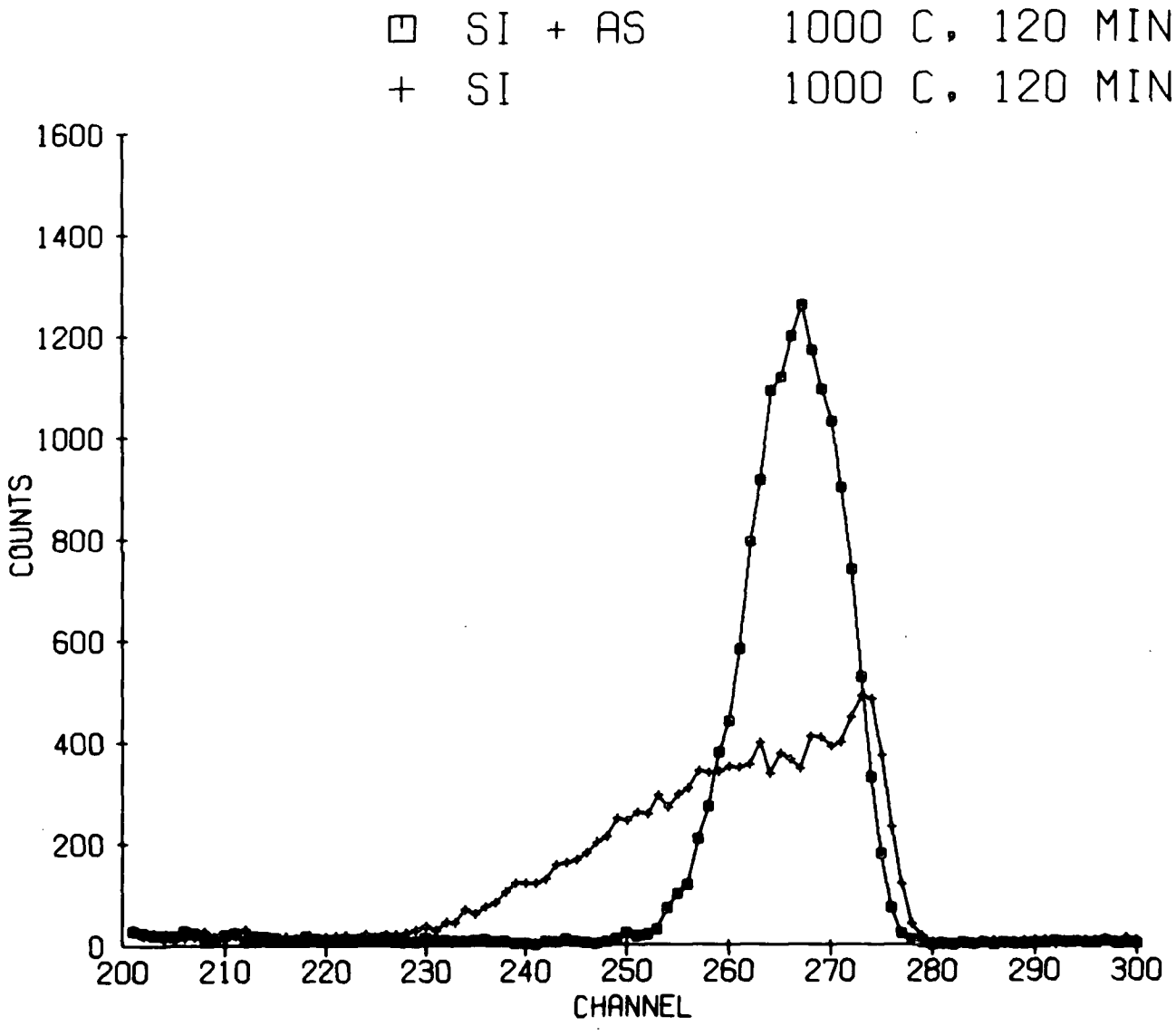
SI + AS 1000 C, 120 MIN
+ SI 1000 C, 120 MIN
COUNTS
1600
1400
1200
1000
800
600
400
200
0
200
210
220
230
240
250
260
270
280
290
300
CHANNEL

Fig. A-11

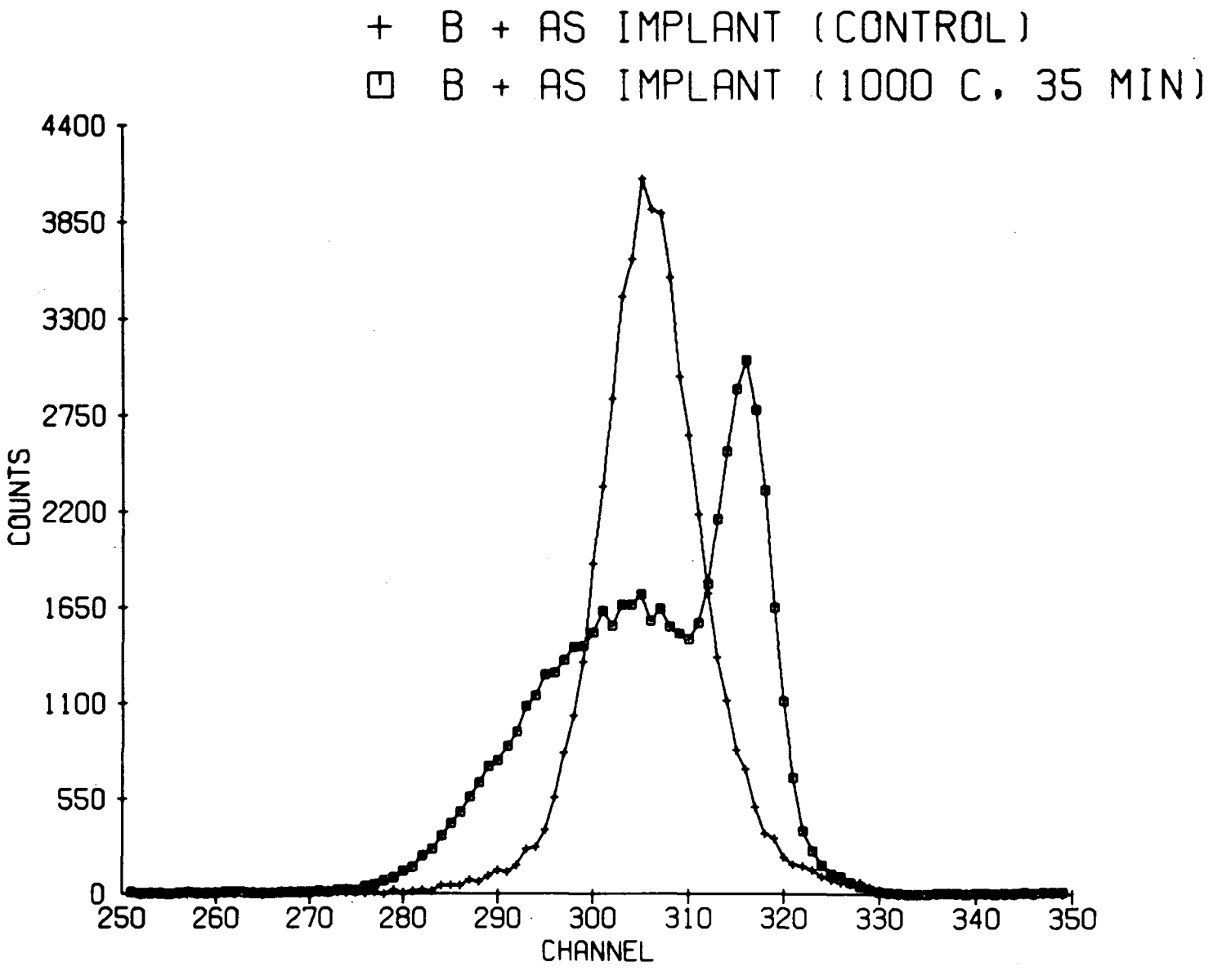
+ B + AS IMPLANT (CONTROL)
B + AS IMPLANT (1000 C, 35 MIN)
COUNTS
4400
3850
3300
2750
2200
1650
1100
550
0
250
260
270
280
290
300
310
320
330
340
350
CHANNEL

Fig. A-12

B. NUCLEAR STRUCTURE

1. K=0 Rotational Bands in ^{174}Yb (R. F. Casten, D. Breitig, W. R. Kane and S. F. Mughabghab

The γ decay of K=0 rotational bands in deformed nuclei has been a subject of much recent interest due to anomalies observed in the de-excitation branching ratios. Thus far, these anomalies have not been resolved. We studied the (n,γ) reaction leading to K=0 states in ^{174}Yb in the hope that the combination of the γ decay information and earlier anomalous two neutron transfer cross sections to the 0^+ states would shed light on the anomalies. The principal findings deduced from the level scheme obtained were that

a. The de-excitation branching ratios of the K=0 rotational bands in ^{174}Yb also deviate from the rotational model predictions.

b. The pattern of deviations differs for each K=0 band in ^{174}Yb.

c. For the lowest K=0 band the pattern of deviations in ^{174}Yb is very similar to the patterns in other rare earth deformed nuclei.

d. The patterns of de-excitations in ^{172}Yb and ^{174}Yb show a striking similarity for corresponding bands.

From these results and detailed calculations of the two- and three-band mixing, the following principal conclusions were reached.

a. The unique pairing character of the 0^+ states in ^{174}Yb does not cause additional significant perturbations that affect the branching ratios, beyond those that occur in the other nuclei.

b. In particular, whatever mechanism causes the anomalous γ decay in ^{174}Yb must be similarly important in ^{172}Yb. Specifically, mixing of the K=0 bands with the γband is unlikely to be important in either nucleus, in contrast to earlier speculations.

c. Neither two-band mixing of each K=0 band with the ground state band, nor three-band mixing including the γ-band, nor the introduction of M1 components in the $I \rightarrow I$ transitions can provide a full explanation of the data.

d. Combining the γ-decay data with the implications of the earlier charged particle reaction results suggests the likelihood that mutual mixing among the excited K=0 bands themselves is an important factor in the probably complex explanation of the de-excitation branching ratios.

2. Study of Levels in ^{200}Hg (D. Breitig, R. F. Casten, G. Cole and W. R. Kane)

The levels of ^{200}Hg up to 3 MeV have been studied by a number of techniques. At Risø, Denmark, high resolution bent crystal γ-ray spectra were measured. At BNL, thermal and resonance neutron capture experiments were performed. In the thermal capture measurements, in addition to singles γ-ray spectra, Ge(Li) - Ge(Li) coincidence data were obtained and γ-γ angular correlations were measured. The latter two were particularly useful for identifying ground state transitions (by elimination) and 0^+ states, respectively. Observation of de-excitation γ-rays, as well as primary capture γ-rays in the resonance experiments helped elucidate the level scheme by comparing the variations in intensities of these radiations from resonance to resonance.

A detailed level scheme up ~ 3 MeV, comprising over 300 transitions, including a large number of newly placed ones and several new levels, has been constructed. Two important results have been the discovery of a 0^+ level at 1515 keV that appears to play an important role in the comparison of the low lying levels with the predictions of a core coupling model, and the probable existence of several 1^- states at ~ 2.5 MeV. This energy is considerably lower than expected for either proton or neutron particle-hole excitations across the N=126, Z=82 shell gaps. A possible interpretation of these states might involve the simultaneous breaking of both a neutron and a proton pair.

The detailed γ-ray de-excitation of the low-lying levels has been compared with calculations of Corvello and Sartoris which involve the coupling of two proton holes to core excitations. While reasonable candidates for each of the model states can indeed be found, they are not always unique and, in fact, many more states are observed below 2 MeV than can be accounted for by the model.

The nucleus ^{200}Hg has been predicted (Wong, 1972) to have a reduced central density (bubble) in its ground state configuration. If true, this would be of considerable importance and the search for similar effects in other nuclei would be stimulated. We are planning to make detailed comparisons of the present γ-de-excitation intensities with calculations of such a model as soon as the latter are completed.

The level scheme (excluding the 1^- levels) for ^{200}Hg deduced in these measurements is shown in the next three pages.

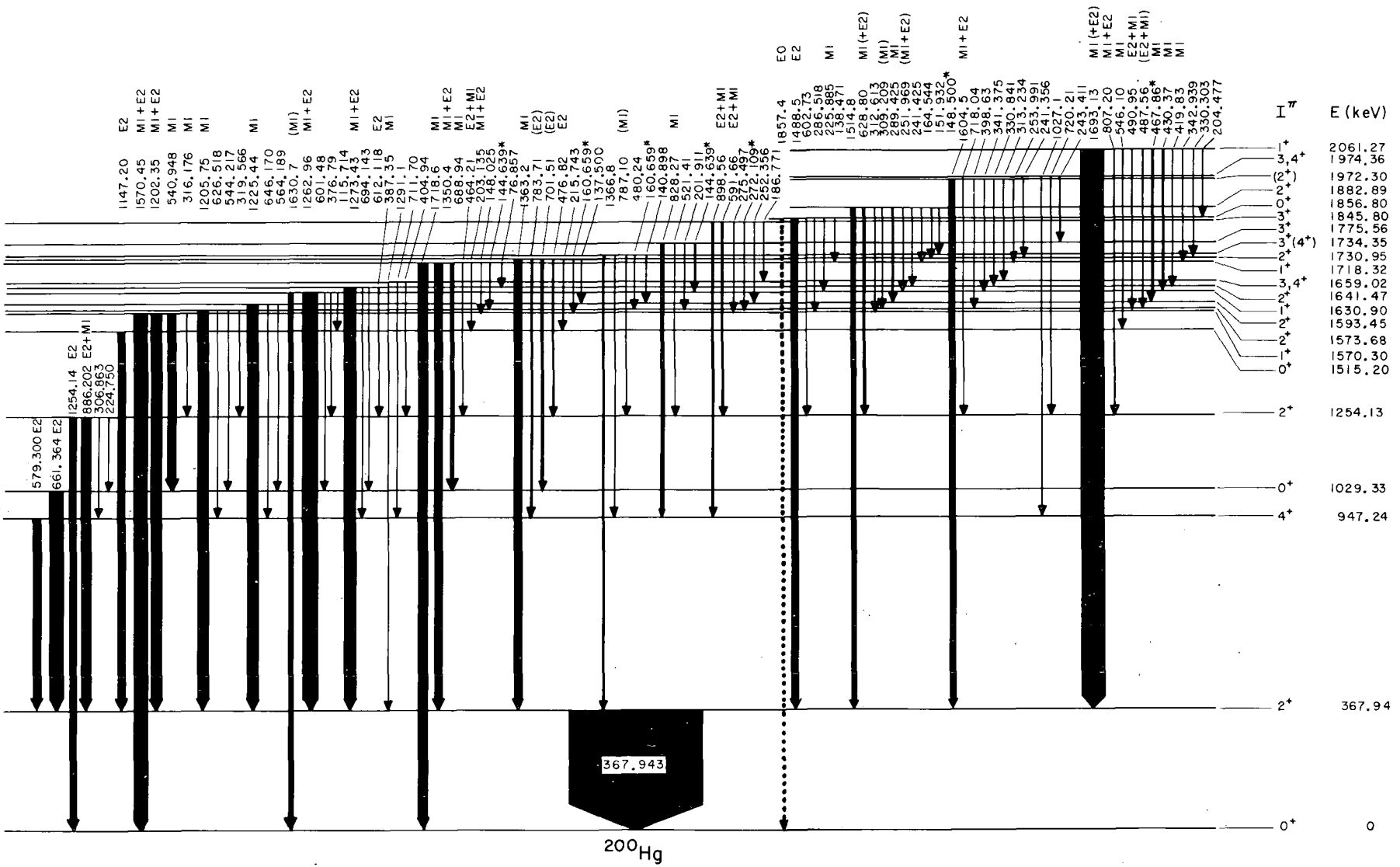
I^π
E (keV)
2061.27
1974.36
1972.30
1882.89
1856.80
1845.80
1775.56
1734.35
1730.95
1718.32
1659.02
1641.47
1630.90
1593.45
1573.68
1570.30
1515.20
1254.13
1029.33
947.24
367.94
0
367.943
200Hg

Fig. B-1

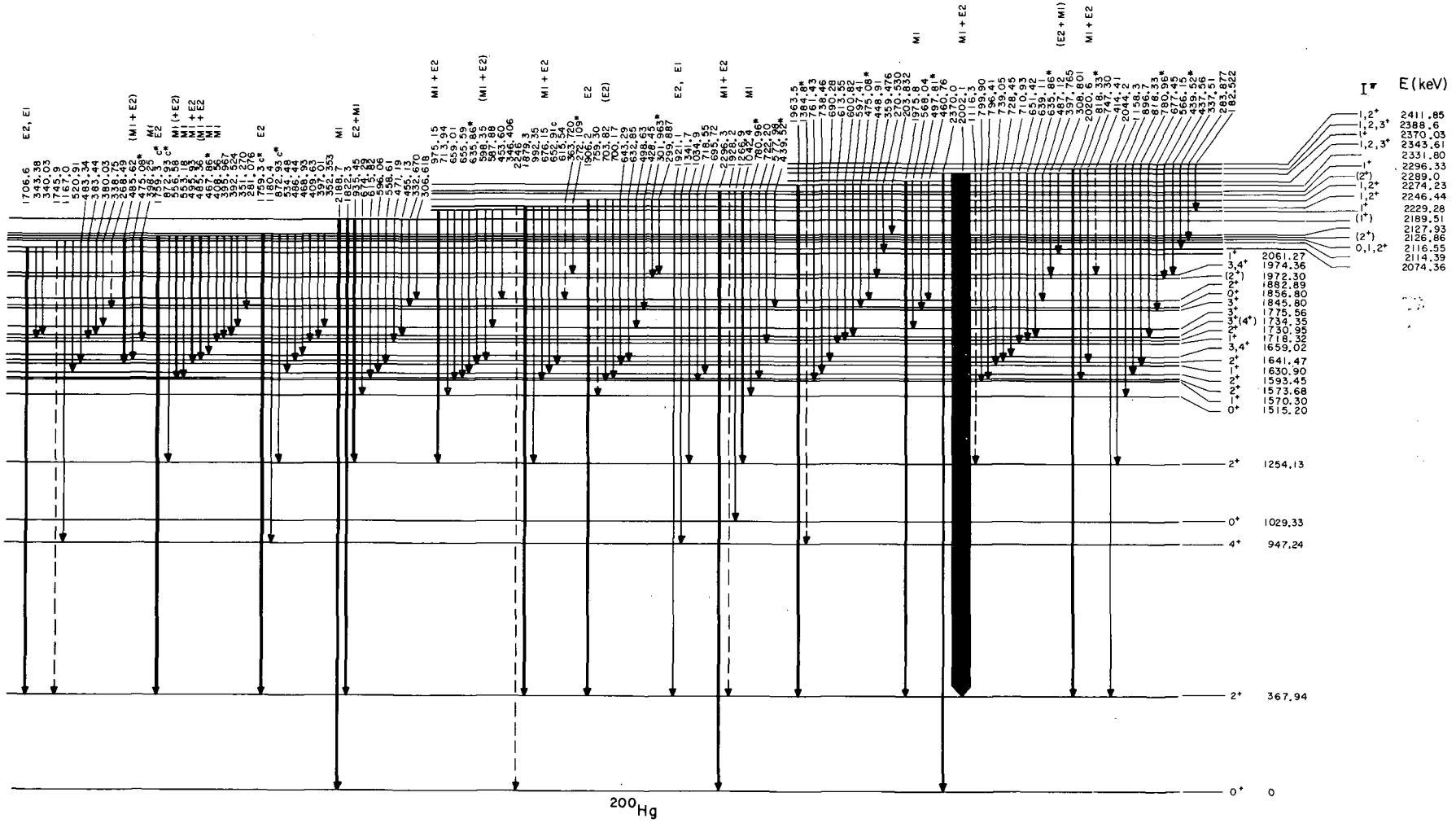
I^π
E(keV)
2411.85
2388.6
2370.03
2343.61
2331.80
2296.33
2289.0
2274.23
2246.44
2229.28
2189.51
2127.93
2126.86
2116.55
2114.39
2074.36
2061.27
1974.36
1972.30
1882.89
1856.80
1845.80
1775.56
1734.35
1730.95
1718.32
1659.02
1641.47
1630.90
1593.45
1573.68
1570.30
1515.20
1254.13
1029.33
947.24
367.94
0
200Hg

Fig. B-2

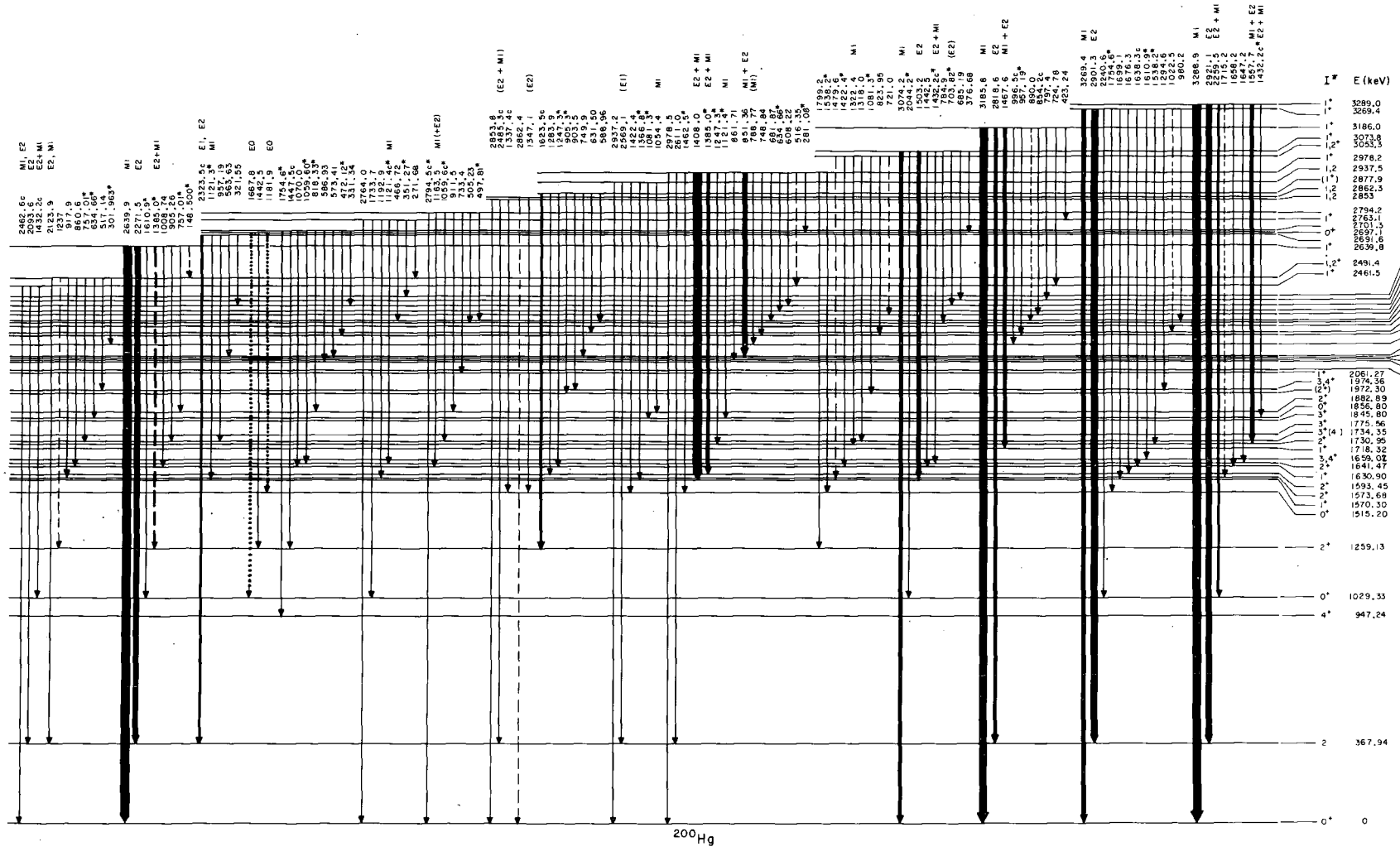
I^π
E (keV)
3289.0
3269.4
3186.0
3073.8
3053.3
2978.2
2937.5
2877.9
2862.3
2853
2794.2
2763.1
2701.5
2697.1
2691.6
2639.8
2491.4
2461.5
2411.85
2388.6
2370.03
2343.61
2331.80
2296.33
2289.0
2274.23
2246.44
2229.28
2189.51
2127.93
2126.86
2116.55
2114.39
2074.36
2061.27
1974.36
1972.30
1882.89
1856.80
1845.80
1775.56
1734.35
1730.95
1718.32
1659.0
1641.47
1630.90
1593.45
1573.68
1570.30
1515.20
1259.13
1029.33
947.24
367.94
0
200Hg

Fig. B-3

C. NATIONAL NEUTRON CROSS SECTION CENTER (S. Pearlstein, M. R. Bhat, H. R. Connell, D. I. Garber, M. D. Goldberg, P. Hlavac, R. E. Kinsey, T. J. Krieger, B. A. Magurno, V. M. May, S. F. Mughabghab, O. Ozer, A. Prince, J. R. Stehn, H. Takahashi)

The huge old SCISRS-I experimental data file has finally been translated into the current CSISRS format and is being incorporated into the CSISRS library. Although done in large part by computer, the translation was a massive task because of human and machine errors in the old file (data points omitted, or duplicated, units wrong, references not right) and these required correction by human hands. As compared with present-day CSISRS entries, these translated entries are generally sparse in auxiliary information (for example, in method, instrumentation, calculation of corrections); but the basic data are there and available. Several tapes of these data, all measured outside the U.S. and Canada, have been sent to the other three World Neutron Data Centers to be checked and entered in the World data file, EXFOR.

The international exchange of data by the Four Data Centers in Paris, Vienna, Obninsk, and Brookhaven is now in full swing. During the year ending March 12, 1973, we have received 238,000 records of data from 245 experimental works in the EXFOR transmission format(very nearly the same as CSISRS) from the three other centers, and we have transmitted to them 50,000 records of data from 150 experimental works. These statistics on the formal transfer of data do not include the informal transfers of data urgently needed but not in final EXFOR format; these informal transfers are quite frequently made for individuals who ask the centers for them. Proposals have been made to broaden EXFOR to include capture gamma spectra and more detailed information on fission processes.

Our evaluated data files have been enriched by the addition of the Swedish SPENG library of data on 28 materials, and by a Russian evaluation of the 92-U-235 fission cross section. These are kept as part of our ENDF/A Library, most of which is not in ENDF/B format.

A fourth version of ENDF/B was proposed at the December 1972 meeting of the Cross Section Evaluation Working Group (CSEWG). NNCSC evaluations of the cross sections of 47-Ag-107, 47-Ag-109, and 53-Cs have been documented in reports soon to be issued.

D. BROOKHAVEN LINAC ISOTOPE PRODUCER

Updating of Brookhaven Linac Isotope Producer publications:

The production of ^{157}Dy for medical use. E. Lebowitz and M. W. Greene. Int. J. Appl. Radiat. Isotopes 22, 789-793 (1971).

^{18}F recoil labeling. E. Lebowitz, P. Richards and J. Baranosky. Int. J. Appl. Radiat. Isotopes 23, 392-394 (1972).

The Brookhaven Linac Isotope Producer (BLIP). BNL 17740. P. Richards, E. Lebowitz, and L. G. Stang. Proc. of the IAEA Symposium on New Developments in Radiopharmaceuticals and Labeled Compounds, Copenhagen, Denmark, March 26-30, 1973.

A status report on the Brookhaven Linac Isotope Producer (BLIP). E. Lebowitz and P. Richards. Presented at the 19th Ann. Meet. of the Soc. of Nucl. Med., Boston, Mass., July 1972. Abstract published: J. Nucl. Med. 13, 449 (1972).

Development of ^{201}Tl for Medical Use. E. Belgrave and E. Lebowitz. Presented at the 19th Ann. Meet. of the Soc. of Nucl. Med. (Works in Progress Session), Boston, Mass., July 1972. Abstract published: J. Nucl. Med. 13, 781 (1972).

COLUMBIA UNIVERSITY

1. NEUTRON SPECTROSCOPY

A. Neutron Resonance Cross Section Measurements, (J. Rainwater, H.I. Liou, G. Hacken, W.W. Havens, Jr., W. Makofske, U.N. Singh, R. Warblen, and F. Rahn)

During the report period, our main emphasis has been on analyzing and publishing data, and the preparation for the impending startup of the newly modified Nevis cyclotron. A number of major papers and reports on our results have been published or submitted for publication. Papers on the neutron resonance spectroscopy and systematics of the separated Yb isotopes and the separated W isotopes have been submitted to the Physical Review. These papers round out our recent work on many of the rare earth isotopes, $150 \leq A \leq 190$, with a paper on the separated even Gd isotopes in preparation and the separated Dy isotopes expected to be ready soon. Our results on the rare earth isotopes, where many of the even-even isotopes provide good test cases for the Dyson-Mehta theory of long and short range correlations between adjacent level spacings, were the first experimental confirmation of this theory. The total cross section, resonance parameters and spin-parity values for Na below 300 keV has been submitted to Nuclear Science and Engineering for publication. An evaluation report on the total radiation widths of the important reactor material ^{238}U has concluded that there is no convincing evidence for quasi-periodic structure in $\Gamma\gamma$ versus energy (apart from a statistical level to level fluctuation of a high chi-squared number of degrees of freedom). The fluctuations in $\Gamma\gamma$ present in many data sets are most likely due to experimental uncertainties in the $\Gamma\gamma$ values themselves. Our best evaluated average radiation width was taken to be $\langle\Gamma\gamma\rangle = 23.55 \pm 0.16$ meV.

The modification of the Nevis synchrocyclotron absorbed a major fraction of our effort. The new work has included (a) installation and testing of the RF system, (b) set up of new collimators and shielding wall for our various new neutron flight paths, (c) re-making of the shielding for the 200 meter flight station, (d) the construction and testing of a new deuterium thyratron pulsing circuit operating at 50 kV, 300 Hz, $\sim$ 15 n sec rise time for rise in deflection of the internal proton beam for neutron production, and (e) the design of a new tungstun-water cooled neutron source and moderator.

B. Results of the Separated Isotopes of Cd (H.I. Liou, J. Rainwater)

The preliminary analysis of the data for natural Cd and the separated isotopes $Cd^{110,111,112,113,114,116}$ has been completed for approximately 530 Cd levels below 10 keV. Energies and isotopic identification of the levels appeared in the last progress report. The values of the s wave strength function obtained from the analysis are 10^4 S_0 = 0.50± 0.10 (Cd^{110}); 0.38±0.06 (Cd^{111}); 0.53±0.09 (Cd^{112}); 0.43±0.07 (Cd^{113}); 0.70 ±0.19 (Cd^{114}) and 0.20±0.06 (Cd^{116}). A separation of s and p wave level populations was made using various statistical tests such as Bayes' Theorum, P-T statistics, Dyson-Mehta Δ test, etc. We found the following values for the p wave strength function 10^4 S_1 = 2.7±0.6 (Cd^{110}); 3.1± 0.8 (Cd^{111}); 2.4±0.5 (Cd^{112}) and 3.1±0.8 (Cd^{114}) to be consistent with our data. The average spacings for s levels were 174±18 eV (Cd^{110}); 24.0±1.5 eV (Cd^{111}); 137±8 eV (Cd^{112}); 22.1±3.8 eV (Cd^{113}); 183±29 Cd^{114}) and 264±38 eV (Cd^{116}). These values for the strength functions and average spacings are summarized in Table B1.

C. The Resonance Parameters for Dy^{163} (H.I. Liou)

The analysis for resonance parameters of the rare earth isotope Dy^{163} has been completed for 113 levels up to 996 eV. Values for E_0 and $g\Gamma_n$ obtained for these levels are presented in Table C1. In favorable cases values of the total radiation width Γ_γ was obtained. The average radiation width was found to be $\langle\Gamma_\gamma\rangle$ = 112 meV (39 levels). Most of the individual Γ_γ values were within 20% of $\langle\Gamma_\gamma\rangle$. The s wave strength function was 10^4 S_0 = (2.08±0.33) in the energy region 0 to 750 eV.

D. Cross Section and Resonance Parameters for Cu (F. Rahn, W. Makofske)

An analysis of our combined 1968 and 1970 data on natural Cu and the separated isotope Cu^{63} was completed during the report period using area analysis to obtain the energies, $ag\Gamma n$ and isotopic identification for the levels below 10 keV. These values are presented in Table D1 along with preliminary values of the spin values J and total neutron widths Γ_n. Final spin assignments will depend on a R-matrix analysis of the data which is presently under way.

E. Results for Cl (U.N. Singh, J. Rainwater)

The analysis of the total cross section of the natural element Cl has been extended to 450 keV, and carefully reviewed in anticipation of

publication in the Physical Review. Figure E1 shows our results of σ versus E up to 450 keV. The σ between levels and the behavior of σ at resonances has been shown separately in this figure. The resonance parameters obtained from an area analysis of the data are given in Table E1 for 35 levels up to 190 keV. In favorable cases we were able to obtain the isotopic identification and spin parity J^{π} of the levels.

F. Extension of our Results for Ta^{181} (G. Hacken, J. Garg, J. Rainwater)

Our previous analysis on Ta^{181} reported on during the last progress period has been expanded to include data obtained in 1970. An example of the data is shown in Figure F1 which shows our T versus E results from 400 to 600 eV. Figure F2 gives the cumulative number of levels N versus E for Ta^{181}. The average spacing was found to be $\langle D \rangle = 4.6$ eV. (up to 250 eV). Table F1 summarzies the level statistics, giving the correlation of nearest neighbor levels, $\rho(S_i, S_{i+1})$, the experimental and theoretical Dyson-Mehta Δ statistic and Δ for the uncorrelated levels picked from a Wigner distribution. Good agreement between the experimental and theoretical Dyson-Mehta Δ statistic exist up to $\sim$250 eV; above this energy the divergence between these quantities is probably due to missing (or spurious) levels in the experimental data set. Figure F3 shows the experimental and Wigner spacing distribution for nearest neighbor levels in Ta^{181} up to 250 eV. A "good" agreement exists to 250 eV and we believe that the 53 observed levels form a complete s population in this energy interval. Figure F4 gives the cumulative sum of $\Sigma g\Gamma_n^o$ versus E. The slope of this curve, insensitive to missing or spurious weak levels, gives the s wave strength function for Ta^{181}. Our best choices for this value are: 10^4 So = 1.67±0.17 (to 1 keV) and 1.92 ±0.14 (to 1.8 keV). The comparison of our experimental distribution of $g\Gamma_n^o$ values and the Porter Thomas distribution is given in Figure F5. To 250 eV, this figure shows that few if any levels have been missed, while to 1 keV a significant number of small levels have not been observed.

Table B1

Isotope	$\langle D \rangle_o$(eV)	$10^4 S_o$	$10^4 S_1$
^{110}Cd	174 ± 18	0.50 ± 0.10	2.7 ± 0.6
^{111}Cd	24.0 ± 1.5	0.38 ± 0.06	3.1 ± 0.8
^{112}Cd	137 ± 8	0.53 ± 0.09	2.4 ± 0.5
^{113}Cd	22.1 ± 3.8	0.43 ± 0.07	
^{114}Cd	183 ± 29	0.70 ± 0.19	3.1 ± 0.8
^{116}Cd	264 ± 38	0.20 ± 0.06	

Table C1

Dy^{163}

E(eV)	$g\Gamma_n$(meV)	Γ_γ(meV)
1.71±0.01	0.92±0.12	
16.23±0.03	10.3±0.6	100±15
19.65±0.03	0.45±0.04	
35.79±0.04	4.4±0.3	
50.27±0.06	1.8±0.2	
55.85±0.08	13±1	140±25
58.97±0.08	43±3	95±20
66.11±0.10	4.4±0.4	
72.00±0.08	1.6±0.5	
75.48±0.10	1.2±0.1	
78.99±0.13	8±1	
86.30±0.14	0.65±0.18	
94.08±0.08	10±1	
105.88±0.10	31±4	120±25
107.18±0.10	14±2	90±20
120.33±0.12	4.9±0.5	
126.58±0.13	8.9±1.5	
127.46±0.13	6.6±1.0	
135.31±0.14	2.8±0.3	
143.38±0.15	7.7±0.9	
144.97±0.15	23±3	85±20
155.02±0.17	43±4	85±20
163.81±0.19	6.2±0.7	
177.18±0.21	2.0±0.4	
185.09±0.22	2.6±0.5	
188.95±0.23	1.7±0.3	
202.90±0.25	8.9±1.5	
205.26±0.26	27±3	110±20
213.74±0.27	3.4±0.5	
224.15±0.30	100±12	140±25
233.54±0.32	3.6±0.5	
250.55±0.18	9.1±1.1	
261.13±0.19	53±6	110±20
268.01±0.19	67±8	125±25
274.17±0.20	15.3±1.8	
281.06±0.21	15.5±2.0	
288.85±0.22	64±9	105±20
296.00±0.29	2.9±0.7	
297.77±0.23	44±6	
306.91±0.46	0.9±0.5	
323.08±0.25	140±20	130±30
324.55±0.26	132±20	100±30
326.93±0.26	175±3.5	
329.73±0.26	8.6±1.8	
342.86±0.28	11.4±2.0	
348.32±0.29	120±18	100±25
368.64±0.31	86±10	120±25
374.96±0.32	1.9±0.7	
382.16±0.33	2.6±0.8	
387.01±0.33	12.2±1.8	
390.44±0.34	27±4	90±20
400.34±0.35	14±3	
403.15±0.35	1.7±0.8	
411.08±0.37	270±30	155±30
420.56±0.38	1.3±0.5	
429.38±0.39	23±3	70±20
454.84±0.43	47±6	150±30
459.21±0.43	15±3	
465.32±0.44	11±2	
479.10±0.46	36±5	150±30
483.55±0.47	40±5	120±25
504.59±0.25	59±7	80±20
516.34±0.26	15±3	
519.83±0.26	11±2	
533.18±0.27	100±15	130±30
542.22±0.28	120±20	135±30
564.29±0.29	31±4	85±25
569.02±0.30	61±8	150±30
580.79±0.31	44±6	130±30
594.52±0.32	49±7	
601.25±0.32	73±10	130±30
615.71±0.34	35±6	75±20
620.77±0.34	50±8	110±25
632.10±0.35	105±18	125±30
637.17±0.35	79±14	135±30
641.96±0.36	81±14	100±30

Table C1

Dy^{163}

E(eV)	$g\Gamma_n$(meV)	Γ_γ(meV)
646.26±0.36	62±10	150±40
652.20±0.47	2.5±1.2	
660.40±0.48	9.5±2.5	
686.95±0.39	12±3	
695.71±0.40	79±12	115±30
709.78±0.53	4±2	
712.49±0.42	38±6	95±30
721.32±0.43	44±6	75±25
732.05±0.44	9.6±2.5	
736.14±0.56	9.8±2.5	
741.69±0.44	11±3	
747.15±0.57	2.6±1.2	
756.05±0.46	26±6	85±30
764.30±0.60	8.8±4.0	
769.93±0.60	3.1±1.5	
776.55±0.61	14±3	
794.40±0.63	27±6	
809.51±0.51	130±30	
812.29±0.51	25±8	
823.04±0.52	24±8	
830.86±0.53	42±9	
846.62±0.69	6.3±3.5	
851.16±0.54	79±16	
857.75±0.70	30±8	
864.92±0.56	26±8	
873.91±0.57	60±14	
899.65±0.30	90±20	
918.71±0.31	44±10	
929.79±0.31	103±25	
935.75±0.80	19±10	
939.49±0.32	130±40	
949.67±0.32	68±18	
957.75±0.83	18±6	
967.35±0.84	24±8	
972.84±0.34	115±30	
980.52±0.86	6.6±4.0	
996.60±0.88	27±9	

$\langle\Gamma_\gamma\rangle$ = 112 meV

S_o = $(2.08\pm0.33)10^{-4}$ for 0-750eV region

Table D1

Cu resonance parameters

E_o(keV)	$ag\Gamma_n$(eV)	Isotope	J	Γ_n(eV)
30.46	0.8	63	-	
29.51	78±8	63	-	
26.87	0.4	65	-	
26.59	26±3	63	-	
25.90	2.7±1	-	-	
25.74	68±7	63	-	
25.45	0.8	-	-	
25.27	5±1	65	-	
25.16	6±1	65	-	
24.90	30±3	63	-	
24.27	10.8±1.5	65	-	
23.80	5.7±0.5	65	-	
23.60	∿0.6	- (63)	-	
23.32	∿0.5	-	-	
23.25	∿0.8	- (63)	-	
22.78	38±4	63	-	
22.01	1.5	- (65)	-	
21.72	2.0	- (63)	-	
21.21	23±3	63	-	
21.14	----	- (63)	-	
20.99	29±3	63	-	
20.91	1.6	- (63)	-	
19.98	20±2	65	-	
18.11	15±3	63	-	
17.86	24±3	63	-	
16.73	0.4	65	-	
16.29	4.1±0.6	63	-	
16.13	5.1±0.6	65	-	
16.06	0.45	63	-	
15.80	5.7±0.5	63	-	

Table D1

Cu resonance parameters

E_o(keV)	$ag\Gamma_n$(eV)	Isotope	J	Γ_n(eV)
15.07	6.4±0.5	63	-	-
14.21	8.0±1.0	65	-	-
13.69	7.2±0.8	63	-	-
13.21	17±2	65	-	-
13.15	32±4	63	2	74±9
12.87	0.07	- (63)	-	-
12.53	3.8±0.4	63	1	14.6±1.6
12.13	0.16	65	-	-
10.83	33±3	63	2	76±7
9.92	30±4	63	1	116±15
9.82	0.2	-	-	-
9.19	25±2	63	2	58±5
8.35	1.5±0.1	63	-	-
7.94	33±3	63	2	76±7
7.92	16±1.5	65	2	83±8
7.62	3.9±0.4	65	1,2	-
7.55	4.6±0.6	63	-	-
7.07	0.42±0.10	63	-	-
6.83	$(49\pm10)\times10^{-3}$	- (63)	-	-
6.44	5.1±0.5	65	2	26.5±2.6
5.81	4.2±0.6	63	2	9.7±1.4
5.39	14.9±1.0	63	2	34.5±2.3
4.85	3.5±0.3	63	1	13.5±1.2
4.48	1.8±0.2	65	1	15.6±1.7
4.39	1.3±0.2	63	-	-
3.91	2.7±0.2	65	1	23.4±1.8
2.64	2.3±0.3	63	2	5.3±.7
2.53	3.4±0.5	65	2	17.6±2.6
2.04	11.6±1.0	63	1	44.7±3.9
1.36	$(2.9\pm0.5)\times10^{-3}$	- (65)	-	-

Table D1

Cu resonance parameters

E_o(keV)	$ag\Gamma_n$(eV)	Isotope	J	Γ_n(eV)
0.994	$(4.8\pm0.8)\times10^{-3}$	63	-	-
0.807	$(1.8\pm0.3)\times10^{-3}$	63	-	-
0.650	$(3.5\pm0.4)\times10^{-3}$	63	-	-
0.578	0.390 ± 0.050	63	2	$.902\pm.116$
0.402	-	- (63)	-	-
0.230	$(3.1\pm0.3)\times10^{-3}$	65	-	-

TABLE E1

$^{35}C\ell$: $I^{\pi} = 3/2^{+}$ $^{35}C\ell$: 75.77%

$^{37}C\ell$: $I^{\pi} = 3/2^{+}$ $^{37}C\ell$: 24.23%

Resonance Parameters

Eo (keV)	2745/Eo (keV) (b)	Isotope	ℓ	J	2745ag/Eo (keV) (b)	$ag\Gamma n$ (eV)
0.398±0.0004	6897	35[a,b]	1			0.028± 0.003
4.248±0.002	646.2	35[b]	1			0.14 ± 0.02
8.314±0.005	330.2	37[c]	0	2	50.00	11.5 ± 1.0
14.788±0.011	185.6	35	0	2	87.90	14.0 ± 2.0
16.344±0.013	168.0		1			2.65 ± 0.30
17.124±0.014	160.3	35		(2,3)	75.94	7.0 ± 1.0
25.570±0.024	107.3	37	(0)	1	9.754	60 ± 10
26.601±0.026	103.2	35	(0)	2	48.87	55 ± 10
27.328±0.027	100.4	37	1	0	3.043	1.5 ± 0.5
27.805±0.027	98.72		1			0.6 ± 0.3
44.121±0.053	62.18		1			4 ± 1
46.607±0.058	58.93	37[c]	0	2	8.924	65 ± 10
51.540±0.067	53.29		1			1.2 ± 0.4
54.900±0.073	49.97					14 ± 4
55.396±0.074	49.58		1			18 ± 4
57.700±0.075	47.56	35	1	2	22.52	46 ± 5
62.686±0.089	43.82		1			35 ± 5
66.7 ±0.1	41.10		1			8 ± 2
68.17 ±0.10	40.29	37[c]	0	2	6.101	55 ± 5
90.253±0.153	30.39					6 ± 3
93.00 ±0.16	29.50	37[c]	0	2	4.466	98 ± 8
103.327±0.186	26.57	35	1			100 ± 20
113.30 ±0.21	24.23	35	1	2	11.48	220 ± 30
				3	16.06	
127.661±0.255	21.50					52 ± 8
133.74 ±0.27	20.55					200 ± 50
134.954±0.277	20.34					50 ± 10
136.322±0.281	20.14					150 ± 40
140.553±0.294	19.53					45 ± 10
142.890±0.301	19.21	35	1			360 ± 50
149.627±0.323	18.35					50 ± 10
165.347±0.380	16.60					48 ± 10
179 ±0.5	15.34					150 ± 50
182.822±0.435	15.01	35	1			900 ±200
188.070±0.453	14.60	35		2	6.915	450 ± 50
190.323±0.462	14.42	35		1	4.097	300 ± 40

a Sample enriched in $^{35}C\ell$, R.M. Brugger et al., Phys. Rev. 104, 1054 (1956).

b $^{35}C\ell(n,p)$ reaction, Y.P. Popov and F.L. Shapiro, Sov. Phys, JETP 13, 1132 (1961).

c Separated isotope, L.A. Toller et al, Phys Rev. 99, 620A (1955).

TABLE F1

Ta^{181} Level Systematics

E (eV)	$\rho(S_i, S_{i+1})$	Δexp	Δ_{D-M}	Δ_{uc}	N(=# of levels)
360	-0.18	1.09	0.72±0.22	1.5	76
300	-0.15	1.10	0.69±0.22	1.4	64
275	-0.17	0.92	0.67±0.22	1.2	59
250	-0.14	0.77	0.64±0.22	1.1	53
200	-0.15	0.66	0.58±0.22	0.9	39
150	-0.13	0.75	0.53±0.22	0.7	30

FIGURE E1

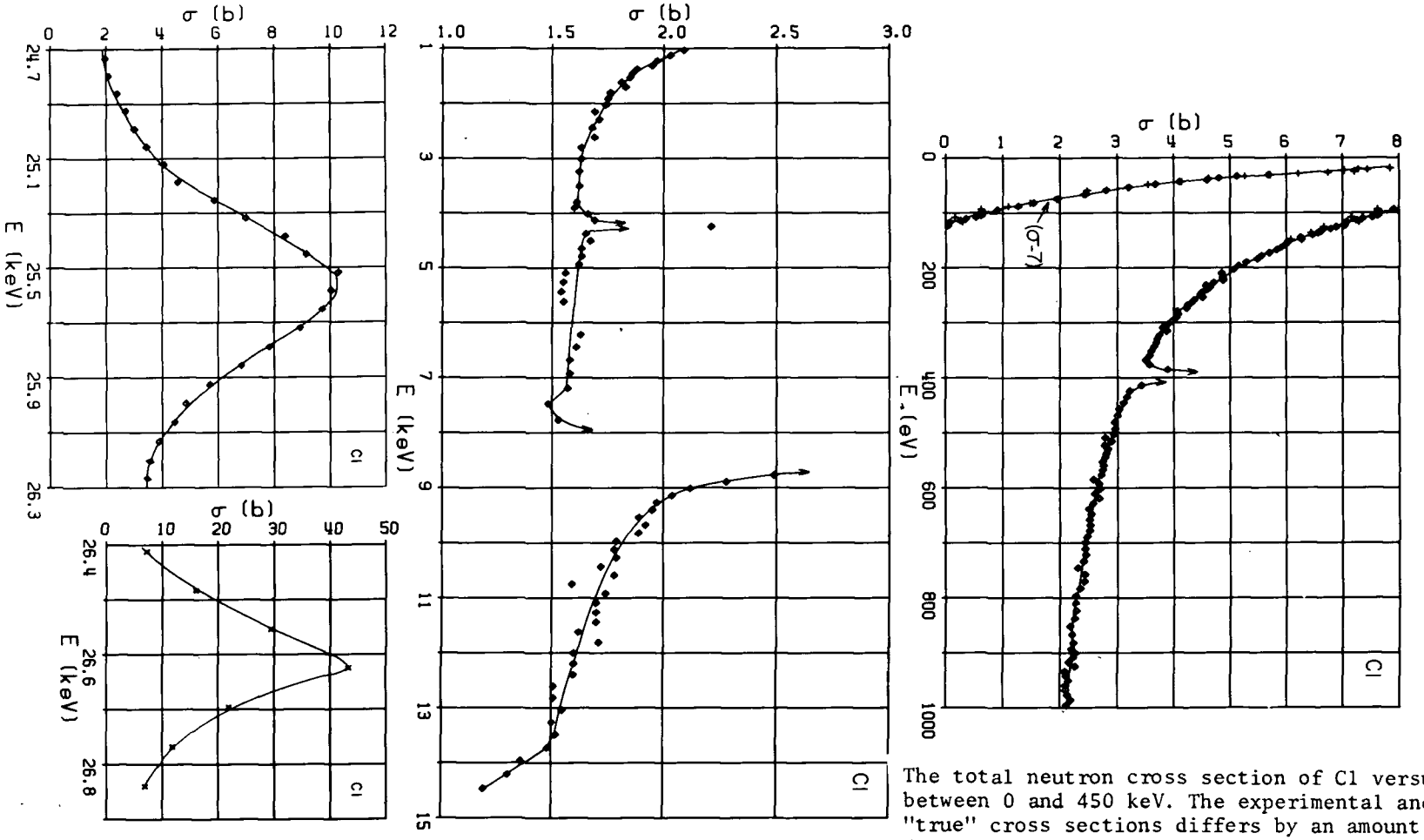

The total neutron cross section of Cl versus E between 0 and 450 keV. The experimental and "true" cross sections differs by an amount which depends on Doppler broadening effects, Resolution effects and the (1/n) values of our samples. The following (1/n) inverse sample thicknesses of the samples were used: (◇) 1/n = 5.05 b/atom; (+) 1/n = 32.6 b/atom and (x) 1/n = 130.9 b/atom

Figure E1 (cont)

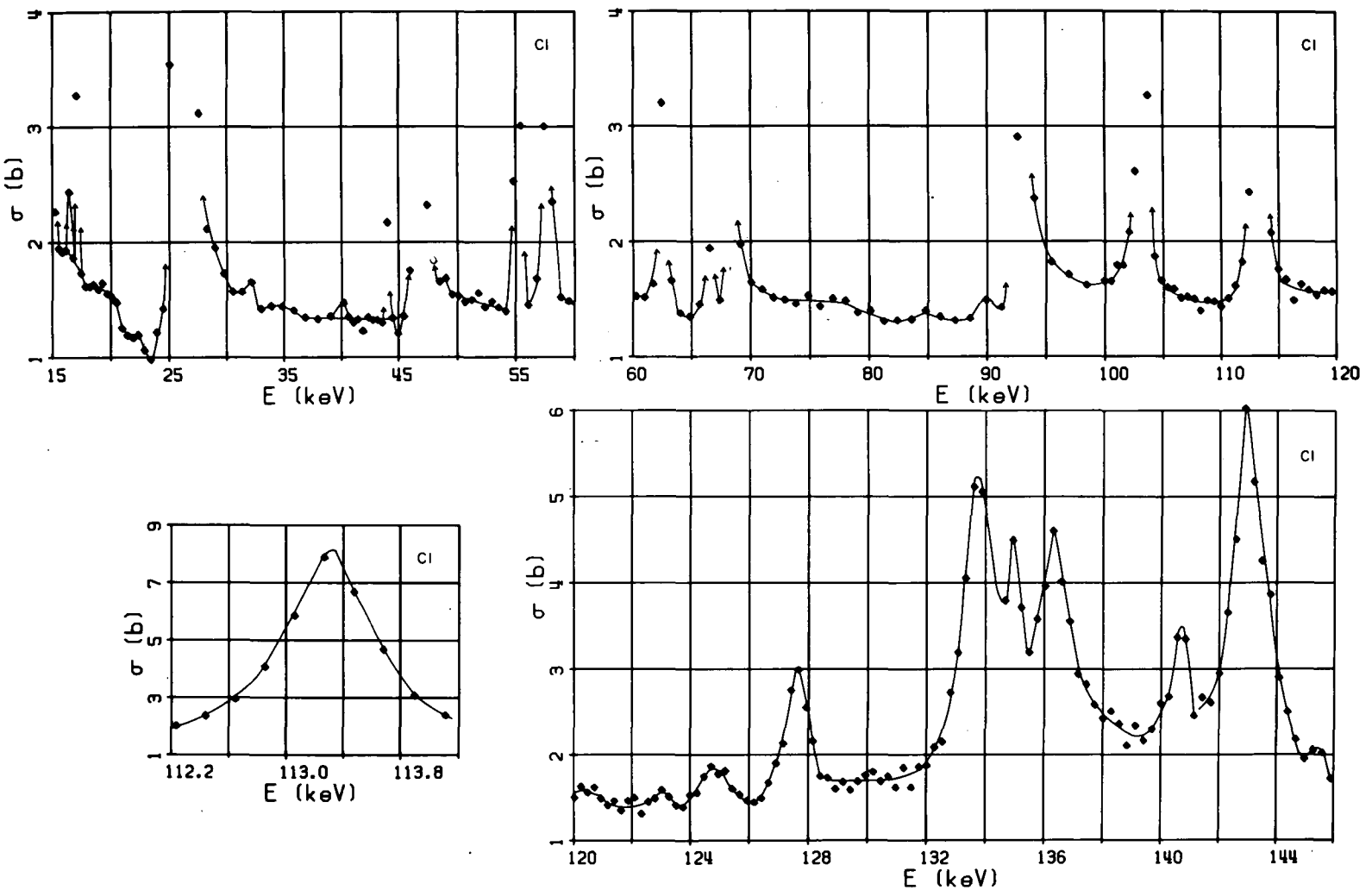

Figure E1 (cont)

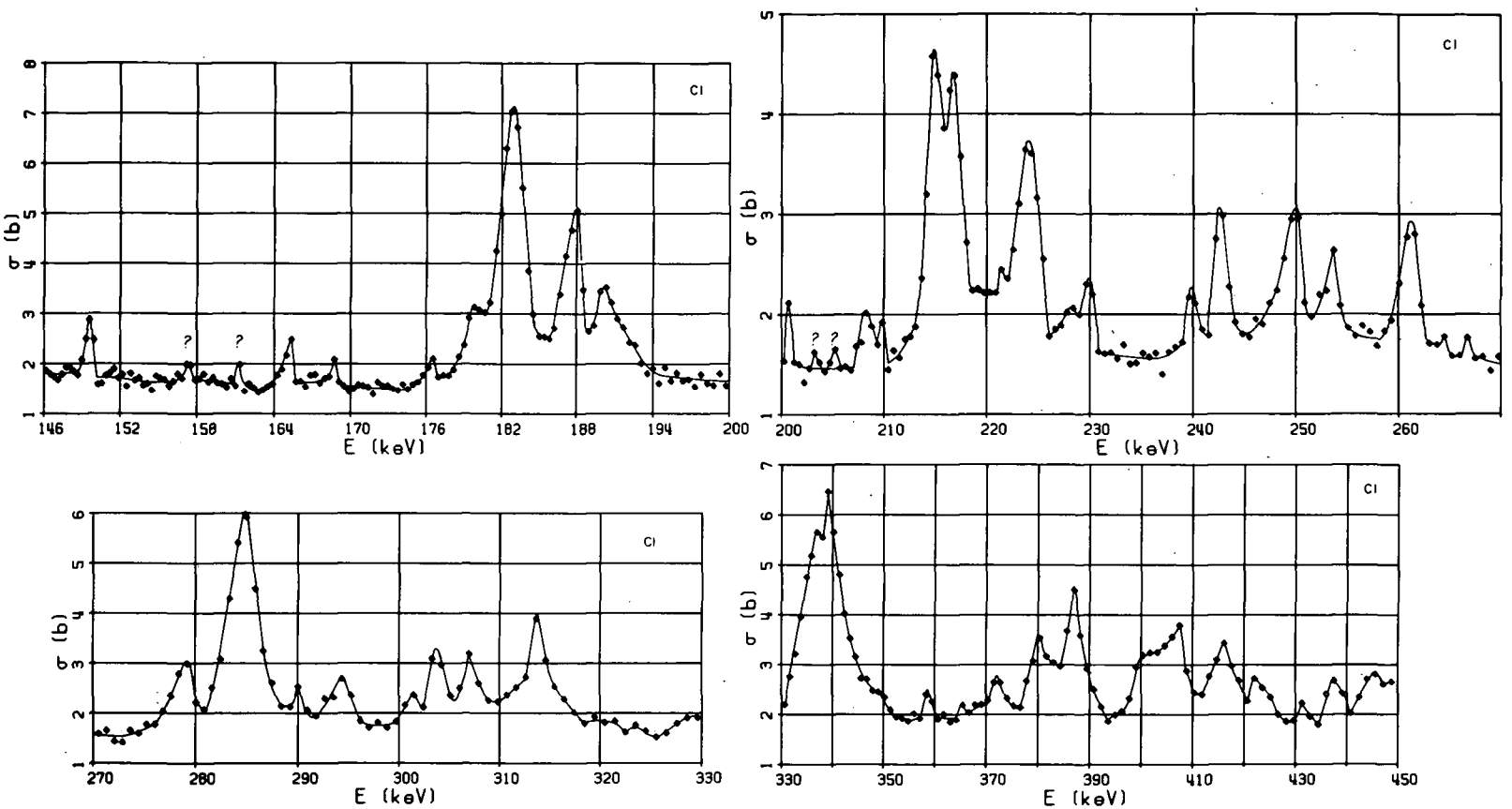

Figure E1 (cont)

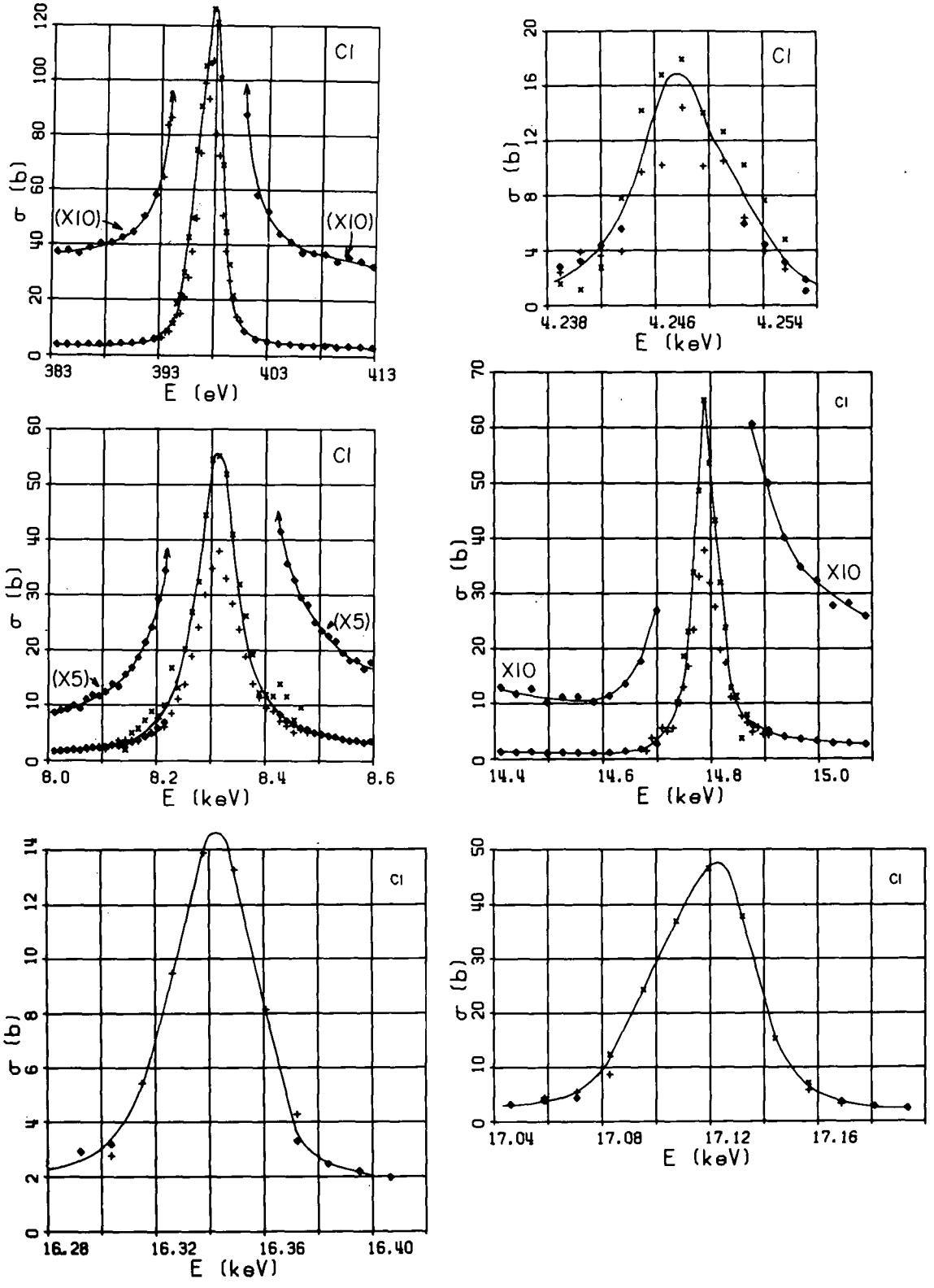

Figure E1 (cont)

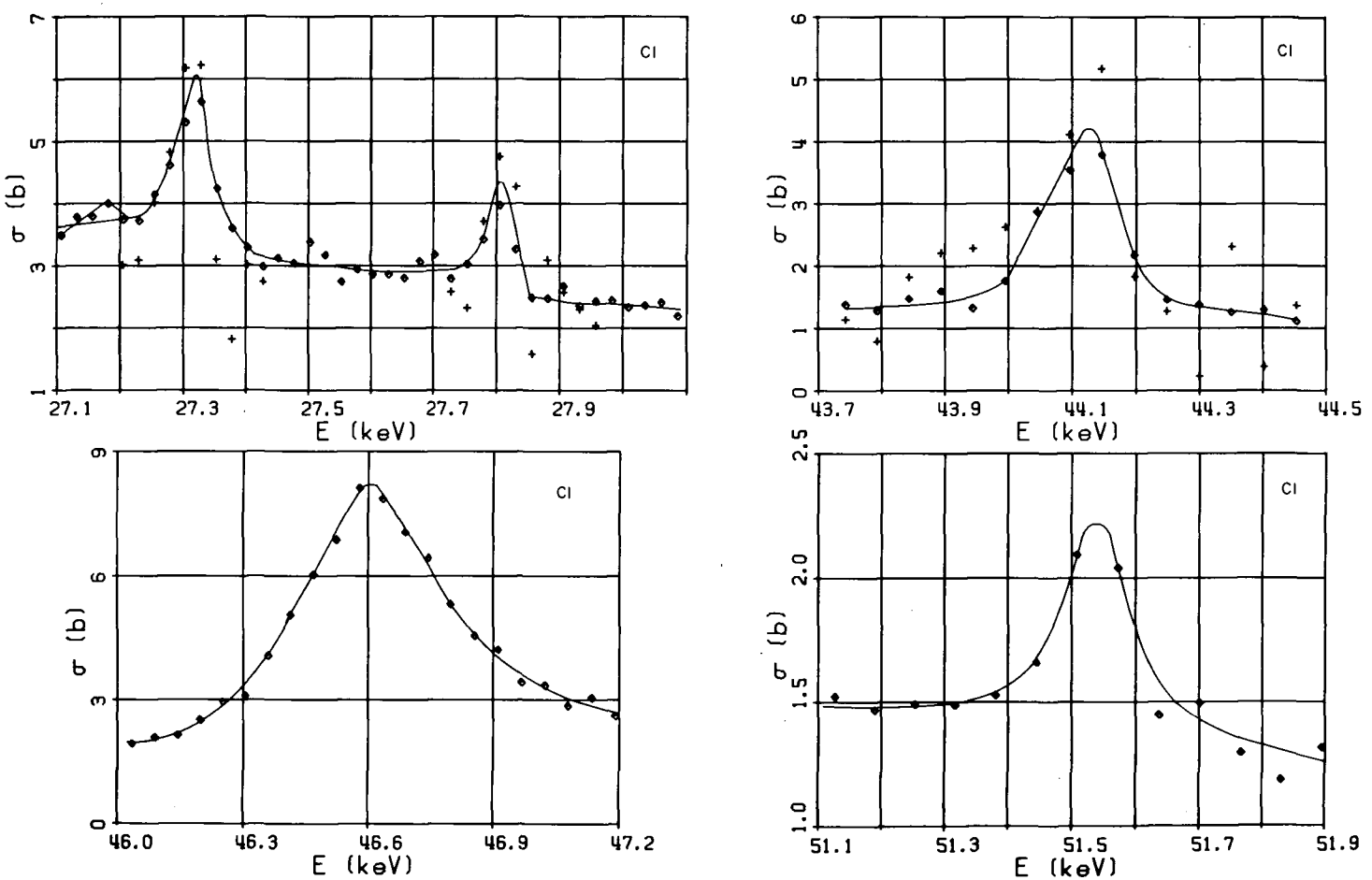

Figure E1 (cont)

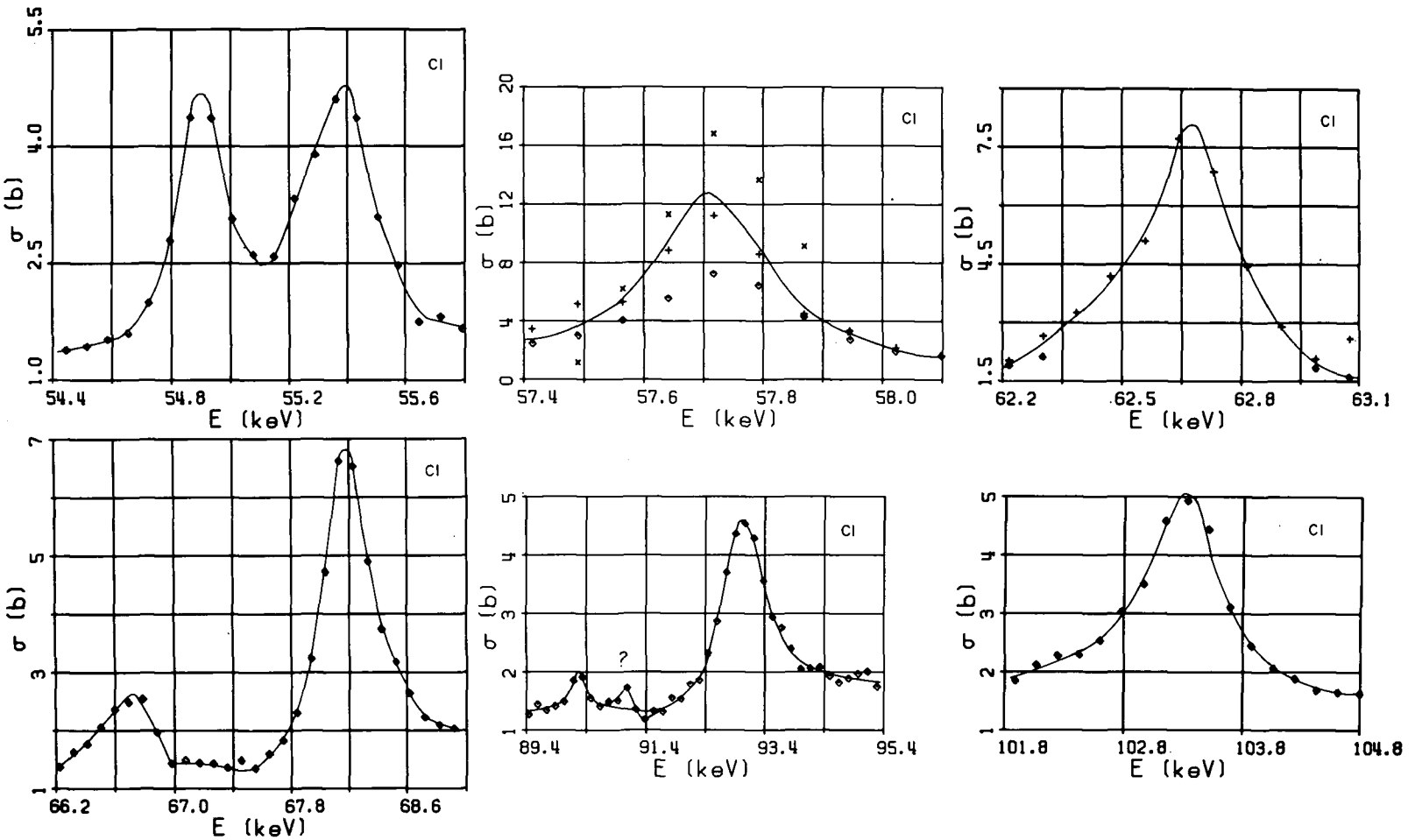

FIGURE F1

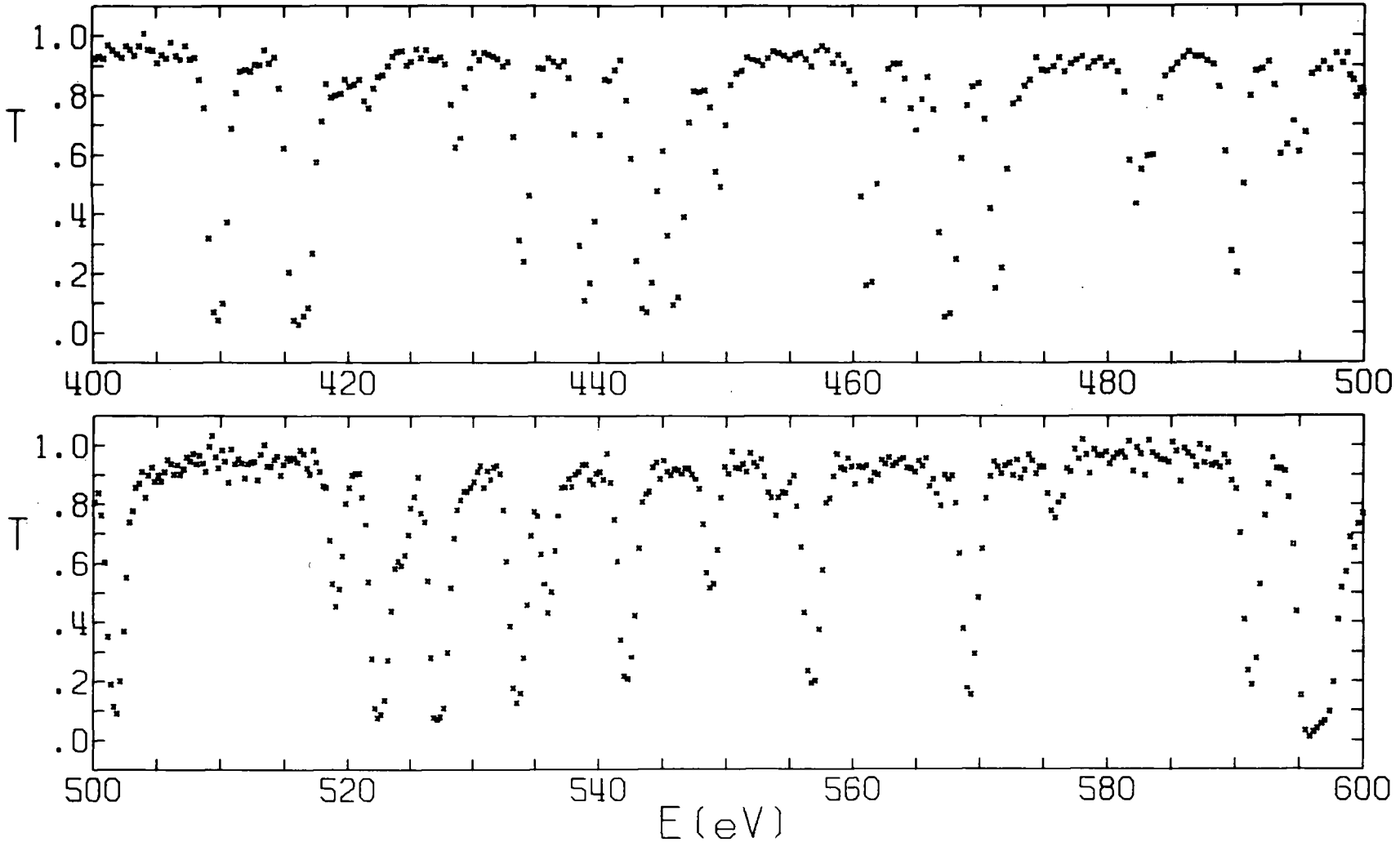

The Transmission versus E in the energy range 400 $\leq$ E(eV) $\leq$ 600 for two sample thicknesses of Ta^{181}. In part (a) the inverse sample thickness is (1/n) = b/atom, in part (b) 1/n =30 b /atom.

Figure F1 (cont)

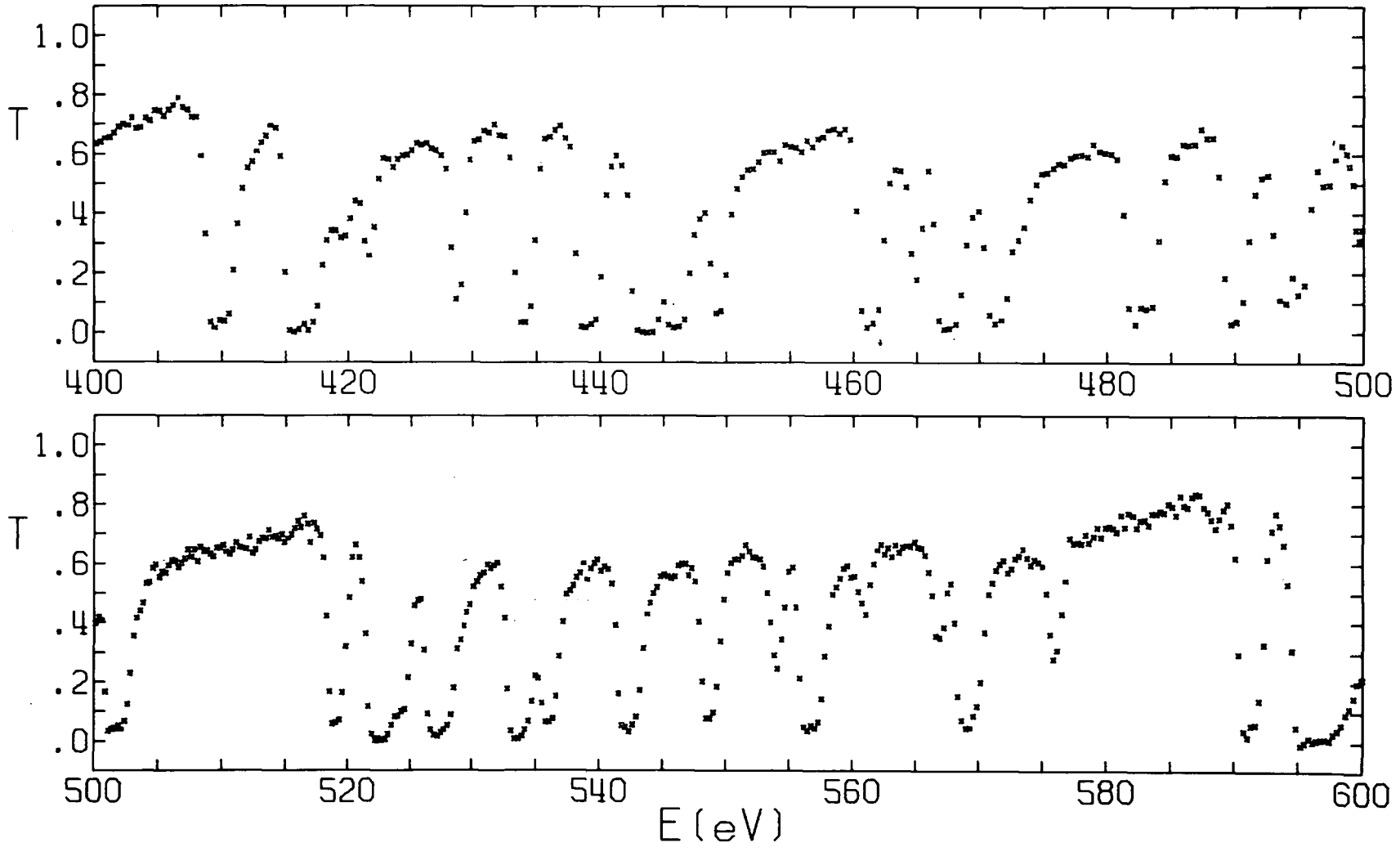

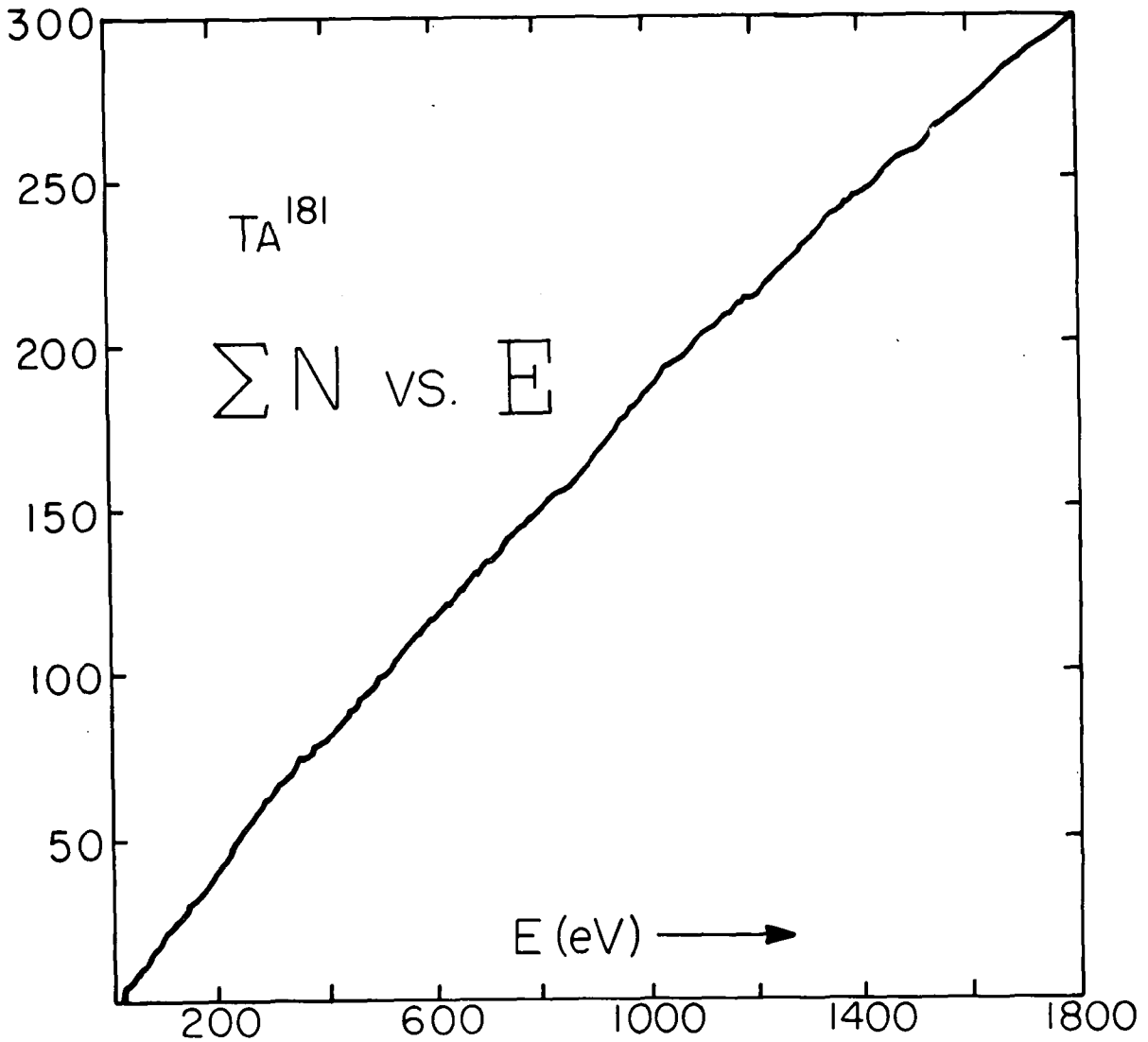

Figure F2 The cumulative sum of the number of observed levels N versus E in Ta^{181} up to 1800 eV. The slope of the curve gives the density of states which is the inverse of the average spacing <D>.

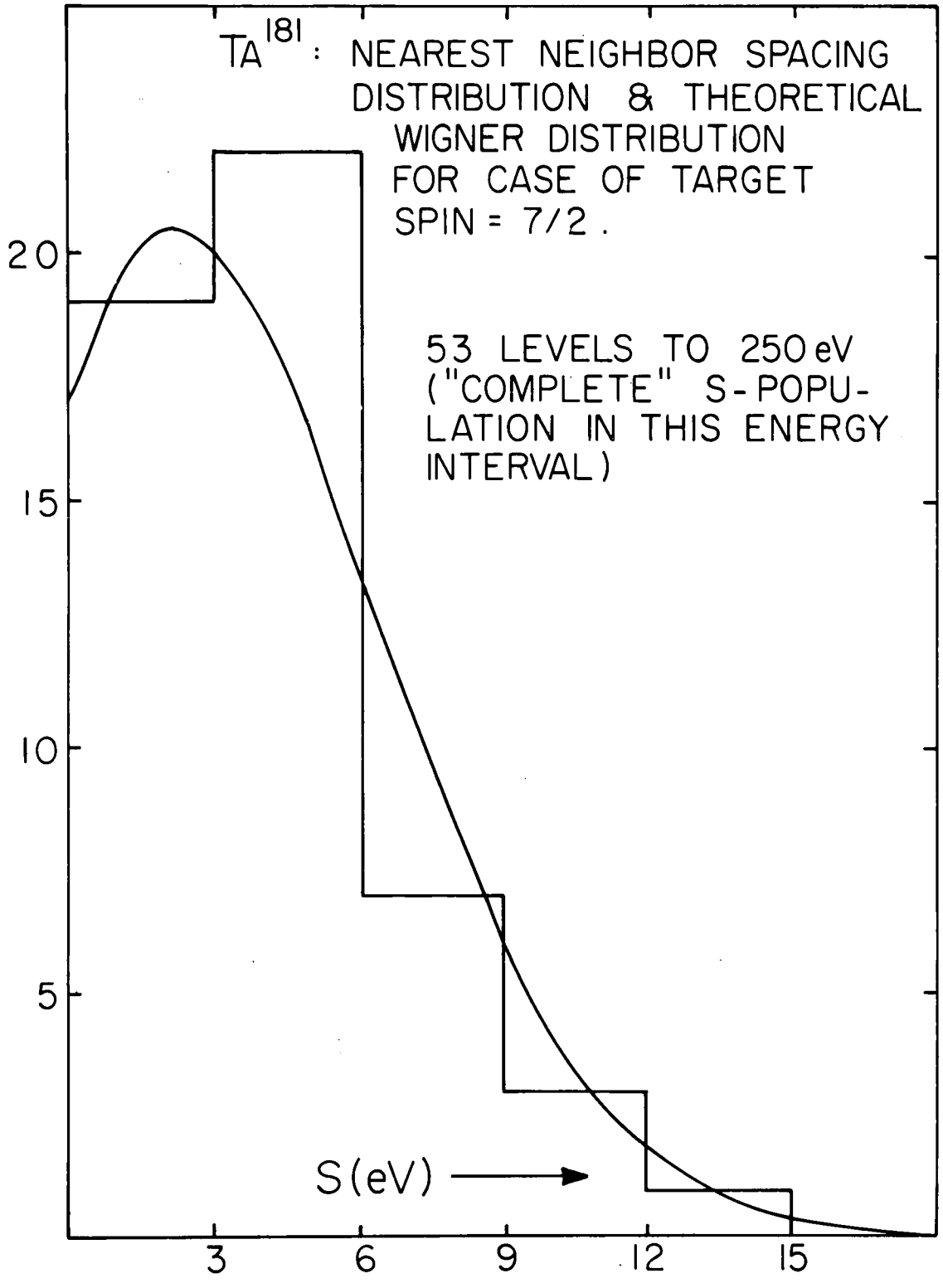
TA181 : NEAREST NEIGHBOR SPACING DISTRIBUTION & THEORETICAL WIGNER DISTRIBUTION FOR CASE OF TARGET SPIN = 7/2 .
53 LEVELS TO 250 eV ("COMPLETE" S-POPULATION IN THIS ENERGY INTERVAL)
20
15
10
5
S(eV)
3
6
9
12
15

Figure F3

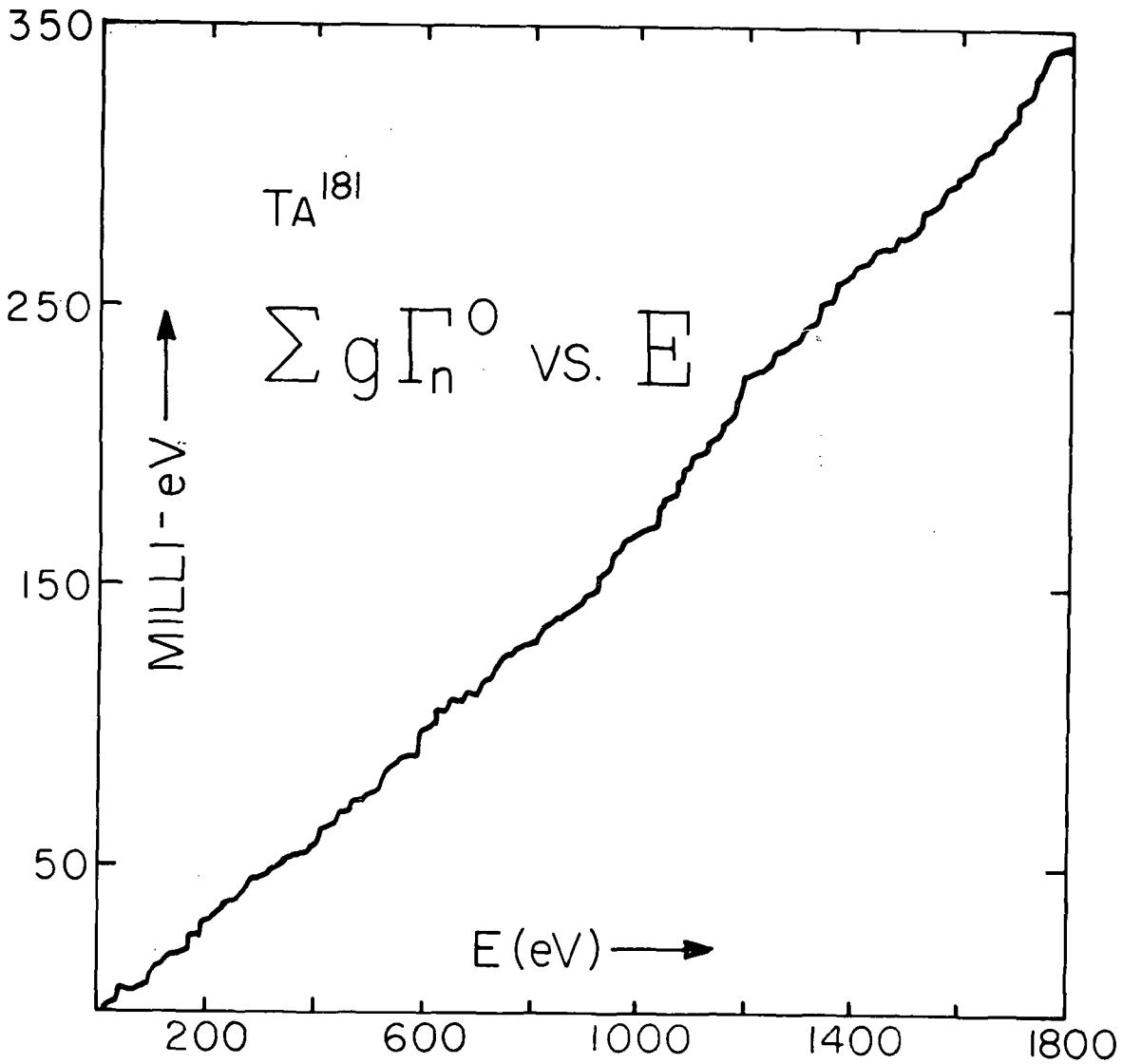

Figure F4

The sum of the product of the statistical spin factor g times the reduced neutron width Γ_n^o versus Energy. The slope of the curve, which is insensitive missing or spurious weak levels, gives the S wave strength function.

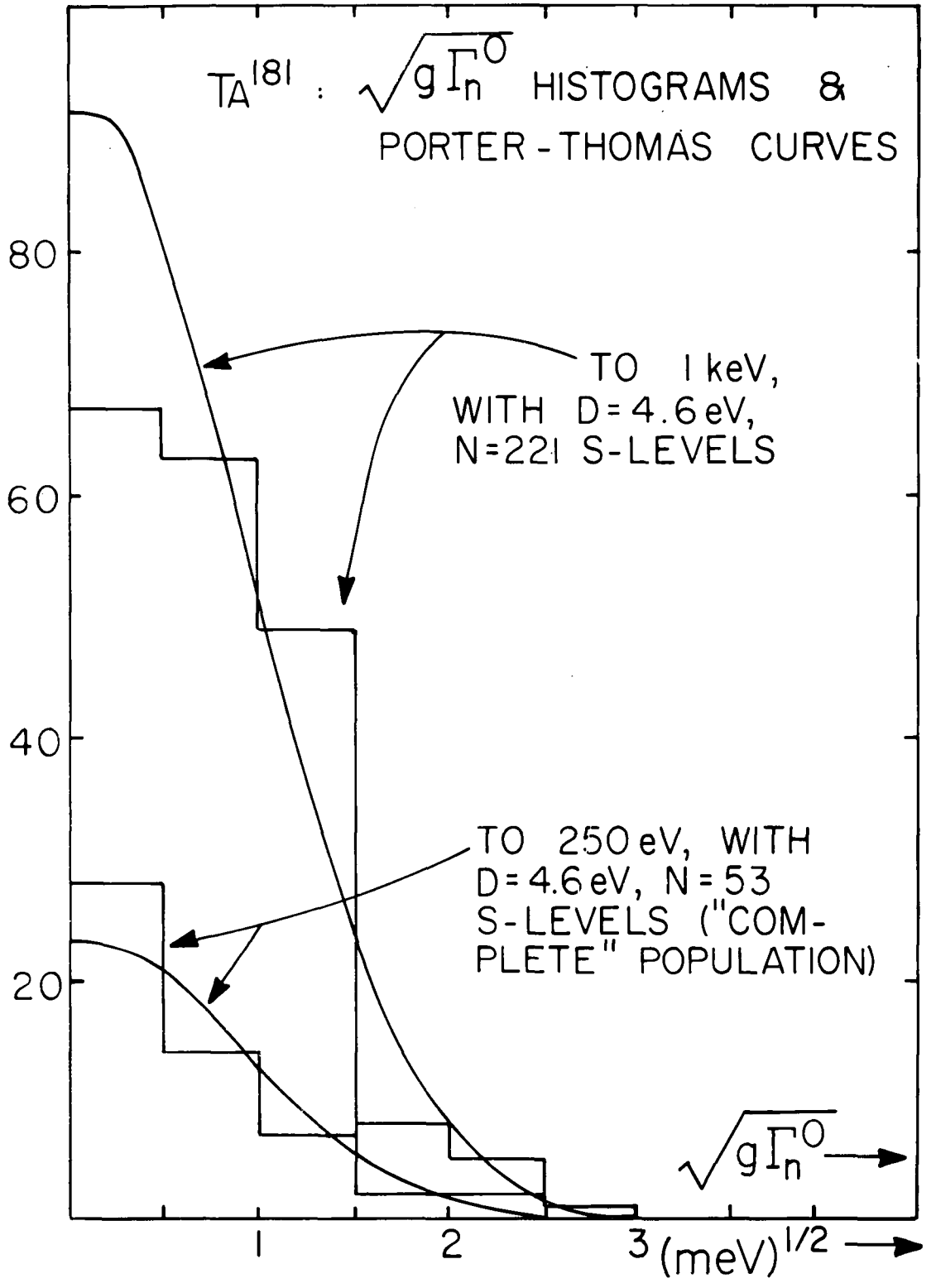

FIGURE F5

A comparison of the experimental and Porter-Thomas distributions for reduced neutron widths. This figure shows that few if any levels have been missed in the interval $0 \leq E(eV) \leq 250$.

G. Precision Measurement of the 2200 m/sec Neutron-Proton Capture Cross Section, (D. Cokinos and E. Melkonian)

A paper, under the above title, is being submitted to the Physical Review for publication with the following abstract:

> The neutron-proton capture cross section at the neutron laboratory velocity of 2200 m/sec has been determined from the time decay of the thermalized neutron population following short bursts of fast neutrons in water samples of widely varying sizes. Use of the intense pulsed neutron beam of the Columbia Nevis Synchrocyclotron enabled elimination of many of the problems encountered in earlier experiments. The present results for this cross section is 332.6± 0.7 mb, which is the most precise of any result obtained by this method and is comparable in accuracy and consistent with the most accurate values determined by any method.

The only measurement of comparable accuracy is that of Cox, Wynchank, and Collie (Nuclear Physics 74, 497 (1965)), who obtained a value of 334.2±0.5 mb, an error assignment which we judge does not reflect all their sources of uncertainty. Their method consisted of observing the decay with time of the integrated neutron population in a large volume of water as contrasted with ours in which a series of smaller volumes was used. With the given error assignments, the two values differ by twice the square root of the sums of the squares of their individual errors, so that the results are essentially in agreement.

Some other measurements of moderate precision have given "low" values in the neighborhood of 325 mb. The fact that the two most precise values (ours and that of Cox et. al.), based on two different techniques with different possible sources of error, are in essential agreement implies that the "low" values obtained by others are probably in error or have uncertainties much larger than claimed.

H. Capture Resonance Parameters of Thulium-169 and Rhodium-103, (J. Arbo, J. Felvinci, E. Melkonian, F. Rahn, C. Ho and W.W. Havens, Jr.)

Partial results from analysis of our resonance capture data for Tm-TM-169, Rh-103, and Au-197 were presented at the meetings of the American Nuclear Society in November, 1972 and the American Physical Society in January, 1973. Additions to our last report include values of $\sigma_o \Gamma_\gamma$ for Tm-169 extended to 1000 eV. (Table H1), and the energies (Table H2) and distribution (Figure H1) of observed resonances for Rh-103 up to 2000 eV. Final results for $\sigma_o \Gamma_\gamma$ from these data should be available for the next report.

Comparing our results with levels reported by A.D. Carlson in NCSAC-38, we tentatively identify the levels at 253.9, 263.2, and 319.6 eV as doublets. Levels reported at 44.6, 83.5, 353.8, 443.8, 866.6, and 988.9 eV are uncertain or not visible in our data. We do observe levels at 427.7, 602.5, 489.3, and 552.8 eV which are not reported by Carlson.

Present analysis effort is directed toward improving the background corrections in our peak-fitting procedure and determining accurate normalizations between the Rh, Au, and Tm runs for various target thicknesses. We intend to make multiple scattering corrections to the measured peak areas.

Capture Resonance Areas: ^{169}Thulium

E_n (eV)	$\sigma_0\Gamma_\gamma$ (barns-eV)	E_n (eV)	$\sigma_0\Gamma_\gamma$ (barns-eV)	E_n (eV)	$\sigma_0\Gamma_\gamma$ (barns-eV)
3.92		296.2	38.	643.5	60.
14.4		297.4	86.	659.7	64.
17.5		319.3	150.	670.3	22.
28.8		320.0	160.	674.3	182.
34.8	370.	325.0	51.	678.5	195.
37.6	25.	333.4	195.	687.4	20.
44.8		346.7	98.	696.1	37.
50.7		358.0	85.	708.3	22.
59.2	311.	364.3	8.	714.7	90.
63.2	34.	377.4	68.	716.8	165.
65.9		379.1	55.	725.4	24.
83.4	165.	391.0	158.	732.8	70.
93.6	36.	400.4	25.	739.8	38.
94.0	500.	408.9	280.	761.1	55.
95.7	30.	414.8	105.	766.1	15.
101.9	11.	415.6	27.	783.6	9.
115.6	250.	416.8	120.	787.9	65.
125.2	130.	433.8	4.	790.4	16.
132.3	10.	441.3	136.	801.	4.
136.0	275.	456.3	24.	803.1	42.
153.6	250.	460.4	40.	809.0	73.
160.7	20.	468.4	85.	829.5	43.
164.4	75.	472.3	43.	843.7	84.
185.4	4.	493.6	30.	842.9	158.
207.8	140.	513.0	138.	851.0	52.
209.8	33.	520.0	102.	853.7	35.
212.2	9.	543.7	17.	867.7	14.
214.0	240.	550.3	85.	881.1	61.
224.3	60.	557.4	125.	891.2	63.
228.3	40.	566.0	175.	897.2	12.
238.7	121.	574.1	147.	911.8	45.
243.8	52.	579.4	19.	934.6	49.
250.8	200.	585.9	32.	940.5	73.
251.6	200.	587.2	75.	949.2	50.
252.2	2.	593.1	88.	958.8	35.
260.4	88.	600.0	170.	986.1	117.
274.0	118.	608.2	60.	989.4	50.
283.6	230.	626.0	130.	998.7	103.
288.8	190.	632.1	77.	1007.	158.

Table H1

1.257	435.6	885.0	1404.5
34.4	447.2	894.5	1430.3
46.7	449.2	913.1	1450.
68.3	450.1	929.0	1461.5
95.8	472.9	954.5	1483.0
98.8	486.8	969.5	1528.6
111.0	489.3	1000.8	1540.3
114.2	492.1	1024.0	1559.2
125.6	505.2	1026.6	1564.2
154.3	526.0	1065.1	1616.
179.5	552.8	1074.5	1666.9
187.3	555.5	1081.8	1692.7
192.3	581.6	1097.0	1706.4
251.4	602.5	1109.0	1732.
254.1	604.6	1153.0	1761.7
263.4	620.7	1185.0	1780.
264.8	646.2	1188.2	1791.
272.4	663.4	1195.	1814.7
290.1	676.3	1203.	1837.6
312.9	683.1	1209.3	1898.2
315.8	691.9	1243.5	1913.1
319.7	701.8	1269.7	1935.1
327.9	727.0	1274.9	1947.6
362.9	741.3	1283.8	1976.
366.5	759.0	1304.3	2003.5
374.2	760.4	1323.0	2053.5
376.9	782.4	1352.5	2078.1
388.4	796.5	1362.3	2094.8
406.3	830.5	1377.9	2108.3
427.7	844.7	1390.6	

OBSERVED RESONANCE ENERGIES OF RHODIUM-103 (eV)

Table H2

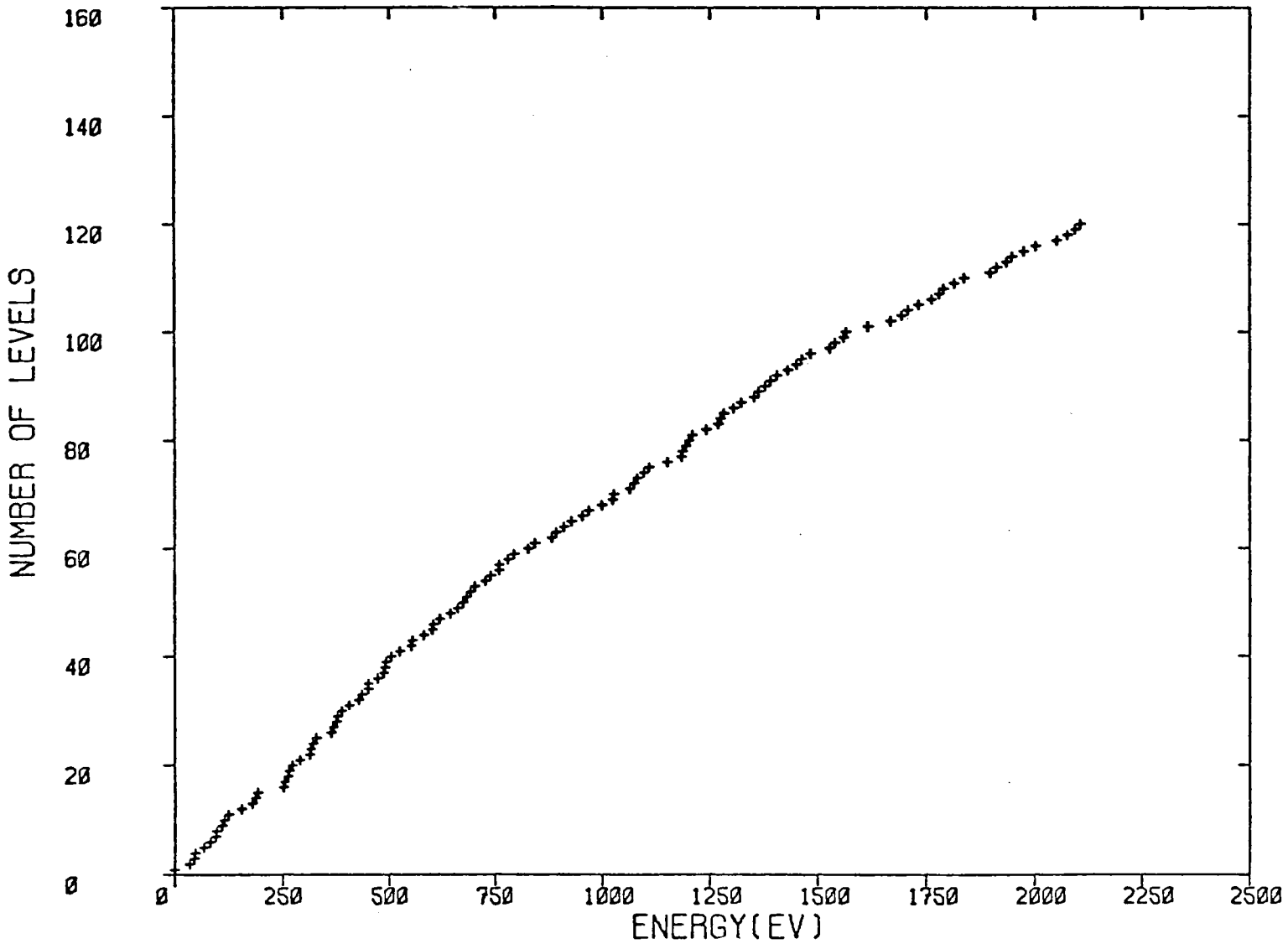

Figure H1. Distribution of Observed Neutron Resonances of Rhodium-103.

I. Smoothing of Cross Section Data, (J.P. Felvinci and E. Melkonian)

Some of the cross section data we have accumulated is of low count rate. This may occur for two reasons: a) a very small amount of sample was available, e.g. only 20 μg of Th-229, and b), in the case of the fission cross section of U-233 and U-235 where a good count rate was obtained, we looked at the cross sections for limited range of the fission fragment pulse heights, again reducing the count rate studied. In considering data of low counts, we frequently see what appear to be additional levels, e.g. split peaks or shoulders on large resonances.

We have presented in previous reports fission resonance areas of Th-229 and noted that the resonance at 4.16 eV could not be fitted by a single Doppler broadened Breit-Wigner formula. As a matter of fact, our data showed distinctly two peaks, one located at 4.10, the other at 4.20 eV (Fig. I1a). We have noticed that the transmission data by R. Coté as presented in BNL-325 also had two peaks at the same energies. We ruled out instrumental effects which would result in a split in the peak.

The consequences of a doublet at 4.16 eV would be serious. Because the ratio of fission to total cross section is 0.6, we would have to assume $\Gamma\gamma$ = 15-20 meV for both of these levels. These values are in disagreement with all observed radiation widths of odd fissile nuclei.

As an aid in resolving a situation like this, we have developed a technique for smoothing data of a better resolution than normally compatible with the Doppler and natural widths. This becomes possible because most of our data have been recorded event-by-event at a basic channel width of 20 ns. For least-squares analysis, a channel width suitable for a given energy region is obtained by summing adjacent channels to get the required resolution. However, by using a channel width 1/4 as large and applying a smoothing procedure, we get the combined advantages of increasing the statistical accuracy of each point, as well as having more points to outline the curve. This smoothing is performed by adding adjacent points weighted by the elements of the Pascal triangle (coefficients of the binomial expansion). Fig. I2a,b show the same data as Fig. I1a but with a channel width of 0.32 μsec. The number "N" indicates the number of points on either side used in the smoothing operation and correspond to the elements in the binomial expansion $(a+b)^{2N}$ (For comparison, Fig. I1b shows the data of Fig. I1a smoothed).

Initially, there appeared to be as many as four levels in Th-229 clustered around 4.16 eV (including a small level on each side). Fig. J2d, with N = 64, corresponds to a smoothing of ∿ 0.7 of the Doppler broadening and indicates that there may be only two levels, a main central peak (4.16 eV) and one on the low (high energy) side (4.40 eV . While the

evidence from fission and total cross section strongly suggests the existence of two central narrow peaks, the present analysis implies that these could be due to statistical fluctuations.

We have also applied this smoothing technique to random data as shown in Fig. 13 a,b with and without smoothing (N = 0 means no smoothing). This smoothing procedure appears to develop an apparent oscillation of fixed frequency. The explanation is that smoothing cuts out higher frequencies in the Fourier expansion leaving a cut-off frequency with the largest amplitude.

This method may also be useful to recover resonances buried in the "noise" of a large background. It may be applicable in the study of the shoulders and bumps on large resonances, to investigate the probability of whether they are due to statistical fluctuation or are real structures. Normal least-square fitting procedures, which calculate the lowest χ^2 for the whole region are not too sensitive to this possibility.

Using this method with our pulse-height cuts in U-233, we have observed resonance-type behavior in bumps at the sides of some large resonances (e.g. 12.76 eV) which were described as interferences in the past. Our analysis indicate either that this bump is a resonance or that the proposed interference depends on the pulse height of the fission fragment, which is not too satisfactory an explanation.

Presently we are scanning some of our past experiments with the help of this technique to discover missed or incorrectly identified levels.

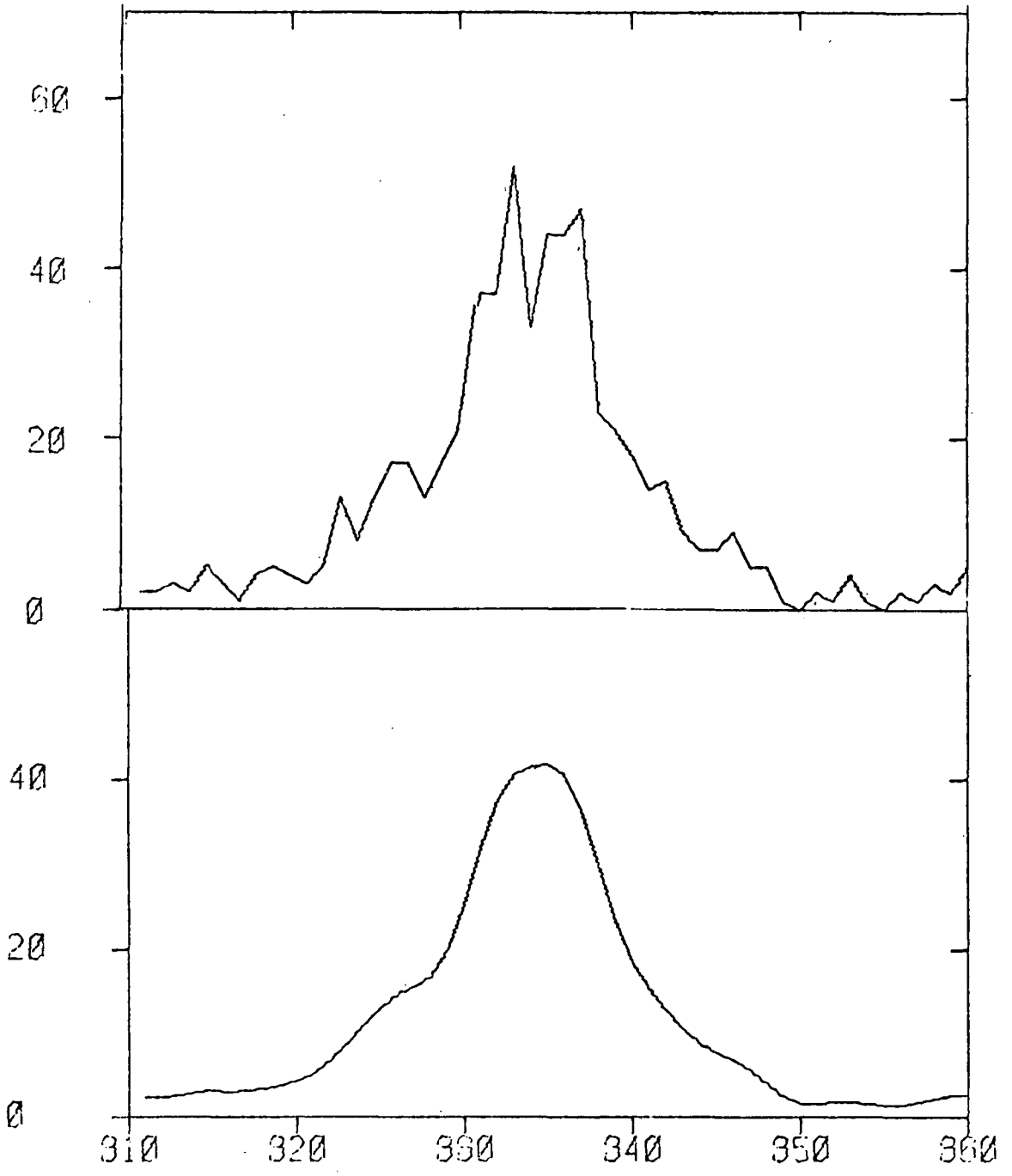

Fig. 11. Th-229 fission yield at 1.28 μs/channel resolution. a) N=0, b) N=4.

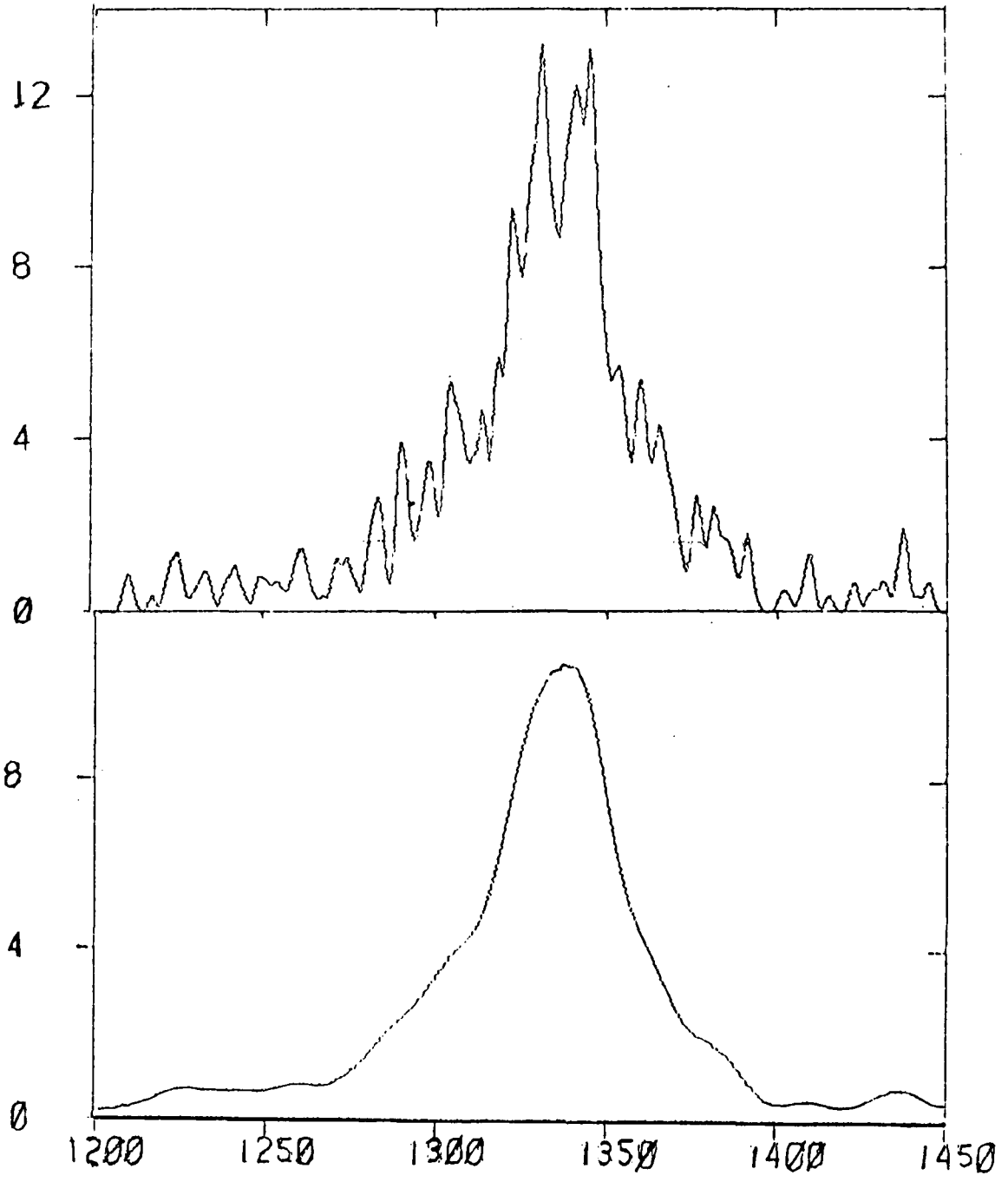

Fig. I2 . Th-229 fission yield at 0.32 μs/channel resolution. a) N=2, b) N=64.

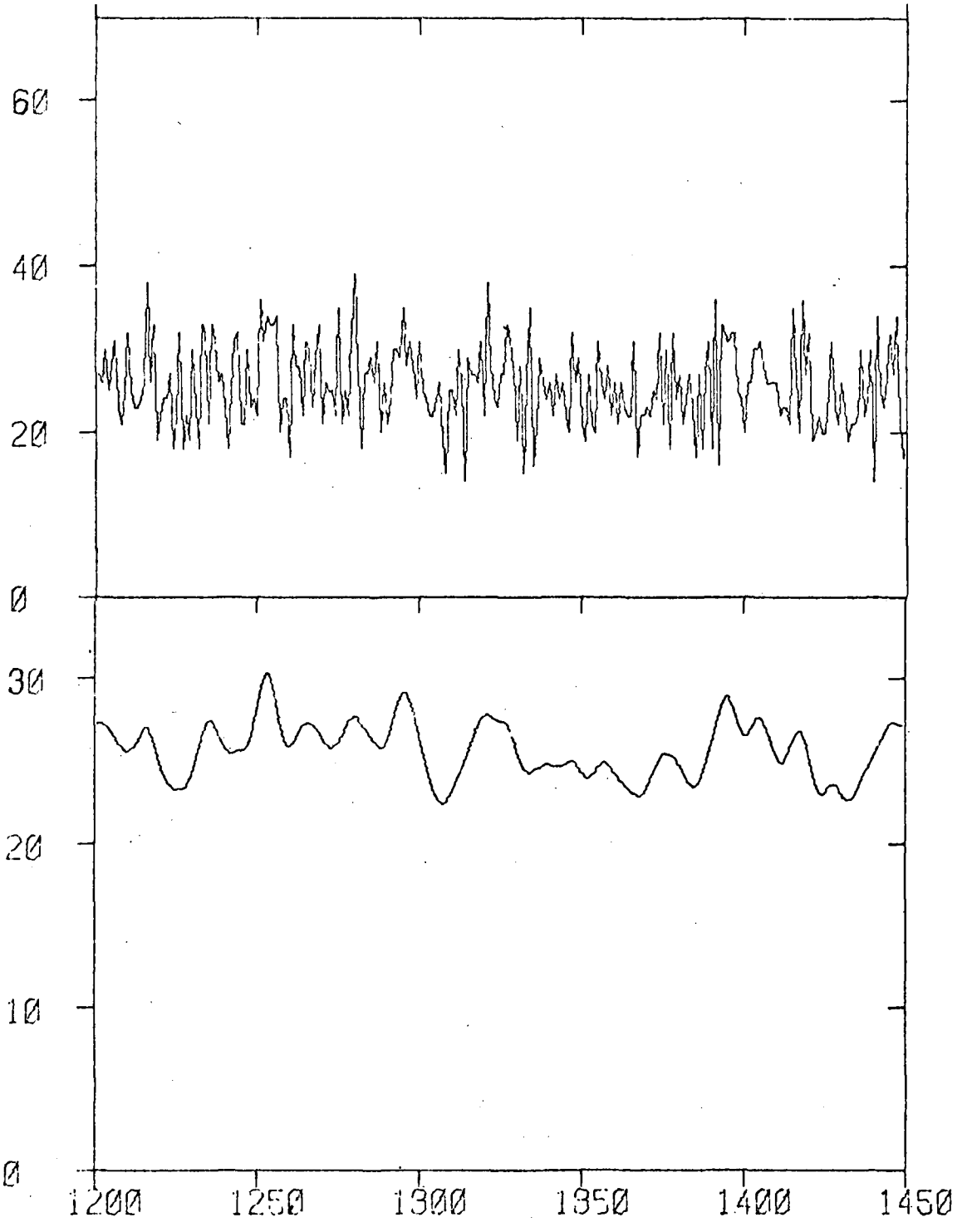

Fig. I3. Random data at 0.32 μs/channel resolution.
a) N=0, b) N=16.

INTELCOM RAD TECH
San Diego, California

A. NEUTRON CROSS SECTIONS

1. Measurements of the $^6Li(n,\alpha)$ Cross Section for Neutron Energies from 1 to 1700 keV (S. J. Friesenhahn)

Preparations for precision measurements of the $^6Li(n,\alpha)$ cross section over the neutron energy, 1 to 1700 keV, are nearing completion. These measurements, part of the standard neutron cross-section program at Rad Tech, will be made using a large ion chamber developed for measurements of the $^{10}B(n,\alpha)$ cross sections completed last year and reported in the last USNDC contribution. A technique has been developed for fabricating the required large area ^6Li-loaded ion chamber plates which involves evaporating ^6Li metal onto thin Aℓ films, and for preventing long-term deterioration of the ^6Li plates. The $^6Li(n,\alpha)$ cross section will be measured relative to the H(n,n) cross section, using the same flux measuring techniques described previously for the $^{10}B(n,\alpha)$ measurements. (This work pertinent to request No. 14 in NCSAC-35.)

2. Measurement of Gamma Ray Production Cross Sections for Carbon and Nitrogen (C. G. Hoot, V. J. Orphan, and V. V. Verbinski)

Initial measurements of gamma-ray production from $(n,x\gamma)$ reactions in carbon and nitrogen have been made using a Linac-pulsed neutron source and a 60 cm^3 Ge(Li) detector. Analysis of the data will yield $(n,x\gamma)$ cross sections for discrete gamma-ray lines, and unfolding of the spectral data for nitrogen will give a measure of the continuum (unresolved or Doppler broadened) gamma-ray contribution to the total gamma ray production cross section. A careful study has been made of the time-dependent background associated with neutrons scattered from the sample into the Ge(Li) detector. In the past, this background has been estimated by replacing the sample with a material (such as Be) having a very low gamma ray production cross section. This assumes that the spectral shape of the neutrons scattered from the sample into the detector is the same for Be and the sample. In the present experiment, the spectrum of neutrons from the sample incident on the Ge(Li) detector will be determined in a supplementary experiment by replacing the Ge(Li) detector with a NE-213 scintillator using pulse-shape discrimination to separate neutron from gamma-ray events. An additional supplementary measurement has been made of the Ge(Li) detector spectral response to neutrons by placing both the Ge(Li) and the NE-213 detectors simultaneously in the direct, but greatly reduced in intensity, neutron beam. Folding the scattered neutron spectrum incident on the Ge(Li) detector with the measured Ge(Li) response to neutrons should provide a more accurate measure of the scattered neutron background.

In Figure A-1, the result of the measurement of the Ge(Li) spectral response to neutrons is shown for neutrons from 6 to 20 MeV. It can be seen that the spectral shape is surprisingly insensitive to incident neutron energy. This was found to be true over the neutron energy range 0.5 to 20 MeV. This result, in addition to simplifying the subtraction of scattered neutron background in the present measurements, demonstrates the validity of the technique used in previous measurements to determine the scattered neutron background (replacing the sample with Be). Since the shape of the Ge(Li) response to neutrons is insensitive to the neutron energy, differences between the scattered neutron spectra from Be and the sample under investigation should have negligible effect on the measured scattered neutron background. (This work pertinent to request Nos. 35 and 42 in NCSAC-35.)

B. INTEGRAL TESTS OF CROSS-SECTION DATA

1. Integral Experiments to Test Gamma-Ray Production and Neutron Scattering Cross Sections of C, N, O, and Fe (L. Harris, J. C. Young, and P. A. Read)

Analysis of the C and N measurements reported in the last USNDC contribution has continued. Preliminary energy spectra of 125° scattered neutrons from the liquid nitrogen sphere are shown in Figure B-1 for ten incident neutron energy intervals. A gamma ray response matrix is being constructed for the NE-213 scintillator to permit unfolding the energy spectra of the secondary gamma rays which were measured simultaneously with the scattered neutrons.

Similar measurements of count rates and energy spectra of scattered neutrons and secondary gamma rays from O and Fe are in progress.

2. Experimental Test of Nitrogen Gamma Ray Production Cross Sections Using a Ge(Li) Detector (V. J. Orphan, C. G. Hoot, and V. V. Verbinski)

Gamma rays from the $^{14}N(n,x\gamma)$ reaction have been measured with a high-resolution Ge(Li) gamma-ray detector for four broad incident neutron energy intervals spanning the range of 4.22 to 15.40 MeV, using the Intelcom Rad Tech Linac pulsed neutron source. These high-resolution measurements made for gamma-ray energies of 0.2 to 10 MeV supplement low-resolution measurements[1] of secondary neutrons and gamma rays made using a proton-recoil scintillator (NE-213). The experimental arrangement was identical to that described by Harris et al.,[1] and, in fact, the Ge(Li) measurements

[1] L. Harris, Jr., G. D. Trimble, and J. C. Young, "Integral Experiment to Test Gamma-Ray Production and Neutron Scattering Cross Sections," Trans. Am. Nucl. Soc. 15, 960 (1972).

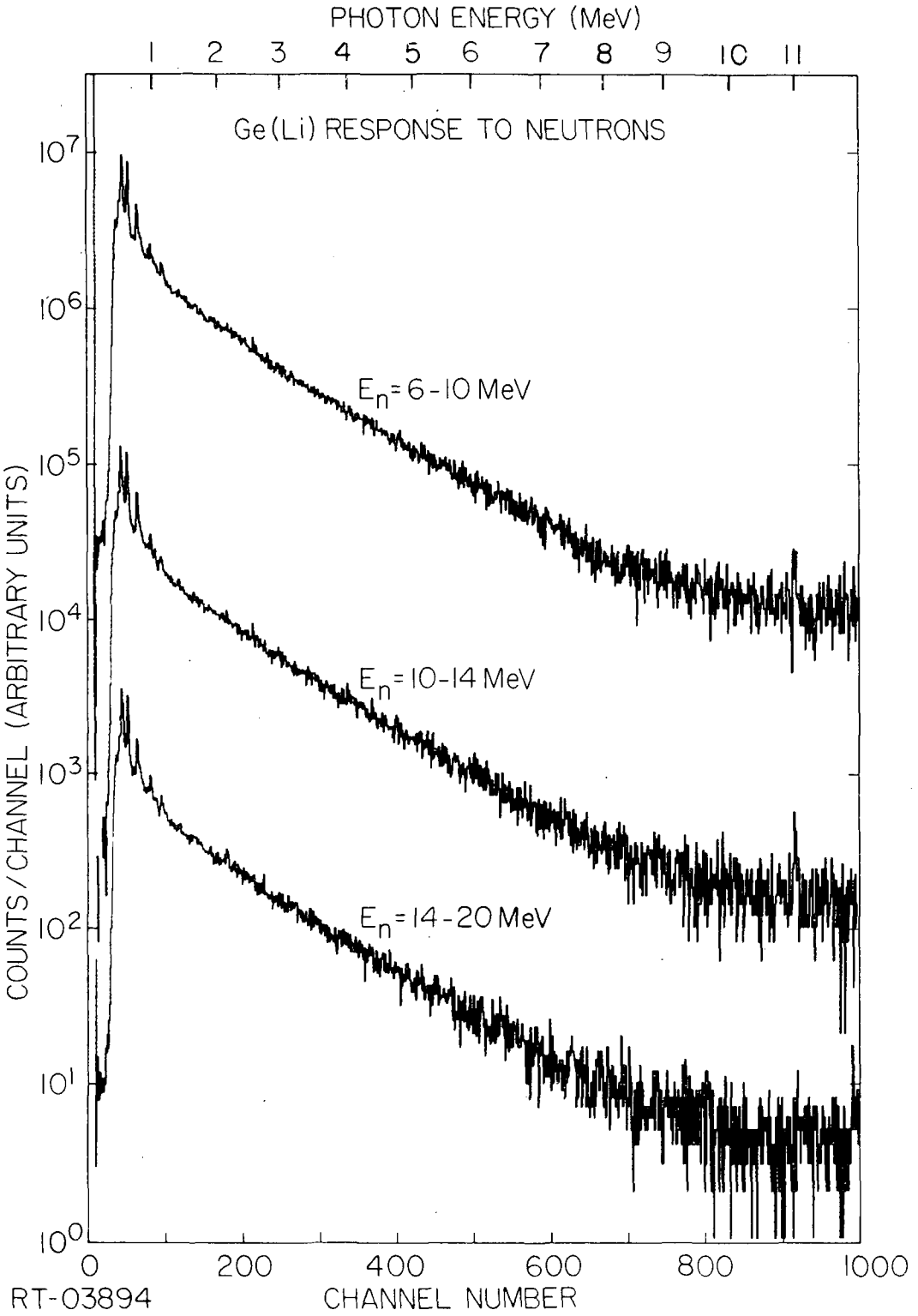

Figure A-1. Response of a 60 cm^3 Ge(Li) detector to incident neutrons between 6 and 20 MeV

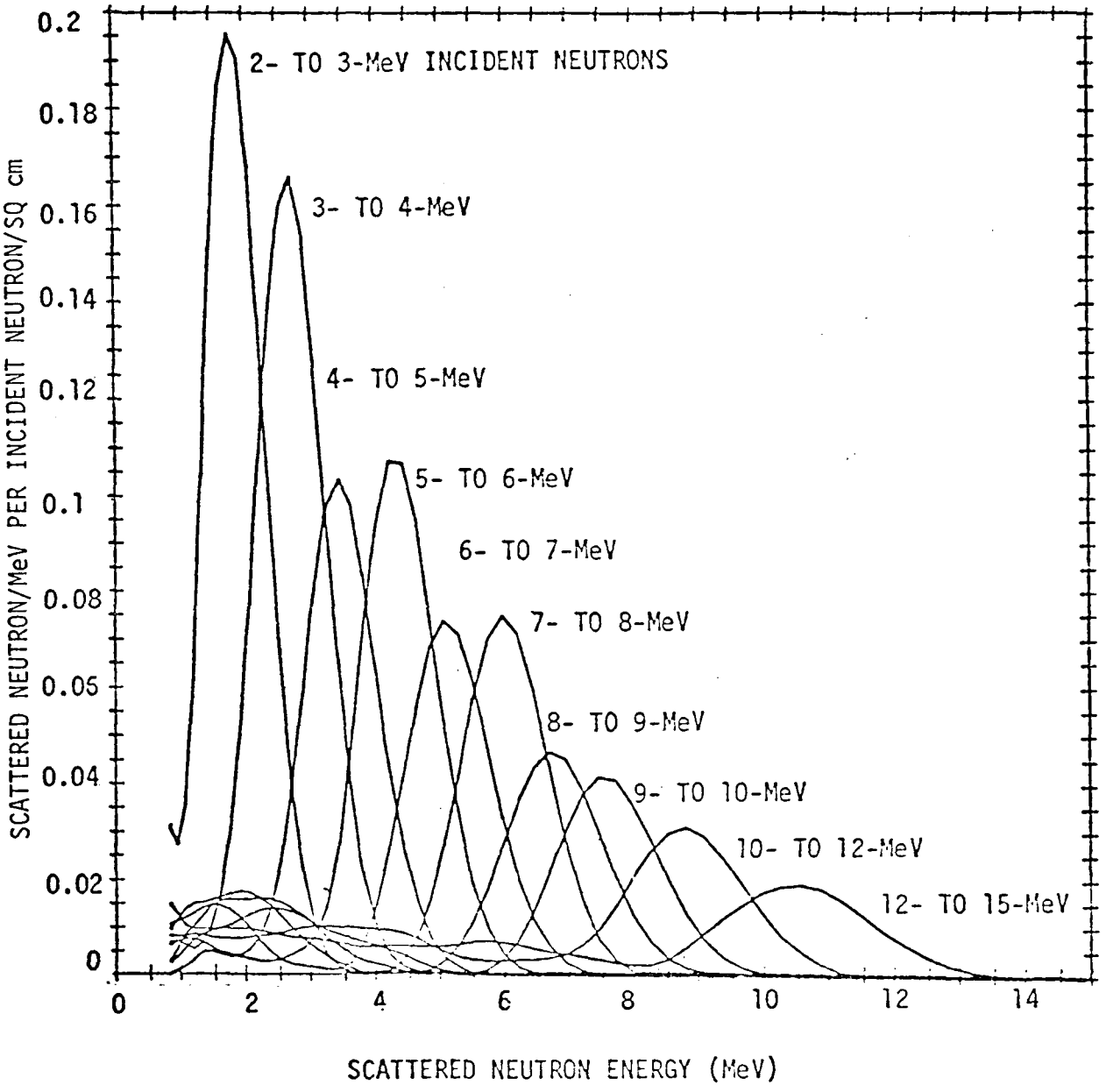

RT-04532

Figure B-1. Measured energy spectra of 125° scattered neutrons from 15 cm diameter liquid nitrogen sphere contained by 2.5-cm-thick styrofoam

reported here were carried out simultaneously with the NE-213 measurements by positioning the Ge(Li) detector on the opposite side of the incident neutron beam from the NE-213 detector at an angle of 125°, with respect to the incident neutron beam.

Figure B-2 shows a typical gamma-ray spectrum with the energies of principal gamma rays from the $^{14}N(n,x\gamma)$ reaction indicated above the corresponding gamma-ray peaks. Measured peak areas (referred to full energy peak counts) for major discrete lines normalized to the incident neutron flux in the corresponding neutron energy interval, are given in Table B-1. The intrinsic detector efficiency (given in Table B-1), the detector sample geometry, and the measured incident neutron energy spectrum[2] will permit calculation of the observed peak area counts using standard radiation transport codes and the latest evaluated cross-section data. Thus, the present data will permit a detailed test of the accuracy of the evaluated cross sections for many discrete lines from nitrogen.

C. CROSS-SECTION EVALUATIONS

1. Evaluations of Magnesium and Copper Cross Sections (M. K. Drake and M. P. Fricke)

Preliminary evaluations for magnesium and copper were completed. The cutoff date for incorporating new experimental data into these evaluations was November 1972. The recommended nuclear data has been sent in ENDF/B-III format to RSIC for incorporation into the DNA Working Library. The magnesium data tape has been assigned identification number MAT 4512 (MOD 0), while the copper has been assigned identification number MAT 4529 (MOD 0). A report documenting these two evaluations has been prepared and will soon be published.

D. FISSION STUDIES

1. Integral Photofission Experiments Near Threshold of ^{238}U and ^{232}Th (T. Gozani)

Low-energy photons are a very powerful tool for studying the fission process in general and the channel theory in particular, because of the small number of possible channels they can excite. The only practical intense sources of low-energy photons, $E_\gamma \leq 6$ MeV, are bremsstrahlung from low-energy Linacs or Microtrons. With such devices, directly measured

[2] L. Harris, Jr., G. D. Trimble, and J. C. Young, "Integral Experiment to Test Carbon and Nitrogen Cross Sections," DNA-2986F, Gulf Radiation Technology (1972).

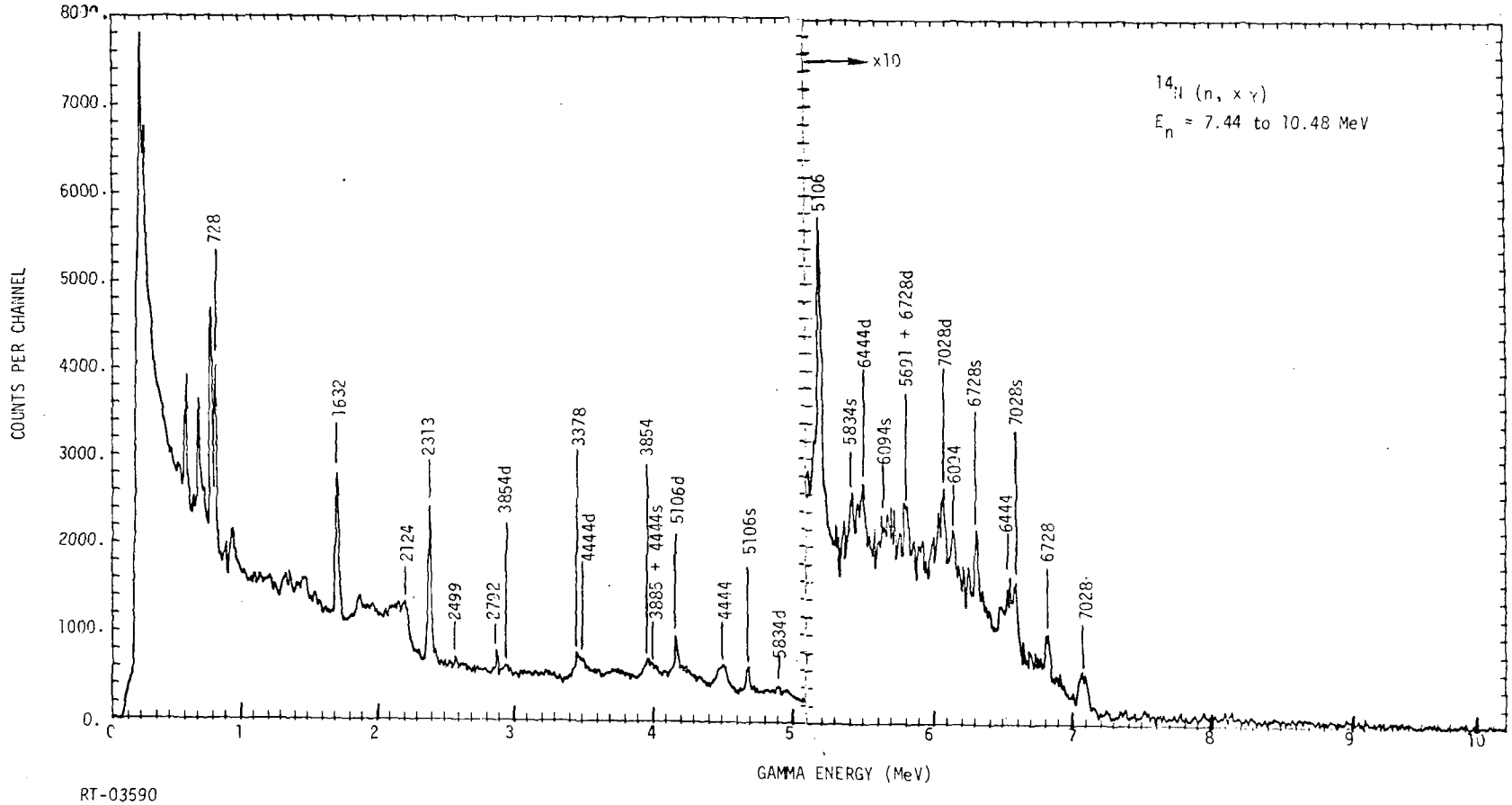

Figure B-2. Gamma-ray spectrum from $^{14}N(n,x\gamma)$ reactions for neutron energies of 7.44 to 10.48 MeV. Energies of principal gamma-ray lines are given in keV; d denotes double-escape peak and s denotes single-escape peak.

Table B-1

OBSERVED GAMMA-RAY PEAK COUNTS FROM $^{14}N(n,x\gamma)$ REACTIONS

E_γ (keV)	$\eta \times 10^3$ [a]	Full-Energy Peak Counts x 10^4 per Incident Neutron in $\Delta E_n/cm^2$			
		ΔE_n [b] 4.22-5.48	ΔE_n 5.48-7.44	ΔE_n 7.44-10.48	ΔE_n 10.48-15.40
728	149.		2.62 (.37) [c]	4.09 (.69)	3.32 (.66)
1632	64.1	2.17 (.06)	5.12 (.10)	4.03 (.05)	2.13 (.13)
2124	48.8	1.30 (.10)	1.84 (.12)	1.11 (.11)	0.80 (.25)
2313	44.6	2.09 (.08)	4.59 (.12)	4.91 (.15)	2.79 (.17)
2499	41.2		0.11 (.05)	0.28 (.07)	0.30 (.09)
2792	36.7		0.36 (.07)	0.63 (.07)	0.65 (.09)
3378	30.4			0.41 (.14)	0.61 (.18)
3684	27.8			0.08 (.06)	1.00 (.12)
3854	26.6				0.73 (.13)
3885	26.2			0.19 (.07)	0.18 (.08)
4444	22.3		1.15 (.09)	2.00 (.16)	1.94 (.17)
4913	19.4		0.19 (.05)	0.42 (.09)	0.33 (.08)
5106	18.2		0.52 (.04)	1.13 (.08)	0.94 (.09)
5691	15.0			0.07 (.03)	0.07 (.04)
5834	14.4			0.12 (.03)	0.19 (.05)
6094	13.1			0.11 (.04)	0.19 (.05)
6444	11.5			0.23 (.03)	0.12 (.04)
6728	10.4			0.17 (.03)	0.33 (.06)
7028	9.26			0.30 (.03)	0.60 (.06)

[a] Intrinsic full-energy peak efficiency

[b] Neutron energies in MeV

[c] Statistical errors given in parenthesis.

quantities are integrals, namely, yields. Previous measurements concentrated on fission fragment angular distribution, and on the fission yields (Y_f) from which the photofission cross section can be derived. The new results reported here concentrate on prompt (Y_n) and delayed (Y_d) neutron yields defined as the number of prompt and delayed neutrons, respectively, emitted per unit gamma-ray dose. The former quantity divided by the fission yield, namely Y_n/Y_f, below the (γ,n) threshold energy, is closely related to the number of prompt neutrons emitted per photofission (ν_n). Y_d/Y_f is closely related to the number of delayed neutrons per fission ($\nu\beta$). Y_n, Y_d, and Y_f were measured simultaneously using the Rad Tech high-current single-section low-energy Linac. Y_f was measured using fission foils sandwiched between solid state track detectors. Y_n and Y_d were measured using a thermalized neutron detector with a suppressed gamma sensitivity.

Targets like ^{232}Th and ^{238}U are very amenable for the study reported here because of their relatively high (γ,n) thresholds (6.4 MeV and 6.1 MeV, respectively), allowing one to investigate the photofission process with no competition from opening neutron channels. Some measurements with ^{235}U and ^{239}Pu targets were made for comparison.

The measured delayed and prompt neutron yields (the latter shown in Figure D-1), as well as the previously measured fission yield in the sub-threshold region of ^{232}Th show clearly the existence of structure in the photofission cross section around 5.7 to 5.8 MeV. Measurements on the other isotopes, namely ^{235}U, ^{238}U, and ^{239}Pu, made under exactly the same conditions did not indicate such a structure.

The ratio Y_n/Y_d (which is related to ν_n and to a much lesser extent to their energy spectrum) was determined as a function of the bremsstrahlung endpoint energy (E_e) from these experiments. It did not show, as expected, significant dependence on E_e around the threshold energy. It did, however, unexpectedly show an increase below the threshold energy for both ^{232}Th and ^{238}U (see Figure D-2). In the case of ^{232}Th the increase is rather dramatic.

Significant increase in the effective delayed neutron fraction in the sub-threshold regions was also observed as indicated by the curves shown in Figure D-3.

2. Correlation Between the Multiplicity and Spectrum of Prompt Fission Gamma Rays (T. Gozani)

The existence and extent of the correlation between energy spectra and the number of prompt neutrons (ν_n) and gamma rays (ν_γ) emitted from a fission is important to the understanding of some aspects of the fission process. This correlation may also appreciably influence the determination

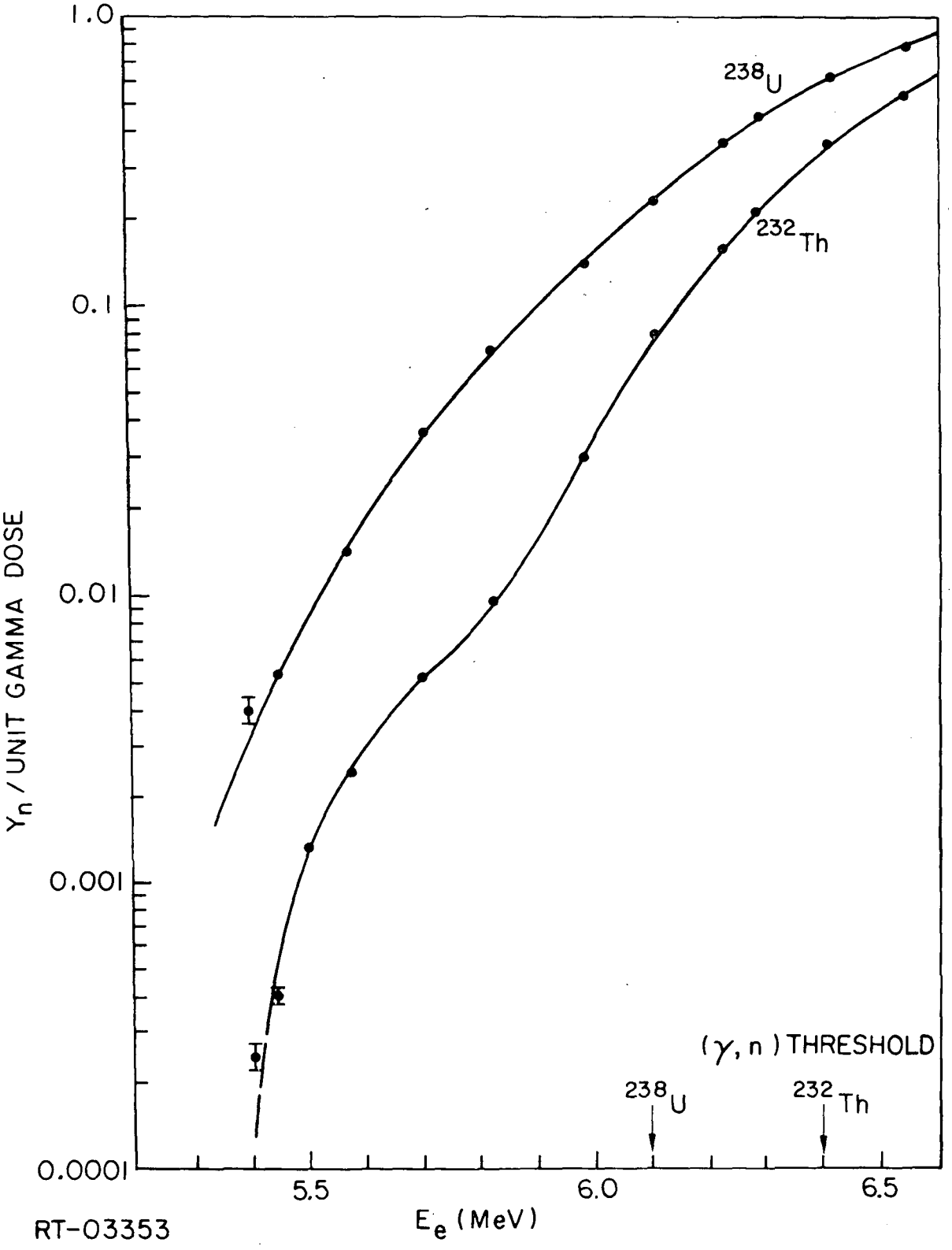

Figure D-1. Prompt neutron yields from photofission of ^{238}U and ^{232}Th

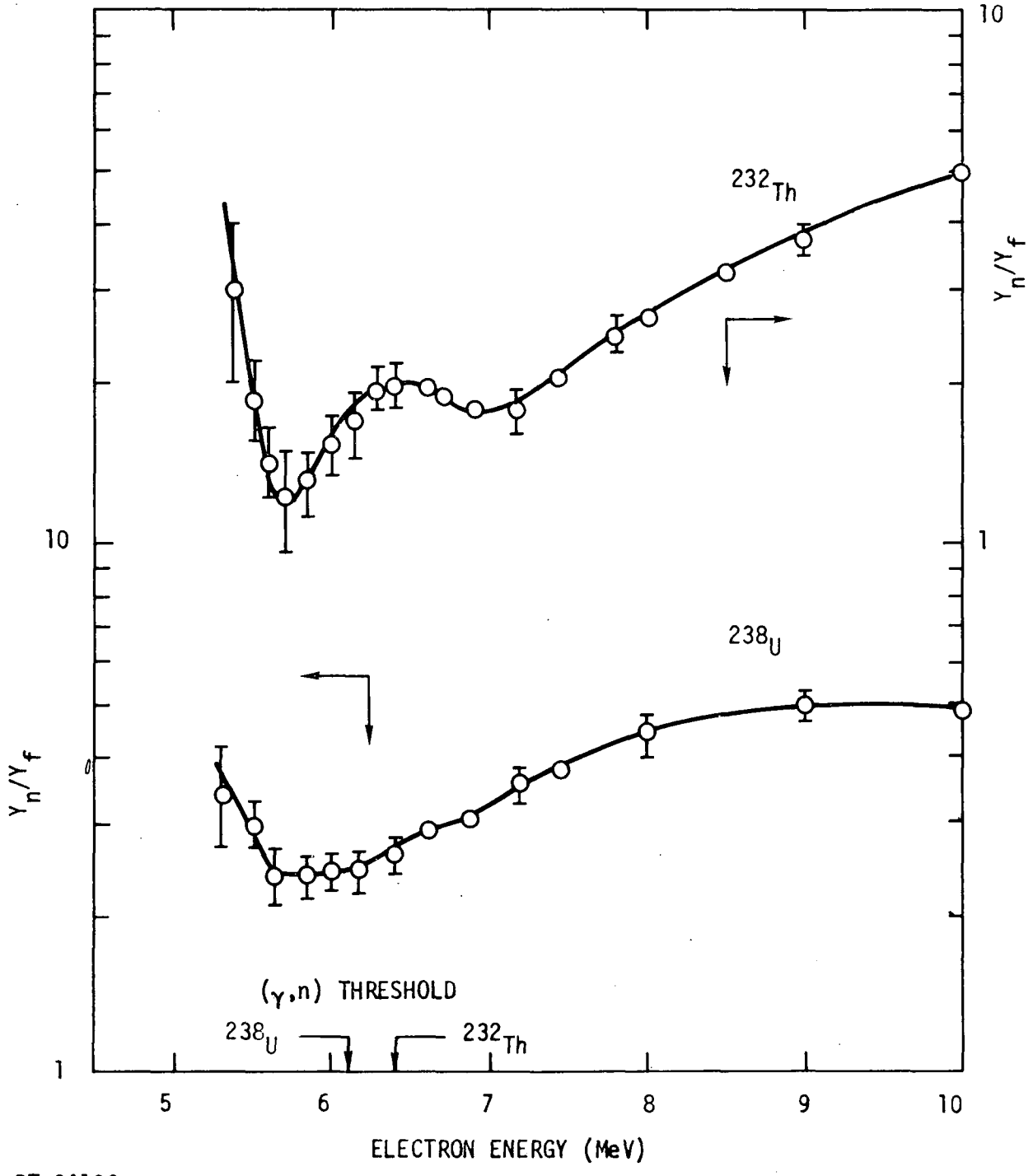

RT-04106

Figure D-2. Ratio of prompt neutron yield to total fission yield versus bremsstrahlung endpoint energy

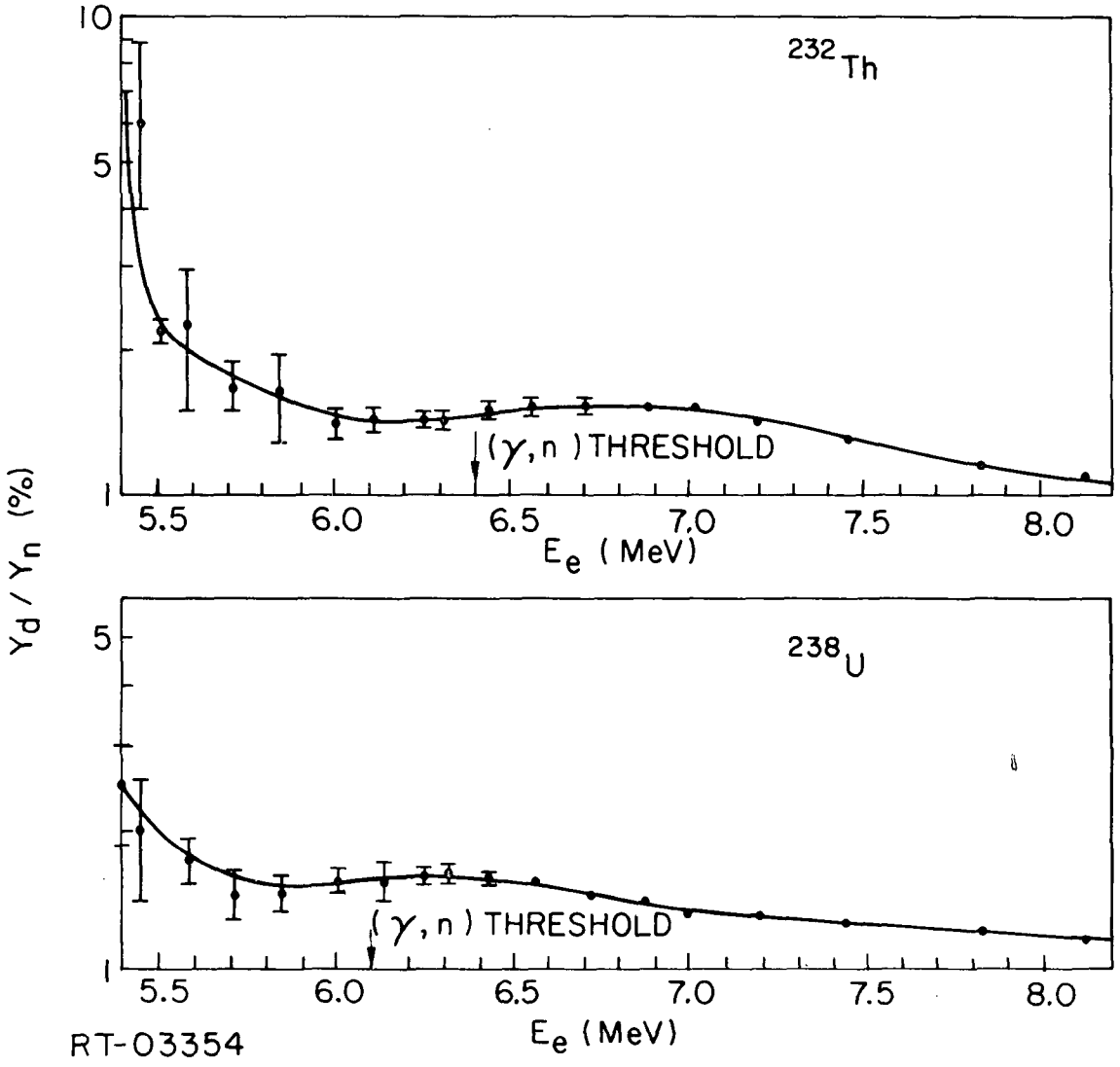

Figure D-3. Ratio of delayed neutron yield to total fission yield versus bremsstrahlung endpoint energy

of the detection efficiency of coincidence detectors, such as the Fission Multiplicity Detector (FMD), which are being used in increasing numbers in the nuclear industry.

In the case of prompt neutron emission from the spontaneous fissioning of ^{252}Cf, there is a strong indication that no correlation exists between the multiplicity of the emitted neutrons and their energy distribution. There are no similar measurements on the gamma multiplicity and its correlation to the energy distribution. This paper describes such a measurement.

The FMD consists of four large plastic scintillators which determine various degrees of the multiplicity by measuring coincidences between any two detectors out of the four, any three detectors out of the four, and all four detectors. The detection efficiency of the FMD is highly dependent on the ν_γ. For example, for a change of ν_γ from 3 to 8, the detection efficiency (for a certain energy bias condition) for any three detectors in coincidence changes from about 0.003 to 0.09. Thus, the FMD with its four detectors scans all gamma-ray multiplicities.

The experimental setup contained a surface barrier fission detector in contact with a small (0.005 μg) ^{252}Cf source placed at the center of the FMD. This geometry ensures almost complete elimination of the effects of any angular correlation between fission fragments and the prompt gamma rays which are detected by the surrounding FMD. When events with the required multiplicity are signaled, a linear gate is opened which lets a linear signal from a large 5 in. x 5 in. NaI(Tℓ) to be processed in a multichannel analyzer. The NaI(Tℓ) thus measures within its resolution limits the prompt fission gamma spectra of a limited range of ν_γ. This range is altered by changing the coincidence requirements from, say, 1 out of 4, 2 out of 4, through 4 out of 4. In addition to these measurements which were made at low bias (∿100 keV), a few measurements were done at higher bias (∿400 keV). In this case, only high-energy gamma rays can fulfill the coincidence requirements.

All spectra obtained with the NaI(Tℓ) were compared to the basic fission spectra, where only the fission detector gated the NaI(Tℓ).

The resultant spectra were rather similar — roughly decreasing exponentially with energy, thus indicating that the multiplicity of the prompt fission gamma rays is, to a large extent, uncorrelated with their energy spectra. A closer examination reveals that spectra taken with high-energy bias on the FMD are slightly softer than the fission spectrum. They show less photons of energy higher than 1.2 MeV by about 10%, while the low-energy region is higher by a few percent. Similar differences, but to a smaller extent, can be observed in the low bias cases. A typical

coincidence spectrum is shown in Figure D-4; also shown in the figure is the ratio of this spectrum to the fission spectrum. The ratio indicates some deficiency in the high-energy portion of the 3-out-of-4 coincidence spectrum.

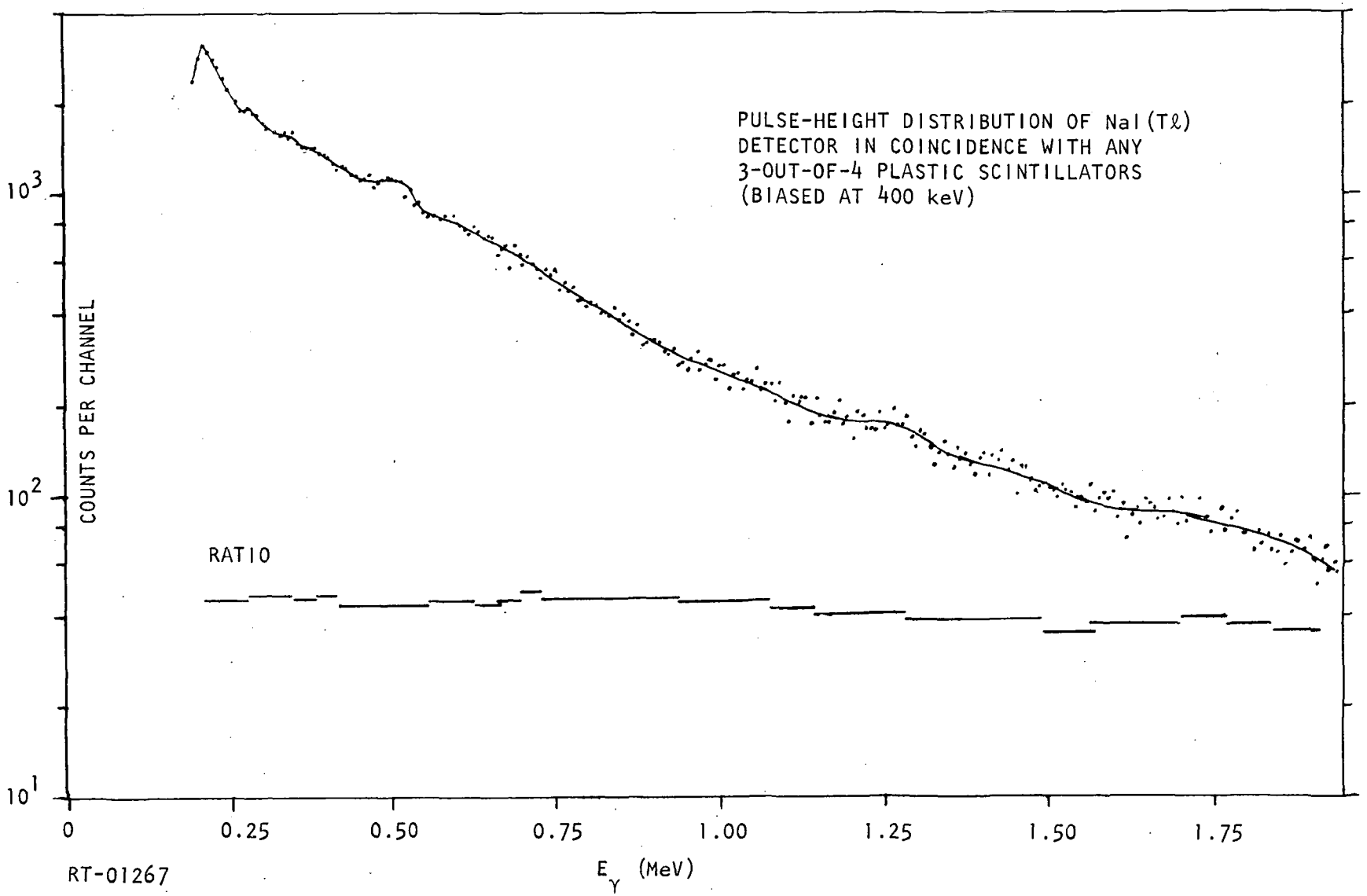

Figure D-4. Fission spectrum measured with NaI detector in coincidence with 3-out-of-4 plastic scintillators. Ratio of coincidence fission spectrum to basic fission spectrum.

UNIVERSITY OF IOWA

A. TOTAL INELASTIC CROSS SECTIONS FOR Li-Li AND Li-Be REACTIONS
(E. Norbeck, J. E. Poling, and P. L. Von Behren)

Lithium and beryllium are low Z materials with many exceptional physical, chemical, and nuclear properties. These elements are likely to be used for various purposes in the high temperature part of devices used in controlled thermonuclear research. Currently, lithium is used in LiD pellets as laser targets. The total inelastic (reaction) cross section has been calculated from elastic scattering data for the reactions $^{6}Li + ^{6}Li$,[1] $^{7}Li + ^{7}Li$,[1] (Fig. A-1) and $^{6}Li + ^{9}Be$ (Fig. A-2). As a check on the calculations, the measured cross sections for the $^{6}Li + ^{6}Li$ reaction were summed at 2 MeV center of mass energy. Estimates of the cross sections of unmeasured groups and continua were added to the sum. The resulting total cross section was found to be within errors for the total inelastic cross section calculated from elastic scattering. The errors for any of the points in the figures could be as much as 40%.

B. $^{9}Be(^{6}Li, 2n)^{13}N$ AND $^{7}Li(^{6}Li, 2n)^{11}C$

These data were extracted from thick-target yield curves.[2] Radioactive products such as ^{11}C may be used as an index of the occurrence of lithium reactions. These reactions are small, but we have evidence that the (^{6}Li, n) reactions are significantly larger.

C. $^{9}Be(^{7}Li, ^{8}Li)^{8}Be$ AND $^{9}Be(^{6}Li, ^{7}Li)^{8}Be$

It is interesting to compare the magnitudes of the cross sections for these two reactions. The (^{7}Li, ^{8}Li) cross section[3] is much larger than for the (^{6}Li, ^{7}Li) reaction.

D. $^{6}Li(^{6}Li, 3\alpha)$

The α-particle spectrum from this reaction shows a large high energy peak that corresponds to the entire Q value, 21 MeV, of the reaction being divided between two of the three α particles. The points shown in Fig. A-1 are the cross sections for producing this high energy peak.

---

[1] The curves were taken from L. L. Pinsonneault and J. M. Blair, Phys. Rev. 141, 961 (1966). Their results were in reasonable (± 40%) agreement with our preliminary results.
[2] E. Norbeck, Phys. Rev. 121, 824 (1961).
[3] E. Norbeck et al., Phys. Rev. 116, 1560 (1959).

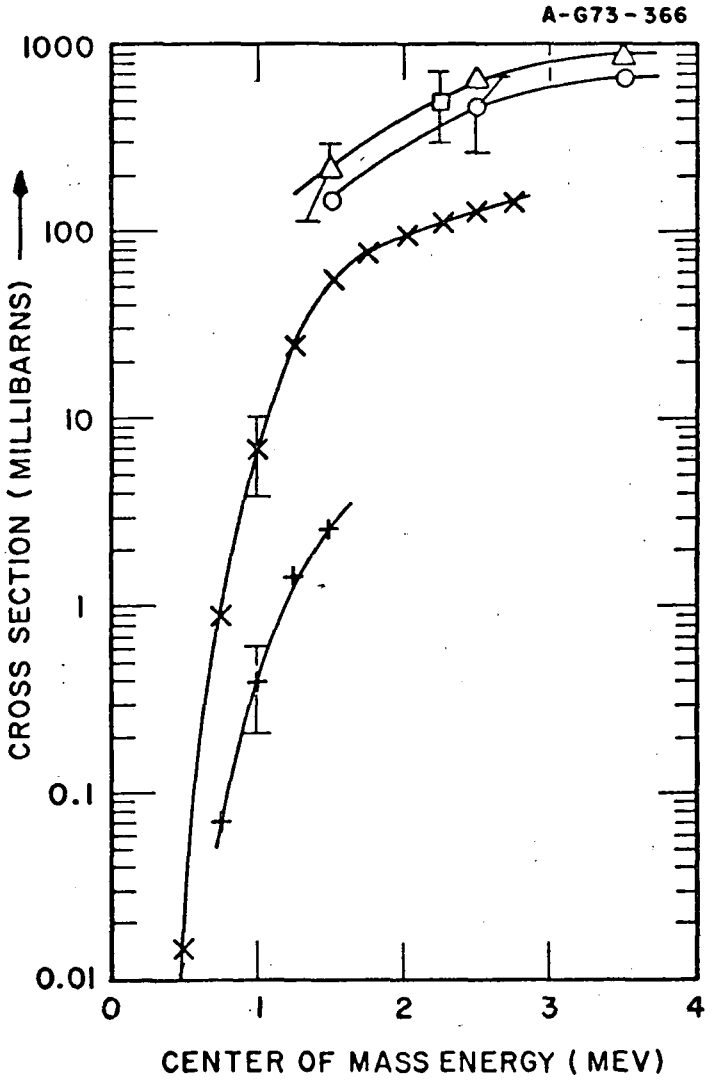

Fig. A-1. Reaction cross sections for lithium projectiles on lithium targets.

(+) $^{7}Li(^{6}Li, 2n)^{11}C$

(x) $^{6}Li + ^{6}Li \longrightarrow 3\alpha$ high energy peak only

(□) $^{6}Li + ^{6}Li$ total inelastic calculated from optical model fit to elastic scattering

(O) $^{6}Li + ^{6}Li$ total inelastic calculated from elastic scattering

(Δ) $^{7}Li + ^{7}Li$ total inelastic calculated from elastic scattering

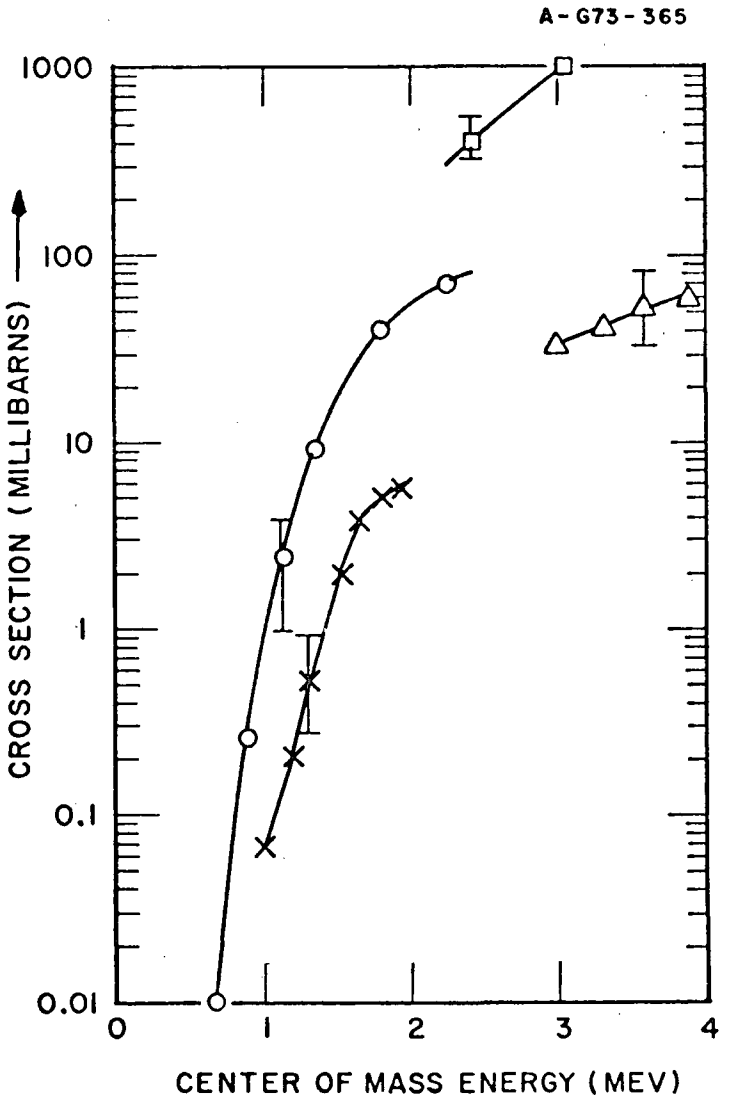

Fig. A-2. Reaction cross sections for lithium projectiles on beryllium targets.

(o) $^{9}Be(^{7}Li, {}^{8}Li)^{8}Be$

(x) $^{9}Be(^{6}Li, 2n)^{13}N$

(□) $^{6}Li + {}^{9}Be$ total inelastic calculated from optical model fits to elastic scattering

(△) $^{9}Be(^{6}Li, {}^{7}Li)^{8}Be$ total ^{7}Li yield

LAWRENCE LIVERMORE LABORATORY

A. NEUTRON PHYSICS

1. ^{235}U Fission Cross-Section Measurements (J. B. Czirr and G. S. Sidhu) Relevant to Requests 388, 389, 390 and 391.

Cross-section measurements are currently underway at the LLL Linac on the ratio of the ^{235}U fission to (n,p) scattering cross section from 2 to 20 MeV.

The fission data are obtained from twelve planar 0.1 mg/cm^2 foils placed in a cylindrical fission chamber. This chamber is rotated relative to the neutron beam in order to compensate for changes in the fission fragment angular distribution with incident neutron energy.

The neutron flux measurement is obtained from a recoil-proton telescope used in ring geometry with a ^7Li-glass scintillator as the proton detector. A 1 mg/cm^2 polyethylene radiator foil is replaced by a deposited carbon foil for background measurements.

Cross-section measurements from thermal to 2 MeV are planned following the completion of the above experiments. The accurate normalization of the high energy data to the well-known thermal values will await these latter results.

2. Fission $\bar{\nu}$ Measurements (R. E. Howe, T. W. Phillips and C. D. Bowman*) Relevant to Requests 395 and 452.

We are currently performing measurements of $\bar{\nu}$ for neutron-induced fission of ^{235}U in the energy range 0.5 to 100 eV. Fast, spectrally-independent detection of the prompt fission neutrons is achieved with the system previously described.**

Recent work has lowered experimental background rates and electronic deadtimes thus greatly reducing the magnitude of corrections applied to the data.

We are hoping to present our results at the IAEA Third Symposium on the Physics and Chemistry of Fission, August 13-17, 1973.

Future plans include completion of $\bar{\nu}$ measurements for ^{235}U from thermal energy up to 15 MeV. We also plan to evaluate $\bar{\nu}$ for ^{239}Pu neutron-induced fission over a similar energy range.

---

* National Bureau of Standards, Washington, D.C.

** USNDC Report, dated 10 November 1971, UCID-15937.

3. Isomeric Fission in ^{243}Pu (J. C. Browne and C. D. Bowman*) Relevant to Request 483.

Analysis of the results from an investigation of γ-decay emission from subthreshold fission groups** to the ground state in the second well for ^{243}Pu indicates the possibility of the existence of two fission isomers for this nucleus, one being the 33-ns isomer already observed and another being much longer-lived (∿100μs). If this is the case, the 33-ns isomer is consistent with being a two-quasiparticle state at an excitation energy of approximately 1.2 MeV above the ground state in the second well (whose excitation energy was previously measured to be 1.86 MeV above the equilibrium ground state). This work has been submitted for presentation at the Third Symposium on the Physics and Chemistry of Fission at Rochester, August 13-17, 1973.

4. Thermal-Neutron Fission Cross Sections of ^{251}Cf and ^{255}Fm (R. C. Ragaini, E. K. Hulet, R. W. Lougheed and J. F. Wild)

The thermal-neutron fission cross sections of ^{251}Cf and ^{255}Fm have been measured by comparison of fission rates with a ^{233}U reference standard. The values obtained are 4800 ± 250 barns for ^{251}Cf and 3400 ± 170 barns for ^{255}Fm. An initially pure sample of 20.3-h ^{255}Fm was fission counted alternately with a ^{233}U standard in the thermal column of the LPTR during its decay to 900-y ^{251}Cf. The atoms of ^{255}Fm-^{251}Cf and ^{233}U present on the thin targets were accurately determined by α-pulse analysis. A value of 531 barns was used for the fission cross section of ^{233}U in calculating the cross sections of ^{251}Cf and ^{255}Fm.

5. Decay of ^{248}Cf (E. K. Hulet and J. F. Wild)

The total half-life of ^{248}Cf has been determined to be 333.5 ± 2.8 d by long-term alpha and fission counting in ionization chambers. In addition, the alpha-to-spontaneous fission disintegration ratio was determined to be 35000 ± 3000, resulting in a SF partial half-life of $(3.2 \pm 0.3) \times 10^4$ y.

The fraction of ^{248}Cf alpha decays proceeding to excited levels in ^{244}Cm was measured by determining the fraction of alpha particles in coincidence with L X-rays arising from internal conversion decay of the excited levels in curium. This fraction, 0.170 ± 0.005, results in a calculated hindrance factor of ≥ 3.1 for decay to the first excited level in ^{244}Cm at 42.9 keV.

---

* National Bureau of Standards, Washington, D.C.
** USNDC Report, dated 10 October 1972, UCID-16136.

6. Transmission Data Analysis for Neutrons on ^{207}Pb (T. W. Phillips and B. L. Berman)

Data from the two-parameter measurement of the neutron total cross section of ^{207}Pb obtained as described in a previous report* is being analyzed to yield information on the decay width, spin, and parity of the levels of ^{208}Pb. The transmission function for neutrons has been obtained for energies between 90 and 1000 keV. The analysis of this transmission function is complicated by interference effects between adjacent levels and interference with the appreciable potential scattering which occurs at these energies. It has been found that to adequately account for these effects a large number of levels must be fit simultaneously. A computer code is being acquired to handle this problem. In the interim, a code which handles up to three levels with two possible spin states has been used. An example of the fit obtained in this manner is shown in Fig. A-1. The parameters for the three levels used in this fit are listed below.

E-resonance (keV)	Width (keV)	Spin and Parity
317.5	0.850	1^-
317.7	4.0	1^+
330.0	8.5	1^-

7. The ^{128}Te (n,γ) and ^{130}Te (n,γ) Cross Sections from 0.5 eV to 7 keV and the Xenon Anomaly in Old Tellurium Ores (J. C. Browne and B. L. Berman)

Preliminary results of this experiment were presented in a previous USNDC report.** Analysis of these data has been completed. Figures A-2 and A-3 show the ^{128}Te (n,γ) and ^{130}Te (n,γ) cross sections along with data taken using a natural tellurium sample. No resonances were observed for ^{128}Te below 425 eV and for ^{130}Te below 1143 eV. Calculation of the resonance absorption integral for the 16 resonances assigned to ^{128}Te and for the 6 resonances assigned to ^{130}Te indicates that the ratio of $^{129}Xe/^{131}Xe$ that could be formed in tellurium ores which were bombarded by a 1/E neutron flux is 3.8 ± 0.55. The measured ratio† in tellurium ores varies from 1.6 to 3.0. The ratio of $^{129}Xe/^{131}Xe$ predicted by thermal-neutron capture alone is 0.6. Therefore, the measured ratio will depend on the thermal/epithermal flux ratio incident on the tellurium ores throughout their history.

---

* T. W. Phillips and B. L. Berman, USNDC Report dated 10 November 1971, UCID-15937.

** J. C. Browne and B. L. Berman, USNDC Report dated 10 October 1972, UCID-16136

† B. Srinivasan, E. C. Alexander, Jr. and O. K. Manuel, J. Inorg. Chem. 34, 2381 (1972).

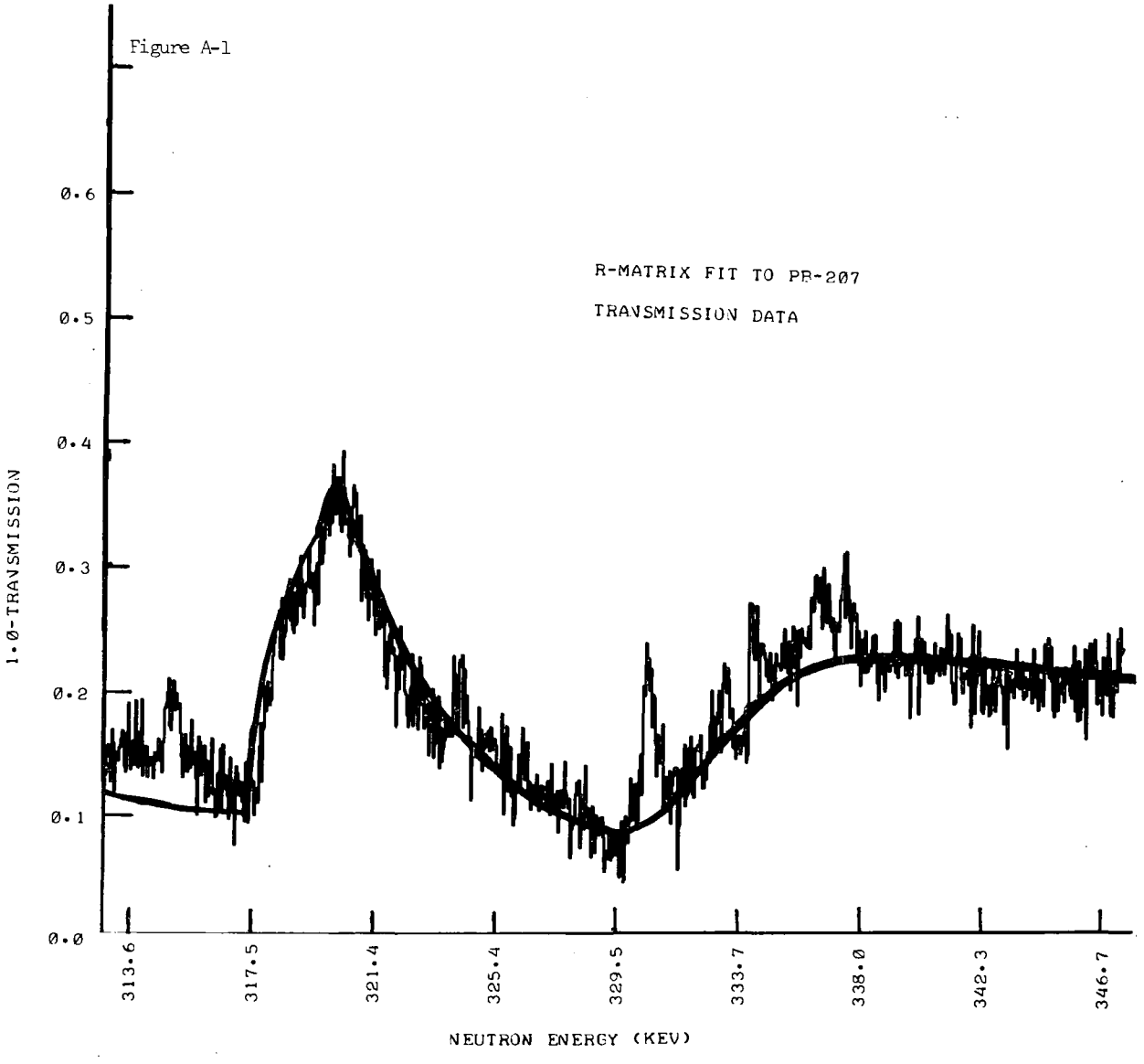
Figure A-1
R-MATRIX FIT TO PB-207
TRANSMISSION DATA
1.0-TRANSMISSION
0.6
0.5
0.4
0.3
0.2
0.1
0.0
313.6
317.5
321.4
325.4
329.5
333.7
338.0
342.3
346.7
NEUTRON ENERGY (KEV)

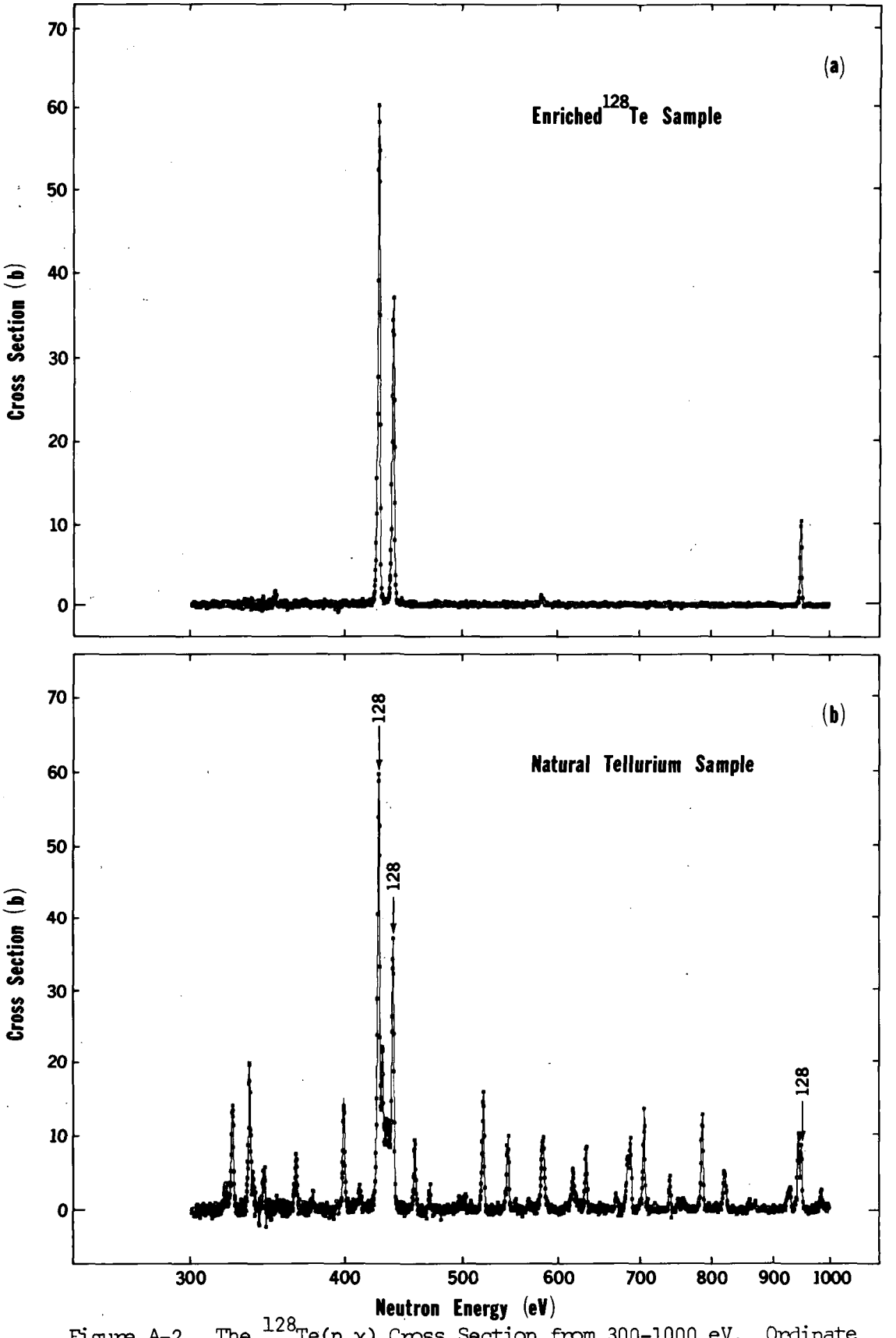

Figure A-2. The $^{128}Te(n,\gamma)$ Cross Section from 300-1000 eV. Ordinate scale for natural Te sample refers to ^{128}Te only.

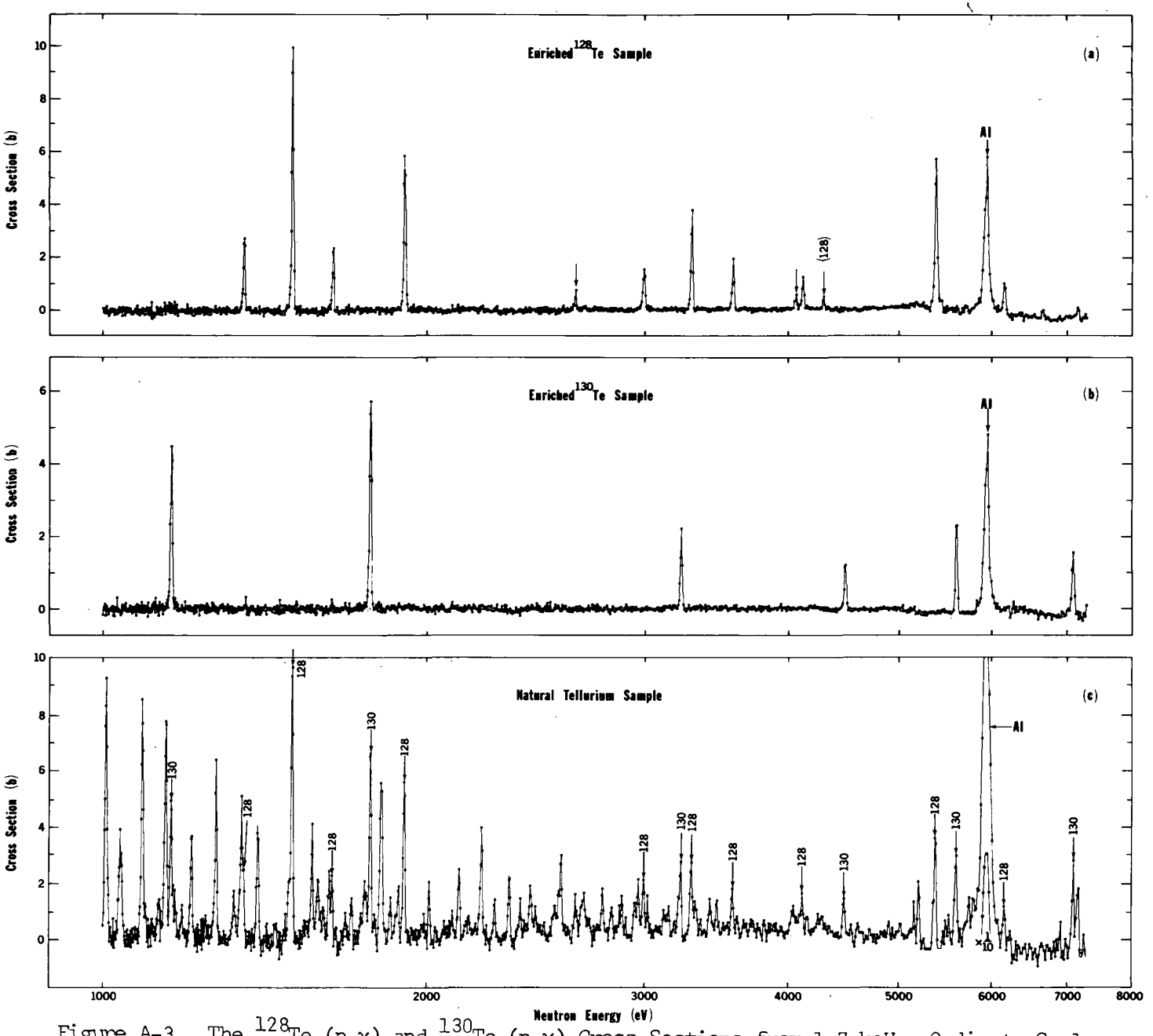

Figure A-3. The ^{128}Te (n,γ) and ^{130}Te (n,γ) Cross Sections from 1-7 keV. Ordinate Scale for natural Te sample refers to ^{128}Te and ^{130}Te resonances only.

Previous neutron total cross-section measurements* on natural tellurium have extracted $ag\Gamma_n^o$ for various resonances in this energy range. (a = fractional abundance of an isotope). Since we can assign resonances to ^{128}Te and ^{130}Te, we can thus obtain values of $g\Gamma_n^o$ for these resonances. These values of $g\Gamma_n^o$ are listed in Tables A-1 and A-2 From the area under these resonances we can also extract values for $g\Gamma_\gamma$ for these resonances which are listed in Tables A-1 and A-2.

Table A-1. ^{128}Te Resonance Parameters

Present Results		Previous Measurements	
E_o	$g\Gamma_n\Gamma_\gamma/\Gamma$ (meV)	$g\Gamma_n^o$ (meV)*	$g\Gamma_\gamma$ (meV)
424.9	14.4	1.20	34
436.4	9.2	0.5	74
944	8.8	0.17	--
1323	5.85	0.09	--
1461	23.7	2.83	39
1587	6.2	0.25	17
1839	26.7	12.3	28
2969	21.2	14.5	22
3268	47.4	1.42	114
3549	27.9	0.5	398
4082	30.1	0.79	75
4256	10.45	0.38	18

Table A-2. ^{130}Te Resonance Parameters

Present Results		Previous Measurements	
E_o	$g\Gamma_n\Gamma_\gamma\ \Gamma$ (meV)	$g\Gamma_n^o$ (meV)*	$g\Gamma_\gamma$ (meV)
1143	7.85	0.32	29
1715	21.5	1.02	44
3201	25.9	0.84	57
4450	31.7	2.0	42

* S. Wynchank, J. B. Garg, W. W. Havens, Jr. and J. Rainwater, Phys. Rev. 166, 1234 (1968).

8. Capture γ-Ray Spectra for ^{181}Ta (n,γ) from 2 eV to 5000 eV. (M. L. Stelts and J. C. Browne)

The spectra of γ-rays from the ^{181}Ta (n,γ) reaction have been measured for incident neutrons in the energy range of 2 eV to 5000 eV using the LLL linac. The γ-rays from the Ta sample located at 13.4 meters from the neutron source were detected by a three-crystal (Ge(Li) - NaI) spectrometer with an energy resolution of 6 keV for 6-MeV photons. The energy scale and absolute efficiency were measured using calibrated radioactive sources and the Cl ($n_{thermal}$,γ) reaction. Data were stored on a magnetic drum in a two-dimensional array of 4096 pulse-height channels by 624 time-of-flight channels. The resolution of the experiment was such that most resonances below 200 eV were resolved.

Figure A-4 shows a portion of the pulse-height spectrum for the highest energy γ-rays obtained by summing over all neutron energies from 2 eV to 60 eV. The ground-state transition is indicated by "GS" and higher excited states by integer labels. All levels seen in the ^{181}Ta (d,p) reaction* and the ^{181}Ta ($n_{thermal}$, γ) reaction** below 1-MeV excitation energy are seen here plus many states not excited in these reactions.

The γ-ray spectra for individual neutron resonances exhibit marked intensity variations from resonance to resonance for the various transitions. Data analysis to extract the partial γ-decay widths for individual resonances is in progress.

9. Capture Cross-Section Measurements (J. B. Czirr and M. L. Stelts)

A paper with the title Capture Cross-Section Measurements for ^{165}Ho and ^{197}Au has been submitted for publication. The abstract for this paper is as follows:

As part of a continuing program to accurately measure neutron-capture cross sections, we have obtained data for ^{165}Ho and ^{197}Au in the 167 eV to 0.6 MeV energy range.

All capture reactions are measured relative to the fission rate of ^{235}U for neutron energies above 800 eV and to the ^{10}B ($n,\alpha_0+\alpha_1$) reaction below 20 keV. In addition, current best estimates of $\sigma_F(^{235}U)$

---

* J. R. Erskine and W. W. Buechner, Phys. Rev. 133, B370 (1964).

** G. A. Bartholomew, J. W. Knowles, G. Manning and P. J. Campion, Atomic Energy of Canada Limited. Progress Report No. 517 (1957), unpublished.

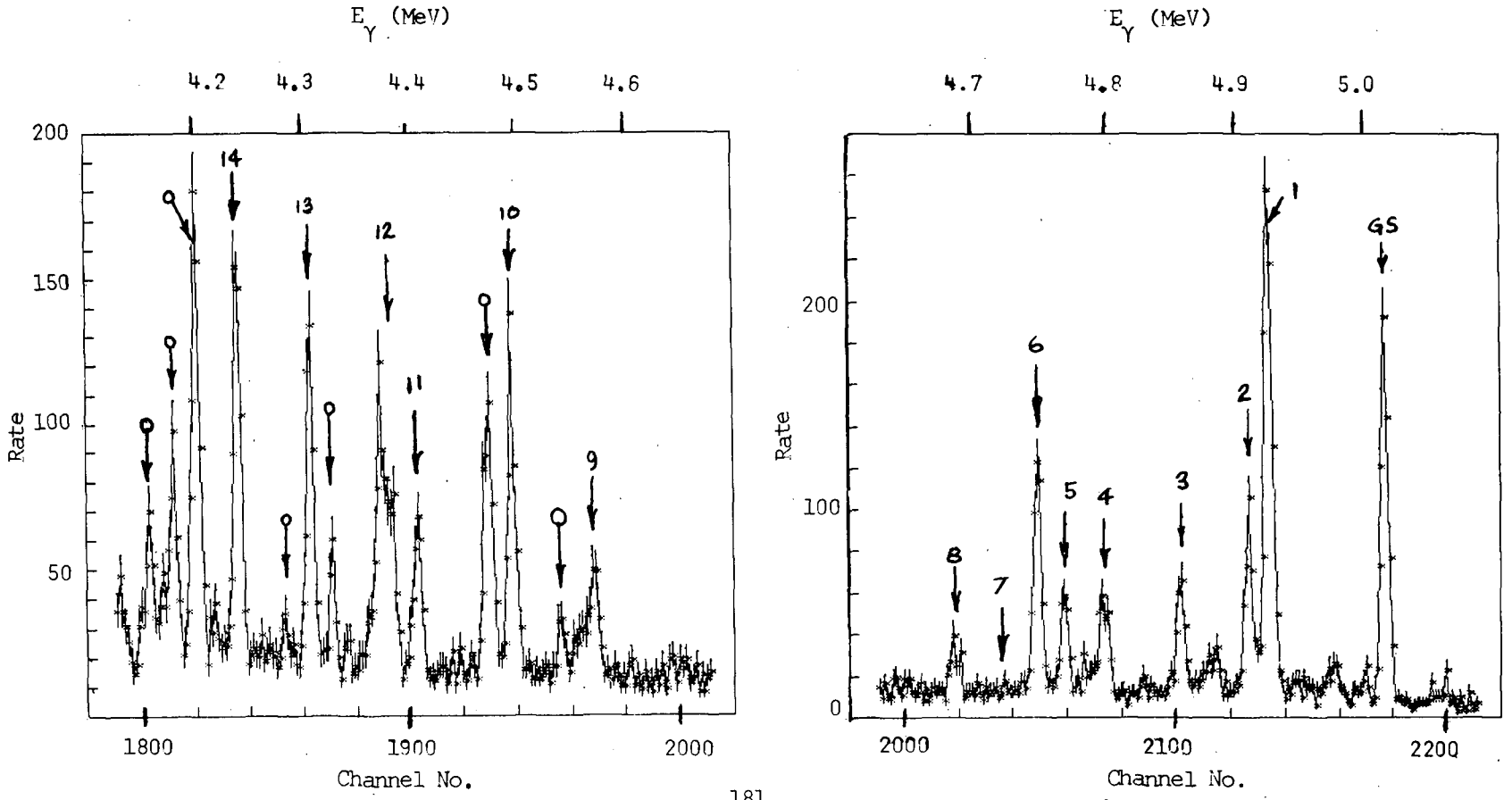

Figure A-4. A portion of the γ-ray spectrum from ^{181}Ta (n,γ) reaction for 2eV $\leq E_n \leq$ 60eV. The γ-ray energies refer to the double-escape peak as measured by the GeLi-NaI three-crystal spectrometer. The numbers listed on the peaks coincide with the levels seen in the ^{181}Ta (d,p) reaction. The peaks shown with an open circle were not observed in the (d,p) study.

and $\sigma_{n,\alpha}(^{10}B)$ are used to convert these ratios to up-to-date capture cross sections. The 3.9 eV "black resonance" of ^{165}Ho is used to normalize all cross sections.

Data have also been obtained for natural In in the 300 eV to 0.6 MeV energy range and will be published in the near future.

10. Cross Sections for Gamma-Ray Production by 14-MeV Neutrons (L. G. Multhauf and S. M. Matthews)

For many elements, γ-ray production cross sections at 14-MeV neutron energy either have not been accurately measured, or can not be determined with confidence due to inconsistencies in reported values. We are undertaking, therefore, to measure this cross section for a range of elements using the high-flux 14-MeV-neutron facility at LLL.

The samples are placed in a ring geometry about the neutron source at a distance of 8 meters from the detector which is shielded from the major sources of neutron-induced background by a 1.9-meter-thick cement wall. In addition, time-of-flight measurements provide a clean separation between γ-rays produced in the sample and scattered neutrons. Preliminary measurements have shown background levels to be very low.

Monte Carlo calculations are being made for each sample material to determine the effects of both γ scattering and neutron multiple scattering. Ring dimensions for each element will be chosen such that these effects are either negligible or small enough that a correction can be made to the spectrum.

The detector systems consist of a 30-cm x 30-cm NaI(Tℓ) annulus operating in an anticompton mode, and having as a central detector either a large volume Ge(Li) crystal or a NaI(Tℓ) well crystal of dimensions selected to optimize the peak efficiency and peak-to-total ratio. The well detector will be used to measure continuum γ-rays. The measured spectra will then be unfolded using measured detector response functions.

We have constructed a set of proton-recoil counters to measure the neutron flux. We will also use isotopic activation for an independent determination of the flux. We have employed, for example, ^{24}Na activation, using the well measured $^{27}Al(n,\alpha)$ cross section.

B. PHOTONUCLEAR PHYSICS

1. Photoneutron Cross Sections of ^{55}Mn and ^{59}Co (R. A. Alvarez, B. L. Berman, F. H. Lewis, and P. Meyer)

We have measured the photoneutron cross sections of ^{55}Mn and ^{59}Co from threshold to 36 MeV using photons from in-flight annihilation of positrons from the new Livermore positron-electron linac. The technique and apparatus used were essentially identical to those employed in a number of previous experiments; a description appears in the literature.* The principal differences in the present measurement were the higher available positron beam currents (which made possible measurements with higher photon energy resolution) than were available on the old Livermore linac, and a remote-controlled target-sample changer, which allowed measurements at each beam energy to be made on each isotope with identical accelerator and beam-transport system tuning. This improvement in the technique provides added confidence that fine structure observed in one isotope but not the other is indeed an effect of the nuclear dynamics and not a fluctuation caused by the apparatus.

Our results are shown in Figs. B-1 and B-2. The photon energy resolution is approximately 90 keV at 10 MeV and 160 keV at 35 MeV. Error bars shown are statistical only. In addition there are several sources of systematic uncertainty, which could introduce overall errors into the absolute cross section of up to about 10% in the region of the giant resonance peak and perhaps 40% at 35 MeV.

In both nuclei the giant resonance is rather broad and is divided into three main groups of substructures. There is a considerable amount of superimposed fine structure from theshold to 25 MeV or higher. Fine structure is evident in the $(\gamma,2n)$ cross section of both isotopes, as well. The integrated total cross sections are 807 MeV-mb for ^{55}Mn and 894 MeV-mb for ^{59}Co, while the integrated $(\gamma,2n)$ cross sections are 166 MeV-mb and 139 MeV-mb, respectively. The $(\gamma,3n)$ cross sections of both nuclei are very small.

C. APPLICATIONS

1. Intense Sources of Fast Neutrons (H. H. Barschall)

Methods for producing intense sources of neutrons of average energy above 10 MeV are investigated for applications in biology, medicine, radiation damage studies particularly for the CTR program, and cross section measurements.

---

* B. L. Berman *et al.*, Phys. Rev. 162, 1098 (1967).

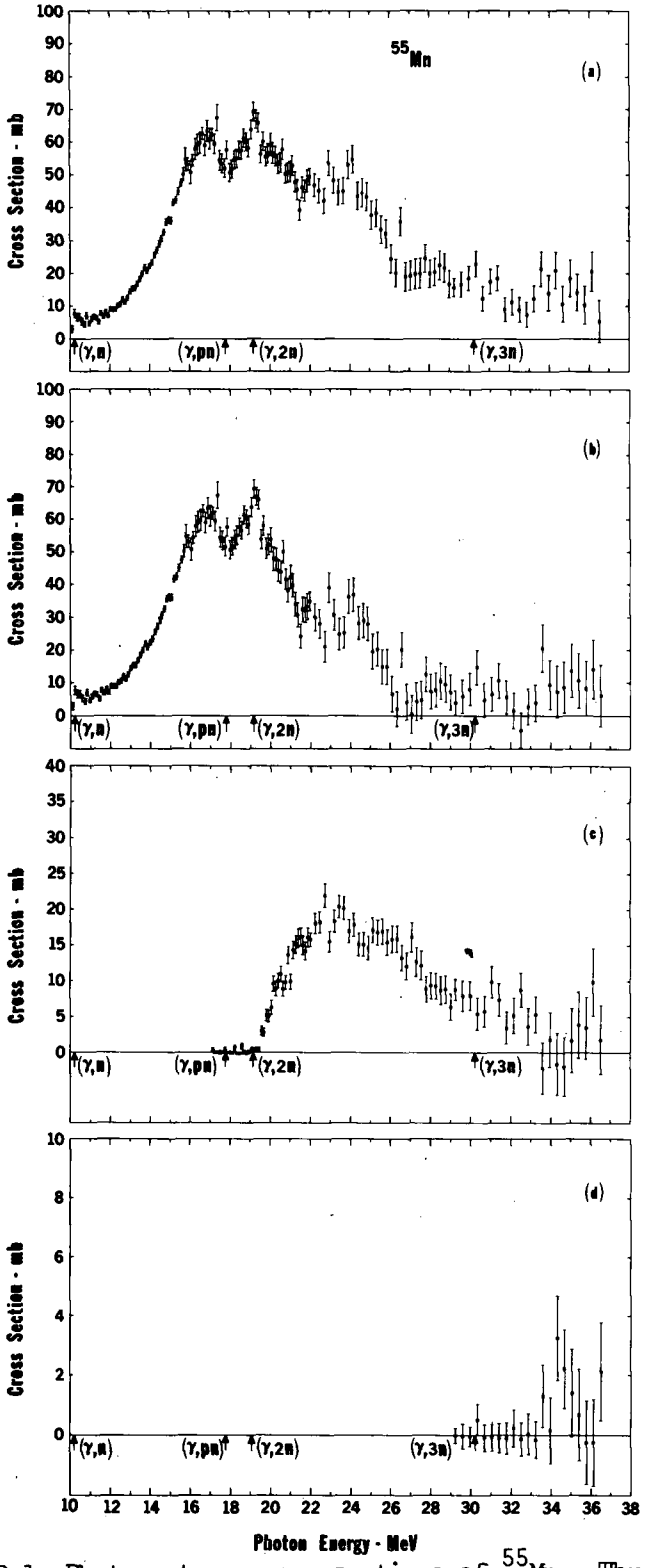

Figure B-1 Photoneutron cross sections of ^{55}Mn. Thresholds are indicated by arrows. (a) Total photoneutron cross section: $\sigma[(\gamma,n) + (\gamma,pn) + (\gamma,2n) + (\gamma,3n)]$; (b) $\sigma[(\gamma,n) + (\gamma,pn)]$; (c) $\sigma(\gamma,2n)$; (d) $\sigma(\gamma,3n)$.

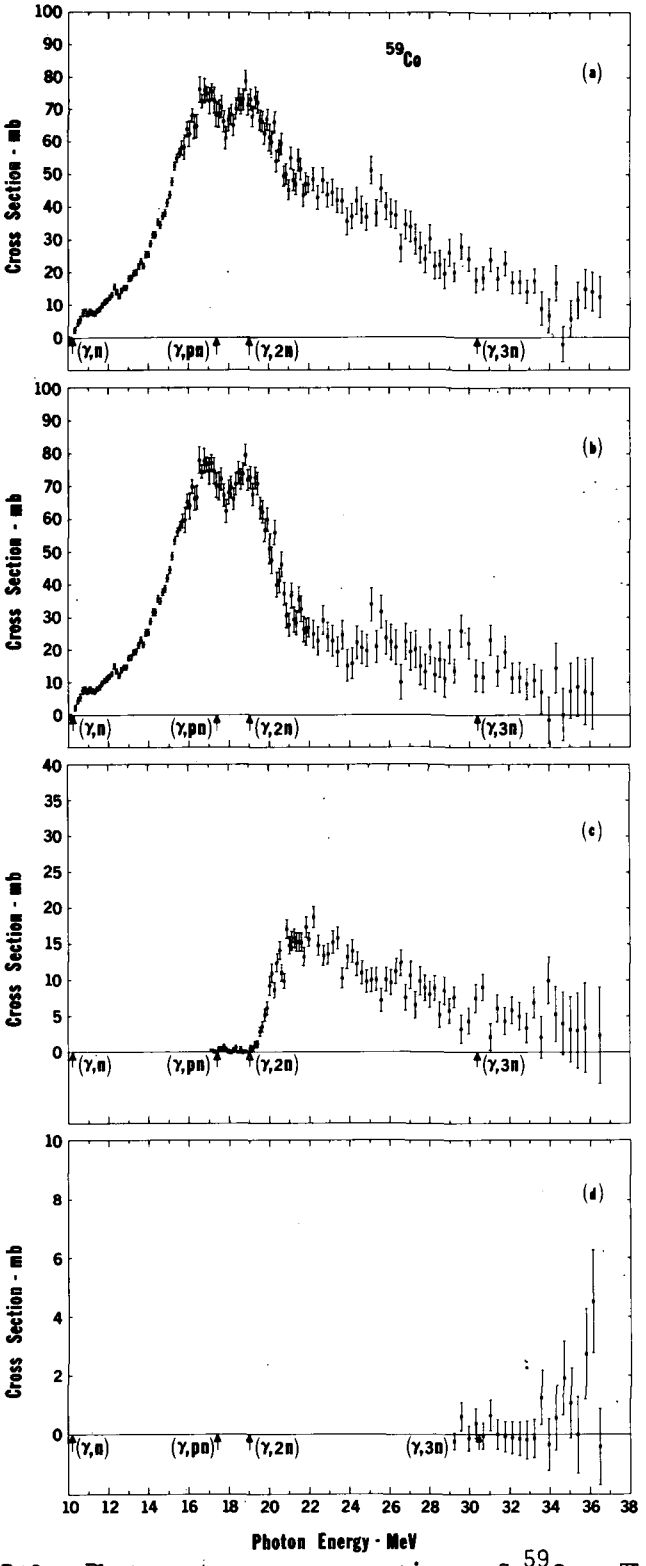

Figure B-2. Photoneutron cross sections of ^{59}Co. Thresholds are indicated by arrows. (a) Total photoneutron cross section: $\sigma[(\gamma,n) + (\gamma,pn) + (\gamma,2n) + (\gamma,3n)]$; (b) $\sigma[(\gamma,n) + (\gamma,pn)]$; (c) $\sigma(\gamma,2n)$; (d) $\sigma(\gamma,3n)$.

(a) Intense source of 15-MeV D-T neutrons. The rotating tritium target previously described has been replaced by a 22-cm diameter target. (UCRL-74285). The new target permits operation at higher source strength. In 30 hours of operation at a source strength between 2.5 and 3.0 x 10^{12}/sec no appreciable decrease in source strength was observed. During this operation a fluence of $10^{17}/cm^2$ was delivered to a small sample for radiation damage studies. A new high-voltage power supply, which is scheduled for delivery in June 1973, should permit operation at higher source strength.

(b) A study of the neutron production from deuteron bombardment of deuterium, lithium, beryllium, and carbon targets has been completed. In UCRL 51310-Addendum, spectra and yields are given for the following conditions:

Target	Deuteron Energy (MeV)	Lab Angle
Thick Li	5 - 19	3° - 32°
Thick Be	3 - 20	3° - 32°
Thick C	12 - 18	3° - 32°
Thin D	16.5 and 18.6	3°, 9°, 32°
Thin Be	5 - 18	3° - 32°

Average neutron energies and available doses are presented in UCRL-51310.

2. Ozone-Tagging for Biomedical Purposes (P. Meyer)

Ozone has been identified as a significant component of ambient air pollution where atmospheric photochemical activity occurs. The importance of ozone (O_3) as a toxicant is recognized and several of its effects have been defined, although the damage mechanism is still uncertain. At present, the distribution of the ozone-uptake throughout the respiratory system is unknown.

We have investigated the possibility of tagging ozone with an oxygen isotope, ^{15}O, a positron emitter with a half life of 122 seconds. With the use of the Anger positron camera* at the Livermore Linac, one can then in principle visualize the distribution of the radioactive ozone (or other gases) by observing the annihilation gamma rays from the decaying oxygen isotope.

The ^{15}O isotope is obtained by irradiating ^{16}O, with bremsstrahlung from the 100 MeV Linac, via a (γ,n) reaction in ^{16}O. The measurement of the ratio of activated to unactivated ozone, O_3^*/O_3, is the object of this experiment. Results using O_2 as a target gas indicate that an O_3 concentration of 1 ppm and a ratio of $^*O_3/O_3$ of 8 x 10^{-10} are the saturation points at the end of an irradiation. All the ozone is trapped at dry-ice temperature and then mixed with a breathing gas in varying proportions for use in a practical application.

*H. O. Anger, Scintillation Camera and Positron Camera in Medical Radioisotope Harming, (IAEA, Vienna, (1959), p. 59.

Preliminary experiments with small dogs have recently been carried out with the 16-inch diameter Anger camera at Livermore. Ozone concentrations used were 1 ppm and 5 ppm. Early results indicate that oxygen as a target gas provides sufficient amounts of tagged ozone to do useful lung function studies with ozone concentrations of perhaps $\geq .1$ ppm. Activated nitrogen, ^{13}N, carbon dioxide, ^{11}C, and oxygen were also used for comparison. Data analysis is in progress at this time.

D. FACILITIES

1. Livermore Cyclograaff Facility (J. C. Davis and J. D. Anderson)

The Livermore Cyclograaff is the successor to the 90" variable energy cyclotron used for basic and programmatic research at Livermore for fifteen years. The 90" cyclotron was shut down and dismantled in February 1971 and the cyclograaff became fully operational for experimental use in late 1972. Easy production of high resolution or pulsed proton beams over the 1-27 MeV energy range was the primary advantage of the cyclograaff as a replacement accelerator. However, the high versatility with respect to particle species, beam energy, and beam intensity as well as significant financial advantages over alternate accelerators were important in the selection of the cyclograaff. The physical layout of the cyclograaff facility is shown in Fig. D-1. Most of the nuclear physics experiments in progress utilize microampere proton beams in either a high resolution mode for charged particle spectroscopy ($\Delta E/E \leq 0.1\%$) or in a pulsed mode for neutron time-of-flight and gamma ray production studies ($\Delta t \sim 1$ ns, $f \sim 5$ MHz). Similar work will be done with the 1-20 MeV deuteron beam. A detailed description of the accelerator facility and the pulsed beam capbilities appears in the June 1973 issue of the IEEE Transactions On Nuclear Science.

E. DATA COMPILATION

1. Atlas of Photoneutron Cross Sections Obtained with Monoenergetic Photons (B. L. Berman)

A compilation, in a uniform format and current as of early 1973, of photoneutron cross-section data obtained with monoenergetic photons from positron annihilation in flight has been issued as UCRL-74622. This atlas was distributed at the International Conference on Photonuclear

Reactions and Applications in March. The USNDC has, of course, expressed its great desire that such a compilation be made available for a variety of applications purposes.

Over the years, a considerable body of data on photoneutron cross sections obtained with monoenergetic photons from the annihilation in flight of fast positrons has been acquired at the Livermore, Saclay, and General Atomic Laboratories. The data on 65 nuclei studied with annihilation photons (49 from Livermore measurements, 25 from Saclay, and two from General Atomic) are gathered together here and presented in a uniform format, in order to serve as a nucleus for a more complete compilation and evaluation (which would include data obtained with continuous bremsstrahlung radiation sources as well). The photonuclear group at the National Bureau of Standards is undertaking such a comprehensive compilation and evaluation, and the data in this atlas will be a major part of it. Meanwhile, these data are available in both graphical and digital form. It is hoped that this service to the physics community will be utilized both for purposes of theoretical analysis and for those associated with applications to other scientific disciplines and technologies.

No attempt was made here to evaluate the data; i.e., to choose between two sets of data for the same nucleus measured at different laboratories, or to compromise between them by presenting a set of recommended intermediate values. It should be noted, however, that the overall agreement and consistency between measurements made at the three laboratories is very good indeed, especially when viewed in the light of the enormous discrepancies between laboratories frequently obtained in the past for bremsstrahlung-induced photonuclear measurements.

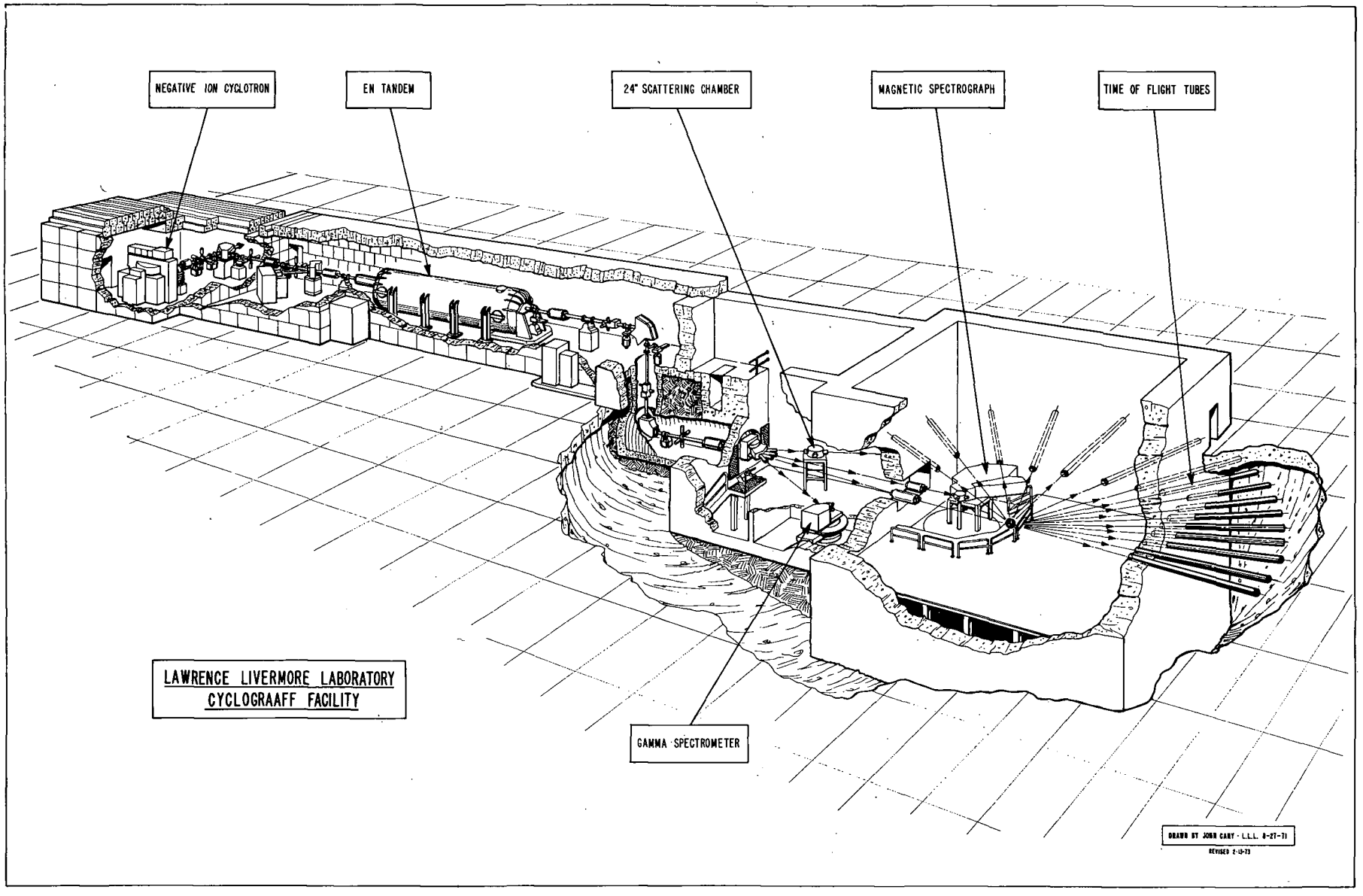
NEGATIVE ION CYCLOTRON
EN TANDEM
24" SCATTERING CHAMBER
MAGNETIC SPECTROGRAPH
TIME OF FLIGHT TUBES
LAWRENCE LIVERMORE LABORATORY
CYCLOGRAAFF FACILITY
GAMMA SPECTROMETER
DRAWN BY JOHN CARY - L.L.L. 8-27-71
REVISED 2-15-73

Figure D-1

LOCKHEED PALO ALTO RESEARCH LABORATORY

A. NEUTRON PHYSICS

1. Neutron Cross-Section Measurements with Polarized Targets (T. R. Fisher, A. R. Poletti,* and B. A. Watson)

The deformation effect in the ^{59}Co + n total cross section has been observed at the neutron energies 1, 1.2, 1.4, 1.6, 2, and 15.9 MeV using an aligned ^{59}Co target. The target was operated at 0.03°K and had an average nuclear alignment of 15.9%. Over the energy range from 1 to 2 MeV, the average change in cross section resulting from nuclear alignment was -41 ± 2.5 mb; at 15.9 MeV, the observed change was -5.9 ± 7.6 mb. From these measurements a value $Q = 0.39 \pm 0.06$ b has been extracted for the quadrupole moment of the ^{59}Co ground state, which is in good agreement with the results using other techniques.

2. Gross-Fission-Product γ-Ray Spectroscopy (W. L. Imhof, L. F. Chase, R. A. Chalmers, F. J. Vaughn, and R. W. Nightingale)

Analysis of the fission-product γ-ray data is continuing, and more results will be reported as they become available.

B. CHARGED-PARTICLE REACTIONS

1. Application of the $^3He(d, p)^4He$ Reaction to the Problem of Measuring ^3He Profiles in Solids (P. P. Pronko,** and J. G. Pronko)

An *in situ* nondestructive probe for measuring the concentration and distribution of helium isotopes in near-surface layers of solids was developed using the resonant $^3He(d,p)^4He$ reaction. Stopping-power effects control the deceleration of the probing beam and bring it into the resonance window. The spatial resolution of the method is defined by the 450-keV full width at half maximum for the resonance cross section. The method has technical value for analyzing potential material problems associated with the implantation of helium in the primary containment wall of controlled thermonuclear reactors.

---

* University of Auckland, Auckland, New Zealand.

** Argonne National Laboratory, Argonne, Illinois.

2. Beta Decay of ^{17}N (A. R. Poletti* and J. G. Pronko)

The delayed neutron spectrum following the β decay of ^{17}N has been observed using the associated-particle time-of-flight method and neutron flight paths of up to 140 cm. The ^{17}N was formed by bombarding a gas cell containing $^{15}N_2$ gas with 2.9-MeV tritons. Three neutron groups were observed. Direct calibration of the time-to-amplitude converter in terms of a 50-MHz frequency standard enabled us to determine the mean energy of the three groups as 1.654 ± 0.024, 1.154 ± 0.014, and 0.385 ± 0.007 MeV. We can assign these groups unambiguously to the neutron decay of the established levels at 5.935, 5.377, and 4.554 MeV in ^{17}O. Further efforts are being made to accurately determine the β-decay branchings to both bound and unbound levels in ^{17}O.

3. A Study of ^{52}Ti Using the $^{50}Ti(t,p\gamma)^{52}Ti$ Reaction (J. G. Pronko, T. T. Bardin, J. A. Becker, T. R. Fisher, R. E. McDonald, and A. R. Poletti*)

The angular correlations of cascading γ rays observed in a collinear geometry with a 5-crystal array of NaI(Tl) detectors were measured. These studies provided information on the previously unobserved level scheme of ^{52}Ti. The data indicate excited states at energies of 1.05, 2.28, 2.44, 3.61, 3.90, and 4.22 MeV and assign spins of J = 2 for the 1.05-, 2.28-, and 2.44-MeV states. The 4.22-MeV state was found to have spin J = 1. In addition, multipole-mixing and branching ratios for the electromagnetic decays of these states were measured. Preliminary lifetime data obtained through the Doppler-shift-attenuation method indicate that the lifetime of the 1.05-MeV state is typical of an E2 decay. Further analysis of lifetime data is presently being pursued.

4. Study of ^{56}Cr Using the $^{54}Cr(t,p)^{56}Cr$ Reaction (T. T. Bardin, J. G. Pronko, A. R. Poletti,* and R. E. McDonald)

The decay modes of the excited states of ^{56}Cr were studied using the technique whereby angular-correlation measurements were obtained in a collinear geometry. An array of 5 NaI(Tl) crystals was used in the collection of the correlation data. The analysis of the data has yielded information on spin assignments as well as branching and mixing ratios of the electromagnetic de-excitations. Further studies regarding the lifetimes of these excited states are in progress.

---

* University of Auckland, Auckland, New Zealand.

5. Unbound States of ^{26}Si (J. G. Pronko, B. A. Watson, D. C. Slater,* and A. Kuhlman*)

The proton decay of the unbound states at 6.32, 6.77, 7.41, 8.08, and 8.62 MeV in ^{26}Si is being studied using the $^{24}Mg(^{3}He,n)^{26}Si(p)^{25}Al$ reaction at a beam energy of 15 MeV. Angular-correlation data measured for the decaying protons (obtained in coincidence with neutrons detected at 0 deg with respect to the beam axis) are being analyzed according to a general formalism which allows channel-spin as well as orbital-angular-momentum mixing in the $^{26}Si \rightarrow {}^{25}Al + p$ exit channel. The above analysis will yield spin information for the unbound states as well as information on the wave-function configurations of these states. Further data analysis is in progress.

6. ^{18}O Excitation Energies and Lifetimes from Ge(Li) Measurements in $^{19}F(t,\alpha\gamma)^{18}O$ Reaction (J. W. Olness,** E. K. Warburton,** and J. A. Becker)

Precision excitation energies and some nuclear lifetimes were obtained for ^{18}O levels with $E_x < 7.1$ MeV. Multi-parameter data-collection techniques were used to store γ-ray spectra measured at $\theta_\gamma = 0$ deg, 45 deg, and 90 deg in coincidence with α groups detected at $\theta_\alpha = 180$ deg populating the various final states in ^{18}O. Analysis of the correlation data also supports previous conclusions on the ^{18}O level spin and parity assignments and in addition restricts the 6351-keV level to J = 1 or 2.

7. Some Nuclear Lifetimes in ^{18}O, ^{18}F, and ^{20}F (E. K. Warburton,** P. Gorodetzky,** and J. A. Becker)

The Doppler-shift-attenuation method was used in conjunction with ^{16}O and ^{18}O bombardment of tritium targets to measure the mean lives of five lines in ^{18}O, ^{18}F, and ^{20}F. The results are [nucleus, E_x (keV), τ_m (psec)]: ^{18}O, 3632, 1.45 ± 0.25; ^{18}F, 1701, 1.16 ± 0.12; ^{20}F, 984, 2.30 ± 0.25; ^{20}F, 1309, 1.10 ± 0.25; and ^{20}F, 1971, 1.40 ± 0.40.

8. Study of ^{18}O Levels with $E_x < 8$ MeV (J. A. Becker, L. F. Chase, D. A. Kohler, and R. E. McDonald)

Levels in ^{18}O were populated with the $^{19}F(t,\alpha\gamma)^{18}O$ reaction. The two-parameter matrix of α-γ coincident pulse heights was collected with good α-particle resolution (40 keV). Angular correlations of decay γ rays associated with individual levels in ^{18}O were obtained, from which

---

* Stanford University, Stanford, California.

** Brookhaven National Laboratory, Upton, New York.

^{18}O level spins, γ-ray branching ratios, and γ-ray multipole mixings were extracted. Results include the spin assignments J = 1 for the 6.19-MeV level, and J = 0 (1) for the 6.86-MeV level.

9. The β Decay of ^{12}B and ^{12}N, and the Second-Class-Current Problem (J. A. Becker, R. E. McDonald, R. Chalmers, and D. H. Wilkinson*)

Relative intensities of the ^{12}B and ^{12}N β branches to the first-excited state of ^{12}C are being remeasured since the ratio of ft (+)/ft (-) for this decay is anomalous. The experiment has been completed and data analysis is underway.

10. ^{42}Ar Excitation Energies and Lifetimes from Ge(Li) Spectroscopy in the $^{40}Ar(t,p\gamma)^{42}Ar$ Reaction (T. T. Bardin, J. A. Becker, T. R. Fisher, and B. A. Watson)

A target of solid Ar prepared by cryogenic techniques was bombarded with 2.9-MeV tritons. Measurements were made of the p-γ coincident pulse-height events. ^{42}Ar branching ratios, excitation energies, and nuclear lifetimes are presently being extracted from these data for levels with $E_x \leq 4.3$ MeV.

11. Gamma-Ray Angular Distributions Following the $^{48}Ti(p,p')^{48}Ti$ Reaction at $E_p = 5.0$ MeV (T. T. Bardin, J. A. Becker, and T. R. Fisher)

Angular distributions of several γ-ray transitions following the $^{48}Ti(p,p')^{48}Ti$ reaction were measured at $E_p = 5.0$ MeV. The measured distributions are compared with distributions predicted on the basis of the compound-nucleus model for the transitions 2.29 → 0.98, 2.42 → 0, 2.42 → 0.98, 3.22 → 0.98, 3.22 → 2.29, 3.36 → 0.98, and 3.37 → 0.98 MeV.

12. Oxygen-Induced Reactions on Several f, p-Shell Nuclei (D. C. Slater,** J. R. Hall,** J. R. Calarco,** R. Avida,** W. E. Meyerhof,** and B. A. Watson)

A 70-MeV ^{16}O beam was used to bombard the targets ^{40}Ca, ^{45}Sc, and ^{48}Ti. Reaction products ranging from ^{4}He to ^{24}Mg were identified with an E-ΔE-T counter telescope. One of the sharp features appears to be that whereas ^{40}Ca stripping and pickup reactions proceeded with almost equal strength, ^{45}Sc stripping reactions were much more intense than pickup reactions. Also α-particle transfer reactions were observed to be stronger than other transfer reactions for all targets.

---

* Oxford University, Oxford, England.
** Stanford University, Stanford, California.

13. Application of Superconductivity to the Detection of Nuclear Radiation (B. A. Watson and T. R. Fisher)

The possibility of using the energy gap of the superconducting state to detect nuclear particles is being investigated. A prescription for making Pb-PbO-Pb junctions has been developed and source-related effects are observed.

14. Polarization Measurements (R. E. McDonald and J. A. Becker)

Polarization of ^{12}B nuclei produced with the $^{11}B(d,p)^{12}B$ reaction and implanted in Au has been measured as a function of ^{12}B recoil angle and incident beam energy. Preliminary NMR spectra have also been obtained; however, line widths were determined by magnetic-field nonuniformities. An improved experimental arrangement is being installed.

LOS ALAMOS SCIENTIFIC LABORATORY, UNIVERSITY OF CALIFORNIA

A. NEUTRON CROSS SECTIONS

1. Prompt Neutrons from ^{257}Fm (Veeser, Hemmendinger, Farrell Balagna, Ford, Hoffman, Wilhelmy)

The measurement of the number of prompt neutrons emitted in the spontaneous fission of ^{257}Fm was completed.

As was reported earlier, $\bar{\nu}$ for ^{257}Fm is about 1.009±0.006 times that for ^{252}Cf. We have noticed, however, that for the 10% of the fragments which have the highest kinetic energies, $\nu \simeq 1.9$ for Fm as compared with 3.0 for Cf. For Fm 90% of these high-energy fragments result from nearly symmetric fissions, while Cf almost never undergoes symmetric fission. It appears, therefore, that fewer neutrons are emitted in symmetric fission than in asymmetric fission. Measurements on a new ^{257}Fm source will begin shortly.

2. Fission Spectra of ^{238}U and ^{235}U as a Function of Incident Neutron Energy (Auchampaugh, Ragan)

Many of the points in the ^{238}U fission neutron energy distribution have been repeated at 90° and some at 55°, with and without PSD. In addition, ^{235}U has been looked at briefly with results similar to those of ^{238}U. A paper with the following abstract has been prepared:

> "The fission neutron energy spectra of ^{238}U and ^{235}U have been measured at the incident neutron energies of 1.3 (^{238}U), 1.7, 4.8, 6.4, 8.8, 17.4, and 22.5 MeV. The spectrum in the fission neutron energy interval from 1.4 to 5.0 MeV has been least-squares fitted with a Maxwellian function for each incident energy to study changes in the shape of the spectrum with excitation energy. For both ^{238}U and ^{235}U the Maxwellian temperature calculated was essentially constant with energy within 1%. Data taken at 22.5 MeV with pulse shape discrimination indicates a slight hardening of the fission neutron spectrum with increasing neutron energy."

3. Inelastic Neutron Spectra as a Function of Neutron Excitation Energy (Auchampaugh, Ragan)

Concurrent with the fission neutron spectra measurements, total neutron emission spectra data were taken using the same geometry but timing with respect to a bunched p or d beam. These data have not been analyzed. It is hoped that from both sets of data temperatures for the

inelastic as well as the fission neutron distributions can be obtained as a function of excitation energy.

4. Gamma-Ray Production (Drake, Silbert, Arthur)

The number of samples for which gamma-ray production cross sections are being measured at 14-MeV neutron energy has been expanded to include tungsten, gold, and lead. A preliminary cross section (~64 mb/sr at 125°) has been calculated for the 0.85-MeV gamma ray from ^{56}Fe. This value agrees with results obtained by several other experimental groups, but is higher than results from Oak Ridge and Gulf Radiation Technology.

Gamma-ray response functions are being remeasured with absorbers to find a consistent way to adjust the peak-to-tail ratio as a function of gamma-ray energy and sample composition.

5. Neutron Polarization Experiments (Keyworth, Seibel)

The neutron polarization experimental program at ORNL which began August 1, 1972, was temporarily halted on January 10, 1973, for the purpose of data analysis and target modifications.

Numerous unexpected problems were encountered at Oak Ridge. Several months were spent repairing leaks, which had not existed at LASL, and reducing background on a flight tube which had previously seen little or no use by ORNL personnel. In addition, a consistently low product polarization, $f_n f_N$, where f_n is the neutron polarization and f_N the target polarization, was without explanation until early January. Extensive diagnostics on the neutron polarization system eliminated that as a source of the problem. Several attempts at magnetic guide fields to prevent depolarization of the neutron beam in transit produced no visible change. In addition, a computer code, LARMOR, to trace the expectation value of the spin of a neutron as it moves through an inhomogeneous magnet field, has been written. Preliminary results indicate that a depolarization of less than 1% should occur for neutrons passing through the magnets utilized in the polarization experiment. A system was then set up to measure precisely the angular distribution of alpha particles from natural decay of ^{237}Np which was presumably polarized. This measurement, which had been performed at LASL on a small sample, had confirmed calculations on the expected extent of ^{237}Np polarization.

The large sample in use at ORNL, however, had not been tested previously because it was not fabricated until after the program at Oak Ridge began. It is now assumed that the aluminum matrix containing the neptunium was not behaving as a good thermal conductor and that a large thermal gradient existed between the neptunium system and the target holder. This problem is, hopefully, being rectified by Clayton Olsen, by

casting a solid sample of target material in a beryllium oxide die. The casting will then be soldered directly to a copper holder, eliminating any matrix.

Although the total polarization was substantially less than had been expected, it was decided to acquire as much data as possible before returning to LASL. To this end, three weeks of prime machine time were scheduled in late December and early January. Machine breakdown reduced this period to nine days. Nevertheless, this effort produced data from which spin assignments of at least 20 intermediate structure resonances below a neutron energy of 3 keV can be made. This has served to verify current theories of a double-humped fission barrier and sheds light on the properties of levels in the second well in the compound system.

It is now expected that, with the previously mentioned target modification, additional measurements on ^{237}Np will result in many more resonances being analyzed, permitting understanding of detailed properties of levels in the second well. In addition, the higher polarization should yield information regarding the transition states in the fissioning nucleus, through determination of the K quantum number. The expected improvement for ^{237}Np extends, perhaps even more dramatically, to measurements on ^{235}U and ^{233}U. A ^{235}U sample was the initial target in the ORNL program, but the reduced polarization compounded with the greater complexity of the ^{235}U fission cross section led us to concentrate on the less fissile but simpler ^{237}Np.

Data reduction codes to convert the Oak Ridge data to a format readable at Los Alamos, to perform background and dead-time corrections, and to convert time-of-flight data to a cross section form have now been written. This should result in rapid processing of future data.

A paper with the following abstract has been submitted to the Third Symposium on the Physics and Chemistry of Fission:

> "The appearance of prominent intermediate structure in subthreshold fission is currently ascribed to coupling between the normal (Class I) compound nuclear states and Class II states belonging to the second minimum in a double-humped fission barrier. This explanation requires that only Class I resonances of a single spin state be enhanced through coupling to a Class II state of the same spin. In order to verify this explanation, the fission (σ_f) and total (σ_t) cross sections of ^{237}Np for resonance energy neutrons have been measured with a polarized neutron beam and polarized target, using time-of-flight methods. Neutrons from the Oak Ridge Electron Linear Accelerator were polarized by transmission through a dynamically pumped proton sample. The ^{237}Np was polarized in a ferromagnetic medium cooled by a ^{3}He-^{4}He dilution refrigerator.

"Spins of the individual fine-structure resonances comprising the first group at 40 eV were found to be of the same spin state, probably 3+. This assumption, taken into consideration with existing K-value determinations for these resonances, would imply that these states fission through more than one K-channel. Spins of at least ten other groups below 2 keV were determined, although any fine structure is unresolved. The majority of these groups belong to the same spin state as does the 40-eV group. Comparisons are made between spin assignments derived from this technique and less direct methods."

6. Absolute Cross Sections for $^{235}U(n,f)$ (Smith, Hansen, Barton, Jarvis)

Work is continuing to check the data processing and write up a paper for publication. After a partial return on foil weight information our preliminary cross section values have been lowered by about 2%. No further large changes are anticipated. Some refinements on scattering corrections may change the cross sections a few tenths of 1%, probably less.

After 30 years of inconsistent measurements, we believe that the present measurement will stand the test of time, particularly the 3 MeV point. After the data are published we believe it would be worthwhile to work over a low energy point around 1 to 1.5 MeV and also at 6 MeV. The 6 MeV region can be firmed up by using the $D(d,n)^3He$ reaction and lapping down into this region as part of a program to measure higher energy of $\sigma_{n,f}(^{235}U)$ cross sections.

7. n-^{3}He and n-T Cross Sections [Seagrave, with Stoler and Goulding (RPI), Berman (LLL), Drosg (U. Vienna)]

a. ^{3}He Total Cross Section

The RPI n-^{3}He total cross section analysis is substantially complete. Stan Hall has adapted the Rice and de Boers free-knots spline-fitting program to replace the LASL Library SMØØTH subroutine in the program GLSHND developed for the deuterium data. It has been applied to three sets of n-^{3}He data separately and collectively, as an aid in testing statistical consistency of the three sets, and to aid assessment of how best to group the data points for a more compact presentation of the results. Spline-smoothed interpolations are available at any energy, and in particular, values have been obtained corresponding to the energies at which LASL n-^{3}He elastic cross sections were obtained by Drosg et al.

b. ^{3}He Elastic and Inelastic Cross Sections

Drosg has reported from Vienna that problems in the data analysis have been resolved, and a final version of the paper should be forthcoming. The integral results shown together with the new total cross sections in Table A-1 have the interesting consequence that the nonelastic cross section becomes approximately constant above 12 MeV. This can be accounted for by the known ^{3}He(n,d)D cross section, the extension of the ^{3}He(,pn)T cross section derived from the new LASL T(p,n)^{3}He measurements of McDaniels et al. [Phys. Rev. C 6, 1593 (1972)], and an assumed envelope of ^{3}He(n,pn)D and ^{3}He(n,2n)2p cross sections similar in shape to the ^{3}He(n,d)D cross section but displaced to higher energies.

c. Tritium Total Cross Section

It has appeared desirable to effect a change of venue for this proposed experiment from RPI to the comparable 250 m time-of-flight facility at the LLL linac, since LLL already has facilities for handling the 250 kCi of T_2 required. No serious obstacle appeared on a trip to LLL in February, and LLL authorities have agreed to the experiment "in principle." The RPI transmission cell design used for measurements on H_2, D_2, ^{3}He, and ^{4}He will be redesigned. In consultation with stress analyst H. Luke, the new design will be based on standard pressure vessel codes for elliptical ends (machinable with tape-controlled equipment at

Table A-1

n-^{3}He Integral Cross Sections (in barns)

En, MeV	7.9	12.0	13.6	14.4	23.7
σ_T (RPI)	1.75	1.28	1.16	1.11	0.71
σ_{el}	1.43	1.04	0.92	0.87	0.48
$\sigma_T-\sigma_{el}$	0.32 ±0.08	0.24 ±0.06	0.24 ±0.05	0.24 ±0.05	0.23 ±0.05
$\sigma_{n,p}+\sigma_{n,d}$	0.306	0.244	0.232	0.224	0.145
$\sigma_{n,pn}+\sigma_{n,2n}$			0.008	0.016	0.070
σ_{ne}			0.240	0.240	0.215

LASL) and utilizing 21-6-9 steel selected for resistance to hydrogen embrittlement, and for high strength and heat treatability. The elliptical end design permits a flatter central end and less bending deformation as well as greater strength than the RPI design. At LLL, beam collimation will be installed for a 3/8-in. diam neutron beam, and a section of vacuum flight pipe can be removed to accommodate about 1.6 m of apparatus in a shelter outside of the main buildings. A cylinder for total containment of the 100 liters of tritium in the event of leakage will also contain an evacuated cell and one containing hydrogen or deuterium. It is proposed to extend measurements down to about 1 keV to compare with recent RPI continuum measurements for deuterium showing a rise in cross section below the energies of the discrete data set. There remains a discrepancy of nearly 50% between the lowest discrete tritium measurement and the zero energy cross section inferred from the deuterium values and the recent LLL coherent scattering ratio of tritium and deuterium [Phys. Rev. C 5, 1952 (1972)].

8. (n,2n), (n,3n) Measurements (Jarmie, Erkkila, Martin, Morrison Hardekopf, the LASL Radiochemistry Group)

Runs have been made near 16 MeV neutron energy using the $D(d,n)^3He$ reaction. It appears that we will, thanks to the techniques that have been developed, be able to make successful bombardments in this region, which has been intractable up to now. A series of isotopes were bombarded and the neutron telescope was used to determine a flux to ~5%. It is expected that fluxes will be measured to 2-3% in the future. Of particular note was the importance of not allowing a significant "self-made" target to build up, where the impacted beam at the target stop provides a spurious neutron producing source. Baking the target between runs should reduce this spurious source.

The analysis of the neutron telescope data has been completed both for this run and for a subsequent run with 24-MeV neutrons from the D(t,n) reaction. Neutron fluxes were measured to an absolute accuracy of about 5% for the 16-MeV run and about 3% for the 24-MeV run.

B. NUCLEAR SPECTROSCOPY: STUDIES OF RADIOACTIVE NUCLEI

1. Decay of Fission-Product ^{126}Sn (Bunker, Starner, Smith, Orth)

An attempt by K. E. G. Löbner (Munich, Germany) to measure the half-life of the 41.9-keV second excited state of ^{126}Sb by a delayed-coincidence technique appears to have been successful. Preliminary analysis gives $T_{1/2}$(41.9 keV) ≈ 15 sec, which slightly exceeds our previous upper limit of $T_{1/2} < 10$ sec, set by radiochemical means. Löbner's final computer analysis of the data has not yet been received.

2. Decay of Fission-Product ^{126}Sb (Bunker, Starner, Orth)

A study of the ^{126}Sb (12-day) $\rightarrow$ ^{126}Te decay has been undertaken for the following reasons: (1) in a recent preprint by S. Shastry, it is concluded from β-γ angular correlation data that the spin of 12-day ^{126}Sb is 7^-, not 8^- as we propose on the basis of our study of $^{126}Sn \rightarrow {}^{126}Sb$. Through reexamination of the ^{126}Sb decay scheme, we may be able to resolve this conflict; (2) the Nuclear Data Group at ORNL is preparing to publish an updated summary of the mass-126 chain, and since there are many disagreements among the published decay schemes of ^{126}Sb, it would greatly simplify the work of the compilers if the more serious inconsistensies could be resolved.

In late September, we produced ^{126}Sb (12 day) at the cyclotron via α-induced fission of ^{238}U. After waiting three weeks to allow ^{127}Sb (3.9 day) to decay down to an acceptable level, we began two-dimensional Ge(Li)-Ge(li) coincidence measurements, as well as singles measurements with three different detectors. To date, we have observed 28 γ-rays attributable to ^{126}Sb, three of which had not been previously observed. We also have shown that three of the γ-rays reported in the most recent study of $^{126}Sb \rightarrow {}^{126}Te$ do not belong to this decay. More importantly, our coincidence results establish uniquely the positions of 17 excited states below 3.5 MeV. Twelve of these states had been proposed earlier, but the evidence was inconclusive, being based mainly on the closure of energy loops.

Another source of ^{126}Sb (12 day) was produced in late January at the cyclotron via α-induced fission of ^{238}U. Measurements were begun in mid-February and are still continuing. One of the most significant new results is the observation of a 208.5-keV γ-transition, which depopulates a level at 2973.9 keV--known previously from $(\alpha,2n\gamma)$ data to have $I^{\pi} = 10^+$. Our data indicate that the 2973.9-keV level is directly β-populated, the associated log $\underline{ft}$ being $\approx$ 9.3. Thus, the ^{126}Sb parent cannot be 7^- as proposed by Shastry, but must be 8^-, in agreement with our $^{126}Sn \rightarrow {}^{126}Sb$ data.

3. Decay of ^{151}Nd (Bunker, Starner, Smith, Nielsen)

An attempt has been made, via theoretical Coriolis-coupling calculations, to explain the deviations in energy from the I(I+1) "law" within the three lowest-lying rotational bands of ^{151}Pm.

Our attempts, via Coriolis-coupling calculations, to obtain theoretical energy fits to the rotational level energies of the N = 4 states in ^{151}Pm, as well as in ^{157}Tb, ^{159}Tb, and ^{165}Ho have revealed major deviations from the Nilsson-model predictions. At the suggestion of S. G. Nilsson, we are exploring the sensitivity of the wave functions (especially those with $K^{\pi} = \frac{1}{2}^+$) to the model parameters. Also, a deformed Woods-Saxon

model code has been obtained from G. Ford and the Woods-Saxon wave functions are being compared against those given by the Nilsson model. The Woods-Saxon code has been modified to calculate and print out Coriolis-coupling matrix elements (both decoupling parameters and j_- matrix elements). It is too early to decide which model (Woods-Saxon or Nilsson) gives a better fit to the data.

C. MATERIALS IDENTIFICATION AND ANALYSIS WITH STOPPED MUONS (Malanify, Umbarger, Augustson, East, Close)

The interactions of stopped muons with nuclei are being studied as is the possibility of using the resulting characteristic muonic x-ray spectra to provide an incisive technique for identification and analyses of fissionable materials.

Some preliminary measurements were done in June and in November 1972 at the NASA Space Radiation Effects Laboratory (SREL). With the availability of the Los Alamos Meson Physics Facility (LAMPF), extensive tests of the assay method will be made in 1973. A study will also be made of the influence of chemical compounds on resulting spectra.

The initial objective is to determine the feasibility of using stopped muons for elemental and isotopic analysis of fissionable material. A subsequent objective is to develop and utilize facilities at LAMPF to establish standard analytical techniques for bulk samples of fissionable materials using stopped muons.

With the muon orbits so close to the nucleus, the energies of the x rays are much greater than those of the corresponding electron transitions. For example, the K_α electronic x rays in uranium are ~95 keV, whereas they are ~6.4 MeV for the same muonic transition. Hence, the radiation is very penetrating and thus permitting analyses of bulk samples. In addition, the interrogating muons are very penetrating, allowing large and/or dense samples to be scanned.

Figure C-1 displays the details of the K_α region for the five metal targets: ^{208}Pb, ^{232}Th, ^{235}U, ^{238}U, and ^{239}Pu. These spectra were recorded with a large volume Ge(Li) detector. Therefore, the figures display the characteristic full energy (FE) as well as the single (SE) and double escape (DE) peaks. Since ^{208}Pb is a "doubly magic" spherical nucleus of ground state spin zero, its spectrum is very simple. The other nuclei, because of their nuclear deformation, display appreciable hyperfine splitting. Table C-1 lists the centroid energies for the K_α ($2P_{3/2}$ to $1S_{1/2}$ and $2P_{1/2}$ to $1S_{1/2}$) transitions displayed in Fig. C-1. This table shows that various fissionable elements display energy shifts of approximately 90 keV, while the uranium isotopes display an energy shift of nearly 30 keV. Both of these energy shifts are clearly observable with the Ge(Li) detector which possesses about 7 keV resolution.

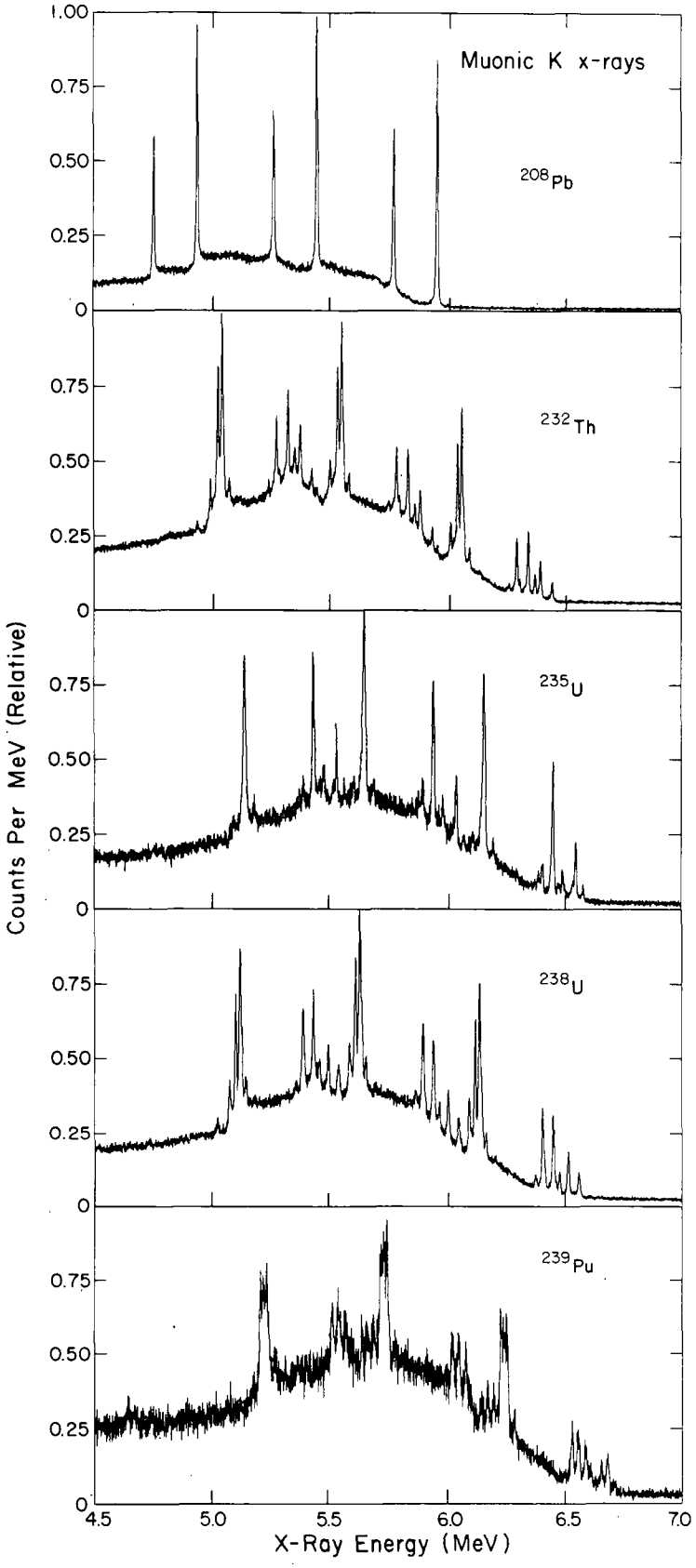

Fig. C-1. Muonic K X-Ray Spectra for ^{208}Pb, ^{232}Th, ^{235}U, ^{238}U, and ^{239}Pu.

Table C-1

K_α Centroid Energies (MeV)

Isotope	$2P_{1/2}$ to $1S_{1/2}$	$2P_{3/2}$ to $1S_{1/2}$
^{208}Pb	5779	5963
^{232}Th	6059	6356
^{235}U	6159	6482
^{238}U	6130	6455
^{239}Pu	6244	6595

Figure C-2 displays the muonic L x-ray spectral region for the same five metal targets: ^{208}Pb, ^{232}Th, ^{235}U, ^{238}U, and ^{239}Pu. The elemental and isotopic shifts are also observed for these x rays. The simple spectrum for ^{208}Pb is again evidence of its value as a calibration standard.

The data presented above clearly demonstrate the elemental and isotopic discrimination aspects of this technique. It now remains to develop this technique at the high-intensity LAMPF facility and to extend the technique to meaningful assays.

D. EVALUATION

1. Evaluation of Neutron Cross Sections for ^{239}Pu and ^{240}Pu (Hunter, Stewart, Hirons)

Cross sections for ^{239}Pu and ^{240}Pu have been evaluated for neutron energies above 25 keV and 40 keV, respectively, and joined to ENDF/B-III evaluations at lower energies.[1] These evaluations have yielded striking agreement with integral experiments and with measurements on nuclear devices. For example, k_{eff} for VERA-11A is predicted to 1/2%. These data are in ENDF/B format and have been processed into multigroup and pointwise files for LASL applications.

---

[1] R. E. Hunter, L. Stewart, and T. J. Hirons, "Evaluated Neutron Induced Cross Sections for ^{239}Pu and ^{240}Pu," Los Alamos Scientific report LA-5172 (in preparation).

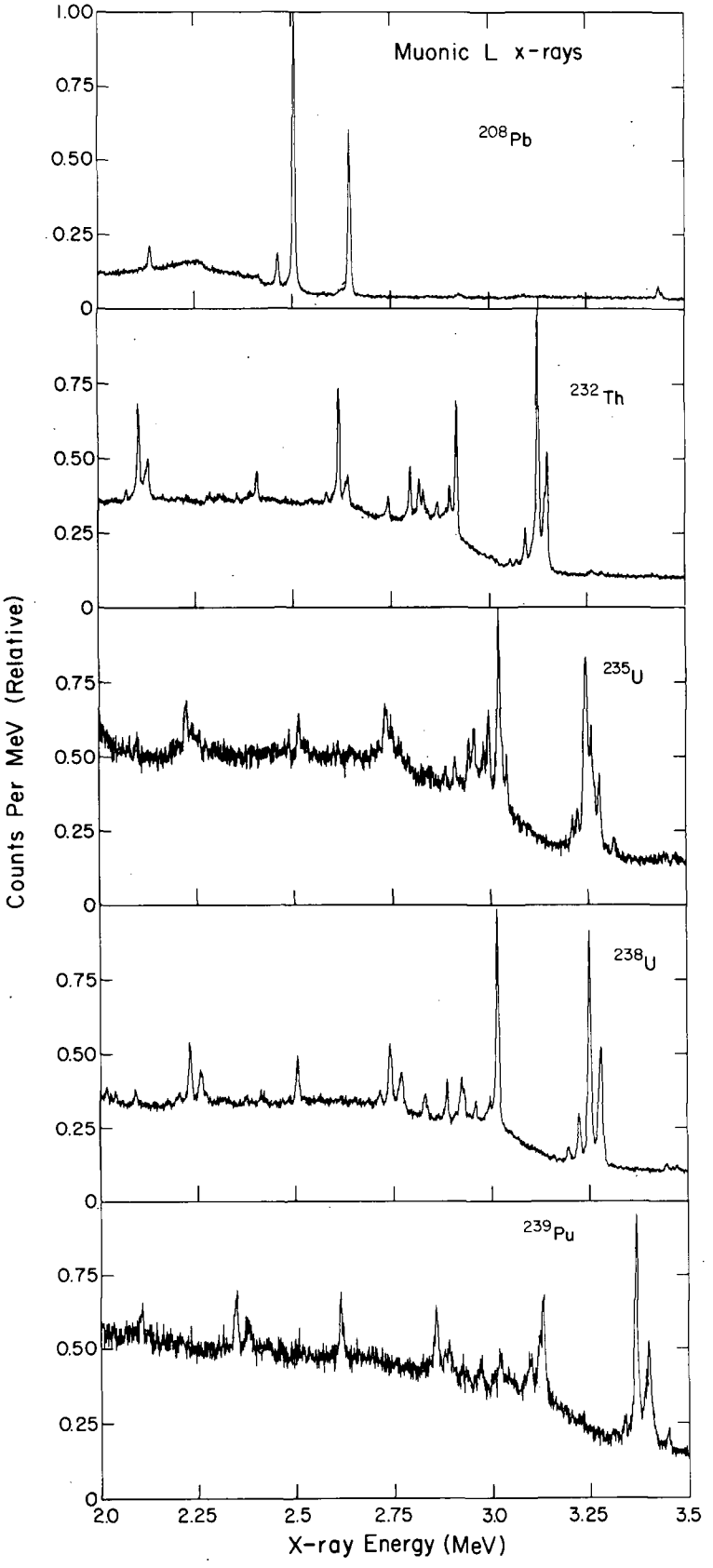

Fig. C-2. Muonic L X-Ray Spectra for ^{208}Pb, ^{232}Th, ^{235}U, ^{238}U, and ^{239}Pu.

2. Elastic Scattering of Nucleons from ^{4}He (Nisley, Hale, Dodder, Jarmie, Young)

An R-matrix analysis of p-^{4}He and n-^{4}He elastic scattering has been done at nucleon energies below 18 MeV. The work has proceeded in two stages. We have analyzed the two reactions independently using all the known data available in this energy range. The data sets have been carefully examined for consistency in the quoted energies, values, and errors, and those points which are obviously inconsistent have been thrown out to produce a "best" data set for each reaction. In the case of p-^{4}He elastic scattering where the "best" data set includes some extremely accurate measurements (errors <1%), the fit is characterized by a χ^2/degree of freedom of 1.00 (the most probable value).

In the second stage, we have analyzed the "best" data sets for the two reactions simultaneously, constraining the neutron and proton R-matrix parameters with a simple model of charge independence. The fit in this case is somewhat worse (χ^2/degree of freedom = 1.17), probably reflecting the simplicity of the charge independent model. However, it is the aim of this simultaneous analysis to make use of the generally more accurate p-^{4}He measurements in determining accurate values of the n-^{4}He differential cross section and analyzing power. The latter quantity is of critical interest to experimentalists engaged in measurements of polarization in nuclear reactions.

3. R-Matrix Analysis of Reactions in the ^{11}B System (Hale, Young, Nisley)

A coupled-channel R-matrix analysis of reactions in the ^{11}B system is in progress. The channel configuration at present includes n-^{10}B, α-^{7}Li, and α-^{7}Li*(0.478), with data being analyzed simultaneously from the reactions ^{10}B(n,n), ^{10}B(n,α_0), ^{10}B(n,α_1), and ^{7}Li(α,α) at energies corresponding to E_n below 1 MeV. Although the level structure of ^{11}B is presumably well known in this energy region, the consistency of data from the above reactions has not been fully tested. For instance, we hope to determine which of several disparate ^{10}B(n,α_0) cross-section measurements in this region is correct. An accurate determination of the cross sections for neutron-induced reactions in the ^{11}B system is desirable, since several of these cross sections are "standards" upon which other measurements are based.

We plan to extend this analysis to higher energies, including at the same time the t-2α channel in order to investigate the tritium production from neutrons scattered on ^{10}B. This information should be of interest in the design and operation of nuclear reactors.

4. Multiple Reaction Correction to Neutron Reaction Cross Sections (Devaney)

The importance of the multiple reaction correction to cross sections above ~0.1 MeV is demonstrated by deriving a simple formula for a thin-slab sample utilizing a limited multigroup, spatially averaged, transport theory, and applying the formalism to a few examples. To illustrate the immediate relevance of the correction, we also apply it to revise an important cross section in current use ($^{238}U\sigma_{ny}$, ENDF/B-III). The correction can be large with thicker samples and at higher energies, especially for radiative capture (exceeding a factor of 10). Our examples indicate that multiple reaction effects must be checked in measuring or evaluating radiative capture, fission, reaction, and gamma production cross sections and their consequent spectra.[1] A paper has been accepted by Nuclear Science and Engineering.

5. A New Evaluation of the Capture Cross Section of Wolfram (Devaney)

A new evaluation of the smooth radiative neutron capture cross section for wolfram and its isotopes between 0.006 and 20 MeV has been completed. The multiple reaction corrections[1] significantly lower the cross section at the higher energies (as much as factors of 2 to 5 or more). The (n,n^1) competition reverses the role of dominant capturing isotope at about 0.23 MeV. The high-energy cross section is expected to show giant resonance collective behavior. A report is in preparation (Los Alamos Scientific Laboratory report LA-5221).

6. MINX - A Multigroup Interpretation of Nuclear X-Sections (Weisbin, Soran, Harris, LaBauve, Hendricks)

MINX is a designer-oriented multigroup processing code with improved resonance and group-to-group transfer capabilities. All pertinent ENDF/B formats are considered and a pseudocomposition independent fine multigroup library with self-shielding factors is generated in CCCC[2] format.

In order to clearly distinguish uncertainties in multigroup constants arising from imprecision in the fundamental cross-section data from those due to numerical approximations required in the averaging procedure, the MINX code enables the user to obtain multigroup sets known to be accurate to within an input specified tolerance (provided one assumes

---

[1] J. J. Devaney, Phys. Rev. Letters, 29, 1567 (1972).

[2] B. M. Carmichael, D. A. Meneley, and D. R. Vondy, "Report of the Subcommittee on Standard Interface Files," prepared for the Committee on Computer Code Coordination (September 1971).

that the data base and weighting function are known explicitly). Only after having reduced the relative error in the calculation to some known measure well below existing uncertainties in nuclear data, can multigroup constants be assigned errors consistent with those uncertainties. The stated philosophy behind the MINX development, therefore, is to reduce the calculation to a sequence of numerical steps, each of which can be defined explicitly and assigned a quantitative error.

MINX has the optional capability to generate and access a linearly interpolable, infinitely dilute, temperature dependent pointwise cross-section library.[1] This feature permits efficient computation of group cross sections with low- and high-temperature Doppler broadening[2,3,4] of single level and multilevel resonance cross sections. A number of recently developed improved algorithms have been incorporated. These include a semianalytic computation for high order elastic and inelastic anisotropic matrices (including energy-angle coupling for discrete inelastic reactions), an exact kernel broadening procedure[2] for linearly interpolable neutron cross sections, and a rapid and accurate method for the generation of transfer matrices from tabulated descriptions of inelastic spectra.

---

[1] C. R. Weisbin, D. R. Harris, M. E. Battat, R. J. LaBauve, W. M. Taylor, G. D. Turner, and R. E. Seamon, "Preparation of Data Libraries for Efficient Retrieval by Continuous Energy Monte Carlo Codes," Trans. Am. Nucl. Soc. 15, 572-573 (1972).

[2] D. E. Cullen, O. Ozer, and C. R. Weisbin, "Exact Doppler Broadening of Evaluated Neutron Cross Sections," submitted as a contributed paper to Am. Nucl. Soc. meeting, Chicago, June 1973.

[3] D. R. Harris and C. B. Noll, "SUMOR (M0271), a FORTRAN-IV Program for the CDC-6600 for Neutron Resonance Cross Sections Including Level-Level Interference and Exact Doppler Broadening," Bettis Atomic Power Laboratory report WAPD-TM-810 (July 1969).

[4] E. Oblow, "Neutron Thermalization in High Temperature Gaseous Media," Thesis, Columbia University (1970).

E. CONTROLLED THERMONUCLEAR RESEARCH

1. Energy Dependent Analysis of the d+^{4}He System (Ohlsen, Lovoi, Dodder)

Because of the growing programmatic interest in the charged particle cross sections which are of importance in fusion reactors, we have accelerated our long-planned analysis of the d+α system via Dodder's R-matrix code "EDA." A great deal of new information is available to us (polarization transfer coefficients, accurate analyzing powers) and we hope to be able to provide a definitive analysis. The data are still being assembled, but we expect to generate a preliminary report in the next month in which the lower region (0-8 MeV) is treated.

2. $D(\vec{d},\vec{n})^3$He Neutron Polarization Transfer Experiments [Salzman, Jarmer (AWU, U. Wyoming), Ohlsen, Martin, Simmons, Donoghue, Morrison]

The 0° data have been submitted as a Physics Letter. The angular distribution data are now being analyzed and will be reported at the Washington meeting of the APS, in a paper with the following abstract:

> "The longitudinal polarization transfer coefficient $K_z^{z'}(0°)$ has been measured for the incident laboratory deuteron energies 6, 8, 10, 11, 12, 13, 14, and 15 MeV. In addition, angular distributions of $K_z^{z'}(\theta)$, $K_z^{x'}(\theta)$, $K_x^{x'}(\theta)$, and $K_x^{z'}(\theta)$ have been measured at a laboratory deuteron energy of 10 MeV for laboratory angles from 0 to 80° in 10° steps. The outgoing neutron polarization was measured with a dipole spin precession magnet and a liquid helium polarimeter. Further, the polarization transfer coefficients $K_y^{y'}(\theta)$ and $K_{yy}^{y'}(\theta)$ have been measured at the same energy but over a laboratory angular range of 0 to 100° in 10° steps using a spin precession solenoid and the liquid helium polarimeter."

3. ^{3}He$(\vec{d},\vec{d})$ Polarization Transfer [Salzman, Lovoi (AWU, UNM), Gruebler (ETH), and Morrison]

A paper with the following abstract has been submitted to the Washington APS meeting:

> "For the elastic scattering of deuterons from ^{3}He at a laboratory angle of 30° and for the laboratory deuteron energies 5.65, 7.11, 8.42, and 9.39 MeV, we have measured the polarization transfer coefficients $K_x^{y'z'}$, $K_{xx}^{x'z'}$, $(K_{xx}^{x'x'}-K_{xx}^{y'y'})$, $K_{xx}^{z'z'}$, $K_y^{x'z'}$, $(K_y^{x'x'}-K_y^{y'y'})$, $K_y^{z'z'}$, $K_{zz}^{x'z'}$, $(K_{yy}^{x'x'}-K_{yy}^{y'y'})$,

and $K_{yy}^{z'z'}$. We have also measured the y axis polarization transfer coefficients (subscripts y and yy above) at a laboratory angle of 45° and for the laboratory deuteron energy of 6.60 MeV. The outgoing deuterons were slowed to 800 keV where the $^3He(\vec{d},\vec{p})^4He$ reaction was used as a polarization analyzer in conjunction with four silicon detector telescopes at θ_{lab} = 54.7°, ϕ = 0, 90, 180, and 270°.

4. d-^{3}He Spin Correlation Experiment [Ohlsen, Hardekopf, Baker (Rice U.), May (Rice U)]

Reduction of the data has been completed. Table E-1 shows the observed spin correlation parameters. These represent the first spin correlation data in d-^{3}He scattering. A paper is in progress. The data are presently being used by Dodder and Hale in their analysis of the 5-nucleon problem.

5. Intense Neutron Source (Emigh, Brolley, Muir)

The major objective of the national CTR program is to contribute to the nation's energy production soon after the turn of the century. One of the milestones to be passed in this program is a thorough knowledge of the effects of high-level neutron irradiation on materials and insulators which are to be used for CTR program. The early needs for a high-fluence 14-MeV neutron source to carry out such relevant studies probably can best be met by the supersonic-gas-target approach.

It is proposed that a 14-MeV Intense Neutron Source (INS) be established at Los Alamos for the CTR program. The 14-MeV neutrons are to be used primarily to study radiation-damage phenomena similar to those anticipated in CTR reactor structural materials. In particular, a typical first wall of a D-T reactor will be subject to a primary current of 4.4 x 10^{13} 14-MeV neutrons per cm^2 sec for a 1 MW per m^2 neutron power loading. The INS facility, with a source yield of 10^{15} neutrons per sec, will produce primary currents greater than 2 x 10^{14} 14-MeV neutrons per cm^2 sec.

The INS will consist basically of two intersecting beams, one of 1.5 A of 270-keV tritium ions and the other of a supersonic jet of deuterium molecules. The collisional intersection of these two beams will be the source of 14-MeV neutrons from the resultant D-T reaction

The INS will provide a unique facility for the measurement of certain 14-MeV neutron cross sections.

One type of cross section measurement which is intensity limited is the determination of activation cross sections where the activation product has a half-life greater than about 100 years. To see why this limit exists, consider a typical activation measurement where the cross section is ~50 mb, the sample mass ~100 mg, the atomic weight ~100 amu,

Table E-1

$^{3}\vec{He}(\vec{d},d)^{3}He$ Spin Correlation Coefficients

Energy	Angle Lab	Angle c.m.	$C_{y,y}$	$C_{yy,y}$	$C_{x,x}$	$C_{zz,y}$	$C_{z,x}$
4.0	30	49.5	-0.086±0.027	-0.002±0.049	-0.046±0.038		
6.0	30	49.5	-0.071±0.017	-0.023±0.029	0.139±0.035		
6.0	60	95.4	0.603±0.037	0.007±0.063	0.082±0.056		
8.0	30	49.6	0.027±0.017	-0.148±0.030	0.126±0.035	0.144±0.029	-0.020±0.022
8.0	*60	60.0	0.411±0.030	0.057±0.054			
8.0	60	95.4	0.413±0.033	-0.120±0.058	0.239±0.051	-0.082±0.055	0.071±0.047
8.0	*30	120.0	0.484±0.043	-0.102±0.073	0.428±0.077	0.438±0.060	0.003±0.049
9.0	30	49.6	0.038±0.012	-0.128±0.020	0.160±0.016		
9.0	60	95.4	0.471±0.023	-0.058±0.041	0.185±0.037		
9.0	*30	120.0	0.568±0.029	-0.407±0.049	0.296±0.040		
10.0	30	49.6	0.085±0.013	-0.181±0.022	0.173±0.017		
10.0	60	95.4	0.463±0.026	0.056±0.047	0.305±0.044		
10.0	*30	120.0	0.639±0.032	-0.359±0.054	0.273±0.047		
12.0	30	49.6	0.086±0.021	-0.206±0.036	0.241±0.057		
12.0	60	95.4	0.341±0.034	-0.011±0.062	0.239±0.063		

*^{3}He recoils detected

the length of irradiation ~1 day, the practical counter background ~100 counts/min, and a detection efficiency ~100%. Since the sample rate should exceed the background, one can derive an approximate relation between the required flux, ϕ, and half-life, $t_{1/2}$, of the activation product; namely, $\phi(n/cm^2\ sec) \geq t_{1/2}\ (sec)$. For example, a small Cockcroft-Walton D-T generator might produce ~3×10^{10} n/sec. At a distance of 1 cm, this produces a flux of 2.5×10^9 n/cm^2 sec and thus a half-life limit of $t_{1/2}$ ~10^2 years. By way of comparison, at the 2-cm position of the INS, where ϕ ~2×10^{13} n/cm^2 sec, the maximum half-life is about 6×10^5 years.

A number of nuclides of interest in various engineering applications have half-lives in the range 10^2 to 10^6 years. To mention a few specific examples, consider the following 14-MeV reactions which occur in the CTR-structural-material candidates Nb and Mo.

a. $^{93}Nb(n,p)^{93}Zr$, $t_{1/2} = 10^6$ y

b. $^{93}Nb(n,2n)^{92g}Nb$, $t_{1/2} > 350$ y

c. $^{92}Mo(n,p)^{92g}Nb$, $T_{1/2} > 350$ y

d. $^{94}Mo(n,p)^{94}Nb$, $t_{1/2} = 2 \times 10^4$ y

e. $^{94}Mo(n,2n)^{93}Mo$, $t_{1/2} = 3 \times 10^3$ y

To measure the cross section for reaction (a) would require the highest flux available at INS ($r \leq 2$ cm), but probably the measurement would be feasible. The only previous measurement of this important activation cross section was performed by proton counting, with relatively poor precision. Thus, a direct activation measurement would be quite valuable. The cross sections for reaction (d) and (e) also could be measured at INS (r ~10 cm and r ~30 cm, respectively).

The cross section for the reaction (b) has been measured recently by neutron counting, with the result $\sigma \simeq 800$ mb. One interesting approach here would be to treat σ as known and use the INS to measure the half-life of ^{92g}Nb. Using the measured cross section rather than the "typical" value of 50 mb, one concludes that this half-life could be measured at INS ($\phi \geq 2 \times 10^{13}$ n/cm^2 sec) even if the half-life is as large as 10^7 y. The ^{92g}Nb half-life would be interesting for a number of reasons, but primarily from the point of view of CTR radioactive-waste-disposal studies. In addition, knowledge of this half-life would allow one to measure the cross section for reaction (c), also using the INS.

All of the calculations described above are based on the assumption of a 100 mg sample mass. Target radioactivity or high cost may limit one to samples of a few micrograms. In this case, the INS facility could

be used for activation cross sections or half-life measurements for materials having activation products with half-lives up to several hundred years. For activities in this range, the INS will provide a unique facility for microgram-sample techniques.

Another area where the INS could make a unique contribution to cross-section measurements is in the area of helium production cross sections. One important example is the reaction $^{7}Li(n,n'\alpha)T$, which is the primary neutron-multiplication reaction in most conceptual fusion reactors. The 14-MeV cross section for this reaction is 330±50 mb. A more accurate measurement of this cross section is a high-priority item in CTR technology. H. Farrar has developed a helium detection system which can accurately determine helium concentrations in solids as low as one part per billion, with sample sizes in the milligram range. The fluence required to produce this much helium in a Li sample is 3×10^{15} n/cm^2. To accomplish this in one day would require a flux of 3×10^{10} n/cm^2 sec (r ~50 cm at INS).

Again drawing from the CTR technology area, the (n,α) and $(n,n'\alpha)$ reactions in structural materials are quite important from a metallurgical point of view. In the Nb-Mo region the (n,α) cross sections are ~10 mb, but for Ta and W they are down to ~1 mb. For the lower cross sections, a flux of 10^{13} n/cm^2 sec is required to generate the one part per billion concentrations needed for analysis in irradiation times ~1 day. Thus, helium production cross sections, as well as certain activation cross sections, could make good use of the highest flux levels available at the INS.

F. OTHER APPLIED PROBLEMS: NEUTRON RESPONSE OF THERMOLUMINESCENT DOSIMETERS (Smith, Donnert, and Alexander, Kansas State U.)

Thermoluminescent dosimeters were irradiated at 0.5 MeV intervals from 2 to 7 MeV and TLD's were also irradiated at 8 and 20 MeV. The TLD's were irradiated to a total dose of about 10^{11} n/cm^2. The neutrons per square centimeter were measured by a proton recoil telescope. At 20 MeV the telescope used the signal from a ΔE window-type silicon surface barrier detector and a NaI photomultiplier E detector. Coincidence was required and the gated E signal hydrogenous foil in and out data were used to calculate the total dose. In the 2-8 MeV runs a simple non-coincidence telescope was used. Various backgrounds were taken including data with no gas in the target as well as lead cone shielding to eliminate gammas from the target. (We measured the total cross section of lead.)

All of the data from 2 to 8 MeV appear to be in good shape. At 20 MeV further work needs to be done, even after an additional shift was

used to unravel the problem of recoil protons occurring outside the proton recoil telescope. These appear to come from the cooling water as well as the fact that scotch tape was used to mount the TLD's. In most irradiations, recoil protons from the cooling water do not cause trouble, but in this particular study they do.

NATIONAL BUREAU OF STANDARDS

A. NEUTRON PHYSICS

1. MeV Neutron Total Cross Sections (R.B. Schwartz, H.T. Heaton, II, J.L. Menke, and R.A. Schrack)

A paper entitled "Total Neutron Cross Sections of ^{235}U, ^{238}U, and ^{239}Pu from 0.5 to 15 MeV" has been presented at the Washington Meeting of the American Physical Society. The abstract follows:

"We have measured the total neutron cross sections of ^{235}U, ^{238}U, and ^{239}Pu in the energy range 0.5 to 15 MeV, using the NBS electron linac as a pulsed neutron source. The high purity uranium and plutonium samples were generously loaned to us by the Los Alamos Scientific Laboratory. The statistical precision was approximately 1% over most of the energy range and the energy resolution was approximately 0.1 nsec/m. Within these limitations there was no indication of any structure (fine or intermediate). The absolute accuracy is estimated to be 1%, and the data are in reasonably good agreement with other recent measurements."

2. KeV Cross Sections (H.T. Heaton, II, J.L. Menke, R.A. Schrack, R.B. Schwartz, and H.S. Camarda)

The past several months have been largely spent in refining our techniques so as to be able to consistently make measurements to an accuracy of 1% or better. A recent measurement of the hydrogen cross section, using the ^{10}B-NaI detector, gave results which agreed to within better than 1% with predictions of the effective range theory, over the energy range 1 keV to 1 MeV. Most of the problems, therefore, seem to be pretty well under control for this detector.

3. Average Neutron Transmission Measurements (H. S. Camarda)

A paper entitled "p Wave Strength Function of As, Nb, Ag, In, Sb, I, Au, and Th" has been presented at the Washington Meeting of the American Physical Society. The abstract follows:

"The good stability of the NBS linac and the excellent signal to noise ratio of the underground time-of-flight facility enable high precision neutron transmission measurements to be made. By covering the energy range 1 keV to 700 keV it is possible to extract R_0^∞ (and hence R'), S_1 and R_1^∞ from the data. The s wave resonance contribution to the average transmission is determined by using published results obtained from the analysis of well resolved levels at low energies. The sample thicknesses used were "thick" in the sense that the s wave self-protection must be fully accounted for at low energies. However, the samples were

still sufficiently thin that any errors introduced by neglecting p wave self-protection are negligible. Theoretical predictions will be compared with these results."

4. $^{10}B(n,\alpha)^{7}Li$ Branching Ratio (G. Lamaze, A. D. Carlson, and M. Meier)

Measurements of the $^{10}B(n,\alpha)^{7}Li$ branching ratio have begun. This work was prompted by recent preliminary measurements[1] of this branching ratio which are significantly lower above 50 keV neutron energy than the evaluation of Irving.[2] The present measurements are being made with a gas proportional counter containing $^{10}BF_3$ and Ar gases. The Ar gas is employed to improve the timing and pulse height resolution of the counter as well as reducing wall and end effects. The counter has a pulse height resolution of about 5% (FWHM) which is adequate for separation of the $^{10}B(n,\alpha_0)^{7}Li$ and $^{10}B(n,\alpha_1)^{7}Li$ events. Neutrons are obtained from the $T(p,n)^{3}He$ reaction. The measurements were made with a 200 kHz pulsed proton beam from the Van de Graaff accelerator so that the time uncorrelated background could be measured between neutron pulses. Initial measurements are being made at 800 keV neutron energy where background due to energy degraded neutrons is clearly separated from the events of interest. The results of these measurements agree well with the evaluation of Irving.

5. Age of ^{252}Cf Fission Neutrons to Indium-Resonance Energy in Water (V. Spiegel)

A cylindrical ^{252}Cf source of 0.762 cm D by 0.762 cm height emitting 1.8×10^{9} neutrons/sec was used as a near point source in the water medium. Three sets of cadmium-covered (0.5 mm) indium foils with diameters 1.00, 3.23, and 4.27 cm were used to measure the indium-resonance activity from 2 to 65 cm.

Integration of the indium activity as a function of the rms source-to-foil distance yielded an uncorrected age value of 28.94 cm^2. Corrections to this value arise from: a) Finite foil thickness; an increase in age of 0.51 cm^2 was made because the foils are current and not flux detectors.[3] b) Water displacement by the source; a decrease in age of 0.08 cm^2 was determined by measuring the effect of increasing the

---

[1] S.J. Friesenhahn, et al., "Measurements of the $^{10}B(n,\alpha_1\gamma)$ and $^{10}B(n,\alpha)$ Cross Sections," Gulf Radiation Technology Report Gulf-RT-A12210 (October 1972).

[2] D.C. Irving, "Evaluation of Neutron Cross Sections for Boron 10," ORNL-TM-1872 (1967).

[3] H. Goldstein, P.F. Zweifel, and D.G. Foster, Jr., Proc. 2nd Int. Conf. Peaceful Uses Atomic Energy, Geneva P/2375 (1958).

linear dimensions of the source by 50% and 100%. This correction is in agreement with the calculations of Mullin.[1] c) Density of water; a decrease of 0.11 cm^2 is necessary to specify the age at a water density of 1.000 gm/ml. Applying these corrections the final value obtained for the age is 29.26 ± 0.42 cm^2.

A summary of the results has been accepted for presentation at the 19th Annual Meeting of the American Nuclear Society to be held in Chicago, Illinois in June 1973.

6. Measurement of Absolute Fission Rates (J. A. Grundl)

Continuing efforts to determine absolute fission rates per nucleus for ^{235}U, ^{239}Pu, ^{238}U, and ^{237}Np in the Coupled Fast Reactivity Measurement Facility (CFRMF) at Aerojet Nuclear Corporation are at an intermediate stage of completion. These measurements are undertaken for the Interlaboratory LMFBR Reaction Rate Program (ILRR) and its associated effort to establish accurate fission product yields for fission activation detectors used in LMFBR fuels and materials tests.[2] Reproducibility, count rate losses, the fraction of fission fragments undetected, and neutron scattering and absorption effects have been investigated and uncertainties assigned. Typical net corrections for fission chamber responses are 1.006 ± 0.002 for a 50 μgm/cm^2 ^{235}U foil and 1.030 ± 0.011 for a 200 μgm/cm^2 ^{238}U foil. Final uncertainty assignments for the absolute fission rates per nucleus remain near ± 3% pending a further investigation of foil masses.

Fission cross section ratios established for the CFRMF central spectrum are as follows:

$$\bar{\sigma}_f(^{238}U):\bar{\sigma}_f(^{235}U):\bar{\sigma}_f(^{239}Pu):\bar{\sigma}_f(^{237}Np) =$$

$$= 1.000:[20.98 \pm 2.2\%]:[24.06 \pm 3.1\%]:[7.44 \pm 3.5\%].$$

7. Intermediate-Energy Standard Neutron Field (ISNF) (J.A. Grundl and A. Fabry*)

An intermediate energy neutron field, permanently established,

---

*CEN-SCK Laboratories at Mol, Belgium.

[1] C. R. Mullin, "The Age of Neutrons from an Anisotropic Shell Source," KAPL-M-RM-1 (25 February 1958).

[2] A low-scatter double fission chamber, and selected foils from the NBS-Los Alamos permanent set of assayed fission foils, were employed in more than fifteen separate irradiations at CFRMF with the reactor operating at power levels between 0.2 KW and 6 KW.

amenable to accurate neutron transport computations, and providing a moderately intense neutron flux (nv ~ 10^9) in the energy range 1 keV to 5 MeV is under construction at the NBS Research Reactor thermal column. Neutron transport computations (DSN and Monte Carlo) of the spherically symmetric arrangement of fission neutron sources and a ^{10}B shell within a 30 cm diameter cavity in graphite show that the neutron spectrum at the center of the system is uniform and may be established reliably by means of calculation.

B. PHOTONUCLEAR PHYSICS

1. Nuclear Scattering of Plane-Polarized Photons (E. Hayward, W. C. Barber*, and F. J. Sazama†)

A beam of plane-polarized, monochromatic photons has been produced by the resonance fluorescence of the well-known 1^+ state at 15.1 MeV in ^{12}C. These have been scattered a second time from natural targets of Cd, Sn, Ta, W, Pt, Au, and Bi. Measurements were made with poor energy resolution of the relative number of photons scattered at 90° parallel and perpendicular to the polarization vector in the incident 15.1 MeV beam. The observation of photons scattered along the polarization vector reflects the contribution of incoherent scattering to the dominant coherent scattering process and results either from permanent nuclear deformation or from the dynamic deformation produced by the coupling of the giant dipole resonance with the quadrupole oscillations of the nuclear surface. The observed intensities of incoherent scattering are of the same order of magnitude for the deformed nuclei and the spherical vibrators and agree roughly with the predictions of the dynamic collective model. No incoherent scattering was observed from the rigid sphere ^{209}Bi.

2. A "Shelf" in the Subthreshold Photofission Cross Section (C. D. Bowman, I.G. Schroder, and C.E. Dick)

In this report we wish to draw attention to the usefulness of the photofission process in the region far below the (γ,n) threshold, and to the phenomena which one encounters there. From consideration of competition between fission and γ-ray decay in the second minimum of the curve of potential energy vs deformation, we show that at low excitation energies the isomeric fission can become more probable than prompt fission. This occurs because as the excitation energy in the second

---

* Massachusetts Institute of Technology, supported by USAEC under contract No. AT(11-1)-3069 and Guest Worker at NBS.

† Harry Diamond Laboratories, HDL Fellow at the American University, and Guest Worker at NBS.

minimum decreases, the penetrability of the outer barrier decreases much more rapidly than the probability for γ-ray decay. When the γ-ray decay becomes competitive, the photofission cross section depends primarily on the penetration of the inner barrier and comparatively weakly on the depth of the potential minimum or the shape of the outer barrier. For isotopes of plutonium and uranium where the two barriers are thought to be of about equal height, the prompt and isomeric fission are equal at a total photofission cross section in the range of 10^{-8} to 10^{-7} barns which obtains near E_γ = 4 MeV. As one decreases the γ-ray energy still lower, the photofission cross section quickly becomes almost completely isomeric fission. Furthermore, the cross section starts to drop much more slowly and a "shelf" in the photofission cross section should develop. The shelf appears because the fission cross section depends only on the penetration of the inner barrier; once the nucleus is in the second minimum configuration it will decay to the deformed ground state (isomer) and then eventually will penetrate the outer barrier regardless of the outer barrier properties, provided that the isomer decays primarily by fission. Since only the inner barrier affects the fission probability at lower energies in contrast to the situation at higher energies where both inhibit the fission process, the net effect is to reduce the slope of the cross section causing a shelf to appear at the lower energies.

The shape of the cross section has been calculated for the case of two parabolic barriers of the same height and width using the Hill-Wheeler[1] relation for transmission through such barriers. The formalism of Lynn[2] is used to relate these barrier transmissions to the resonance width and spacing of the class I and class II states. The results of the calculation are presented in Fig. 1 where three curves representing different values of the barrier curvature (thickness) parameter hw. The cross section on the shelf is all isomeric or delayed fission since the process causing the shelf has isomer formation as one of the steps in the fission process. At higher energies, the fission is mostly prompt. The dot-dashed line shows the cross section where the prompt and delayed fission are equal. Note that this cross section is only weakly dependent on the barrier curvature.

With several hundred microamp electron beams and mica fission detectors viewing about 100 mg/cm^2 thickness of fissile material, we believe that cross sections as low as 3×10^{-13} barns can be studied. This should be enough sensitivity to study this sub-barrier phenomena in considerable detail.

---

[1] D. L. Hill and J. A. Wheeler, Phys. Rev. 89, 1102 (1953).

[2] J. E. Lynn, in Proceedings of Second IAEA Symposium on Physics and Chemistry of Fission, 439 (1969).

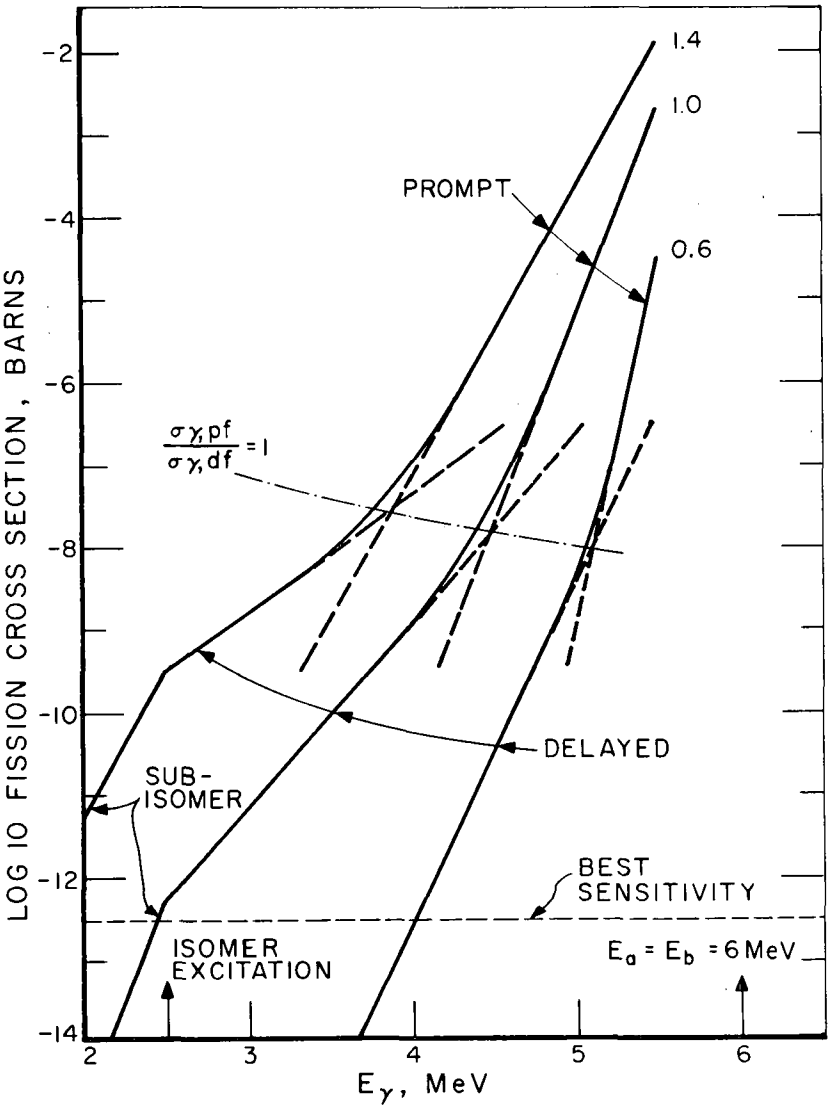

Fig. 1. The predicted photofission cross section well below the barrier is shown for values of $\hbar\omega_a = \hbar\omega_b = 1.4$, 1.0, and 0.6 MeV. The ordinate shows the $\log_{10}$ of the photofission cross section in barns and the abscissa is the photon energy in MeV. The calculation was carried out for inner and outer barriers of identical shape, and height of 6 MeV above the ground state. The isomer excitation energy is taken to be 2.5 MeV.

C. APPLIED NUCLEAR PHYSICS

1. Isotopic Analyses by Electron Scattering (S. Penner)

High energy elastic electron scattering provides a method for measuring the isotopic composition of thin target foils. The method is essentially a form of mass spectroscopy, using the dependence of recoil energy on target mass. The high resolution (7 parts in 10^4) NBS electron scattering facility can resolve better than one mass unit for $A \leqslant 40$. The first practical use of this capability was to determine the impurities in a ^{14}C target. Contaminants ranging from ^{9}Be to ^{40}Ca were detected.

2. ^{11}C Production (W. R. Dodge)

From a biomedical viewpoint, ^{11}C is a biologically useful radioisotope. We have attempted to produce "carrier-free" ^{11}CO by bremsstrahlung irradiation of graphite moss of (.002-.0018)-cm strand diameter in and O_2 environment. Comparison of the 20.5-minute activity in the gaseous efflux from the graphite moss-O_2 cell to the activity in the graphite moss indicated about 1% of the ^{11}C produced was converted into ^{11}CO and $^{11}CO_2$. The low conversion efficiency to ^{11}CO was due to the fact that only (2-3)% of the recoiling ^{11}C nuclei get out of the graphite strands. Our absolute yields were about 1 mCi/kW-g/cm^2 at an electron bombarding energy of 35 MeV. With graphite moss of smaller strand diameter (.0005-cm) and with our linac operating at 45 MeV and 16 kW of beam power, we should be able to produce ~ 10 Ci of ^{11}CO in a 30-minute bombardment.

^{11}C activities in the mCi range are used for most biomedical diagnostic and irradiation purposes. Hence, NBS could provide useful quantities of ^{11}C to biomedical users whose transportation times from NBS plus chemical preparation times were less than 2-3 hours.

3. Radioactivity Decay Schemes (D. D. Hoppes and A.T. Hirshfeld)

A program to investigate and evaluate decay schemes of nuclides useful as radioactivity standards has assumed as a first goal an overall consistency check of detector efficiency, decay scheme information and source calibration using all gamma-ray emitting standards issued by NBS. A Ge(Li) detector (1.8 keV FWHM at 1.33 MeV) has been incorporated into a high-stability system using a fast 8192 channel ADC and automatic computer analysis. Error quotations are based on an analysis of multiple runs on each sample; pulse pile-up corrections are based on simultaneous analysis of a peak introduced by a 50 Hertz pulser.

A plot of efficiency times energy vs energy in the region of 500-1400 keV shows about 1% deviations from a smooth curve for 12 gamma

rays from 9 nuclides (^{85}Sr, ^{207}Bi, ^{137}Cs, ^{94}Nb, ^{88}Y, ^{65}Zn, ^{60}Co, ^{22}Na), using available decay-scheme information and calibrations. The origin of these deviations, and those for other nuclides, are being checked. The calibration of the detector is being extended to other energies, and analysis schemes suitable for the x-ray region are being investigated.

4. Secondary Particle Spectra from Neutron Interactions with Tissue (R. S. Caswell and J. J. Coyne)

Abstract of an article published in Radiation Research 52, 488 (1972) follows:

"Theoretical calculations have been made of the secondary particle spectra for p, d, α, ^{9}Be, ^{11}B, $^{12,13,14}C$, $^{14,16}N$, and ^{16}O produced by interactions of 1- and 14-MeV neutrons with a four-element tissue containing the elements H, C, N, O. Detailed neutron cross-section data has been used in the calculation. Both "initial" spectra of the secondary particles as produced by nuclear reactions and the "equilibrium" spectra produced by particles slowing down are determined. This work is the first step in development of a quantitative description of the "physical" stage in the action of neutron radiation on biological materials. The spectra are input information for energy deposition studies for neutron microdosimetry and for models of the biological action of neutron radiation.

D. DATA COMPILATION

1. Photonuclear Data Center (E.G. Fuller, H.M. Gerstenberg, and H. Vander Molen)

NBS Special Publication 380, Photonuclear Reaction Data, 1973 was published in March. This 125-page book contains a complete index to all measurements in the field published in the period from 1955 to 1972. In addition, a brief summary is given of the gross features of the giant resonance. Included are the energy at which the cross section peaks, the maximum value reached by the cross section, the width of the "resonance" at half maximum, and the two cross section integrals which are most useful for estimating yields, $\sigma_{-0}(E_m)$ and $\sigma_{-1}(E_m)$. Data are presented both in tabular as well as graphical form for all nuclei where measurements have been made. Where a number of measurements have been made for a single nucleus, the parameters tabulated were taken from the single measurement which was felt to give the most representative picture for that nucleus.

Related to this publication is the invited paper, Photonuclear Physics, 1973, Where We Are and How We Got There, presented (EGF) at the Asilomar Conference on Photonuclear Reactions and Applications (March 1973). This contained a very brief history of the field, a review of

the data now available, and finally, a summary of the results of a world-wide survey made in early 1973 of existing and proposed facilities and programs in photonuclear physics.

2. Photon Cross Sections (J. H. Hubbell and G. L. Simmons*)

A compilation of x-ray cross section data at wavelengths used by crystallographers, produced in collaboration with LLL, is in page proof stage.[1]

Work continues on the DNA-sponsored intercomparison and evaluation of existing quasi-independent photon cross section compilations (NBS, LLL, LASL, Sandia, Kaman, and Gulf General Atomic). Results of the first phase of this intercomparison are available as a series of NBS reports.[2] We expect to determine and assemble an interim DNA "best set" by January 1974, using portions of the above existing sets plus new theoretical photoeffect results by J. Scofield (LLL) and scattering results by D. Cromer (LASL) and by R. T. Brown (LASL).

Through participation in the Shielding Subcommittee of CSEWG (Cross Section Evaluation Working Group, AEC) we are continuing to examine, update, and expand the ENDF/B photon cross section library tape.

3. Beta Radiation Data (M. Martin,† N. B. Gove,† and M.J. Berger)

Martin and Gove at ORNL with the collaboration of Berger are preparing a comprehensive compilation of data on beta radiation emitted by a large number of nuclides used in nuclear technology and medicine. This involves (a) extension and updating of data on the mean number of beta particles per disintegration and their average and maximum energies, and the "R90" range in water, and (b) a tabulation of the complete beta spectra both for the complete complex beta spectrum consisting of several components with different endpoint energies, and for the individual components separately.

---

* Science Applications, Inc., Huntsville, Alabama.

† Oak Ridge National Laboratory.

1 J. Hubbell, W. McMaster, N. DelGrande and J. Mallett, X-Ray Cross Sections and Attenuation Coefficients, Sec. 21 of International Tables for X-Ray Crystallography, Vol. 4 (in press).

2 G.L. Simmons and J.H. Hubbell, Comparison of Photon Interaction Cross Section Data Sets. I. Storm-Israel and ENDF/B, NBS 10668 (unpublished); II. Biggs-Lighthill and ENDF/B, NBS 10818 (unpublished); III. NSRDS-NBS 29 and ENDF/B, NBS 10842 (unpublished); IV. Kaman and ENDF/B, NBS 10847 (unpublished); V. Photran and ENDF/B, NBS 10848 (unpublished); VI. McGuire and Kaman Photoeffect Data (in NBS editorial review).

E. FACILITIES

1. Above-Ground Neutron Facility (S. Penner)

The neutron source building was finally completed by the contractor in December 1972. Since then, major emphasis has been on installation of beam transport equipment to guide the linac electron beam to the new source. Completion of this phase is scheduled for May 1973. By judicious scheduling, we have been able to keep the old 40 m underground flight path in operation for all but one month during the installation process. Installation of the above-ground flight paths and end stations is now beginning. Initially, we will provide three paths, the longest being 200 m.

2. Positron Source (S. Penner)

Initial testing of the positron acceleration system for the NBS linac began in January 1973. To date, we have obtained positron currents of 7 na. Beam energies from 20 to 40 are available. So far, we have restricted electron beam power on the converter to under 15 kw (the linac is capable of over 40 kw), and have not attempted to focus the electron beam to the small spot size needed for optimum positron capture. Operation of the converter under these limitations has been completely satisfactory. We will begin to use electron beam focusing within the next few weeks, and expect to achieve positron currents in excess of 0.1 μA.

3. 3-MeV Van de Graaff Facility (A.D. Carlson, M. Meier, and G. Lamaze)

Since the last report, there has been generally good performance from the Van de Graaff accelerator although some down time has been experienced as a result of the development of a slow pulsing system. Design studies show that an appreciable increase in the pulsed beam on target can be achieved by the introduction of a quadrupole magnet at the accelerator exit. Modifications are currently being planned for the beam transport system which will be implemented when the quadrupole arrives later this year.

Some delay has been experienced at ORNL in the development of the thin tritiated targets to be used in the associated particle facility. The electronics have been acquired for this system and experimental studies preliminary to final hardware design will proceed as soon as the targets are received. The interfacing of the on-line computer which has been ordered from Datacraft Corporation is presently being designed.

NAVAL RESEARCH LABORATORY

A. NEUTRON RESONANCE SPECTROSCOPY

1. Neutron Resonances in ^{185}Re and ^{187}Re up to 3 keV (A. Stolovy, A.I. Namenson, and J.A. Harvey*)

The neutron resonances in the target nuclei ^{185}Re and ^{187}Re are interesting from several points of view. The level spacing for both isotopes is only about 4 eV, so that many resonances can be observed to yield good cases for statistical analysis. These isotopes are in the region of a peak in the s-wave strength function. Also, previous work at the NRL linac[1] has indicated the presence of an intermediate structure state in ^{187}Re. With these considerations in mind, we have extended these measurements to much higher neutron energies.

In collaboration with personnel at ORNL, our NaI detector arrangement[1] was installed at the 80 meter station of the ORELA facility. Data were taken on capture gamma-rays associated with the resonances using separated isotopes. The resolution was sufficient to yield well resolved data up to about 3 keV, comprising hundreds of levels in each isotope. This massive amount of data is now being analyzed to obtain the following information:

a. Estimates of $g\Gamma n$ for as many levels as possible
b. Probabilities that the levels are due to p-wave neutrons
c. A search for intermediate structure
d. s-wave strength function determinations
e. Distribution of $g\Gamma n^0$ values
f. Distribution of level spacings.

Figures A-1, A-2, and A-3 are representative time-of-flight spectra for three different energy regions in ^{185}Re, showing the quality of the data. Many small resonances, probably due to p-wave neutrons, can be seen. We now have data on about 10 times as many resonances as we had previously.

Although we did not take data with different sample thicknesses, it is possible to obtain estimates of $g\Gamma n$ by making use of the parameters which have been measured[2,3] for resonances below 100 eV. An average

---

* Oak Ridge National Lab., Oak Ridge, Tenn.

[1] Stolovy, Namenson, and Godlove, Phys. Rev. C4, 1466 (1971).

[2] Friesenhahn, Gibbs, Haddad, Frohner, and Lopez, J. Nucl. Energy 22, 191 (1968).

[3] Ideno, Asami, Nakajima, Ohkubo, and Fuketa, J. Nucl. Sci. and Tech. 9, 261 (1972).

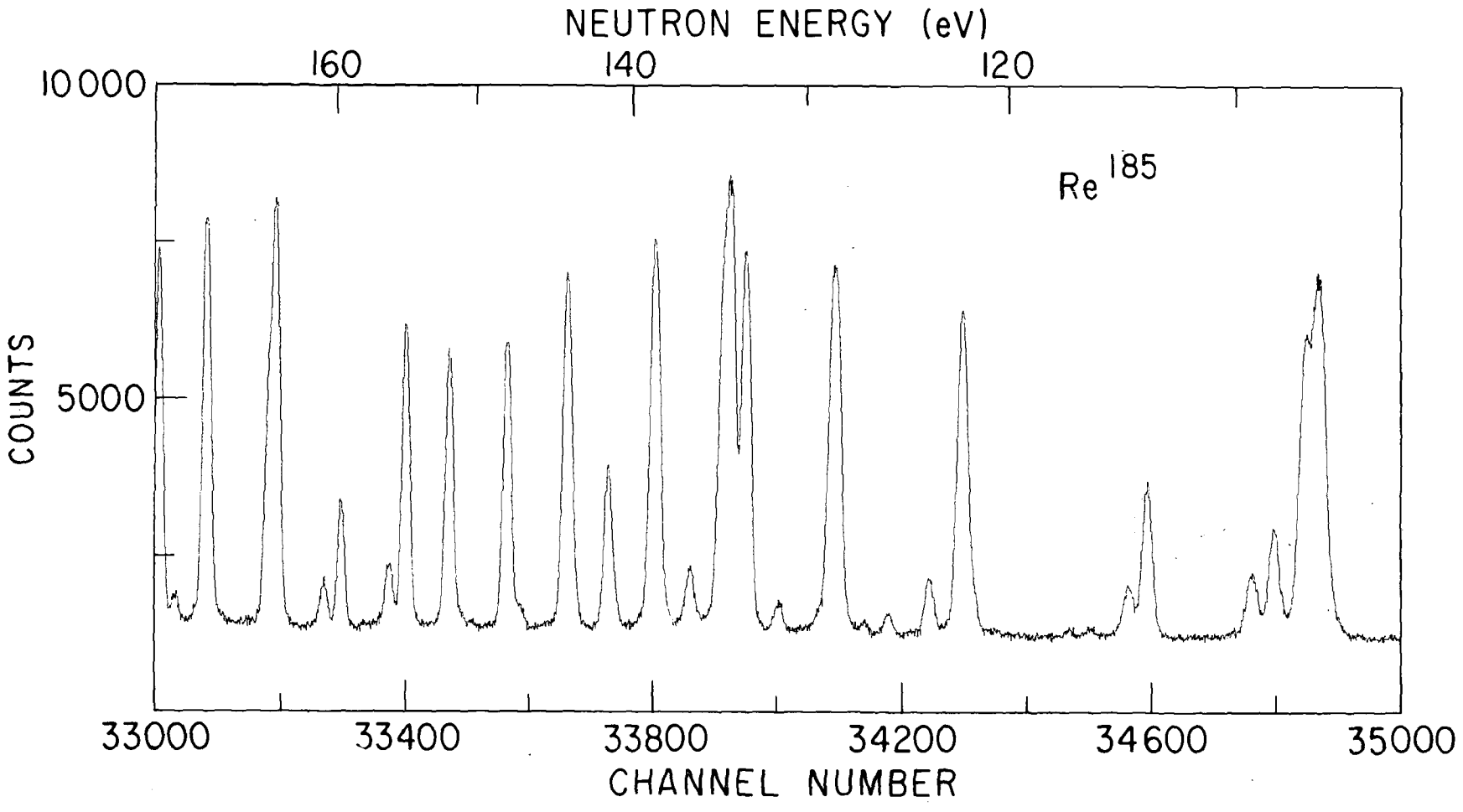
NEUTRON ENERGY (eV)
160
140
120
10000
5000
COUNTS
Re 185
33000
33400
33800
34200
34600
35000
CHANNEL NUMBER

Fig. A-1

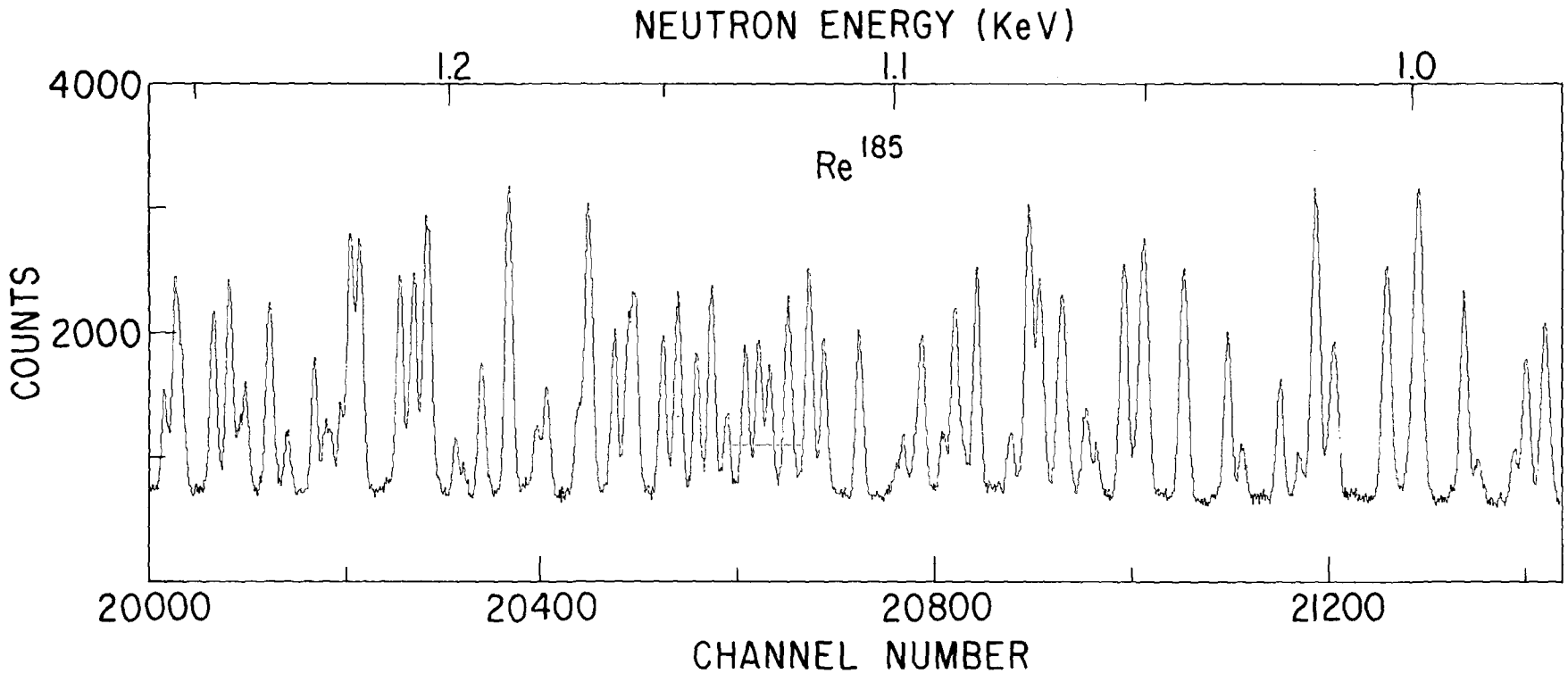
NEUTRON ENERGY (KeV)
1.2
1.1
1.0
4000
2000
COUNTS
Re 185
20000
20400
20800
21200
CHANNEL NUMBER

Fig. A-2

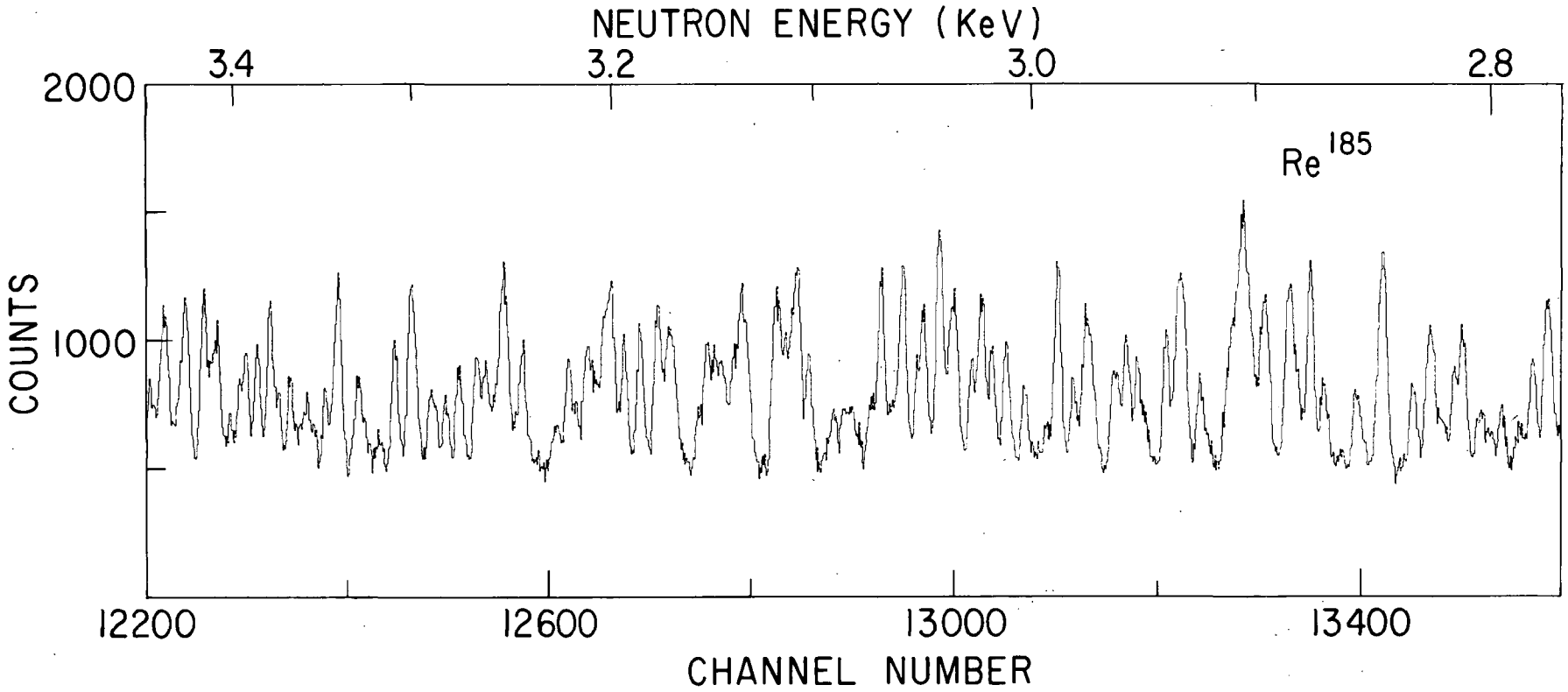
NEUTRON ENERGY (KeV)
3.4
3.2
3.0
2.8
2000
1000
COUNTS
Re 185
12200
12600
13000
13400
CHANNEL NUMBER

Fig. A-3

constant of proportionality is obtained between our observed peak areas and calculated values using known parameters and accounting for the effects of sample thickness, Doppler broadening, neutron spectral shape, and transmission through a ^{10}B filter. Once this constant is obtained, it can be used to obtain estimates of $g\Gamma n$ for higher energy resonances by an iterative procedure on a computer. We take $\Gamma\gamma$ to be a constant. This assumption introduces the major cause of uncertainty in our values of $g\Gamma n$. We can then calculate the probabilities that the resonances are due to p-wave neutrons by a Bayes' theorem formalism.[1]

The data were taken with two integral bias levels: 4 MeV (essentially primary transitions), and 1 MeV (used to normalize the high bias data). Coceva et al.[2] have indicated that one can search for intermediate structure in the gamma exit channel by looking at this normalized primary transition intensity as a function of neutron resonance energy. They claim to have found structure of this kind for the target ^{115}In. We have similarly indicated the presence of intermediate structure for ^{187}Re, but none for ^{185}Re. Preliminary results on our new data do not indicate any obvious intermediate structure in either isotope. Even the previously observed peak in ^{187}Re is greatly reduced due to the appearance of new resonances and the superior resolution of overlapping resonances.

The resonances in these two isotopes provide excellent statistical samples. We plan to analyze the s-wave level spacings in terms of the Dyson-Mehta statistic for a two-level population (since both spins $J = I \pm \frac{1}{2}$ are present), and for comparison with a Wigner distribution. The distribution of the $g\Gamma n^o$ values will be compared to a Porter-Thomas distribution, and s-wave strength functions will be calculated.

B. CONTROLLED THERMONUCLEAR RESEARCH

1. Neutron Energy Spectra from Exploding Wires (F.C. Young, S.J. Stephanakis, D. Mosher, and I.M. Vitkovitsky)

Yields of more than 10^{10} neutrons have been observed from plasmas produced by exploding-wire discharges (10^{12} W) of deuterated polyethylene fibers.[3] Evidence for neutron production in such plasmas by d-d

---

[1] L.M. Bollinger and G.E. Thomas, Phys. Rev. 171, 1293 (1968).
[2] Coceva, Corvi, Giacobbe, and Stefanon, Phys. Rev. Letters 25, 1047 (1970).
[3] Stephanakis, Levine, Mosher, Vitkovitsky and Young, Phys. Rev. Letts. 29, 568 (1972).

thermonuclear fusion and by collective ion acceleration has been reported.[2] The contribution to the neutron yield from various sources was based on measurements of the neutron activation produced in various delayed-activation counters and on neutron isotropy measurements. In this report the results of neutron-energy-spectrum measurements by the time-of-flight (TOF) technique are presented. These measurements were carried out in order to assess more reliably the relative importance of neutron production by collective ion acceleration in the energetic discharge.

The TOF counter consists of a 2" diam. x 2" encapsulated liquid scintillator (NE-213) coupled to a 56AVP photomultiplier. To avoid the initial x-ray flash, the counter is surrounded completely by one inch of lead and is located 14.73 ± 0.03 meters from the fiber source. In addition, 3" of lead shielding is located 2.5 meters from the fiber in the neutron flight path for x-ray attenuation. Neutrons reaching the scintillator must also pass through a 0.5" inch brass wall on the vacuum chamber containing the fiber. The counter is located at an angle of 68° to the fiber axis and is enclosed in an aluminum container for electromagnetic shielding. The aluminum anode used in previous measurements[2] has been replaced with a carbon anode to minimize x-ray production. Also a mechanism for positioning the wire tautly across the diode gap is used to insure good fiber geometry.

The results of TOF measurements for initial fiber diameters of 0.0003" to 0.006" are shown in Fig. B-1. The anode output of the phototube is photographed on an oscilloscope set at 5 V/cm and 200 nsec/cm. The time scale on the photographic display was calibrated with a 2 Mhz pulser. The initial 15 V pulse on the TOF traces corresponds to the x-ray flash, and 2.45-MeV neutrons from d-d thermonuclear fusion arrive at the detector 630 nsec after the x-ray flash. The neutron energy scale is measured relative to the initial x-ray peak. An uncertainty of ± 25 nsec in zero time due to the duration of the discharge corresponds to an uncertainty in neutron energy of 16% at 14 MeV and 8% at 2.5 MeV. The onset of a neutron group at 2.5 MeV is apparent in the traces obtained for 0.006", 0.004" and 0.002" diam. fibers. On the other hand, pulses corresponding to neutrons of up to 10 MeV are apparent in the trace obtained for a 0.0007" diam. fiber.

Total neutron yields, as measured by a Ag-activation counter,[1] for various fiber diameters are given in Table B-1. These results are based on a Ag-counter calibration corresponding to 2.5-MeV neutrons. The variation of neutron yield with fiber diameter is consistent with the energy spectra observed in Fig. B-1. However, the yields for the

[1] Young, Stephanakis, Vitkovitsky, and Mosher, IEEE Tranc. Nucl. Sci. NS-20, 1, 439 (1973).

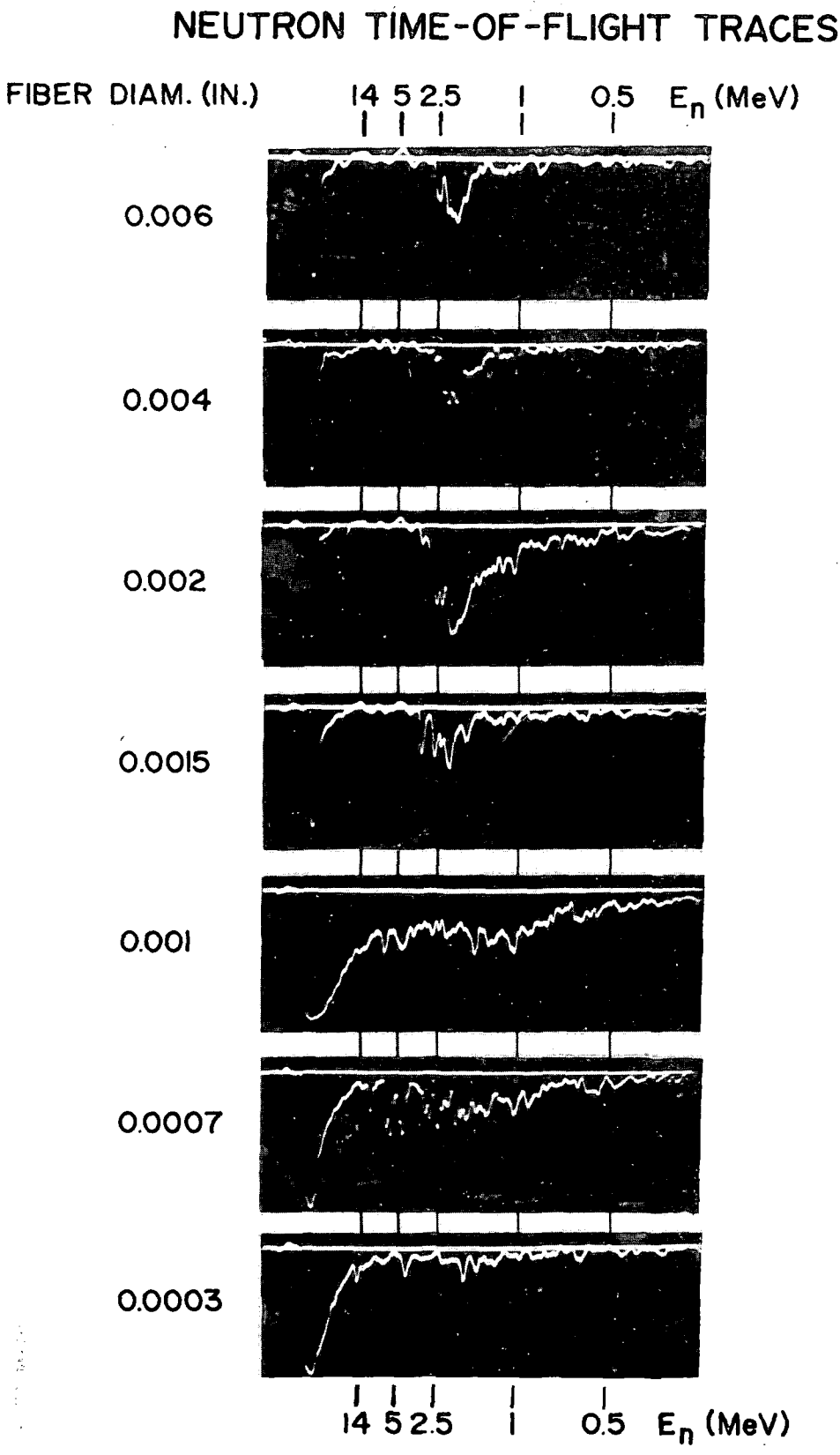
NEUTRON TIME-OF-FLIGHT TRACES
FIBER DIAM. (IN.)
14 5 2.5 1 0.5 En (MeV)
0.006
0.004
0.002
0.0015
0.001
0.0007
0.0003
14 5 2.5 1 0.5 En (MeV)

Fig. B-1

smaller diameter wires are underestimated by using the 2.5-MeV neutron energy calibration. The sensitivity of the Ag counter decreases by about two as the neutron energy increases from 2.5 to 14 MeV. It is estimated that the number of events for each trace in Fig. B-1 ranges from about 25 for the 0.004" diam. fiber to about 100 for the 0.0007" diam. fiber.

The dramatic change in the neutron energy spectrum for a change in initial fiber diam. from 0.002" to 0.001" suggests that the dominant neutron production mechanism is changing with wire diameter. For d-d thermonuclear fusion a nearly monoenergetic neutron group of 2.5 MeV is expected. The low energy tail observed in the spectra for 0.006", 0.004" and 0.002" diam. fibers is presumably due to neutron scattering by shielding in the flight path and/or in the environment. The detector geometry and environment are not ideal to minimize such scattering. It is estimated that only 5% of the neutrons emitted within the solid angle of the detector are not scattered by lead and brass shielding in the flight path. The broad energy spectrum observed for the smaller diameter fibers indicates that ions of several MeV are produced in the discharge. Under these conditions energetic neutrons may be produced by $d(d,n)^3He$ or $^{12}C(d,n)^{13}N$ reactions in the plasma. Neutrons from the latter reaction may also be produced by the collective acceleration[1] of deuterons onto the carbon anode. The production of 10-MeV neutrons by the $d(d,n)^3He$ reaction requires that deuterons be accelerated to at least 5 MeV in the discharge. For the $^{12}C(d,n)^{13}N$ reaction, at least 9.5-MeV deuterons are required to produce 10-MeV neutrons.

In conclusion, measurements of neutron energy spectra by time-of-flight from exploding 0.006", 0.004" and 0.002" diam. deuterated polyethylene fibers are consistent with a thermonuclear fusion mechanism, but the spectrum measured for smaller diameter fibers implies that positive ions of several MeV energy are produced in the discharge.

---

[1] J.D. Lawson, Particle Accelerators 3, 21 (1972).

Table B-1

Neutron Yields from Exploding Wires

Initial Fiber Diameter (in.)	Total Neutron Yield (10^9 neutrons)
0.006	1.9
0.004	1.6
0.002	4.9
0.0015	3.1
0.001	4.9
0.0007	5.3
0.0003	2.2

OAK RIDGE NATIONAL LABORATORY

A. NEUTRON PHYSICS

1. Integral Neutron Scattering Measurements on Carbon From 1 to 20 MeV*,** (G. L. Morgan, T. A. Love and F. G. Perey)

The spectrum of neutrons above ~1 MeV scattered by a thick (3.81 cm) carbon ring has been measured as a function of the incident neutron energy over the range from 1 to 20 MeV. Data were taken for three angles: 60°, 90°, and 135°. A linac (ORELA) was used as a neutron source with a 47-m flight path. Incident energy was determined by time of flight while scattered spectra were determined by pulse-height unfolding techniques. The results of the measurement are presented in forms suitable for comparison to calculations based on the evaluated neutron data files.

---

*Abstract of ORNL-TM-4157.
**Relevant to Request Nos. 32 and 34.

2. Valency Model of Radiative Neutron Capture in $^{88}Sr(n,\gamma)^{89}Sr$* (R. R. Winters†, O. A. Wasson††, and R. L. Macklin)

The total capture cross section of the reaction $^{88}Sr(n,\gamma)^{89}Sr$ was measured from 2.5 to 400 keV neutron energies at the Oak Ridge Linear Electron Accelerator using a fluorocarbon liquid scintillator as a γ-ray detector. The capture events were weighted using the Total-Energy Weighting method of Macklin. The resonance energies, neutron widths, and total radiative widths were determined. The ground state partial radiative widths are also obtained from the relative size of the high energy part of the γ-ray spectrum. A comparison of these partial widths with the predictions of the valency model of neutron capture will be presented.

---

*To be presented at the Washington, D. C. APS Meeting, April 23-26, 1973.
†Denison University
††Brookhaven National Laboratory

3. Mass and Total Kinetic Energy Distributions from the Spontaneous Fission of ^{246}Cm* (Frances Pleasonton, Robert L. Ferguson, Franz Plasil and Curtis E. Bemis, Jr.)

Energies of coincident pairs of fission fragments from spontaneous fission of ^{246}Cm have been measured with silicon surface barrier detectors.

Fragment mass and total kinetic energy distributions have been deduced and compared to those obtained from a companion experiment, using the same apparatus, on ^{252}Cf (SF). For ^{246}Cm(SF) the first and second moments of the fragment distributions, in terms of "provisional" masses in amu and post-neutron-emission kinetic energies in MeV, are as follows: $\langle m_H \rangle$ = 139.5; $\langle m_L \rangle$ = 106.5, σ_m = 6.6; $\langle E_K \rangle$ = 181.3; σ_{EK} = 10.8. Our results are compared with recent work[1] on other Cm isotopes and other trans-Pu elements.

---

*To be presented at the Washington, D. C. APS Meeting, April 23-26, 1973.
[1]See, for example, K. F. Flynn, B. Srinivasan, O. K. Manuel and L. E. Glendenin, Phys. Rev. C 6, 2211 (1972); D. C. Hoffman, G. P. Ford and J. P. Balagna, Phys. Rev. C 7, 276 (1973).

4. Half-Value Thickness Measurements of Ordinary Concrete for Neutrons from Cyclotron Targets* (H. M. Butler, K. M. Wallace and C. B. Fulmer)

Half-value thicknesses (or half-value layers) of ordinary concrete were determined for neutrons emitted from a variety of cyclotron beam-target combinations. Targets of carbon, aluminum, copper and tantalum were each bombarded with beams of protons, deuterons, alpha particles, and carbon ions at the Oak Ridge Isochronous Cyclotron. Measurements were made of neutron attenuation by an 80 cm thick wall for each target-beam combination. For protons, deuterons, and alpha particles a range of bombarding energies were used; maximum neutron energies were as high as 60 MeV. The half-value thicknesses for neutrons from all of these particle-target combinations are in the range of 9-10.5 centimeters.

---

*To be presented at the 1973 Annual AIHA Conference, Boston, Massachusetts, May 20-25, 1973.

5. Total Cross Section of Calcium* (J. L. Fowler, C. H. Johnson and N. W. Hill)

We have measured the total cross section of calcium (96.96% ^{40}Ca) from 60 keV to 1000 keV with energy resolution ranging from ~0.1 keV to ~1.0 keV. For the neutron detector at the 200-meter time-of-flight station of the Oak Ridge Electron Linear Accelerator, we used the plastic scintillator, NE-110. Delayed 0.5-MeV gamma rays from the source were removed by a 2-cm filter of ^{238}U. The delayed 2.2-MeV gamma-rays were removed by both the filter and by the use of a differential pulse height window for the detector. From the widths of narrow unresolved resonances, we determined the neutron energy resolution as a function of neutron energy as

follows: $\Delta E/E = 0.0004\ [1 + 3.5\ E(\mathrm{MeV})]^{1/2}$. This empirical formula corresponds to an uncertainty in distance of 4 cm and a time spread to 5 nsec. In the range of our measurements up to 1000 keV we see ~100 resonances, about 1/6 of which we identify as s-wave resonances from their heights and shapes. Below 600 keV we see 2.5 times the number of resonances reported in the literature.

---

*To be presented at the Washington, D. C. APS Meeting, April 23-26, 1973.

6. ^{241}Pu Neutron Total Cross-Section Measurements at ORELA* (F. B. Simpson†, J. A. Harvey and N. W. Hill)

Neutron total cross-section measurements for ^{241}Pu are in progress at ORELA in the energy range from 0.5 eV to ~8 MeV. An 80-meter flight path is used with accelerator pulse widths of 30 to 4 nsec, resulting in an energy resolution $\Delta E/E$ of $0.0007\ \sqrt{1 + 4E(\text{in MeV})}$. Measurements are made with a ^{6}Li glass detector from 0.5 eV to 100 keV and with an NE-110 scintillation detector from 10 keV to 8 MeV. Backgrounds are $\lesssim$ 1%, with a major part of it being constant room background at low energies, 2.23-MeV gamma rays (with a 16-μsec decay period) from H-capture in the moderator at keV energies with the ^{6}Li glass detector, and a background in the keV measurements with the NE-110 detector due to neutrons being moderated (with a 5-μsec leakage period) by the detector and producing gamma rays from capture in the detector. Three different sample thicknesses are being measured and are cooled to liquid nitrogen temperature. The samples are 5/8 in. diameter metallic discs with thicknesses of 0.006 in., 0.026 in. and 0.126 in. The ^{241}Am was separated from the plutonium oxide sample just before converting the oxide to metal.

---

*Relevant to Request No. 474.

†Aerojet Nuclear.

7. Further Search for Intermediate Structure in the Re Isotopes* (A. Stolovy†, A. I. Namenson†, and J. A. Harvey)

As an extension of data taken previously[1], neutron resonances up to about 3 keV in the target nuclei ^{185}Re and ^{187}Re were observed at the 80-meter station of the ORELA facility. Data on several hundred resonances were obtained in each isotope. Four large NaI detectors were used to observe capture gamma rays as a function of time of flight. For each resonance, the intensity of the capture gamma rays above 4.0 MeV was divided by the intensity of capture gamma rays above 1.0 MeV. We then look for trends in this normalized primary transition intensity as a function of neutron energy. Our earlier data[1] appeared to show evidence for the

presence of an intermediate state in the compound nucleus ^{188}Re, similar to the structure reported by Coceva et al.[2] for ^{115}In. The data taken at ORELA comprise an order of magnitude more resonances than we had previously. We find no evidence for additional intermediate structure in either isotope. The data will be analyzed to obtain estimates of $g\Gamma_n$, and various statistical tests will be applied.

---

*To be presented at the Washington, D. C. APS Meeting, April 23-26, 1973.

†Naval Research Laboratory

[1] A. Stolovy, A. I. Namenson, and T. F. Godlove, Phys. Rev. C4, 1466 (1971).

[2] C. Coceva, F. Corvi, P. Giacobbe, and M. Stefanon, Phys. Rev. Letters 25, 1047 (1970).

8. Neutron Fission Cross Section of ^{249}Cf wrt ^{235}U, using 128 μg Sample* (J. W. T. Dabbs, C. E. Bemis, N. W. Hill, M. S. Moore† and A. N. Ellis†)

Time-of-flight measurements of the neutron-induced fission cross section of ^{249}Cf have been performed at ORELA, using an ultrapure 128 μg sample of ^{249}Cf and compared with that of a 458 μg sample of ^{235}U measured simultaneously in the same flight path. Identical diffused junction fission fragment detectors[1] were used. An α-particle count rate of 10^7/sec caused substantial deterioration of the ^{249}Cf detector during each overnight run. A total of ~7 x 10^5 Cf events were recorded. Previous measurements[2] using an underground nuclear explosion gave results down to ~20 eV, with comparable resolution. Eleven new resonances were found between 0.3 eV and 20 eV, including a very large resonance at 0.71 eV of total width ~0.15 eV and σ_o ~4000 b. This resonance accounted for ~75% of the total fissions recorded.

---

*To be presented at the Washington, D. C. APS Meeting, April 23-26, 1973.

†Los Alamos Scientific Laboratory

[1] Solid State Radiations, Los Angeles, CA 90064, Model 600-PIN-125.

[2] M. G. Silbert, LASL Report LA-5042 MS; to be published.

9. Validity of the Valence Neutron Model for ^{98}Mo*,** (G. W. Cole†, R. E. Chrien†, R. C. Byrd†, S. F. Mughabghab†, G. G. Slaughter and J. A. Harvey)

Measurements of neutron capture gamma-ray spectra from ^{98}Mo taken at the HFBR chopper and later at the Oak Ridge Electron Linear Accelerator (ORELA) have indicated that for large neutron widths, the partial radiative

widths for ^{98}Mo are well predicted by a model which ascribes the radiative strengths to the motion of a valence p-neutron outside a ^{98}Mo core. The detailed extension of the model to higher neutron energies is made possible by additional total cross-section measurements at ORELA from which neutron widths and resonance parities may be derived. For these measurements a thick sample of 0.043 atoms/barn was used with a 78.2 meter flight path to give a nominal resolution of 0.06 ns/meter. Parameters were derived for resonances up to approximately 100 keV; detailed comparisons with the valence model, however, were restricted to energies below 10 keV. The validity of the model in this region is discussed.

---

*Presented at the New York APS Meeting, January 29 - February 1, 1973.
**Relevant to Requests 222 and 223.
†Brookhaven National Laboratory

10. The Neutron Total Cross Section of ^{248}Cm*,** (R. W. Benjamin†, C. E. Ahlfeld†, J. A. Harvey and N. W. Hill)

Neutron time-of-flight transmission measurements were made with 13.0 mg of 97% pure ^{248}Cm, using the Oak Ridge Electron Linear Accelerator. Data were collected from the cadmium cut-off to 3 keV. The small diameter (1.6 to 4 mm) cylindrical samples were cooled with liquid nitrogen to reduce Doppler broadening. The thickest sample had an inverse thickness of 637 barns/atom, which made possible the identification of forty resonances in ^{248}Cm below 3 keV. The average resonance spacing below 1 keV is about 50 eV. The first five resonances (7.25 eV, 26.9 eV, 35.0 eV, 76.1 eV, and 98.9 eV) are suitable for shape analyses to obtain Breit-Wigner, single-level resonance parameters. Results of the preliminary analyses will be presented.

---

*To be presented at the Washington, D. C. APS Meeting, April 23-26, 1973.
**Relevant to Request No. 523.
†Savannah River Laboratory, Aiken, S.C.

11. Prompt Gamma Rays Emitted in the Thermal-Neutron Induced Fission of ^{233}U, ^{235}U, and ^{239}Pu and the Spontaneous Fission of ^{252}Cf*,** (Frances Pleasonton, Robert L. Ferguson, and H. W. Schmitt)

A series of four experiments, corresponding to four different fission reactions (see title), were performed to determine the average energy $\bar{E}_\gamma$ and average number $\bar{N}_\gamma$ of gamma rays emitted within ~5 nsec after fission as functions of fragment mass m and fragment total kinetic energy E_K. All

results for $\overline{E}_\gamma(m)$ and $\overline{N}_\gamma(m)$ exhibit a saw-tooth behavior. Further, the $\overline{E}_\gamma(m)$ results for all four cases are nearly congruent, as are the $\overline{N}_\gamma(m)$ results. The similarity of these functions to that describing the number of neutrons emitted in fission, $\nu(m)$, is shown. The average photon energy $\overline{\varepsilon}$ has also been obtained as a function of m, and all quantities have been obtained as a function of E_K as well. Trends in all of these results are qualitatively understood in terms of fragment nuclear structures.

---

*To be presented at the Washington APS Meeting, April 23-26, 1973.

**Relevant to Request Nos. 358 and 449.

12. Fast Neutron Capture Cross Sections for Silicon* (B. J. Allen† and R. L. Macklin)

One of the continuing programs at the Oak Ridge Electron Linear Accelerator is the measurement of fast neutron capture by stable isotopes. A flight path of 40 meters and 3-5 ns pulses give an energy resolution of about 0.2% FWHM over an energy range 2.5 - 1000+ keV. Where there is a special interest in the inverse photonulcear reaction it is possible to study the partial radiative widths of capture resonances by simply recording the detector response above an appropriate high bias level separately. The high efficiency at good resolution and low neutron sensitivity of the detector system make this an attractive alternative to NaI(Tl) or Ge(Li) detector work when the excited states of the compound nucleus are an MeV or two above the ground state as in ^{207}Pb+n and ^{28}Si+n.

Total neutron capture has been run with a 0.027 atom/barn sample of natural silicon. As expected, most of the resonances observed are from the 92.2% abundant ^{28}Si target. The average radiative width (for resonances of assigned spin) is 4.6 eV. The wide range (0.4 to 14.5) and suggestion of correlation with neutron width may favor nonstatistical capture mechanisms. An 808 keV resonance shape comparison with the photo-nuclear ^{29}Si+γ data of Jackson and Toohey[1] indicating a doorway state in the reaction will require better statistics, a thicker sample, and a high bias.

---

*Presented at the International Conference on Photo-Nuclear Reactions and Applications, March 26-30, 1973 at Pacific Grove, California.

†Present address: Australian Atomic Energy Commission, Lucas Heights, Australia.

[1] H. E. Jackson, R. E. Toohey, Phys. Rev. Letters 29, 379 (1972).

13. Neutron Total Cross Sections for Kilovolt Neutron Energies*

(W. M. Good, J. A. Harvey and N. W. Hill)

Neutron transmission studies have continued, of nuclides whose neutron resonant spacings are of the order of a kilovolt. The energy range of study generally is about 1 keV to 400 keV and separated isotopes are employed.

Continuing as of one year ago, $^{29,30}Si$, $^{40,42,43,44}Ca$, $^{47,49}Ti$, $^{54,57}Fe$, $^{204,206,207,208}Pb$ are in various stages of study and to these have been added $^{90,91,92,94,96}Zr$, $^{33,34}S$ and ^{6}Li.

Very little information is generally available on total cross sections $^{29,30}Si$, $^{33,34}S$ (Ref. 1). Hence the resonant energies observed for these nuclides in the present measurements are listed in Table I.

On account of ORELA's high resolution, many levels are expected to be observed in present transmission measurements which were unobservable before, excepting possibly for the earlier capture measurements (capture can be a bit more sensitive to narrow resonances than transmission). In Table I are listed the resonances observed in $^{54,57}Fe$ in the present measurements. The most recent data for comparison is Hockenbury et al.[2] and Rohr and Müller.[3]

No listing is provided of the resonance levels observed in $^{90,91}Zr$ (Ref. 4). However, a scan of the raw Zr transmission data indicates many small resonances not resolved in the previous measurements.[5] In the energy interval from 3 keV to 70 keV on which only 13 resonances were then reported, there now appears at least 35.

---

*Relevant to Request Nos. 10, 165, 173, 182, 189 and 197.

[1] CINDA 72, Vol. 1, IAEA Vienna (1972).

[2] Hockenbury, Bartolome, Tatarczuk, Moyer, and Block, Phys. Rev. 178, 1746 (1969).

[3] G. Rohr and K. N. Müller, Z. Phy. 227, 1 (1969).

[4] Measurements on $^{90,91}Zr$ were made in collaboration with Mr. Richard E. Toohey, Physics Division, Argonne National Laboratory. Samples were courtesy of Dr. A. B. Smith, Argonne National Laboratory.

[5] W. M. Good and H. Kim, Phys. Rev. 165, 1329 (1968).

Table I. Listing of Resonances Observed in the Target Nuclides $^{29,30}Si$, $^{33,34}S$, $^{54,57}Fe$. In $^{54,57}Fe$, * = new, ** = previously observed but different energy assignments.

^{29}Si keV	^{30}Si keV	^{33}S keV	^{34}S keV	^{54}Fe keV	^{57}Fe keV
15.29	2.235	13.44	30.37	7.813	1.628
38.79	4.98	17.63	118.5	9.476	3.973
159.6	63.43	23.93	231.3	11.169*	4.746
184.5	185.8	30.37	301.3	14.455	6.276
336.7	235.1	52.17	317.6	30.628*	7.215
385.4	302.7	53.54	357.2	39.053*	7.934
553.2	413.5	59.06	362.5	51.533*	12.847
650.3	644.4	77.84	396.6	52.1	13.286*
	747.6	81.46	435.7	55.341*	13.966
	849.9	87.50	464.0	72.089	18.224
		101.2	470.8	98.820	21.049*
		151.6	510.2		21.284
		168.7	642.5		28.624
		178.3	800.6		29.680
		197.3	814.5		37.078*
		221.7	839.5		39.361*
		228.8	851.0		41.643
		238.4	893.7		41.958*
			935.8		47.164
			1019		49.917*
			1089		52.644*
			1125		56.539
			1193		61.786
			1313		65.416*
			1352		74.331*
			1391		77.528
			1450		83.812*
					88.089*
					89.816*
					91.672*
					93.912*
					101.695**
					109.866**
					118.832**

14. Tungsten Neutron Elastic- and Inelastic-Scattering Cross Sections From 4.34 To 8.56 MeV* (W. E. Kinney and F. G. Perey)

Measured natural tungsten neutron elastic- and inelastic-scattering cross sections are presented and shown to be in good agreement with the results of others. An evaporation model of inelastic scattering was found to be applicable with nuclear temperatures in agreement with previous results but with total inelastic cross sections larger by as much as 20% than measured nonelastic cross sections. ENDF/B W (Mat 1060-63) elastic angular distributions agree with our data at angles less than 50° but do not at larger angles. The ENDF/B nuclear temperatures are 10-15% lower than experimental temperatures.

*Abstract of ORNL-4803.

15. Gamma-Ray Production Due to Neutron Interactions with Nitrogen for Incident Neutron Energies Between 2.0 and 20 MeV: Tabulated Differential Cross Sections*,** (J. K. Dickens, T. A. Love and G. L. Morgan)

Numerical values of differential cross sections for gamma rays produced by neutron reactions with nitrogen have been obtained for neutron energies between 2.0 and 20 MeV for θ_{γ} = 90 and 125 deg using a NaI spectrometer. These data consist of neutron and gamma-ray production group cross-section values of $d^2\sigma/d\omega dE$ for $0.7 \leq E_{\gamma} \leq 10.5$ MeV, with gamma-ray intervals ranging from 20 keV for $E_{\gamma} \leq 1$ MeV to 250 keV for $E_{\gamma} \sim 9$ MeV. Neutron energy intervals varied from 1 MeV for E_n = 2 to 10 MeV to 3 MeV for E_n = 14 to 20 MeV.

*Abstract of ORNL-4864
**Relevant to Request No. 42.

16. Gamma-Ray Production Due to Neutron Interactions with Copper for Incident Neutron Energies Between 1.0 and 20 MeV: Tabulated Differential Cross Sections*,** (J. K. Dickens, T. A. Love and G. L. Morgan)

Numerical values of differential cross sections for gamma rays produced by neutron reactions with copper have been obtained for neutron

energies between 1.0 and 20 MeV for θ_γ = 125 deg. The $d^2\sigma/d\omega dE$ values were obtained using a NaI spectrometer. These data consist of neutron and gamma-ray production group cross-section values of $d^2\sigma/d\omega dE$ for $0.7 \leq E_\gamma \leq 10.5$ MeV, with gamma-ray intervals ranging from 20 keV for $E_\gamma \leq 1$ MeV to 160 keV for $E_\gamma \sim 9$ MeV. Neutron energy intervals varied from 0.5 MeV for E_n = 1 to 5 MeV to 3 MeV for E_n = 14 to 20 MeV.

---

*Abstract of ORNL-4846.

**Relevant to Request No. 127.

17. Gamma-Ray Production Due to Neutron Interactions with Tungsten for Incident Neutron Energies Between 1.0 and 20 MeV: Tabulated Differential Cross Sections*,** (J. K. Dickens, T. A. Love and G. L. Morgan)

Numerical values of differential cross sections for gamma rays produced by neutron reactions with tungsten have been obtained for neutron energies between 1.0 and 20 MeV for θ_γ = 125 deg. The $d^2\sigma/d\omega dE$ values were obtained using a NaI spectrometer. These data consist of neutron and gamma-ray production group cross-section values of $d^2\sigma/d\omega dE$ for $0.7 \leq E_\gamma \leq 10.5$ MeV, with gamma-ray intervals ranging from 20 keV for $E_\gamma \leq 1$ MeV to 160 keV for $E_\gamma \sim 9$ MeV. Neutron energy intervals varied from 0.5 MeV for E_n = 1 to 8 MeV to 3 MeV for E_n = 14 to 20 MeV.

---

*Abstract of ORNL-4847

**Relevant to Request Nos. 324 and 325.

18. Measurement of the ^{238}U Capture Cross Section for Incident Neutron Energies up to 100 keV*,** (G. de Saussure, E. G. Silver, R. B. Perez, R. Ingle and H. Weaver)

The neutron capture cross section of ^{238}U was measured for incident neutron energies between 5 eV and 100 keV using a pulsed electron linac neutron source and the time-of-flight technique. Capture gamma rays were detected by a large liquid scintillator located on a 40-m flight path. The incident neutron flux was monitored by a $^{10}BF_3$ ionization chamber. The cross section was normalized by the saturated resonance technique.

This memorandum contains a brief description of the experimental technique and a discussion of the results. A complete tabulation of one of the measurements is given in the appendix.

---

*Abstract of ORNL-TM-4059; also to be published in Nuclear Science and Engineering.

**Relevant to Request Nos. 421 and 422.

19. Simultaneous Measurements of the Neutron Fission and Capture Cross Sections for ^{235}U for Neutron Energies from 8 eV to 10 keV*,** (R. B. Perez, G. de Saussure, E. G. Silver, R. W. Ingle, and H. Weaver)

Simultaneous measurements of the neutron fission and capture cross sections of ^{235}U have been performed at the Oak Ridge Electron Linear Accelerator (ORELA) for neutrons with energies between 8 eV and 10 keV. These cross sections were measured relative to the standard $^{10}B(n,\alpha)$ reaction cross section.

The comparison of the present ^{235}U capture cross section with the values from other available sources shows that below 200 eV there is general agreement within an error band of $\pm 5\%$. In the keV energy region, the average difference observed rises to $\pm 12\%$.

The fission cross section results presented here agree with a worldwide compilation of fission data typically within a 3% error in the entire range of neutron energies investigated in this work.

The values of alpha, capture-to-fission ratio, exhibit a remarkable amount of structure superimposed on the featureless behavior predicted by Bohr's fission channel theory.

---

*Abstract of ORNL-TM-3696; also to be published in Nucl. Sci. Eng.

**Relevant to Request Nos. 388, 389, 390, 393 and 394.

20. Multilevel Effects in the Unresolved Resonance Region of the Cross Sections of Fissile Nuclides* (G. de Saussure and R. B. Perez)

For the specification of the cross sections of the fissile isotopes in the neutron energy region of unresolved resonances, the single-level formalism is often used while an analysis of the cross sections in the resolved region indicates that a multilevel formula may be more appropriate. In this paper we compare the statistical properties of the cross sections generated using the single-level formalism with those obtained by a multilevel formulation. The multilevel parameters were chosen so as to give the same average cross sections as the single-level formalism. The comparison indicates that there are small but significant differences between the statistical properties of the cross sections obtained with the multilevel formalism and those obtained with the single-level formula. The differences are probably too small, particularly when Doppler broadening is considered, to affect reactor calculations.

*To be presented at the Chicago APS Meeting, June 1973; submitted to Nucl. Sci. Eng. for publication.

21. General Sensitivity Theory for Radiation Transport* (E. M. Oblow)

The theoretical framework of a general approach to sensitivity analysis using adjoint functions is introduced and developed for practical application. Sensitivity and the context in which it is used is defined quantitatively in terms of adjoint functionals. The physical meaning and applicability of such a definition are then discussed with reference to both analytic and predictive studies. Connections are made between the general approach and perturbation theory for predictive applications. Specific formulations useful in cross-section sensitivity work are described in detail.

*Abstract of ORNL-TM-4110.

22. Neutron Yield from a Small High Purity $^{238}Pu\ O_2$ Source*
(J. K. Bair and H. M. Butler)

The neutron yield from a small high purity $^{238}Pu\ O_2$ source has been measured to be 1.705×10^4 neutrons per second per gram of ^{238}Pu with an accuracy of better than 1%.

*Submitted for publication in Nuclear Tech., Technical Note.

23. Neutron Capture in Fluorine Below 1500 keV* (R. L. Macklin and R. R. Winters†)

Neutron time-of-flight radiative capture data taken at the Oak Ridge Electron Linear Accelerator have been analyzed for single level resonance parameters. Ten resonances were found, with parameters as indicated, listing E_o (keV), J value assumed, and Γ_γ (eV) in order. 27.07(2)1.4 $\pm$ .3, 48.7(1)1.7 $\pm$ .4, 97.0(1) $<$ 6.0 $\pm$ 1.8, 269(1)3.5 $\pm$ 0.8, 270(1) $<$ 4.4, 386(1)7 $\pm$ 2, 490.5(0) $>$ 10 $\pm$ 3, 595(1) $>$ 12.6 $\pm$ 2, 1460(1) $>$ 11 $\pm$ 3. Values of total width were also found for these resonances. Two resonances are very narrow and their capture areas yield estimates of $g\Gamma_n$. At 43.5 keV $g\Gamma_n$ = 0.86 $\pm$ .02 eV if J $\geq$ 1 or Γ_n = .42 $\pm$ .1 eV if J = 0, and at 173.5 keV $g\Gamma_n$ = .35 $\pm$ .10 eV. The increase of nearly an order of magnitude in radiative width with increasing energy up to 600 keV is notable. Twelve large resonances between 1600 and 5000 keV were not analyzed for capture because of detector sensitivity to the inelastic scattering channels which open in that energy region.

*Submitted to Phys. Rev. for publication.

†Denison University, Granville, Ohio.

24. Cross-Section Sensitivity of Breeding Ratio in a Fusion-Reactor Blanket* (D. E. Bartine, R. G. Alsmiller, Jr., E. Oblow and F. R. Mynatt)

In a reactor operating on deuterium-tritium fusion, it is necessary that the blanket surrounding the plasma have a tritium breeding ratio larger than unity,[1] (more than one tritium nucleus produced per incident neutron). In this paper, the sensitivity of this breeding ratio to changes in neutron cross sections in a model fusion-reactor blanket is studied using linear perturbation theory.[2] The blanket model used is the standard model that has been proposed for comparison of neutronics codes.[3] All of the transport calculations were carried out with the one-dimensional discrete

ordinates code ANISN,[4] using P_3S_{12}, while the code SWANLAKE[5] was employed in the sensitivity studies. The cross-section data were taken from ENDF/B-III, MAT. 1164 for Nb, MAT. 1115 for ^{6}Li, MAT. 1116 for ^{7}Li, and MAT. 1165 for C.

The sensitivity which is numerically equal to the percent change in the breeding ratio due to a 1% increase in the indicated element's cross sections was -0.20% for Nb, +0.12% for ^{6}Li, +0.13% for ^{7}Li, and +0.06% for C. Sensititivities were also calculated for all partial cross sections (elastic, inelastic, etc.). All results are directly proportional to the assumed change in cross sections; i.e., to estimate the effect of a 2% increase in the cross sections, the values given should be multiplied by 2. However, if $\delta R/R$ becomes large, the analysis becomes invalid. In general, the total sensitivity of the breeding ratio to changes in the cross sections is quite low. The results indicate that the sensitivity is considerably influenced by the energy dependence of the tritium-production cross sections in ^{6}Li and ^{7}Li.

---

*To be presented at the Chicago ANS Meeting, June 10-15, 1973.

[1]D. Steiner, Nucl. App. Tech. 9, 83 (1970).

[2]D. L. Prezbindowski and H. A. Sandmeier, Trans. Am. Nucl. Soc. 11, 193 (1968).

[3]D. Steiner, private communication (1972).

[4]W. W. Engle, Jr., "A Users Manual for ANISN, a One-Dimensional Discrete Ordinates Transport Code with Anisotropic Scattering," K-1693, Computing Technology Center, Union Carbide Corporation (1967).

[5]D. E. Bartine, F. R. Mynatt and E. Oblow, ORNL-TM-3809 (to be issued).

25. Neutron Fission and Absorption Cross-Section Measurements for ^{239}Pu, ^{240}Pu, ^{241}Pu and ^{241}Am* (L. W. Weston and J. H. Todd)

The neutron fission and absorption cross sections for ^{239}Pu, ^{240}Pu and ^{241}Pu were measured from thermal-neutron energies to 20 keV. In addition, the absorption cross sections of ^{240}Pu and ^{241}Am were measured from thermal-neutron energies to 200 keV. The ratio of the capture and fission cross sections, $(\sigma_c)/(\sigma_f)$, could be determined up to 200 keV for ^{239}Pu and ^{241}Pu.

The general trends of the ^{239}Pu and ^{241}Pu data have been reported previously.[1] The average absorption cross section of ^{240}Pu is in agreement with that reported by Hockenbury.[2] The shape of the two sets of data

is in good agreement over the range of overlap. The present data, which are normalized to the thermal cross section, are about 10% lower than that of Hockenbury at keV neutron energies. Both these normalizations are appreciably higher than ENDF III, however, all of the data on which ENDF-III was based have been renormalized upward. The average absorption cross section for ^{241}Am was in good agreement with ENDF-III up to 20 keV and is appreciably higher thereafter. There were little previous data on ^{241}Am available in the energy range from 20 to 200 keV.

These results, although not complete, have been reported to the ENDF-IV committee and will be considered in the revision of the ENDF data.

---

*Relevant to Request Nos. 449, 450, 455, 474 and 479.

[1] L. W. Weston and J. H. Todd, Trans. Am. Nucl. Soc. 15, 480 (1972).

[2] R. W. Hockenbury, W. R. Moyer and R. C. Block, Nucl. Sci. Eng. 49, 153-161 (1972).

B. CHARGED PARTICLE FISSION STUDIES

1. Photon Dose Rates from the Interactions of 200-GeV Protons in Iron and Iron-Lead Beam Stops* (T. A. Gabriel and R. T. Santoro)

The calculated photon dose rates from the long-lived ($\tau_{1/2}$ > 1 min) beta- and gamma-active nuclides produced when 200-GeV protons are incident on a semi-infinite cylindrical iron beam stop having a radius of 40.64 cm (16 in.) are compared with the calculated photon dose rates from long-lived beta- and gamma-active nuclides produced by 200-GeV protons in semi-infinite beam stops having a 30.48-cm (12 in.) radius iron core but surrounded by either 5.08 cm (2 in.) or 10.16 cm (4 in.) of lead. Data are also presented comparing the calculated photon dose rates from the long-lived beta- and gamma-active nuclides produced when 200-GeV protons are incident on semi-infinite cylindrical iron beam stops having radii of 10.16 cm (4 in.), 20.32 cm (8 in.), 30.48 cm (12 in.), and 40.64 cm (16 in.).

*Abstract of Particle Journal Vol. 4, 169-186 (1973).

2. Calculations for Cancer Radiotherapy with Negatively Charged Pions* (Principal Investigator - R. G. Alsmiller, Jr.)

Very approximate estimates indicate that about 60,000 lives per year might be saved if new and improved radiotherapeutic techniques for cancer treatment were available. The use of negatively charged pions is one possible method of obtaining the needed improvement since these particles, because of their physical properties, make it possible, in principle, to deliver highly concentrated radiation doses to small localized regions. The calculational program described here is directed toward the following broad objectives: assessing the biological effect and radiotherapeutic value of negative-pion beams, ascertaining the influence of beam parameters on the dose, LET spectra, cell-survival probabilities, and oxygen-enhancement ratios, and providing quantitative data to aid in planning and understanding biological and therapeutic exposures.

*Part A Introduction of ORNL-TM-4159.

3. A Compariative Study of the Use of Photons, Neutrons, Protons, Negatively Charged Pions, and Heavy Ions in Cancer Radiotherapy* (Principal Investigator - R. G. Alsmiller, Jr.)

Radiotherapy, which is an important aid in the treatment of cancer, is used on about one-half of all cancer patients. Very approximate estimates

indicate that about 60,000 lives per year might be saved if new and improved radiotherapeutic techniques were available. To obtain these needed improvements, a variety of particle types - neutrons, protons, negatively charged pions, and heavy ions - has been proposed for use in radiotherapy. The purpose of the program discussed here is to carry out calculationally an objective comparative study of the therapeutic value of these various particles and the commonly used ^{60}Co gamma rays. The calcualtional techniques and cross-section data that are being utilized will be verified insofar as possible by comparisons with available experimental data.

---

*Part B Introduction of ORNL-TM-4159.

4. Fragment Kinetic Energies from ^{18}O-Induced Fission of ^{246}Cm*
(H. Freiesleben†, Franz Plasil, Robert L. Ferguson, Curtis E. Bemis, Jr. and H. W. Schmitt)

Recently it was predicted on the basis of a static scission model (SSM)[1] that total fragment kinetic energies $\langle E_K \rangle$ are larger than those predicted with the liquid drop model (LDM) when $250 \lesssim A < 290$. In a search for this effect, we measured $\langle E_K \rangle$ in bombardments of ^{232}Th and ^{246}Cm with 94-, 105- and 126-MeV $^{18}O^{5+}$ ions. Correlated energies of fission fragment pairs were measured with silicon surface barrier detectors; fragment mass and total kinetic energy distributions were deduced. The results for Th + O are in good agreement with the LDM prediction. A preliminary analysis of the Cm + O data shows a smaller $\langle E_K \rangle$ than the LDM predicts. This result, however, does not necessarily invalidate the SSM since the shell effects that lead to prediction of a large $\langle E_K \rangle$ may be washed out above the 50-MeV excitation energy of our ^{264}104 compound nucleus. In addition, the possibility of fission following incomplete momentum transfer has not been ruled out.

---

*To be presented at the Washington, D. C. APS Meeting, April 23-26, 1973.

†University of Rochester.

[1]H. W. Schmitt and U. Mosel, Nucl. Phys. A186, 1 (1972).

C. PROTON INDUCED REACTIONS

1. Total Neutron Yields from the Proton Bombardment of $^{17,18}O$* (J. K. Bair)

The $^{17}O(p,n)^{17}F$ reaction has been observed for the first time in the energy region from threshold to 5 MeV. Total neutron production cross sections measured with good resolution are given. The reaction threshold is determined to be 3743 ± 6 keV. High resolution total neutron cross sections are also given for the reaction $^{18}O(p,n)^{18}F$ from threshold to 4 MeV.

*Submitted to Phys. Rev. for publication.

2. Energy Levels of ^{94}Ru Observed with the $^{96}Ru(p,t)$ Reaction* (J. B. Ball, C. B. Fulmer, J. S. Larsen† and G. Sletten†)

The level structure of the neutron-magic nucleus ^{94}Ru, up to an excitation energy of 4 MeV, has been studied by means of the (p,t) reaction. Particular emphasis was placed on a search for excited 0^+ levels, none of which have been reported previously. Among new levels observed in this study are 0^+ levels at 2.995, 3.615 and 3.770 MeV, and the 3^- octupole vibration at 2.965 MeV.

*Submitted to Nuclear Physics for publication.

†The Niels Bohr Institute, University of Copenhagen, Denmark.

3. The ^{110}Pd, $^{116}Cd(p,p'\gamma)$ Reactions* (J. A. Deye†, R. L. Robinson, and J. L. C. Ford, Jr.)

The possibility of extending our knowledge about higher-energy collective-type states among the vibrational nuclei by observing gamma rays from states excited by inelastically scattered protons has been examined. Gamma rays from ^{110}Pd and ^{116}Cd were detected in coincidence with inelastically scattered protons; the incident protons had energies of 12 and 13 MeV. Gamma rays, most of them previously unreported, were observed from 17 levels in ^{110}Pd and 14 levels in ^{116}Cd below ~ 2.5 MeV. The results are compared to predictions of a phonon-model interpretation of the levels. Evidence is shown for the existence of the three-quadrupole phonon quintet in ^{110}Pd.

*Submitted to Nuclear Physics for publication.

†Radioisotope Lab., General Hospital, Cincinnati, Ohio.

4. Neutron Hole States in ^{138}La and ^{140}Pr* (V. D. Helton†, J. C. Hiebert† and J. B. Ball)

Protons accelerated to 30 MeV were used to investigate low-lying states in the odd-odd nuclei ^{138}La and ^{140}Pr with (p,d) reactions. The elastic scattering of 30 MeV protons and 23 MeV deuterons was also studied to determine optical potentials. Experimental angular distributions are compared with distorted-wave Born approximation calculations to extract spin, parity, and spectroscopic factors for levels up to 432 keV of excitation in ^{140}Pr and 530 keV in ^{138}La. Comparisons with the simple shell-model predictions and extended shell-model calculations are presented. The ^{140}Pr levels appear experimentally to have an almost pure particle-hole structure whereas the ^{138}La levels exhibit substantial mixing.

---

*Nuclear Physics A201, 225-246 (1973).

†Cyclotron Institute, Texas A&M University, College Station, Texas 77843.

5. Effective Interactions and the ^{40}Ca(p,p') Reaction* (G. R. Satchler)

The excitation of the lowest 3^- and 5^- levels in ^{40}Ca is studied using a microscopic description. The long-range part of the Hamada-Johnston potential is shown to be a good effective interaction especially when supplemented by a phenomenological imaginary term. Transition densities are constructed from hole-particle RPA wave functions normalized to give the correct electric transition rates. Various wave functions and other interactions are studied. Other features of the calculations are discussed.

---

*Submitted to Z. für Physik for publication.

6. Differential Cross Sections for the Production of Neutrons from the Bombardment of ^{12}C and ^{27}Al by 63-MeV Protons.* (J. W. Wachter, R. T. Santoro, T. A. Love and W. Zobel)

Differential cross sections in energy and angle have been obtained using time-of-flight spectroscopy for secondary neutrons produced in the reactions of 63-MeV protons with ^{12}C and ^{27}Al. Neutron energy spectra are given for laboratory angles of 20°, 45°, 60°, and 135° for energies > 10 MeV. The NE-213 efficiency was calculated using the 05S Monte Carlo code.[1] Comparisons between the Al cross sections and the predictions of the intranuclear cascade model of Bertini[2] show good agreement at medium angles.

The data do not show the predicted quasi-free scattering peak at 20°, although the energy-integrated cross sections agree. The calculated cross section at 135° is low by a factor of 3 to 4.

---

*Presented at the January APS Meeting, January 29 - February 1, 1973.

[1] R. E. Textor and V. V. Verbinski, ORNL-4160, 1968.

[2] H. W. Bertini, Phys. Rev. 131, 1801 (1963); with erratum Phys. Rev. 138, AB 2 (1965).

7. Systematics of Fragment Mass and Energy Distributions for Proton-Induced Fission of ^{233}U, ^{235}U, and ^{238}U* (S. C. Burnett†, H. W. Schmitt, R. L. Ferguson, F. Plasil and Frances Pleasonton)

Thin targets of ^{233}U, ^{235}U and ^{238}U were bombarded with protons of several energies between 7 and 13 MeV. Correlated energies of fission fragment pairs were measured with silicon surface barrier detectors. Fragment mass vs. total kinetic energy distributions were deduced, and their systematic variation with bombarding energy was studied. It was found that the yield in the valley of the mass distributions for symmetric divisions increases with increasing excitation energy, and that the peaks move slightly toward symmetry. The average total kinetic energy for mass divisions with one fragment mass $\simeq$ 132 amu was found to decrease with increasing excitation energy, while for other mass divisions little change was observed. The average overall total kinetic energy was found to decrease with increasing bombarding energy, and widths of both the kinetic energy distributions and the mass distributions were found to increase somewhat. The results are discussed in terms of fragment shell effects which appear to persist to our highest excitation energy (~ 18 MeV), and also in terms of the two-component fission hypothesis.

---

*Submitted to Phys. Rev. C for publication.

†U. S. Atomic Energy Commission, Washington, D. C. 20545.

8. Fission of ^{209}Bi by 36.1 MeV Protons: Search for an Asymmetric Component in the Mass Distribution, and Neutron Emission Results* (Franz Plasil, Robert L. Ferguson, Frances Pleasonton and H. W. Schmitt)

A thin deposit of ^{209}Bi was bombarded with 36.1 MeV protons from the Oak Ridge Isochronous Cyclotron and correlated energies of fission fragment pairs were measured with silicon surface barrier detectors. The

mass-yield distribution obtained from these energies was compared with the radiochemical results of Sugihara, Roesner and Meadows; we do not confirm the existence of the small asymmetric peak that appears in the wings of their distribution. Studies of statistical uncertainties and dispersion effects in our experiment indicate that they are not large enough to wash-out such peaks. The average number of neutrons emitted as a function of fragment mass was obtained from a cumulative yield calculation and is consistent with an earlier measurement for ^{4}He-induced fission of ^{209}Bi. Pre-neutron-emission mass and kinetic energy distributions are presented.

*Phys. Rev. C 7, 1186-1197 (1973).

D. ALPHA INDUCED REACTIONS

1. Neutron Shell Structure in ^{125}Sn by (d,p) and (α,^{3}He) Reactions* (C. R. Bingham† and D. L. Hillis††)

Differential cross sections for ^{124}Sn(d,p) at 33.3 MeV were measured in 5° increments from 12.5° to 47.5° lab. The resolution was about 30 keV FWHM. The (α,^{3}He) spectra with ~ 55 keV resolution were obtained at 15° and 20° lab. with 65.7 MeV α particles. Spectroscopic factors were obtained by comparison with distorted wave calculations. Consistent spectroscopic factors were obtained from the (d,p) and (α,^{3}He) reactions. Spin assignments and spectroscopic factors were obtained for several levels which were not characterized in previous neutron-transfer studies. Sums of spectroscopic factors and centers of gravity are presented for the levels observed. Essentially all the neutron strength remaining in the neutron shell between N = 50 and N = 82 was located. Most of the strength in the $2f_{7/2}$, $3p_{3/2}$, and $1h_{9/2}$ levels of the next major shell was located. The spectroscopic factors sums and the centers-of-gravity are compared with the results of pairing theory.

*Submitted to Physical Review for publication.

†ORNL and the University of Tennessee.

††University of Tennessee.

2. Absolute Neutron Yields from Thick Target $^{NAT}C(\alpha,n)$* (J. K. Bair)

Recent measurements of the neutron yield resulting from the α-particle bombardment of carbon have disclosed an error in the data reported in the literature. New values are given for the thick target yield of neutrons for α-particle energies between 2 and 9 MeV.

---

*Submitted to Nuclear Science and Engineering, Technical Note, for publication.

3. Total Neutron Yield from the (α,n) Reaction on $^{21,22}Ne$* (F. X. Haas† and J. K. Bair)

Compound states of high excitation in $^{25,26}Mg$ have been observed, with good resolution, in the total neutron yield from α-particle bombardment of $^{21,22}Ne$. Bombarding energies were from 1 to 5 MeV. Analysis of the areas under the yield curves give α-particle strength functions of $\bar{S}_\alpha = 0.031 \pm 0.021$ for $^{21}Ne + \alpha$ and $\bar{S}_\alpha = 0.026 \pm 0.012$ for $^{22}Ne + \alpha$. For astrophysical purposes these strength functions are used to extrapolate the averaged cross sections to lower energies.

---

*Submitted to Physical Review for publication.

†Mound Laboratory, Miamisburg, Ohio.

4. Total Neutron Yield from the Reactions $^{13}C(\alpha,n)^{16}O$ and $^{17,18}O(\alpha,n)^{20,21}Ne$* (J. K. Bair and F. X. Haas†)

Compound states of high excitation in ^{17}O and $^{21,22}Ne$ have been observed, with good resolution, in the total neutron yield from the reactions $^{13}C(\alpha,n)^{16}O$ and $^{17,18}O(\alpha,n)^{20,21}Ne$. Bombarding α-particle energies were approximately from 1 to 5 MeV. Analysis of the area under the excitation curves gives α-particle strength functions of $\bar{S}_\alpha = 0.029 \pm 0.030$ for $^{13}C + \alpha$, 0.030 ± 0.023 for $^{17}O + \alpha$ and 0.022 ± 0.010 for $^{18}O + \alpha$. For astrophysical purposes these strength functions are used to extrapolate the average cross sections to lower energies.

---

*Submitted to Physical Review for publication.

†Mound Laboratory, Miamisburg, Ohio.

E. HEAVY ION INDUCED FISSION

1. Fission and Complete Fusion Measurements in ^{40}Ar Bombardments of ^{58}Ni and ^{109}Ag* (H. H. Gutbrod†, H. C. Britt††, B. H. Erkila††, R. H. Stokes††, M. Blann†††, and F. Plasil)

Thin targets of ^{58}Ni and ^{109}Ag have been bombarded with 288 MeV ^{40}Ar ions from the Berkeley SUPER-HILAC. A particle telescope consisting of a gas proportional ΔE counter and a silicon surface barrier E detector was used to measure all reaction products ranging from elastically scattered argon ions to complete fusion products. Fission fragments and transfer products were also detected. A good separation between fission fragments and other reaction products was possible in the case of the ^{109}Ag + ^{40}Ar reaction. Angular distributions were obtained from 4° to 180° in the laboratory system. Elastic scattering was used to obtain energy and angular calibrations.

In the case of ^{109}Ag + ^{40}Ar, the complete fusion cross section, σ_{CF}, was found to be 610 mb. The fission fragment angular distribution is characterized by a $1/\sin\theta$ function, and the integrated fission cross section was found to be 1160 mb. Thus essentially all of the estimated total reaction cross section σ_R of 1875 mb is accounted for. For ^{58}Ni + ^{40}Ar, σ_{CF} was found to be $\approx$ 870 mb.

Results have been interpreted in terms of a model in which fission competes with other modes of de-excitation of the compound nucleus, and in which the effects of angular momentum on the fission barrier are taken into account. It was found that for ^{109}Ar + ^{40}Ar, the calculated ratio σ_{CF}/σ_R was 0.17 compared with the experimental result of 0.33 and for ^{58}Ni + ^{40}Ar, the calculated ratio was 0.25 compared with a measured value of 0.47. The model seems to overestimate the fission contribution for the reactions investigated in this work. The implications of this conclusion are discussed.

---

*Submitted to the IAEA 3rd Symposium on the Physics and Chemistry of Fission, Rochester, New York, August 13-17, 1973.

†G.S.I. Darmstadt, Germany.

††Los Alamos Scientific Laboratory, Los Alamos, New Mexico.

†††University of Rochester, Rochester, New York.

2. Cross Sections for $^{61}Ni(^{16}O,X)$ Reactions* (J. C. Wells, Jr.† Jung Lin†, R. L. Robinson, H. J. Kim and J. L. C. Ford, Jr.

We have determined absolute cross sections for different exit channels for reactions induced by bombardment of ^{61}Ni with ^{16}O ions between 38 and 51 MeV. Targets were 1 mg/cm^2 enriched ^{61}Ni with Au backing. Cross sections were obtained from yields of gamma rays from residual radioisotopes, and from prompt gamma rays from the target. Identification of the products was based on gamma ray energies and intensities, and on the half-lives, in the case of the radioisotopes. Due to the proximity of the Coulomb barrier (E≈42 MeV), all of the cross sections increase rapidly with energy.

---

*To be presented at the Washington, D. C. APS Meeting, April 23 - 26, 1973.

†Tennessee Technological University, Cookeville, Tennessee.

3. In-Beam γ Rays from the $^{28}Si(^{16}O,2p)^{42}Ca$ Reaction* (H. J. Kim, R. L. Robinson, W. T. Milner, J. C. Wells, Jr.† and J. Lin†)

The yields and angular distributions of the prominent in-beam γ rays from the ^{16}O bombardment of ^{28}Si were investigated for bombarding energies of 24 to 42 MeV. To ascertain the origin of some of the γ rays, the in-beam γ rays from the 36- and 42-MeV ^{16}O bombardment of ^{29}Si and ^{30}Si were also studied. The γ rays from the stretched E2 transitions between the lowest-lying 6^+, 4^+, 2^+ and ground states of ^{42}Ca dominate the ^{16}O + ^{28}Si singles spectra. Above 36-MeV bombarding energy the side-feeding intensities for the 4^+ and 2^+ states are less than 25% and the production of ^{42}Ca proceeds mainly via the 6^+ state. The γ-γ coincident spectrum measured at 42 MeV with two large-volume Ge(Li) detectors shows that the 6^+ state is fed by many γ rays.

---

*To be presented at the Washington, D. C. APS Meeting, April 23 - 26, 1973.

†Tennessee Technological University, Cookeville, Tennessee.

4. Lifetime Measurements of 8^+, 10^+ and 12^+ Rotational States in ^{164}Dy* (D. C. Hensley, N. R. Johnson, W. T. Milner, G. B. Hagemann† and L. L. Riedinger††)

Rotational states up to spin 12 in ^{164}Dy were populated by inelastic scattering of 153 keV ^{40}Ar from a thick target of ^{164}Dy. Gamma rays were detected in two Ge(Li) detectors at 0° and 90° to the beam and were recorded in coincidence with ^{40}Ar ions backscattered (160°) into an annular detector. Lifetimes were inferred from the Doppler broadened shapes of

the γ-transitions: $8^+ \rightarrow 6^+$, $10^+ \rightarrow 8^+$, and $12^+ \rightarrow 10^+$ by comparing the observed line shapes to those calculated taking into account the stopping power of projectiles and recoiling ions as well as the reaction kinematics and detector geometry. The results are presented as the ratio of the experimental B(E2) to the B(E2) predicted by the rigid rotor model, and, because of some uncertainty in the absolute value of the stopping power, the ratios have been scaled so that the ratio for the $(8^+ \rightarrow 6^+)$ transition is 1.0; $(10^+ \rightarrow 8^+) = 1.18 \pm 0.1$; and $(12^+ \rightarrow 10^+) = 1.35 \pm 0.2$. Measurements in ^{160}Dy are in progress.

---

*To be presented at the Washington, D. C. APS Meeting, April 23 - 26, 1973.

†Niels Bohr Institute.

††University of Tennessee, Knoxville, Tennessee.

5. High Spin States in ^{164}Yb and ^{160}Er* (P. H. Stelson, G. B. Hagemann, D. C. Hensley, R. L. Robinson, L. L. Riedinger† and R. O. Sayer††)

The ^{156}Gd(^{12}C,4n)^{164}Yb and ^{152}Sm(^{12}C,4n)^{160}Er reactions at 74 MeV were used to excite high spin states in the residual nuclei. γ-γ coincidences with Ge(Li) detectors were used to relate γ-rays to the g.s. band. The systematic decrease of γ-ray intensity with increasing spin was helpful in placing observed γ-rays. In ^{164}Yb the 20→18 γ-ray intensity was about 10 percent of the 4→2 γ-ray intensity. For ^{164}Yb we confirm the previous results of the Jülich group (to 16+). New γ-rays are found at 543.2 and 632.5 keV which are assigned to decay of the 18+ and 20+ states, respectively. Tentative evidence was obtained for a 713.0 keV γ-ray from decay of the 22+ state. Several discrete γ-rays were observed which feed into the g.s. band at the spin 10-12 region. In ^{160}Er we observed γ-rays of 556.1 and 640.0 keV which are assigned to decay of the 18+ and 20+ states, respectively

---

*To be presented at the Washington, D. C. APS Meeting, April 23 - 26, 1973.

†University of Tennessee

††Furman University

6. Heavy-Ion-Induced Fission of Nuclei in the Region of Silver* (Franz Plasil, Robert L. Ferguson and Frances Pleasonton)

Studies of heavy-ion-induced fission of light nuclei have been initiated at the Oak Ridge Isochronous Cyclotron. Thin targets of ^{107}Ag were bombarded with 165 MeV ^{20}Ne ions. Surface barrier silicon detectors were used to detect coincident pairs of fission fragments and to measure fragment kinetic energies. Mass and total kinetic energy distributions were obtained from the correlated energy data by means of an iterative center-of-mass calculation. The fragment angular correlation was also measured, as was the fission cross section, σ_F, relative to Rutherford scattering. σ_F for ^{107}Ag and 165 MeV ^{20}Ne was found to be 172 mb. This value is about four times greater than that obtained from earlier track detector measurements. The angular correlation, which provides a measure of momentum transfer, was found to be slightly asymmetric, indicating a small contribution from three-body reactions.

The mass distribution was found to be symmetric, and the average total kinetic energy to be 90 MeV. Measured widths of the mass and total kinetic energy distributions were compared with the liquid drop model, which predicts the mass distribution to be broad (43 amu FWHM), and the total kinetic energy distribution to be narrow (17 MeV FWHM). The measured width of the mass distribution (36 amu FWHM) is, as expected, greater than the width of the kinetic energy distribution (27 MeV FWHM), but the measured values differ substantially from those predicted by the liquid drop theory.

Calculations of σ_F have been made on the basis of a model in which fission competes with other modes of de-excitation of the compound nucleus, and in which the variation of the fission barrier with angular momentum is taken into account. The calculated upper limit on σ_F was found to be 730 mb which is greater than the observed fission cross section of 172 mb. It is concluded that in addition to fission and to complete fusion of target and projectile, other reaction channels play an important role.

---

*Submitted to the IAEA 3rd Symposium on the Physics and Chemistry of Fission, Rochester, New York, August 13-17, 1973.

7. Single-Nucleon Transfer Reactions and Inelastic Scattering Induced by ^{11}B Ions Incident on ^{208}Pb* (J. L. C. Ford, Jr., K. S. Toth, D. C. Hensley, R. M. Gaedke†, P. J. Riley††, and S. T. Thornton†††)

^{208}Pb was bombarded with 72-MeV ^{11}B ions accelerated in the Oak Ridge Isochronous Cyclotron. With the use of a 60-cm long, 3-wire, position sensitive proportional detector placed in the focal plane of a broad-range magnetic spectrograph all four single-nucleon transfer reaction products

were identified. Angular distribution measurements have been completed for five final states in ^{209}Bi populated in the reaction ^{208}Pb(^{11}B,^{10}Be) and for three states in ^{207}Pb populated in the reaction ^{208}Pb(^{11}B,^{12}B). The differential cross sections are single peaked and smooth. Once again, as reported earlier[1] for the analogous reaction ^{208}Pb(^{12}C,^{11}B)^{209}Bi, the indication is that for the proton stripping reaction the peak angles remain constant with increasing excitation energy in ^{209}Bi. Angular distributions for inelastic scattering to the 3^-, 5^- and 2^+ states at 2.62, 3.20, and 4.10 MeV in ^{208}Pb were also measured.

---

*Presented at the Symposium on Heavy-Ion Transfer Reactions, Argonne, Illinois, March 15-17, 1973.

†Trinity University, San Antonio, Texas.

††University of Texas, Austin, Texas.

†††University of Virginia, Charlottesville, Virginia.

[1] J. S. Larsen et al., Phys. Letters 42B, 205 (1972).

OHIO UNIVERSITY ACCELERATOR LABORATORY

A. TANDEM ACCELERATOR PROGRAM

1. Structure Studies of Light Nuclei with Neutrons

a. States in ^{12}B Observed in Neutron Elastic Scattering from ^{11}B (C.E. Nelson, S.L. Hausladen and R.O.Lane)

The elastic differential cross section for the scattering of neutrons from ^{11}B has been measured for 45 neutron energies between E_n = 2.2 MeV and E_n = 4.5 MeV using the Ohio University time-of-flight spectrometer. A two channel, three level R-matrix analysis of the data has been completed. The experimental results (connected for finite geometry effects and detector efficiency), expressed as the expansion coefficients derived from a least squares fit to the differential cross section (c.m.) are shown in Figure A1, versus laboratory neutron energy. Also shown are the state assignments deduced from the R-matrix analysis and the corresponding R-matrix fit to the data. These narrow states previously seen as resonances in the total neutron cross section at E_n = 2.45 MeV, E_n = 2.58 MeV and E_n = 3.5 MeV have been assigned $J^\pi = 3^+$, $J^\pi = 3^-$ and $J^\pi = (1)^+$, respectively, based on this analysis. In addition, two previously unobserved broad resonances at E_n = 2.7 MeV and E_n = 3.8 MeV have been assigned $J^\pi = 1^-$ and $J^\pi = (1)^+$ respectively.

---

b. A Study of the Level Structure of ^{11}B (S. L. Hausladen, C. E. Nelson and R. O. Lane)

Elastic scattering differential cross sections for ^{10}B were made using the Ohio University fast neutron time-of-flight facility. Measurements were made between 1.5 and 4.4 MeV at 50 keV intervals. A two-level, four channel R-matrix analysis with non-diagonal R° was made using the present data, the elastic scattering data at lower energies,* differential polarization data,** and the $^{10}B(n,\alpha)^7Li$ data† for both the ground state and first excited state α-particle groups. The result of the R-matrix analysis to all these data is the solid line shown in Figs A2 and A3. The states identified in ^{11}B are the following: 1) $J^\pi = 9/2^-$ (ℓ_n=1) at E_x = 13.12 MeV (E_n = 1.83 MeV), 2) $J^\pi = 5/2^+$ or $7/2^+$(ℓ =2) at E_x = 13.17 MeV (E_n = 1.88 MeV), 3) $J^\pi = 11/2^+$ (ℓ =2) at E_x = 14.0 MeV (E_n = 2.82 MeV), and 4) $J^\pi = 3/2^+$, $5/2^+$ or $7/2^+$ at E_x = 15.2 MeV (E_n = 4.2 MeV). In addition to these states, states used in a previous analysis* with spins $5/2^+(\ell=0)$ at E_x = 11.60 MeV, $5/2^-(\ell_n=1)$ at E_x= 11.94 MeV, and two levels of $7/2^+(\ell_n=0)$ at E_x = 10.60 MeV and 11.79 MeV were

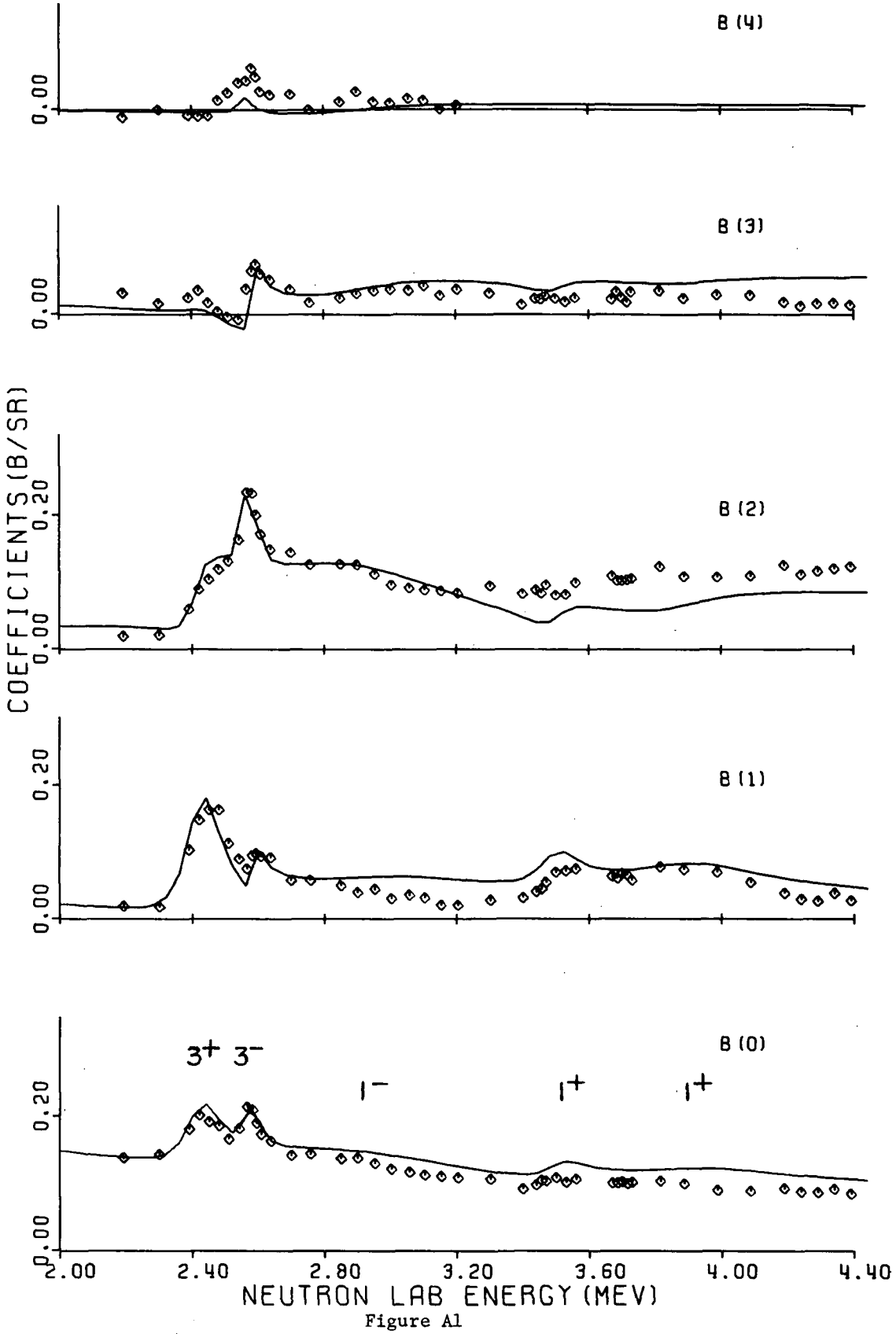
B (4)
B (3)
B (2)
B (1)
B (0)
COEFFICIENTS (B/SR)
0.00
0.20
3+ 3-
1-
1+
1+
2.00
2.40
2.80
3.20
3.60
4.00
4.40
NEUTRON LAB ENERGY (MEV)

Figure A1

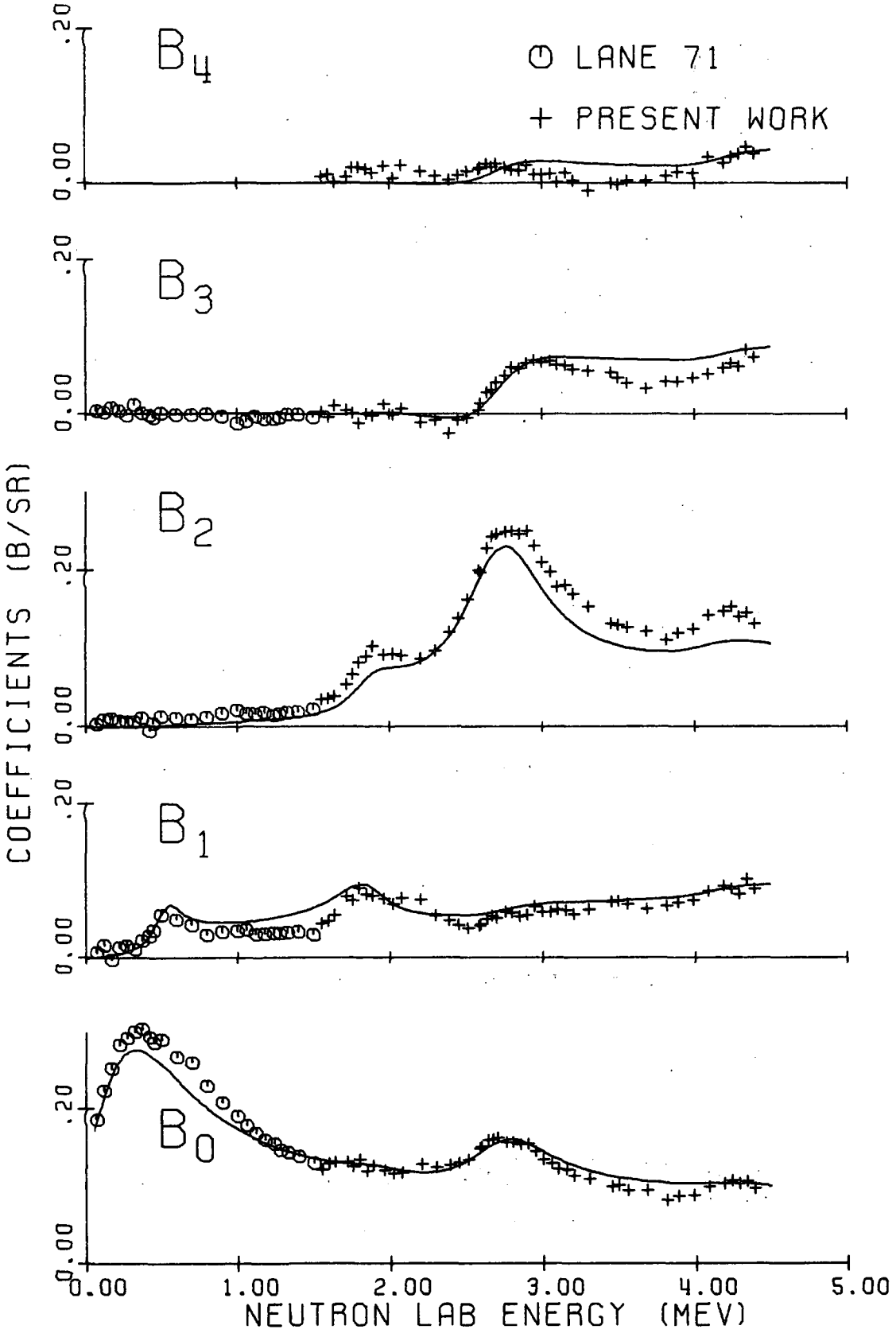
B4
B3
B2
B1
B0
LANE 71
PRESENT WORK
COEFFICIENTS (B/SR)
.20
0.00
0.00
1.00
2.00
3.00
4.00
5.00
NEUTRON LAB ENERGY (MEV)

Figure A2

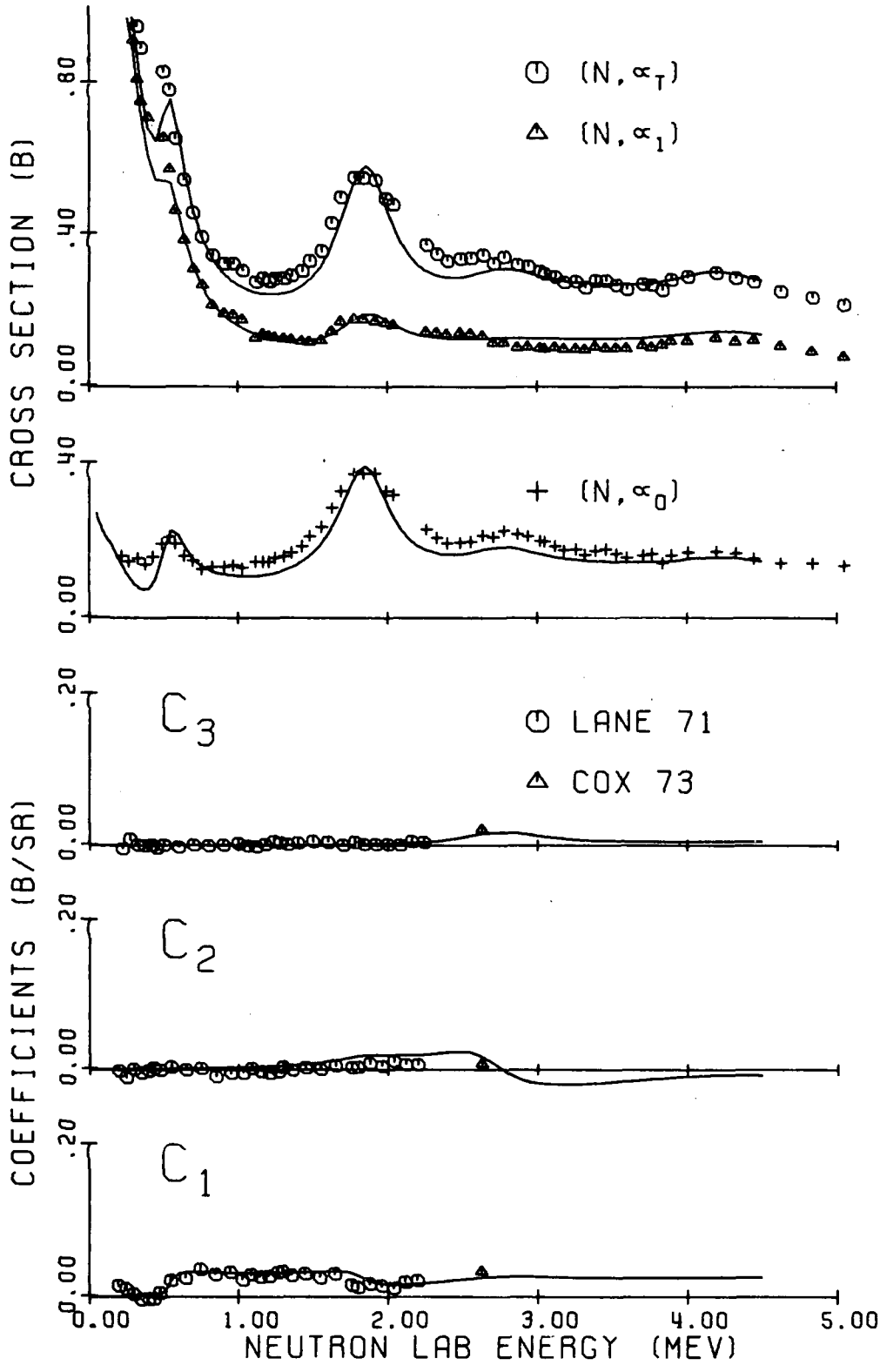
CROSS SECTION (B)
.80
.40
0.00
(N,α_T)
(N,α_1)
.40
0.00
(N,α_0)
COEFFICIENTS (B/SR)
.20
0.00
C_3
LANE 71
COX 73
.20
0.00
C_2
.20
0.00
C_1
0.00
1.00
2.00
3.00
4.00
5.00
NEUTRON LAB ENERGY (MEV)

Figure A3

used in this analysis. The results of the present analysis are consistent with other known reactions leading to states in ^{11}B in this energy region such as $^{10}B(n,n'\gamma)^{10}B(.717)$†† and the $^{7}Li(\alpha,n_0)^{10}B$ and $^{7}Li(\alpha,n_1)^{10}B(.717)$ reaction.††† The constraints imposed by fitting not only the elastic scattering data but also the polarization and $^{10}B(n,\alpha)^{7}Li$ data with the multi-level, multi-channel R-matrix formalism give a consistent quantitative interpretation of the level structure of ^{11}B above the neutron binding energy.

---

* Lane, Hausladen, Monahan, Elwyn, Mooring and Langsdorf, Jr., Phys. Rev. C4, 380(1971).

** Cox, Knox, Lane and Finlay, Nucl. Phys. A203, 89(1973).

† Irving, Oak Ridge National Laboratory Report No. ORNL-TM-1872, 1967 (unpublished).

†† Day and Walt, Phys. Rev. 117, 1330 (1960).

††† Van der Zwan and Geiger, Nucl. Phys. A180, 615 (1972).

2. Measurement of Differential Elastic and Inelastic Cross Sections for C, Al, Fe, Ni, Nb, and In at 12 MeV (J. D. Carlson and J. Rapaport)

Angular distributions of neutrons scattered from C, Al, Fe, Ni, Nb and In have been measured between 70° and 145°. The elastic cross sections have a relative uncertainty of ∿2% based only on counting statistics. The cross section for the excitation of the 2^+ (0.845 MeV) level in ^{56}Fe has been measured with a relative uncertainty of ∿5%. The elastic and inelastic cross sections for Fe are shown in Figure A4. The elastic data has been corrected for flux attentuation and multiple scattering. The inelastic data has been corrected for flux attentuation.

The solid curves shown in Figure A4 are optical model calculations. The parameters used in these calculations were determined from (p,p) and (p,n) scattering data independent of neutron scattering measurements.*,**,†

---

* Carlson, Lind and Zafiratos, Phys. Rev. Lett. 30 (1973) 99.

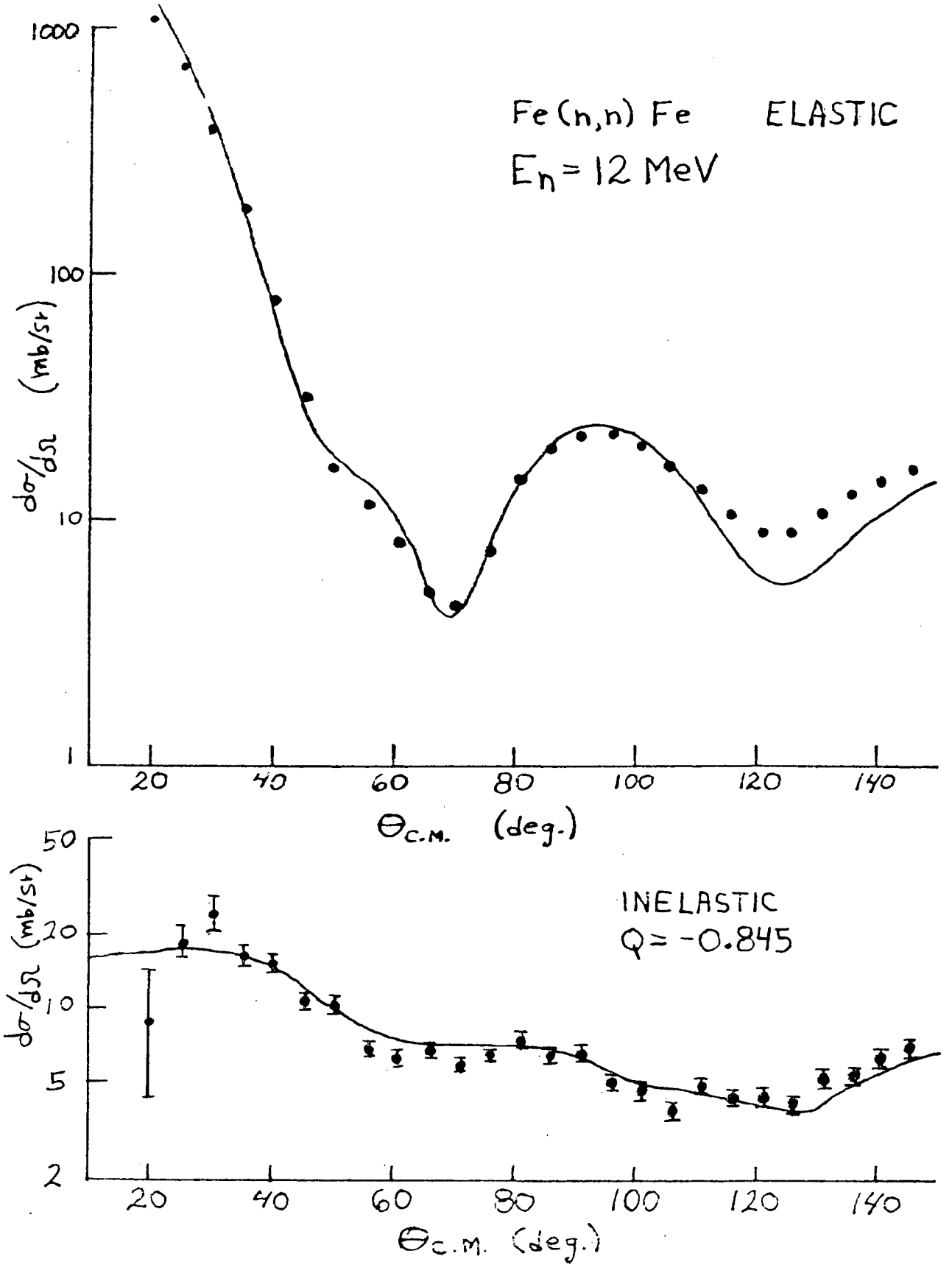
Fe(n,n) Fe ELASTIC
E_n = 12 MeV
1000
100
10
1
dσ/dΩ (mb/st)
20
40
60
80
100
120
140
$\theta_{c.m.}$ (deg.)
INELASTIC
Q = -0.845
50
20
10
5
2
dσ/dΩ (mb/st)
20
40
60
80
100
120
140
$\theta_{c.m.}$ (deg.)

Figure A4

** J. D. Carlson, Ph.D. Thesis, Univ. of Colorado (1972).

† Carlson, Lind and Zafiratos, to be published.

3. (p,n) Reactions on ^{96}Mo and ^{98}Mo (C. M. McKenna, R. W. Finlay, J. Rapaport, J. Crawford, G. Doukellis and H. J. Kim*)

Energy levels in ^{96}Tc and ^{98}Tc were studied by means of the (p,n) reaction on ^{96}Mo and ^{98}Mo, and the (p,nγ) reaction on ^{98}Mo. Proton bombarding energy was varied between threshold and 5.45 MeV. Outgoing neutron groups were observed by means of a pulsed-beam time-of-flight spectrometer. Angular distributions for ^{96}Mo(p,n)^{96}Tc were measured at proton energies in the vicinity of and at the isobaric analog resonances at 5.384 MeV. Absolute time scales were established by measuring neutrons from the ^{7}Li(p,n)^{7}Be and ^{65}Cu(p,n)^{65}Zn reactions. Results for the ground state Q-values and level schemes are being obtained.

---

* Oak Ridge National Laboratory

4. Neutron Elastic and Inelastic Scattering Measurements Between 10 and 28 MeV

Gas Target for Monoenergetic Neutron Production (J. D. Carlson)

A simple, low mass, small volume gas target for the production of monoenergetic neutrons by means of the D(d,n)^{3}He, T(d,n)^{4}He, and T(p,n)^{3}He reactions has been constructed and tested. The gas cell is similar in design to one which has been used at Los Alamos Scientific Laboratory.* The charged particle beam enters the cell through a thin window of Molybdenum or Havar which is held in place between a pair of "O" rings. The beam is stopped in a layer of platinum which forms the end of the gas cell. The cell has a length of approximately 3 cm. The entrance aperture has a diameter of 0.5 cm.

The performance of the gas cell has been quite satisfactory. When filled with 1100 TORR of deuterium gas a 5 μm M_0 entrance window was able to operate at beam currents in excess of 20 μA (4 MeV proton beam). At a beam current of 10 μA it was possible to increase the gas pressure to 3100 TORR before a rupture occurred with a 5 μm M_0 foil. A 10 μm M_0 foil was found to be capable of operating at a pressure of 4800 TORR and a beam current of 14 μA (4 MeV proton beam).

---

* McDaniels, Berqvist, Drake and Martin, NIM 99 (1972) 77.

5. ^{11}C Production by a Tandem Van de Graaff for Medical Uses
(A. G. Perris, R. O. Lane, J. D. Matthews and J. Y. Tong)

The $^{11}B(p,n)^{11}C$ reaction was used to produce ^{11}C with high yields suitable for medical uses. This reaction was considered to be advantageous over the widely used $^{10}B(d,n)^{11}C$ because of the higher abundance of ^{11}B in natural boron, the lower background and the 6-MeV resonance in $^{11}B(p,n)^{11}C$ which has a high cross section. Protons of 6-MeV from our Tandem bombarded the B_2O_3 target with beam currents of 2 μA. The B_2O_3 disk was placed in a cell through which He gas flowed as a carrier. The cell was separated from the accelerator vacuum by a Havar window of thickness 2 mgr/cm^2. The activity was collected as $^{11}CO_2$ and ^{11}CO using liquid N_2 traps, solid NaOH traps and Ag_2O traps. For the chemical traps the $^{11}CO_2$ to ^{11}CO production ratio was determined. The activity collected in the traps was determined using ^{68}Ge as a standard source. Typical yields of the production were approximately 13 x 10^3 μCi/μA·h. A total activity of about 50 mCi was collected in a run of 100 minutes.

B. NUCLEAR THEORY

1. Core-coupling Model Applied to Odd Nickel Isotopes
(P. Hoffmann-Pinther and J. L. Adams)

We are attempting to fit the odd nickel isotopes from 59 to 65 using the core-coupling model in the quasiparticle representation. The various parameters are varied in order to fit both energy levels and neutron spectroscopic factors. Wave functions are also found for each level.

---

2. Core-coupling Model Applied to ^{90}Y (P. Hoffmann-Pinther and J. L. Adams)

We have fit ^{90}Y in the core-coupling model with the inclusion of a zero-range neutron-proton residual interaction. Both energy levels and wave functions are calculated.

C. A-CHAIN COMPILATIONS

Level Schemes for Nuclei with A=142 and A=143

(J. F. Lemming* and J. Rapaport)

Level schemes and decay characteristics have been compiled for all nuclei with mass number 142. Experimental data, adopted values, comparison with theory and arguments for spin and parity have been obtained.

The 1967 version of Nuclear Data Sheets for A=143 is now in the process of being revised.

---

* Nuclear Information Research Associate, supported by National Science Foundation through the National Academy of Sciences-National Research Council

RENSSELAER POLYTECHNIC INSTITUTE

A. CROSS SECTION MEASUREMENTS

1. Resonance and Thermal $\bar{\nu}$ Measurements on ^{239}Pu*
(R.W. Hockenbury, R.L. Reed and R.C. Block)

The prompt fission neutron average multiplicity $\bar{\nu}$ of ^{239}Pu has been measured at the RPI LINAC from 0.01 to 100 eV using a fission chamber and a 0.75 m dia. Gd-loaded liquid scintillator. Values of $\bar{\nu}$ have been determined for 22 resonances with standard deviations ranging from 0.2 to 0.5%. The $\bar{\nu}$ values fluctuate significantly from resonance to resonance, and statistical tests of the values indicate that their distribution is consistent with two or more populations. There is a tendency for higher $\bar{\nu}$ values to be associated with resonances with spin J = 0^+ while almost all the lower values correspond to resonances of spin J = 1^+. In the 0.3 to 0.01 eV range, $\bar{\nu}$ increases with decreasing energy, with $\bar{\nu}$ for the 0.3 eV resonance significantly lower than the value at 0.0253 eV. From 0.10 to 0.011 eV, $\bar{\nu}$ increases with a slope of approximately 0.6%. These new data follow the same trend with resonance energy as the earlier results of Weinstein et al. if their data in the 40 to 100 eV region are re-normalized downward slightly. Comparisons have also been made to recent measurements at Oak Ridge and Saclay. In the resonance region, our results also show the same trend with resonance energy as the results reported by Oak Ridge, but the Oak Ridge $\bar{\nu}$ values do not show the tendency to divide into groupings as do the RPI and Saclay data. On the other hand, our results do not show the same trend with energy as the Saclay results, and in particular there is a strong reversal in the two sets of data for the $\bar{\nu}$ values of the 41.4 and 44.6 eV resonances.

*Req. No. 503

2. Neutron Multiplicity Measurements on ^{233}U and ^{235}U*
(R.L. Reed**, R.W. Hockenbury and R.C. Block)

Measurements of prompt neutron emission as a function of incident neutron energy for fission of ^{233}U and ^{235}U have been made using multiplate fission chambers and a Gd-loaded liquid scintillator tank. The neutron source was the R.P.I. LINAC and incident neutron energies were determined by the time-of-flight method. Nubar values were determined for ^{235}U in the thermal to 30 eV energy range and for ^{233}U in the thermal to 100 eV energy range. Nubar was measured to be constant to 0.1% in the thermal region from 0.10 to 0.011 eV for both ^{235}U and ^{233}U. In the epithermal energy region, relative nubar values were determined for

** Now at Savannah River Laboratory, S. C.

each resolvable resonance and the data were normalized to the well established thermal values. For ^{235}U, the distribution of the resonance nubar values cannot be fit by a single population. If one assumes two populations, then $\bar{\nu}$ falls into two groups separated by about 0.5% with mean values of 2.406 ± 0.002 and 2.417 ± 0.002. Statistical errors (standard deviations) for the ^{235}U resonance nubar values range from 0.1% to 0.3%. The maximum deviation from the average of all the resonance nubar values is 0.7% while the maximum difference between any two resonance nubar values is 1%. Resonance spin assignments for ^{235}U are made based on the assumed nubar grouping. The ^{233}U resonance nubar values also exhibit variations not consistent with a single population. However no definitive groupings as for ^{235}U are observed. The errors on the ^{233}U resonance nubar values range from 0.1% to 0.5% with maximum deviations from the average of 1% and maximum resonance-to-resonance differences of 2%.
*Req. No. 417, 447

3. ^{60}Ni (n,γ) TOFXPHA Data*
(P.H. Brown, R.C. Block and J.R. Tatarczuk)

The intensity of γ-ray transitions from the ½- s-wave neutron capturing state in ^{60}Ni to the 2nd excited state (½-, E_γ = 7534 keV) and ground state (3/2-, E_γ = 7817 keV) have been measured in 12 time-of-flight bins. The 12 time-of-flight bins extend from the large s-wave resonance in ^{60}Ni at 12 keV down to thermal (via Cd difference). The ratio of the ground state to the 2nd excited state transition is found to be a constant ($\approx$1.6) over this neutron energy range. In addition a strong transition to the 1st excited state (5/2-, E_γ = 7750 keV) is observed following capture in the p-wave resonance at E_n = 2.2 keV. This 1st excited state transition is ~10 times stronger than the ground state transition and ~4 times stronger than the 2nd excited state transitions in this neutron energy region.
*Req. No. 193

4. KeV Neutron Elastic Scattering Cross Sections in Iron and Nickel*
(R. Zuhr and K. Min)

The latest differential elastic scattering cross section data for natural iron and nickel have been analyzed. These measurements, which incorporated all the experimental modifications previously reported, represent a marked improvement in accuracy over earlier results. The data were averaged, using 10 keV bins, over the energy range from 10 to 650 kilovolts, giving statistical errors ranging from less than 1% at low energies to a maximum of 6% at the upper limits. The raw angular distributions were corrected for multiple scattering, and then least square fitted in order to provide results in terms of fourth order

Legendre Polynomial coefficients. These results provide differential scattering cross sections of resolution not previously available below 300 kilovolts.
*Req. No. 147

5. Average Resonance Parameters in the Unresolved Resonance Region of Uranium and Tantalum*
(T.Y. Byoun, R.C. Block and T. Semler+)

The average resonance parameters in the energy range from 10 to 100 keV have been determined from the average transmission and the self-indication data[1,2]. The analytical model[2,3] has developed for the analysis of the above data. The results for tantalum and depleted uranium (99.8% ^{238}U and 0.2% ^{235}U) are listed in Tables A-1 and A-2.

* Supported by NASA Grant NGR 33-018-134
+ NASA Lewis Research Center, Cleveland, Ohio

6. Increased LINAC Beam Current with a Model 12 Gun
(W.R. Moyer, J.R. Tatarczuk and R.C. Block)

An RPI designed pulser and an ARCO Model 12 high current electron gun were recently installed in the LINAC to increase the peak electron beam current on target. The new pulser is capable of emitting 40 amperes into a 50 ohm resistive load, matching the characteristics of the model 12 cathode under high current operation. The pulser consists of (i) a pulse-forming network composed of a pair of Raytheon RT 3333 avalanche transistors in series plus selected lengths of open-ended coaxial cable, (ii) an intermediate pulse amplifier composed of a Machlett ML-8538 planar triode and (iii) a final pulse amplifier composed of four ML-8538 triodes in parallel. Rise and fall times of $\sim$2 nsec were achieved over a range of pulse widths (FWHM) from $\sim$5 to 200 nsec.

---

1. T. Y. Byoun, R. C. Block and T. Semler, Conf. 710301, Col. 2, 3rd Neut. Cross Sect. and Tech. Conf. (1971).
2. T. Y. Byoun, R. C. Block and T. Semler, Conf. 720901 (Book 2), Sept. 1972 ANS Topical Meeting on New Development in Reactor Physics and Shielding.
3. T. Y. Byoun, R. C. Block and T. Semler, to be published.

TABLE A-1

Best-Fit Average Resonance Parameters of Tantalum
In The Energy Range From 10 keV to 100 keV

	S-wave ($\ell = 0$)	P-wave ($\ell = 1$)
Strength Function (10^{-4})	$1.6^{+0.3}_{-0.2}$ (*)	$0.4^{-0.2}_{+0.3}$
Level Spacing (eV)	$4.3^{-0.5}_{+1.5}$	$2.15^{-0.25}_{+0.75}$
Radiation Width (meV)	$60.0^{-5.0}_{+3.5}$	$72.0^{-9.0}_{+6.0}$
Scattering Length, R' (fermi)	8.19(#)	

(*) The error limitations given for all the parameters correspond to the values which yield the average difference between the experimental values and theoretical values as follows:

$$\overline{\Delta R} = \left| \frac{1}{N} \sum_{i=1}^{N} (R_i^{exp} - R_i^{cal}) / R_i^{exp} \right| = 2.0$$

(#) It is assumed that channel radius, R, is the same as R', that is, $R^{\infty} = 0.0$.

TABLE A-2

Best-Fit P-wave Strength Functions For ^{238}U

Different Scattering Lengths.

	Best Fit Parameters(*)			ENDF/B-III	
	(A)	(B)	(C)	(D)	(E) (#)
$S_1 (10^{-4})$	$1.58^{+0.1}_{-0.1}$	$1.94^{+0.1}_{-0.2}$	$2.40^{+0.1}_{-0.2}$	1.75	1.27
D_1 (eV)	$11.3^{-2.0}_{+2.0}$	$11.3^{-3.5}_{+3.0}$	$11.3^{-2.0}_{+3.0}$	6.67	6.90
$\overline{\Gamma}_{\gamma 1}$ (meV)	$47.5^{-8.4}_{+8.4}$	$43.8^{-13.6}_{+11.6}$	$37.0^{-6.6}_{+9.8}$	23.5	28.0
R' (fm)	9.30	9.20	9.0	9.20	9.60
R (fm)	8.74	8.74	8.4	8.4	8.74
R^{∞}	-0.065	-0.053	-0.071	-0.095	-0.098
S_o (10^{-4})	1.0			1.05	1.0
D_o (eV)	20.7			20.0	20.7
$\overline{\Gamma}_{\gamma 0}$ (meV)	23.0			23.5	23.0

(*) The uncertainties given for S_1, D_1, and $\overline{\Gamma}_{\gamma 1}$ correspond to the values which yield the average difference between the experimental values and theoretical values as follows:

$$\overline{\Delta R} = \left| \frac{1}{N} \sum_{i=1}^{N} \left(R_i^{exp} - R_i^{cal} \right) / \delta R_i^{exp} \right| = 2.0$$

(#) R' = 9.6 fermi, taken from Columbia measurement .

A maximum peak beam current of 6 amperes was measured on target (for $\leq$ 40 nsec pulse widths) whereas the total peak emission from the gun was about 25 amperes. Recent tests at the Argonne linear accelerator* show that a higher powered buncher should increase the peak target current from 6 amperes to at least 20 amperes. The pulser and Model 12 gun have been in service for over five months and have functioned very reliably. The gun (while cold) was let down to atmospheric pressure three times during this period, and each time the gun reactivated and returned to normal operation.

7. High Resolution Capture and Total Cross Sections of ^{54}Fe and ^{61}Ni**
(H. D. Knox, M. V. Costello, R. W. Hockenbury and R.C. Block)

High resolution capture and total cross section measurements on ^{54}Fe and ^{61}Ni have been undertaken in the 10 to 200 keV neutron energy range. The over all timing resolution in these experiments is approximately 19 nsec. The capture measurements have been completed and the transmission measurements are underway.

8. Subthreshold Fission Induced by Neutrons on ^{238}U
(R. C. Block , R. W. Hockenbury, R. E. Slovacek+, E. B. Bean+ and D. S. Cramer+)

Subthreshold fission has been observed for neutrons incident upon ^{238}U below 100 keV. Two prominent subthreshold groups of resonances are clustered about the 720 and 1210 eV ^{238}U resonances. The fission widths for these two resonances are (1.2 $\pm$ 0.3) meV and (0.12 $\pm$ 0.03) meV respectively. Additional subthreshold groups are observed at approximately 2.5, 7.5, 11, 15, 27 and 35 keV. From these data the second potential well is deduced to lie about2.2 MeV above the first potential well in the double humped potential barrier. The average ^{238}U subthreshold fission cross section is 87 $\pm$ μb in the neutron energy range $10 \leq E_n \leq 30$ keV; in the energy interval $30 \leq E_n \leq 100$ keV, this cross section is 40 $\pm$ 12 μb. The two groups at 722 and 1210 eV are shown in the upper part of Fig.A-1; the reduced neutron widths are shown in the lower part. The ^{238}U fission data from 2 to 40 keV are shown in Fig.A-2.

---

* G. Mavrogenes (private communication)

** Req. No. 155, 162, 187, 188

\+ Knolls Atomic Power Laboratory

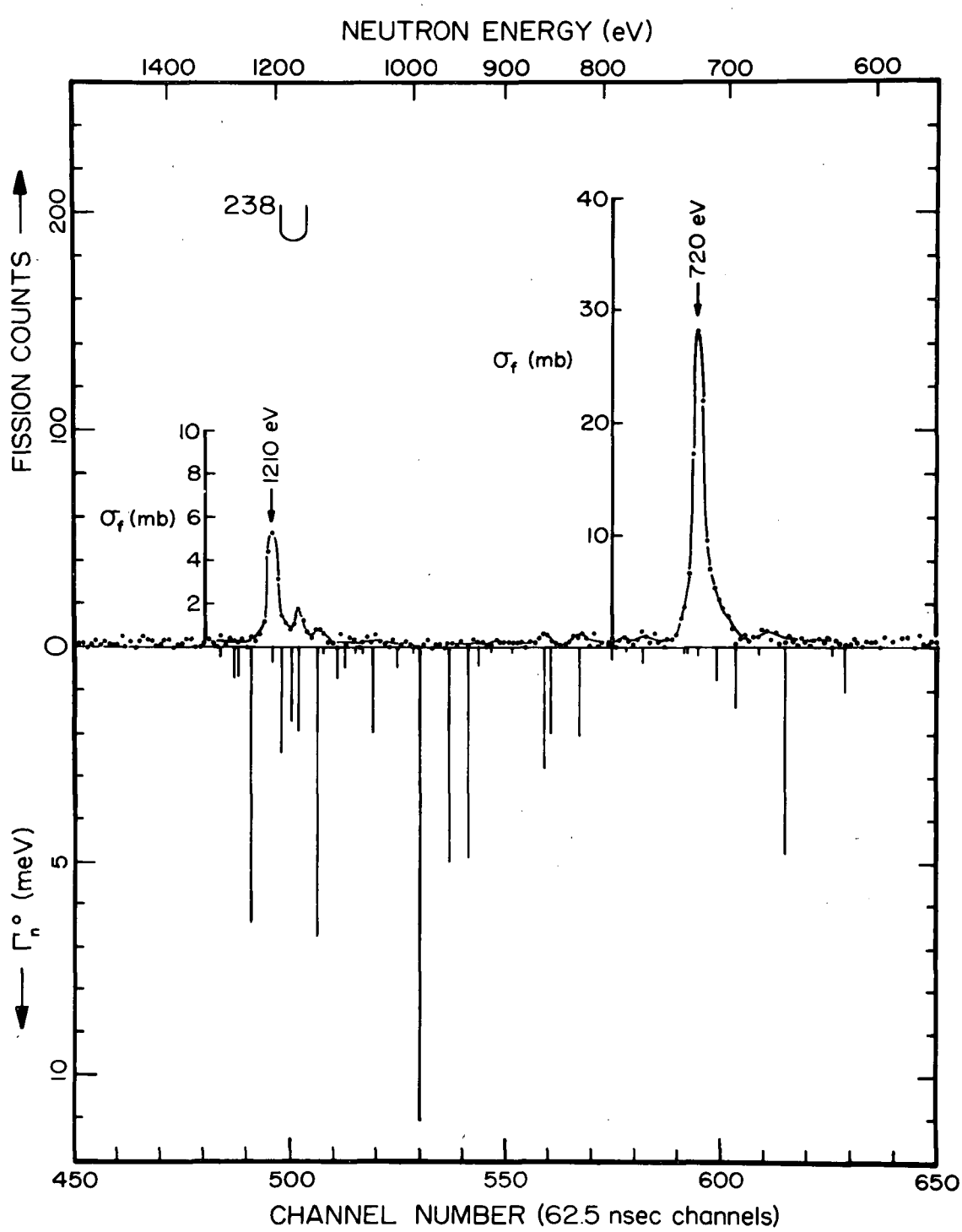
NEUTRON ENERGY (eV)
1400
1200
1000
900
800
700
600
238U
FISSION COUNTS
200
100
0
σf (mb)
10
8
6
4
2
1210 eV
40
30
20
10
720 eV
Γn° (meV)
5
10
450
500
550
600
650
CHANNEL NUMBER (62.5 nsec channels)

Fig. A-1.

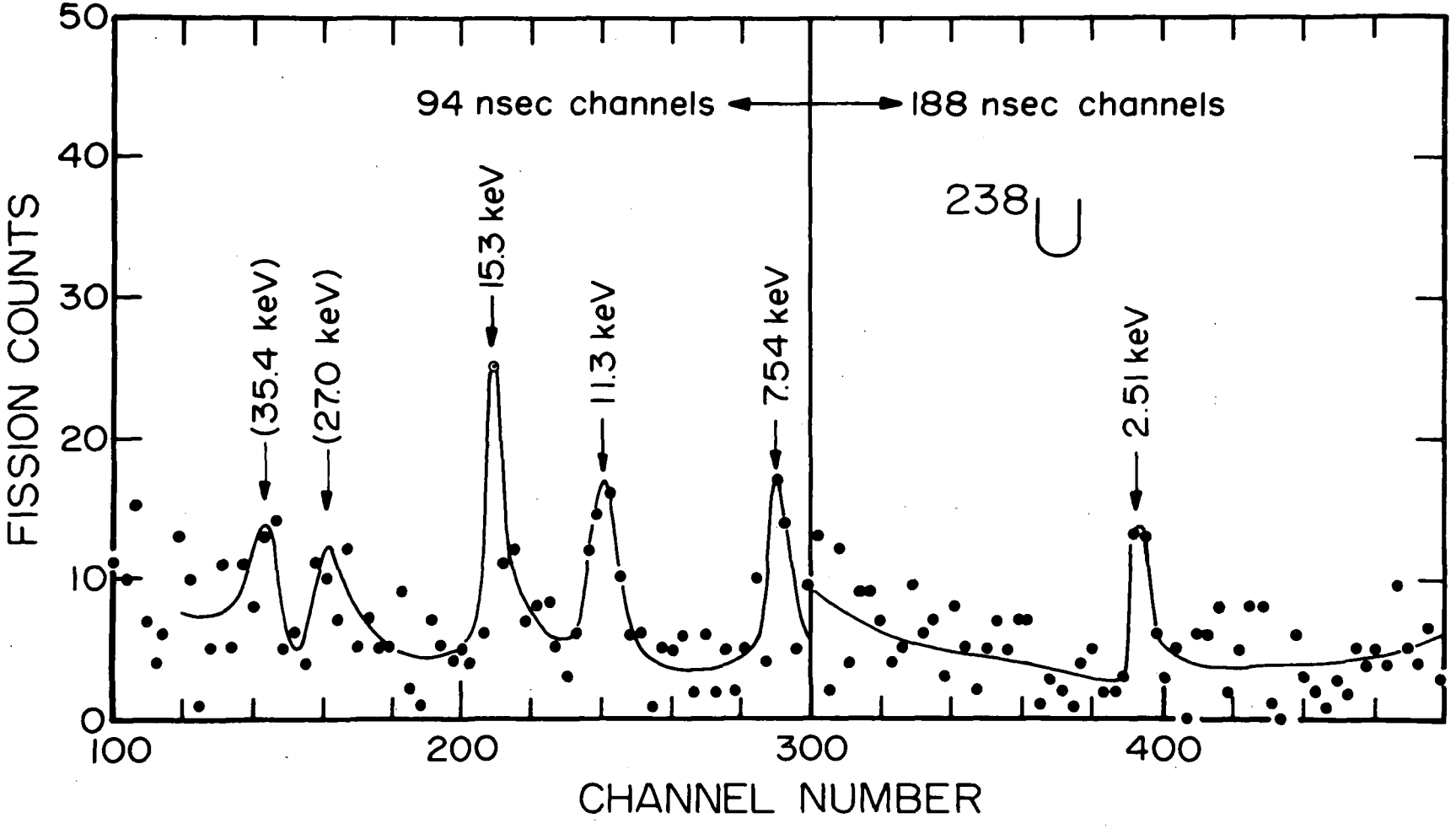
94 nsec channels
188 nsec channels
238U
(35.4 keV)
(27.0 keV)
15.3 keV
11.3 keV
7.54 keV
2.51 keV
FISSION COUNTS
CHANNEL NUMBER
0
10
20
30
40
50
100
200
300
400

Fig. A-2.

B. NUCLEAR THEORY

1. Optical Model Calculations
(P. J. Turinsky, J. Sierra)

As previously reported, an angular momentum (ℓ) dependent optical model was found necessary in order to simultaneously fit the s- and p-wave neutron strength functions and potential scattering radius over the mass range 40 to 240 for low energy neutrons. By the addition of an (ℓ) dependent imaginary surface term, the deep strength functions minima and maxima and oscillatory potential scattering radius were accurately predicted in the mass region of strongly spherical nuclei. Above mass number 140 where the 2^+ vibrator state becomes low lying, our calculation has been extended by performing coupled-channel calculations with the JUPITØR program. Allowing 0^+-2^+ coupling, using deformation parameters β_{2^+} and excitation energies E_{2^+} from E2 transition data and our previously determined (ℓ) dependent global optical parameters, excellent agreement to the strength functions and potential scattering radius over the mass range 40 to 240 was obtained. Total, shape-elastic and reaction cross sections versus mass number and energy have also been calculated. Comparison of our calculated total cross section with the energy averaged experimentally obtained total cross section for low energy neutrons ($<$ 300 keV) indicates good agreement. Some problems were encountered about mass numbers 90 and 140 due to both strong mass number and energy sensitivity. Unfortunately these mass ranges nearly coincide with peak fission product productions, the particular elements where prediction capability is most required for reactor physics calculations.

To justify the(ℓ)dependent optical imaginary surface potential employed, 2p-1h calculations within the framework of coupled-channel calculations are being carried out. Considering an (A-1) inert target core, last bound particle and incident neutron, shell model potentials are used to model the inert core-particle interactions and a delta function potential is used to model the particle-particle interaction. This leads to a simple coupled-channel equation whose solution provides the optical potential. These calculations are near completion.

2. Correlations Between Reduced Neutron and Radiative Widths
(M. Lubert, R. C. Block, N. C. Francis)

The strong correlations between the reduced neutron and radiative widths for the chromium and nickel isotopes reported by RPI[1] have been examined. A capture model which includes both a channel and compound nucleus component was formulated. The capture mechanism was examined through the analysis of the ground state transitions in the (γ,n) experiments[2,3] for ^{57}Fe, ^{53}Cr, and ^{61}Ni as well as the ^{60}Ni (n,γ) experiment. The partial radiative widths, correlations between the partial radiative and reduced neutron widths, compound nucleus partial

radiative widths, neutron capture cross section and estimates of the total radiative widths were determined. The primary results are as follows:

The absence of (γ,n) experimental correlations between the Γ_{γ_i} and Γ_n^0 is due to two factors. First, this correlation is reduced by the random compound nucleus partial radiative amplitude which adds coherently to the channel amplitude. Second, the experimental correlations may be reduced because of experimental error. The (γ,n) experiments are difficult to perform and subject to area and background uncertainties.

The correlations observed at RPI between the reduced neutron and radiative widths for the nickel and chromium isotopes can be interpreted as due to correlations between the partial radiative and reduced neutron widths for several final states where the interference between the channel and compound nucleus is negligible. This indicates that non-statistical effects such as channel capture are important.

The resonance line shape determined by the theory are asymmetric. Although the experimental evidence is not conclusive, asymmetries in (n,γ) and (γ,n) have been observed. The experimental and theoretical line shapes exhibit constructive interference below and destructive interference above the resonance. This characteristic shape is expected when the channel width is greater than the compound nucleus width.

The model developed should be used in the analysis of experiments in which channel effects are non-negligible. The use of Breit-Wigner theory should be avoided in these cases.

If one examines the iron, chromium and nickel (n,γ) spectra[4] for resonance neutrons, a slow variation with energy is observed. A similar pattern is found in the p-wave analysis[5] of the 1150 eV level in ^{56}Fe. The preliminary results of a study at RPI for the ground and first excited states in ^{61}Ni show similar results. It is exciting to consider that the channel compound theory developed would hold for both s and p state resonances.

---

1. Stieglitz, R. G. et al. Nucl. Phys. A163, 592 (1971).
2. Baglan, R. J. UCRL-50902, August 170.
3. Jackson, H. E., Strait, E. N., Phys. Rev. C4, 1314 (1971).
4. Allen, B. J. et al. AAEC E200, October 1969.
5. Chrien, R. E., et al. Phys. Rev. C1, 973 (1970).

If one has measured the partial cross section to some final state for an isotope, this analysis can determine the reduced width. This provides another method, besides the (d,p) reaction, for calculating the reduced width.

The channel cross section shapes differ from the Breit-Wigner theory. In particular, the channel cross section below the resonance is greater than the Breit-Wigner cross section. As neutrons diffuse through materials such as iron, the neutron flux is depressed at the resonance and is large at the total cross section minima positions. At these latter energies, the difference between the channel and compound nucleus cross sections is large and the channel reaction rate can be significant.

C. INTEGRAL CHECKS OF CROSS SECTION DATA

1. Fast Neutron Transport in Bulk Media

(E. R. Gaerttner, N. N. Kaushal, B. K. Malaviya, A. N. Mallen and M. Becker)

Measurement of fast neutron spectra in a 6 ft. cube sodium assembly, are nearing completion[1]. These data which span a neutron energy range from 100 eV to upwards of 10 MeV, are to be compared with theoretical spectra calculated by means of transport theory code DTF-IV[2] and the cross section data from various ENDF/B files including version ENDF/B-III. Preliminary calculations have already been made and show a fair overall agreement between the measurements and the calculations. However, there are areas of disagreement in the few-MeV range and there may be discrepancies in the calculated and measured amplitudes in the low keV range. A more detailed investigation of these errors and further calculations are in progress.

Also continuing is further evaluation of similar data for other assemblies such as iron, depleted uranium and aluminum. Recently an evaluation was made, of the contribution of the $^{238}U\ (n;n',\gamma)$ cross section to the neutron spectrum in a depleted uranium assembly[3]. It was concluded that such a cross section, in the magnitudes recommended for adoption in the ENDF/B file by certain authors[4,5], would lead to large discrepancies in the measured and calculated spectra in our depleted uranium assembly. We have, therefore, made a recommendation that the $^{238}U\ (n;n',\gamma)$ cross section as proposed by Fricke and Niell[4] be not adopted.

1. A. N. Mallen, N. N. Kaushal, B. K. Malaviya and E. R. Gaerttner, Linear Accelerator Project Annual Technical Report, COO-3058-27, Rensselaer Polytechnic Institute (1972).

2. K. D. Lathrop, "DTF-IV, A Fortran-IV Program for Solving the Multigroup Transport Equation with Anisotropic Scattering", LA-3373, Los Alamos Scientific Laboratory (1965).

3. Martin Becker and Narinder N. Kaushal, "An Assessment of Proposed (n;n',γ) Data Based on Measured and Calculated Spectra in Depleted Uranium" submitted for publication (1973).

4. M. P. Fricke and J. M. Neill, Nucl. Sci. Eng. 50, 392 (1973).

5. H. H. Hummel and W. M. Stacey, Jr., Nucl. Sci. Eng. 50, 397 (1973).

T. W. Bonner Nuclear Laboratories - Rice University

A. NEUTRON PHYSICS

1. Organic Scintillator Neutron Detector Efficiency: A Comparison of Experimental Results with Predictions (R. Plasek, V. Valković, and G.C. Phillips)

Absolute efficiency points in the neutron energy range 2-10 MeV were taken for a 7.62 cm x 12.75 cm NE-218 liquid organic scintillator, utilizing the $d(d,He^3)n$ reaction. The results were compared with two theoretical efficiency predictions: (1) Program "DETEFF"[1] and (2) Program OSS.[2] The agreement with DETEFF was quite good; however, the predictions of OSS varied considerably from the experimental points, both in absolute magnitude and in shape.

2. Spatial Localization Effects in the $^2H(d,pd)n$ Reaction (W. von Witsch, G. S. Mutchler, G. C. Phillips, and D. Miljanic)

A phenomenological explanation has been proposed for the pronounced peaks observed in some coincidence spectra of the $^2H(d,pd)n$ reaction at low relative energies in the proton-neutron system.[3] It has been shown that the density of states formalism of Phillips, Griffy, and Biedenharn[4] which includes explicitly the fact that the p-n system is produced in a spatially localized state can describe the observed spectral shapes with the pure, isospin allowed, $^3S_1$ proton-neutron final-state interaction. In addition, the model satisfactorily describes the case of low relative energy between the deuteron and neutron.

---

[1] S. T. Thornton and J. R. Smith, Nucl. Instr.&Meth. 96(1971) 551.

[2] R. E. Textor and V. V. Verbinski, Report ORNL-4160. V. V. Verbinski et al, Nucl. Instr. & Meth. 65(1968)8.

[3] W. von Witsch, M. Ivanovich, D. Rendic, J. Sandler, and G. C. Phillips, Phys. Rev. C2(1970)2144.

[4] G. C. Phillips, T. A. Griffy, and L. C. Biedenharn, Nucl. Phys. 21 (1960)327.

B. FEW BODY PROBLEMS

1. Deuteron Break-up Reactions and Mass 3 Excited States (R. Plasek, V. Valkovic, R. Liebert, D. Miljanic, and G. C. Phillips)

In order to obtain information about mass 3 excited states proton-induced and deuteron-induced deuteron break-up have been studied. Charged particle-charged particle and neutron-charged particle coincidences have been measured. Excitation curves for the $p+d \rightarrow p+d^*$ reaction have been measured in the bombarding energy interval $E_p = 7.5 - 12.5$ MeV at $\theta_{d^*,C.M.} = 50^o$, 60°, 75°, 80°, and 90°. The reaction $d+d \rightarrow n+p+d$ has been studied with kinematical conditions corresponding to small relative energies in the n-d system. All measured spectra can be reasonably well explained assuming nucleon-nucleon and nucleon-deuteron quasi-free scattering and nucleon-nucleon final state interactions.

2. Quasi-Free Scattering in the $^6Li(d,dd)^4He$ Reaction at Low Bombarding Energies (D. Miljanic, T. Zabel, R. B. Liebert, V. Valkovic, and G. C. Phillips)

Deuteron-deuteron quasi-free scattering contributions in the $^6Li(d,dd)4He$ reaction have been measured for deuteron bombarding energies of 6-11 MeV. Experimental results are analyzed using the plane wave impulse approximation. Distortion effects are found to be strong at these energies. Extracted clustering probabilities and widths of momentum distributions are compared with results from other quasi-free scattering reactions on ^6Li.

3. Rescattering of α on d in the Reaction $p+^9Be \rightarrow d+^8Be \rightarrow d+\alpha+\alpha$ (E. V. Hungerford and T. M. Williams)

By detecting the d and the α going away from the deuteron in coincidence, it should be possible to observe a decrease in counts when the angle between the other α and the deuteron approaches 0° in the C.M. system. At a slightly higher energy in which rescattering cannot occur, this drop in coincidences should not be observed.

4. A Search for Rescattering in the $d + {}^{10}B \rightarrow 3\alpha$ Reaction (V. Valković, D. Miljanić, R. B. Liebert, and G. C. Phillips)

The reaction ${}^{10}B(d,\alpha\alpha){}^{4}He$ has been studied under kinematic conditions appropriate for the observation of the rescattering process $d + {}^{10}B \rightarrow {}^{8}Be^{*} + \alpha_1 \rightarrow \alpha_2 + {}^{8}Be_{g.s.} \rightarrow \alpha_1 + \alpha_2 + \alpha_3$. The experiment has been performed as a study of the excitation curve for the sequential decay $d + {}^{10}B \rightarrow \alpha_2 + {}^{8}Be_{g.s.} \rightarrow \alpha_1 + \alpha_2 + \alpha_3$. The bombarding energy interval was chosen such that the first step in the rescattering process was the formation of ${}^{8}Be^{*}$ resonances at 16.63 and 16.93 MeV. Coincidence and single counter spectra were analyzed.

5. Energy Dependence of the Cross Section of the ${}^{11}B(p,\alpha\alpha){}^{4}He$ Reaction (D. Miljanić, V. Valković, D. Rendić, and G. C. Phillips)

The α-α coincidence spectra from the ${}^{11}B(p,\alpha\alpha){}^{4}He$ reaction have been measured in the bombarding energy interval $8.5 \leq E_p \leq 9.5$ MeV. The bombarding energies were chosen such that the rescattering process involving the first step formation of the ${}^{8}Be^{*}$ (16.63 MeV) state was allowed. The angular settings of the two alpha-particle detectors were chosen in such a way as to observe the α-α final state interaction in the ${}^{8}Be^{*}$(2.9 MeV) state. The observed structure in the excitation curve was analyzed.

6. (${}^{16}O$,np) and ${}^{16}O$,nα) Reactions on Some Light Nuclei (G. C. Phillips, R. Plasek, R.B. Liebert, R. Wheeler, D. Miljanić, and V. Valković)

Nuclear reactions with three particles in the final state resulting from the bombardment of ${}^{9}Be$, ${}^{10}B$, ${}^{12}C$, and ${}^{13}C$ targets with 30 and 36 MeV ${}^{16}O^{(5+)}$ ions have been studied. Neutron-proton and neutron-alpha particle coincidences have been measured for the geometry $\theta_{p,\alpha} = \theta_n$. Transitions to ground and excited states of residual nuclei have been observed. The obtained results were analyzed in terms of different final state interactions between the particles in the outgoing channel.

7. $^3\vec{He}(\vec{p},p)^3He$ and $^3\vec{He}(\vec{d},d)^3He$ Spin-Correlation Experiments (Donald May and Stephen Baker in collaboration with G. Ohlsen and R. Hardekopf of LASL)

Analyses of the data obtained at LASL on spin-correlation in $^3\vec{He}(\vec{p},p)^3He$ and $^3\vec{He}(\vec{d},d)^3He$ is in process. A phase shift analysis incorporating the proton scattering data will be used to extract a more precise value for the P-wave coupling parameter ϵ (1^-) in the region of 8 MeV. The method of Bolsterli and Hale[1] will also be used to parameterize the higher partial waves and hence to extract a measure of normalization of the large-radius part of the ^3He wavefunction.

8. Pressurized Target of Polarized ^3He (Robert Simpson and Donald May)

A pressurized target of polarized ^3He is under construction to investigate the effect of ionizing radiation on the relaxation time of the polarization.

C. NUCLEAR SPECTROSCOPY

1. Tests of G Parity and Isospin Conservation by Nuclei β Decay (E.V. Hungerford)

A system has been designed and constructed to measure the ft-values of short-lived β decay isotopes. Comparison of the ft-values between isospin multiplets gives a test of G parity and isospin.

2. The $f_{5/2}$ Resonance in ^{41}Sc (T. Jurgensen and C. M. Class)

An optical-model parameterization of the scattering of protons by ^{40}Ca has been obtained that describes well both low energy ($E_p \leq 5$ MeV) structural features of ^{41}Sc and the higher energy ($E_p \geq 12$ MeV) scattering cross sections and polarization. An interesting implication of the parameterization is that it locates the $f_{5/2}$ shape-elastic resonance at $E_p \simeq 6.5$ MeV. This result furnishes a key to

---

[1] M. Bolsterli and G. Hale, Phys. Rev. Lett. 28 (1972)19.

understanding the behavior of both the proton-capture and -scattering cross sections in the neighborhood of this energy that heretofore have been intractable to analysis. In particular it is seen, with the help of the Lane-Robson formalism, that the scattering cross section is accounted for, in the main, by the coupling between the shape resonance and a half-dozen strong f5/2 compound nucleus resonances. Further work is in progress to refine this description of the cross sections.

3. The Magnetic Moment of ^{41}Sc (R. W. Dougherty, Jr. and C. M. Class)

The method of measurement of the magnetic moment of the ground state of the ^{41}Sc nucleus ($E_{max}(\beta^+)$ = 5.5 MeV, $\tau_{1/2}$ = 0.6 sec) involves the detection of nuclear magnetic resonance as a relaxation of beta-decay anisotropy due to the polarization of the scandium recoil nuclei when produced with the ^{40}Sc(d,n) stripping reaction. The hardware and experimental procedure for the measurement has proved capable of measuring beta-decay asymmetries as low as 2%. Of concern at the present time is the various polarization relaxation processes operative in the recoil stopping media.

D. NUCLEAR THEORY

1. Symmetrization of Arbitrary 3-Particle Wave Functions (John E. Beam)

A proper treatment of the quantum mechanical 3-body problem for identical particles requires symmetrization (for bosons) or antisymmetrization (for fermions) of the wave function. If one introduces parameter coordinates[1] then the complete (anti) symmetrization can explicitly be carried out on kernel functions of known form, independently of the form of the particle-particle interaction or of the corresponding unsymmetrized wave function. If the parameter coordinate functions are chosen to be Dirac delta functions, one can obtain a useful angular momentum decomposition which reduces the 6-dimensional parameter coordinate integrals to 2-dimensional ones.

---

[1] Karl Wildermuth and Walter McClure, "Cluster Representations of Nuclei," Springer Tracts in Modern Physics (Springer-Verlag, Berlin, 1966), vol. 41, p. 49.

E. APPLIED PHYSICS

1. Cross Sections for X-ray Production Induced by Protons of 2.5-12 MeV (R. B. Liebert, T. Zabel, H. T. Larson, D. Miljanić, V. Valković, and G. C. Phillips)

K-shell electron ionization cross-sections have been obtained from x-ray production measurements on thin Mn, Fe, Ni, Cu, Zn, Ag, Cd, Y, and Mo targets as a function of bombarding energy between 2.5 and 12 MeV. These results are compared with the predictions of the Merzbacher-Lewis Born Approximation, Binary Encounter Theory, and Semi-classical Approximation.

2. X-ray Production Cross-Sections and K_α/K_β Ratios Observed with Proton and Oxygen Beams (R.P. Chaturvedi, R. B. Liebert, R. M. Wheeler, T. Zabel, D. Miljanić, V. Valković, and G.C.Phillips)

K-shell electron ionization cross-sections for protons between 3 and 11 MeV and oxygen ions between 15 and 42 MeV are measured for $20 \leq Z \leq 51$ to give a simultaneous comparison of the agreement with theory for bombarding energy and Z dependence. K_α/K_β ratios and line positions are studied as a function of energy and exciting particle.

3. Trace Element Analysis of Blood Serum (R. B. Liebert, R. P. Chaturvedi, D. Miljanić, G.C. Phillips, V. V. Valković, R. M. Wheeler, and T. Zabel (Rice) and M. J. Hrgovčić, M.D. (Diagnostic Clinic, Houston)

We are studying normal blood serum and serum obtained from patients with malignant lymphoma. From an investigation of many samples from a composite batch of normal blood bank donors sera we have tested the charged particle induced x-ray emission technique for trace element analysis. Our present accuracy is in the 5-15% range for traces in the range of 1-3 ppm. Comparison of patients' conditions with trace element levels in blood serum is now in progress.

4. Trace Element Analysis of Mouse Tissue (R.M. Wheeler, R. B. Liebert, D. Miljanić, G. C. Phillips, V. Valković, and T. Zabel (Rice) and R. H. Withers and L Milas (M.D.Anderson Hospital & Tumor Institute)

The liver and spleen of normal mice and mice with transplantable fibrosarcoma have been studied. We have found that mice with advanced fibrosarcoma can be distinguished from normal mice by changes in contents of several trace elements. Encouraged by these results we will study the changes in trace element concentrations which occur from the time the sarcoma is implanted in a mouse until the sarcoma has reached an advanced stage.

5. Comparison of Proton Induced X-ray Emission, X-ray Fluorescence, and Atomic Absorption Techniques for Trace Element Analysis of Blood Serum (R. M. Wheeler, R. B. Liebert, D. Miljanić, G.C. Phillips, V. Valković, and T. Zabel (Rice) and P. Ong (M.D. Anderson Hospital and Tumor Institute)

Independent measurements of trace element content in 100 samples of human blood serum have been performed. A comparison of results for copper levels in the sera indicates that atomic absorption gives the best results, followed by x-ray fluorescence and proton induced x-ray emission. We are currently attempting to improve all phases of the proton induced x-ray emission technique.

6. Trace Element Analysis Along Human Hair (V. Valković, R. B. Liebert, D. Miljanić, G. C. Phillips, R. M. Wheeler, and T. Zabel)

We have examined 11-inch long samples of women's hair at 3/4-inch intervals, representing a growth of approximately two years. In all cases we have found substantial elemental variations with length. The origin of these variations is uncertain but would seem to be due in large part to external sources. We conclude that a much larger sampling of subjects is necessary before any accurate conclusions are possible.

7. Automated Analysis of X-ray Spectra (R. B. Liebert and R. M. Wheeler)

Two programs have been written for the IBM-1800 computer which allow automated on-line analysis of x-ray spectra produced by bombardment of biological targets with heavy charged particles. Program STRIP is used to analyze standard spectra by a non-linear least squares technique to obtain K_α/K_β ratios, relative yields with respect to dopant elements, and relative widths of x-ray lines as a function of x-ray energy. Program SPEEL uses these results to do

fast on-line analysis by a linear least squares routine while new data are collected. Comparison with STRIP output allows results to be expressed directly in parts per million.

8. Trace Element Analysis by Proton Bombardment of Aerosols (R. Boustany, R. E. Liebert, R. M. Wheeler, V. Valković, and G. C. Phillips)

Preliminary development work has been done to develop targets for proton-induced x-ray fluorescence which will minimize evaporation of trace elements and be compatible with mass production techniques. Aerosols produced from $Fe(NO_3)_3$ solutions have been bombarded with 3 MeV proton beam in a helium atmosphere and a sensitivity of the order of 1 ppm for a 20 minute run at 200 namps has been observed. Variation of the beam energy and aerosol geometry to optimize proton energy loss, target uniformity, and self-absorption is expected to improve this sensitivity figure.

F. INSTRUMENTATION

1. He^- Ion Source for the Rice Tandem (R. Y. Rodgers and E. V. Hungerford)

A Li exchange He^- ion source has been constructed for the Rice tandem. About 0.5 microamp of He^- has been obtained. Replacement of the oven and heater control should allow this current to be increased by at least a factor of two.

2. Technique for Alignment and Placement of Multi-Wire Proportional Counters (E. V. Hungerford, T. Williams, J. A. Flick, W. P. Madigan, and G. C. Phillips)

A system for the alignment of Multi-wire Proportional Counters (MWPC) with respect to a magnet is being designed using a mirror in the magnet and aligning the magnet with a transit equipped with auto-reflection target. The mirror can then be rotated to make an accurate turn through any desired angle. This will allow correct placement of MWPC behind the magnet.

3. A Multiwire Proportional Counter (MWPC) Photon Camera (G. W. Pfeufer and G.C. Phillips)

We are engaged in the development of a MWPC photon camera for use in localizing the Bragg peak energy deposition in the treatment of tumors with high LET radiation. By localizing the source of gamma-rays from the target in the reaction $^{19}F(p,\alpha\gamma)^{16}O$, existing counter systems are being presently tested for application in this program. Since the counters are relatively insensitive to photons, the gamma-rays are converted to an electron-positron pair in a suitable foil. The electron and positron are detected in two consecutive x-y counters. Using computerized ray tracing, based on these coordinates, the point of conversion can be determined. The bisection of these rays is taken as the photon direction which can be traced back to the target. These preliminary studies will indicate the resolution to be expected from the system and disclose paths of further development.

4. IBM-1800 Software (D. Mann, B. Smith, and K. McGrath)

Progress is continuing in the incorporation of a final version of two-lab capability into the BONAR Data Acquisition System.

5. 6 MV Van de Graaff Accelerator (J. R. Risser)

It is increasingly practical to use the accelerator for experiments to above 4 MeV due to improved conditioning of the accelerator tube and improvement in beam-defining equipment. It appears finally that the design characteristics are achievable. With further conditioning of the accelerator tube, energies of 5 MeV and above appear attainable. Neither the ion optics of the terminal nor design of the extended pressurizing tank appear to introduce limitations.

Pulse-bunching of deuterons and protons have been achieved and appears satisfactory. For protons, 2 ns pulse widths and 1 microampere average beams (10^6 sec^{-1} repetition rate) have been obtained.

TRIANGLE UNIVERSITIES NUCLEAR LABORATORY

A. NEUTRON AND FISSION PHYSICS

1. Resonance Cross-Section Measurements with Continuous Beam (J. G. Malan,* W. F. E. Pineo, E. G. Bilpuch, H. W. Newson)

Rechecking of the Sr cross-section data with the improved version of the R-Matrix Multilevel code (see Section A15) is almost complete. The extracted resonance parameters and the already published 2p-1h doorway results will form the subject matter for a paper on intermediate structure.

2. Resolved Neutron Total Cross Sections and Intermediate Structure (J. Clement, B.-H. Choi, W. F. E. Pineo, M. Divadeenam, H. W. Newson)

A short paper giving the details of doorway structure observed in Si total neutron cross-section data is in preparation. The resonance structure observed in Sulfur data will be combined with the results of higher energy cross-section data (to be analyzed in the future) to look for doorway effects.

Analysis of ^{209}Bi partially resolved data has been completed. The results have been included in a paper submitted (see Section A-12b) to Annals of Physics.

An R-Matrix fit to the Duke and Rensselaer ^{60}Ni neutron cross-section data is completed with the help of our improved version of the Multilevel R-Matrix code. See Section A-15 . An abstract based on these findings has been submitted to the forthcoming Washington American Physical Society meeting.

A comprehensive paper giving the details of resonance cross sections for three Pb isotopes is in preparation. Experimental reduced widths will be compared to theoretical predictions of both particle-vibration and 2p-1h doorway models for ^{206}Pb and ^{208}Pb. See Section A-12b.

---

* Now at the Atomic Energy Board of the Republic of South Africa.

3. Averaged Cross Sections, Strength Functions, and Intermediate Structure (W. F. E. Pineo, M. Divadeenam, E. G. Bilpuch, H. W. Newson)

Part II of our series on Strength Functions and Average Total Cross Sections is ready for submission to Annals of Physics. The abstract follows.

"Average neutron total cross sections have been measured in the keV region for natural samples of the rare earths Ce, Nd, Gd, Tb, Dy, and Ho, and for the separated isotopes ^{144,146,148}Nd and ^{149,152}Sm. The measurements were combined with those made here (TUNL) and elsewhere including new measurements of the average cross sections of KCl, Sc, V, Mn, Co, Cu, Zn, As, Se, CsI, and Hg to give a total data set which is comprised of the cross sections of most of the natural elements and many separated isotopes. All of the cross sections were averaged over hundreds of keV and the resulting averaged cross sections were compared to various optical-model calculations. The agreement of the spherical optical-model calculations with the data is only fair below A = 140 and very poor above that. The calculations using deformed potentials agree much better with the data especially above A = 140 but there is still room for improvement.

The s-, p-, and d-wave strength functions, R' and the p-wave phase shift were all extracted from the average cross sections of the nuclei specifically mentioned above by the Duke average cross section method. The values of R' were combined with other measurements made both at TUNL and elsewhere to give a comprehensive data set which was then compared to available optical-model calculations which use deformed potential wells. The calculations agree fairly well with the data. Measurements of R' indicate that it rises much more rapidly at A = 140 than would be predicted by the spherical optical model and confirm the rapid rise predicted by the deformed model. Similarly, a rise in R' is evident around mass number A = 50, however, enough experimental points are not available for a detailed comparison with theory."

Part III of the above mentioned series is in final stages of preparation for submission to Annals of Physics.

4. Charged Particle Fission (F. O. Purser, J. R. Boyce, D. E. Epperson, E. G. Bilpuch, H. W. Newson, H. W. Schmitt*)

a. Analysis of Fission Cross Section Measurements

Fission cross section analysis has continued utilizing the computer program PHROG to analyze the statistical decay process in multi-chance fission events. Current results indicate that the Gilbert and Cameron level density formalism, with slight modifications, is adequate to reproduce the gross features of the cross section data. Modifications necessary included reduction of shell effects on level densities for both the saddlepoint and neutron decay channels and introduction of an A dependent collective or "deformation energy" into the neutron decay process for even N nuclei. Results of the analysis provide quantitative measurements of the amount of first-, second- and third-chance fission present for the Neptunium nuclei $^{234}Np \rightarrow {}^{239}Np$ for an excitation energy range from 10 to 35 MeV as well as Γ_n/Γ_f ratios for these nuclei as functions of energy and previously measured effective fission thresholds for ^{253}Np through ^{236}Np. A paper based on these results is in the final stages of preparation.

b. Mass and Kinetic Energy Distributions

The mass and kinetic energy measurements have been extended through measurements of $^{233}U + p$ at 1 MeV intervals from 7 to 15 MeV. These studies will be continued to cover all of the Uranium isotopes for the proton energy range covered by the cross section data.

c. Cross Section Measurements

Additional fission fragment angular distributions have been measured for ^{233}U and ^{234}U to provide more detailed measurements of the angular anisotropy at lower energies. These measurements, extending from below second chance threshold to above third chance threshold, are designed to obtain more accurate information regarding angular momentum effects for proton use in analysis of the mass and kinetic energy measurements.

A portion of the experimental and analytical work described above is covered in detail in the Ph.D. dissertation of J. R. Boyce. The abstract follows:

---

* Oak Ridge National Laboratory, Oak Ridge, Tennessee.

"The Cyclo-Graaff facility at Triangle Universities Nuclear Laboratory located on the Duke University campus was used to measure proton induced total fission cross sections for the uranium isotopes ^{233}U, ^{234}U, ^{235}U, ^{236}U, and ^{238}U. The 90° differential cross sections were measured for the incident proton energy range $4.5 \leq E_p \leq 31.0$ MeV in 250 keV and smaller energy steps with a maximum beam-energy spread of 5 keV at 30 MeV. In addition over 100 fission fragment angular distributions were measured at angular intervals of 10° between 20° and 160° and were analyzed to determine fission fragment anisotropies as a function of excitation energy. The angular distribution results were combined with the 90° differential cross sections to obtain accurate proton induced total fission cross sections. Targets used were supplied by Oak Ridge National Laboratory and were of isotopic purity greater than 99%. Surface barrier fission fragment counters were used to detect fission fragments.

A method of analysis has been developed and demonstrated whereby first, second, and third chance fission contributions to the total yield are estimated. The method utilizes the optical model to describe the formation of the compound system and a statistical formalism to describe the de-excitation of the excited compound nucleus in either fission or neutron channels as the dominant decay mechanism. The analysis of cross section ratios for different isotopes clearly indicates that conventional optical models overestimate the proton total reaction cross section for incident proton energies below the Coulomb barrier. An empirically adjusted reaction cross section is therefore used for the compound nucleus formation cross section used in the calculations. The sensitivity of the analysis to various assumptions and model parameters is discussed.

The analysis of the measured cross section data results in the determination of previously unreported fission thresholds and the energy dependence of neutron to fission branching ratios, Γ_n/Γ_f, for all isotopes studied. The formulation is general enough to allow

"incorporation of refinements based on the current state of nuclear theory."

5. A Fermi Gas Model for Fission (H. W. Newson)

This model is now being refined and readied for publication.

6. Cross-Section and Polarization in (^{3}He,n) Reactions from ^{12}C and ^{13}C from 8 to 22 MeV (T. C. Rhea, R. A. Hardekopf,* P. W. Lisowski, J. M. Joyce,** R. Bass+, R. L. Walter)

All the cross-section and neutron measurements between 8 and 22 MeV have been completed for the ground-state neutron group from ^{12}C(^{3}He,n) and ^{13}C(^{3}He,n) now. Elastic-scattering cross-section and polarization data have been obtained for the ^{13}C(^{3}He,^{3}He) reaction at 20 MeV. The latter data have been fit with optical-model parameter sets. These parameters and the earlier ^{12}C(^{3}He,^{3}He) parameters obtained at our lab have been employed in DWBA calculations in attempts to explain the 18-22 MeV ^{12}C(^{3}He,n) and ^{13}C(^{3}He,n) data. The final calculations give a reasonable description for ^{12}C but a fit for ^{13}C could not be obtained.

7. Polarization Produced in The (d,n) Reactions on ^{9}Be and ^{11}B (J. Taylor,++ G. Spalek,‡+ Th. Stammbach,‡‡ R. L. Walter)

Before submitting these data for publication new DWBA calculations will be made using parameters recently obtained from optical-model searches on cross-section and polarization data for (d,d) reactions on light nuclei. This should clarify the situation on the lack of success of DWBA to explain the ^{9}Be(d,n_1) reactions for E_d = 3-4 MeV and ^{11}B(d,n_0) and ^{11}B(d,n_1) reactions for E_d = 7-12 MeV.

---

* Now at Los Alamos Scientific Laboratory, Los Alamos, New Mexico

** Now at East Carolina University, Greenville, North Carolina

\+ Now at Frankfurt University, Frankfurt, Germany

++ Now at Armed Forces Institute of Pathology, Washington, D. C.

‡+ Now at University of Wisconsin, Madison, Wisconsin

‡‡ Now at Schweiz. Inst. f. Nuklearphysik, Zurich, Switzerland

8. Polarization of Neutrons from the D(d,n) Reaction from 6 to 22 MeV (G. Spalek, R. A. Hardekopf, P. W. Lisowski, Th. Stammbach, J. M. Joyce, R. L. Walter)

Two papers describing the D(d,n) analysis have appeared in Nuclear Physics A191 (1972) 449, and A191 (1972) 460.

9. Neutron Scattering Studies Utilizing Polarized Neutrons Produced with Polarized Deuteron Beams (P. W. Lisowski, T. C. Rhea, C. E. Busch, T. B. Clegg, R. L. Walter)

Neutron beams having a polarization of $\sim$ 0.6 have been produced by initiating the $D(\vec{d},n)^3He$ reaction with vector- and tensor-polarized deuteron beams. The following progress has been made.

a. $^3He(n,n)$ Reaction

Polarization angular distributions have been obtained at 8, 12, and 17 MeV by scattering from a ^3He gas scintillator. A report on the data will be given at the Washington meeting of the American Physical Society.

b. $^4He(n,n)$ Reaction

Angular distributions of the asymmetry produced by scattering polarized neutrons from a ^4He gas scintillator have been obtained at 14 and 17 MeV. These data have been corrected for finite geometry effects and multiple scattering. An experimental investigation of the effect on the $^4He(n,n)$ asymmetry due to neutron scattering from the stainless steel scintillator walls showed the corresponding correction to be small. Comparisons to existing optical-model and phase-shift predictions are being made. A report on the data will be given at the Washington meeting of the American Physical Society.

10. Transfer Polarization Studies in $(\vec{p},\vec{n})$ Reactions (P. W. Lisowski, T. B. Clegg, R. L. Walter)

0° polarization-transfer coefficients have been deduced from measurements of the neutron polarization produced in the $^{11}B(\vec{p},\vec{n})$ and $^{13}C(\vec{p},\vec{n})$ reactions for proton energies from 8.5 to 15 MeV. Additional geometry corrections need to be calculated before final values are obtained, but preliminary results show that the transfer coefficients exhibit a strong energy dependence.

11. Polarization Transfer at 0° in the $D(\vec{d},\vec{n})$ Reaction (P. W. Lisowski, C. E. Busch, T. B. Clegg, R. L. Walter)

The $D(\vec{d},\vec{n})$ reaction at 0° is known to be a superior source of fast polarized neutrons. Knowledge of the neutron polarization depends on two quantities for a vector- and tensor-polarized incident beam. These quantities, the polarization-transfer coefficient and the 0° analyzing power, must therefore be accurately known if the $D(\vec{d},\vec{n})$ reaction at 0° is used as a neutron source. In this experiment the transfer coefficient was measured. The transfer for deuteron energies between 4.0 and 15.0 MeV in 0.5 steps. The analyzing power was measured from 2.0 to 15.5 MeV in 0.5 MeV steps. Geometry corrections to the data need to be calculated, but preliminary results indicate that both quantities have values nearly energy-independent over the range investigated.

12. Theoretical Investigation of Neutron Cross Section Measurements (M. Divadeenam, B.-H. Choi, W. P. Beres,* S. Ramavataram,** K. Ramavataram,** H. W. Newson)

a. Shell Model

(1) Even-Odd Compound Nuclei

An abstract based on ^{29}Si 2p-1h doorway calculations has been submitted to the American Physical Society Washington meeting (April 23-28, 1973).

A severely restricted 2p-1h basis was used for predicting $1/2^+$ doorways in ^{209}Pb. A doorway at 900 keV neutron energy was predicted with a very small escape width. These results were in complete disagreement with the experimental situation. In order to check the applicability of the 2p-1h model for ^{209}Pb, calculations are underway which make use of all the available neutron and proton single particle and holes states in the Pb region. When the lowest predicted $1/2^+$ state is normalized to $4S_{1/2}$ state in ^{209}Pb two $1/2^+$ doorways are predicted below 1 - 2 MeV neutron energy. Escape widths for these doorways will be calculated to compare with experiment. In addition calculations will be performed for p- and d-wave doorways.

---

* Now at Wayne State University, Detroit, Michigan

** Université Laval, Quebec, Canada

Considering the $3p_{1/2}$ neutron orbit to be a particle state for ^{206}Pb + n case a 2p-1h diagonalization will be performed for $1/2^+$. Such a calculation is expected to predict several s-wave doorways below 1 MeV neutron energy. These theoretical results will form a part of the comprehensive paper planned for Pb isotopes. See Section 2.

Further 2p-1h calculations for ^{41}Ca d-wave resonances are postponed until the high $E_n > 600$ keV energy ^{40}Ca + n data is analyzed for resonance parameters.

Since the last report no progress has been made on the $^{92,98}Mo$ isotope.

(2) Odd-Odd Compound Nuclei

Following an initial success of the application of a generalized R-Matrix theory incorporating the Feshbach doorway formalism for s-wave resonances in $^{90}Y(^{89}Y + n)$ compound nucleus, calculations are being extended to p-wave doorways. The Shell-Model code used previously was too restrictive in its application. As a first step the formalism is being generalized to handle any given J^{π} for calculating matrix elements and subsequent diagonalization procedure to predict doorway energies, reduced widths and cross sections.

b. Particle-Vibration Model

(1) Even-Odd Compound Nuclei

To understand the s-wave resonance structure observed in Ni isotopes the particle-vibration model seems to be appropriate. Particle-vibration doorways based on the collective octopole state and one of the f- or p-shell single particle states ($[3^- \otimes 1f_{5/2}]$) are too low in energy to be associated with continuum s-wave doorways. It is possible to construct states with configurations $[2^+ \otimes 2d_{5/2}]$ and $[2^+ \otimes 2d_{3/2}]$ which could lie in the low energy neutron region. The $2d_{3/2}$ and $2d_{5/2}$ neutron single particle states are generated with a real Woods-Saxon Well with spin-orbit force for $^{56,58,60,62,64}Ni$ isotopes. The predicted bound single particle states are at about the same negative neutron energy (but decreasing slightly with A) for all the Ni isotopes. In addition the used Woods-Saxon Well depth gets shallower as one goes from ^{56}Ni to ^{64}Ni. s- and d-wave Particle-Vibration doorway widths and reduced widths are calculated for resonances based on low lying 2^+ excited states in Ni isotopes. The ^{60}Ni + n doorway predictions are compared to experimental reduced widths and these will be discussed at the Spring Washington American Physical Society meeting. (See Section 2.)

The procedure outlined above could be extended to all even-even target nuclei in the f-p shell region.

In the case of the ^{41}Ca compound nucleus, shell model 2p-1h model cannot predict negative parity states, the only alternative being particle-vibration model or the 3p-1h excitations, which is very difficult to handle. Calculations for p-wave doorways are planned. The 1p-2 phonon model has been successfully applied to predict spreading widths Γ_d for $1/2^+$ ^{207}Pb and ^{209}Pb doorways below one MeV neutron energy. A short paper incorporating these calculations has been submitted to Physical Review. The abstract follows:

> "The nuclear spreading widths of the ^{207}Pb and ^{209}Pb $1/2^+$ doorway resonances are calculated in a particle-vibration model. The hallway states are of the particle-2 phonon type. The fine structure in ^{207}Pb is essentially due to the availability of many hallways (some with large matrix elements) and their proximity to the doorway. The ^{207}Pb and ^{209}Pb $1/2^+$ doorway spreading widths are found to be in line with the experimental situation."

A paper giving the predicted γ-ray widths for the ^{207}Pb $1/2^+$ doorway has been published in Physical Review C7, 862 (1973). The abstract follows:

> "Small admixtures of doorways $d'\rangle$ in with the dominant doorway $d\rangle$ are shown to account for the possibility of γ decay from the neutron fine structure associated with the doorway $d\rangle$. The example of low-lying $1/2^+$ resonances in ^{207}Pb is investigated via the particle-vibration model with the important doorway $d'\rangle$ for E1 γ decay found to be that based on the 1^- giant dipole resonance in ^{208}Pb."

(2) Even Mass Compound Nuclei

A paper based on the application of the weak coupling particle-vibration model to compound nuclei ^{208}Pb and ^{210}Bi has been submitted to Annals of Physics as a Part of our series on Intermediate Structure. The abstract

follows.

> "The weak coupling particle-vibration model is extended to low-lying neutron resonances in certain even-even or odd-odd nuclei by coupling the extra particle to core excited states of the odd mass target. The odd hole or particle in the target is treated as a passive spectator. ^{208}Pb and ^{210}Bi are studied as test cases and the calculated resonance quantities are in good general agreement with the average features of high resolution experiments. The resonances in ^{208}Pb and ^{210}Bi are related to the same intrinsic doorway in ^{209}Pb. The ^{210}Bi data is presented here for the first time."

This model will be extended to suitable cases: viz ^{15}N + n case.

c. Particle-Rotation Model

Nuclei in the s-d shell region are generally considered to be rotational in structure. The target nucleus ^{28}Si is considered as a test case to apply the Feshbach unified reaction theory to predict doorways and escape widths. Levels corresponding to both N = 2 and N = 3 oscillator shells are calculated in the framework of the Nilsson model. $1/2^-$ and $3/2^-$ states for N = 3 in the continuum region are associated with the observed p-wave doorway effects reported earlier. Escape widths for these resonant states and energy shifts are calculated making use of a surface peaked quadrupole interaction. An abstract based on these findings has been submitted to the forthcoming Washington American Physical Society meeting (April 23-28, 1973).

13. Computer Program MODSNOOP for Strength Functions And Single Particle Reduced Widths (B.-H. Choi, M. Divadeenam)

MODSNOOP will be suitably modified to input imaginary potential point by point as a function of distance. In addition, the program will be tested for calculating proton single particle widths.

14. Computer Program for Calculating Nucleon Resonance Scattering States And Widths for Even-Even Deformed Nuclei Within The Framework of Feshbach's Unified Reaction Theory (B.-H. Choi, M. Divadeenam)

The program generates band mixed states both in the bound and continuum regions making use of the Nilsson Model. In addition it evaluates nucleon escape widths, level shifts for resonant states. Effect of including channel coupling will be considered next.

15. Multilevel R-Matrix Computer Programs SEEK and INEL for Analyzing High Resolution Neutron Cross Sections (J. C. Clement, B.-H. Choi)

Two new interactive total neutron cross section R-matrix codes have been developed. They are SEEK and INEL. Both codes greatly enlarge cross section analysis capabilities of the previous R-Matrix code. Both codes use an energy dependent quadratic R^{∞} term for each partial wave up to F and a maximum of 100 resonances. Resonances outside the region being fit are automatically included in an energy dependent R^{∞} term by the code. An energy dependent resolution function allows analysis of both time-of-flight as well as monoenergetic neutron data. Provision has also been made for resolution function shapes other than gaussian. The first code, SEEK, will automatically minimize χ^2/point by varying the energy and width of each resonance along with R^{∞}. Such a χ^2 minimization usually reveals cases of spin misassignment at the same time the resonance parameters are optimized. The second code, INEL, will handle one inelastic channel in addition to the elastic one, without χ^2 minimization. Both codes have been optimized to run in a minimum amount of time.

B. CHARGED PARTICLE REACTIONS

1. Fine Structure of Isobaric Analogue States--Charged Particle Scattering (E. G. Bilpuch, G. E. Mitchell, H. W. Newson, D. Flynn, D. Outlaw, N. H. Prochnow,* W. N. Wilson, R. O. Nelson)

a. The Nickel Isotopes

The work on the nickel isosopes has been published for $1.8 < E_p < 3.3$ MeV. We are now planning to extend the elastic excitation function for ^{58}Ni up to 4.2 MeV using the high-resolution system developed for the 4 MeV Van de Graaff accelerator.

b. The Iron Isotopes

We have extended the elastic measurements of ^{54}Fe up to $E_p \simeq 4$ MeV using the high-resolution system on the 4 MeV Van de Graaff. About 64 levels were observed from 3.26 - 4.04 MeV. Analysis of these data is in progress. Further runs are planned on this isotope in the near future.

c. The Titanium Isotopes

A paper on the ^{48}Ti data has been published: "High-Resolution Proton Scattering from ^{48}Ti", Nuclear Physics A194, 353 (1972). A second paper on ^{46}Ti has also been published: "High Resolution Proton Scattering on ^{46}Ti", Nuclear Physics A199, 571 (1973).

The reaction $^{50}Ti(p,p)$ was also studied and the analysis of these data is complete. Approximately 200 resonances were analyzed and a paper is being prepared for publication.

d. Calcium Isotopes

Differential cross sections were measured in $^{42}Ca(p,p)^{42}Ca$ at 160°, 135°, 105°, and 90° from 1.2 - 3.0 MeV. The overall energy resolution was 325 - 400 eV. Spins, parities, partial widths, and total widths were extracted for 170 resonances. Two non-fragmented analogue states were identified. Identification of a third analogue state is tentative. Coulomb displacement energies and spectroscopic factors were determined for these analogue states. Differential cross sections were measured in $^{44}Ca(p,p)^{44}Ca$ at 160°, 135°, 105°, and 90° and in $^{44}Ca(p,p_1)^{44}Ca$ at 160°, 135°, and 105° from 1.6 - 3.0 MeV. Spins, parities, partial widths, and total widths were extracted for 429 resonances. Three highly-fragmented analogue states and two non-fragmented analogue states were identified. Coulomb displacement energies and spectroscopic factors were determined for each of these analogue states.

e. Silicon and Sulfur Isotopes

Analysis of the high-resolution elastic scattering study of ^{30}Si is nearing completion. Techniques have been developed for making good high-resolution CdS targets which will be used for a similar study of the ^{34}S elastic scattering excitation function in the very near future.

f. ^{92}Mo

A study has been made of the analogue of the first excited state of ^{93}Mo by means of high-resolution elastic proton scattering with the ^{92}Mo(p,p)^{92}Mo reaction. This study was made feasible by the success of the high-resolution neutral-beam feedback system on the FN Tandem accelerator. Beam energy resolution was typically 450 to 550 eV for the region from 5.13 to 5.43 MeV for which the elastic-scattering excitation function at 165°, 125°, and 90° was measured. The presence of the s-wave analogue in this region caused an enhancement of the background s-wave states near the analogue creating a "classic" example of the Robson fine-structure distribution due to a mixing of the strength of the analogue with the background states.

Since inelastic proton decay was too weak to be observed, the excitation function was analyzed in the single channel, multi-level case. Due to an observed level density of approximately one level per two keV in the vicinity of the analogue it was found necessary to include the effects of as many as 75 resonances in each calculation. A total of 126 $1/2^+$ resonances were observed and fit using our R-Matrix code. The fine-structure distribution of reduced widths versus energy was fit yielding a resonance energy of 5.245 MeV and a spreading width of $\sim$ 15 keV. A paper is now being prepared for publication.

g. Analysis of Fine-Structure Distributions

An analysis of the analogue state fine-structure distributions measured in this laboratory is in progress. In the case of strong mixing of the analogue with the background resonances (spreading width $\gg$ level spacing) the entire distribution can be fitted to

$$S(E) = S_o \frac{(E-E_x - \Delta)^2 + \omega^2/4}{(E-E_x)^2 + \Gamma^2/4} ,$$

when S(E) is the strength function γ^2/D, three analogues have been well fit to this form, (^{40}Ar $3/2^-$, ^{44}Ca $1/2^-$, and ^{92}Mo $1/2^+$), yielding parameters S_o, D, ω, and ω_o. The fit parameters in each case satisfy a consistency relation due to Lane.[1]

In the case of weak or intermediate mixing $\omega_o \lesssim D$, the above equation applies only in the wings of the distribution, and an automatic parameter search does not yield reliable estimates of the parameters of the distribution. Some of these parameters (ω_o,Δ) can in many cases be estimated directly from the data. Most of the analogues seen in the mass region A = 50 - 65 are examples of weak mixing, with $\omega_o \leq 10$ keV.

[1] Isospin in Nuclear Physics, ed. D. H. Wilkinson, North Holland Publishing Co., Amsterdam, 1969.

2. Fine Structure of Analogue States--The Capture Reaction (G. E. Mitchell, E. G. Bilpuch, T. Dittrich, W. C. Peters, D. Vaughn, J. F. Wimpey)

a. ^{58}Fe

A letter entitled "Multi-Channel Study of Fine Structure of an Analogue State in ^{59}Co" has been published: Physics Letters 24B, 422 (1972). The abstract follows:

> "The fine structure of the analogue of the ground state of ^{59}Fe has been studied by the $^{58}Fe(p,p)$, (p,p') and (p,γ) reactions. The fine-structure widths for these three channels are correlated. Evidence for correlations in the decay of fragmented analogue states in the 1f-2p shell is summarized and interpreted."

b. ^{54}Cr

A paper entitled "Multi-Channel Study of Fine Structure of an Analogue State in Mn^{55}" has been accepted for publication in Nuclear Physics. The abstract follows:

> "The $^{54}Cr(p,p)$, $(p,p_1\gamma)$ and (p,γ) reactions were studied in the vicinity of the fragmented analogue of the ground state of ^{55}Cr. The overall proton energy resolution was about 350 eV. γ-rays were detected with both NaI(Tℓ) and Ge(Li) detectors. Elastic and inelastic proton widths and partial and total γ-ray widths were measured for each of the eight fine structure states of the analogue. The analogue to antianalogue strength was small. The width for the ground state transition was 1.4 eV, while the width estimated from the strength of the β decay of the parent state is 0.4 eV. Correlations were observed between the fine structure widths in the p,p_1 and γ_0 channels, indicating that the analogue is a common doorway for these channels. Strong correlations were also observed among other γ-ray channels."

c. ^{62}Ni

The $p_{3/2}$ fragmented analogue state at E_p = 2.65 MeV has been studied in some detail. Strong correlations were observed between partial widths in some of the channels. Analysis of these data is nearing completion.

A paper entitled "Electromagnetic Decay of Fragmented Analogue States" has been presented at the International Conference for Photonuclear Reactions in Asilomar, California. This paper discussed our results on ^{54}Cr, ^{58}Fe and ^{62}Ni and will be published in the proceedings of that conference.

d. ^{44}Ca

An excitation function for $^{44}Ca(p,\gamma)$ was measured using a 4" x 4" NaI(Tl) detector. The overall proton resolution was 350 - 400 eV for this experiment. More than 350 resonances were seen in the (p,γ) reaction from E_p = 1.56 to 2.28 MeV. The data are being analyzed to determine level densities. Further studies of the fragmented analogue states in this energy region are planned using an 80 cc GeLi to study the details of the γ-ray decay.

e. Electromagnetic Transition Strengths--Non-Analog Resonances

The γ-ray decay of a number of $s_{1/2}$ resonances observed in $^{58}Fe(p,p)$ and $^{62}Ni(p,p)$ were studied to compare with the behavior of the γ-ray decay of analogue states in these nuclei. Information was also obtained on electromagnetic transition strengths. In ^{59}Co about 30 E1 transitions were measured (average strength $\sim 10^{-4}$ W.u.); in ^{63}Cu about 50 E1 transitions were measured (average strength about 10^{-4} W.u.). These nuclei are also favorable cases for study of higher multipole transitions, since there are a number of low-lying f states. Preliminary results indicate the presence of some E3 and M2 transitions.

3. Statistical Properties of Nuclei from Proton Resonance Reactions (E. G. Bilpuch, G. E. Mitchell, H. W. Newson, J. D. Moses, W. M. Wilson)

The statistical properties of the resonances observed in $^{42}Ca(p,p)$ and $^{44}Ca(p,p)$ were investigated for both sets of data, and in particular, an attempt was made to determine the number of missed or misassigned levels in a single sequence of levels. The nearest-neighbor spacing distributions indicate that levels are more often misassigned than missed. For example, the superposed spacing distribution of the $3/2^+$ and $5/2^+$ levels in $^{44}Ca(p,p)^{44}Ca$ shows fewer levels missed (when compared with theory) than either of the single-sequence distributions. The number of missed or misassigned levels in a single sequence proved (in every case)

to be too large to be predicted exactly by the sensitive Dyson F-statistic. The F-test cannot be applied to a superposed sequence. The F-test does, however, qualitatively substantiate the conclusions obtained from the spacing distributions. Notably, the F-statistics for the $1/2^-$ levels in $^{44}Ca(p,p)^{44}Ca$ indicate that the sequence has very few missed or misassigned levels.

The number of missed levels was estimated for each sequence by comparing the reduced width distributions with the Porter-Thomas distribution. The corrected number of levels for the $1/2^-$ and $1/2^+$ sequences compared favorably with the theoretical level densities. The $3/2^-$ and $3/2^+$ densities were too small in every case.

4. Studies of The Gamma Decay of Excited Levels of ^{51}Ti (G. P. Lamaze,* C. R. Gould, N. R. Roberson, D. R. Tilley)

Preparation of a paper on this subject, based on the Ph.D. dissertation of G. P. Lamaze, is in progress.

5. Gamma Decay of Excited Levels of ^{38}Ca (E. C. Hagen, N. R. Roberson, C. R. Gould, D. R. Tilley)

Additional measurements on ^{38}Ca by means of $^{36}A(\tau,n\gamma)$ utilizing an implanted target and a gas cell are planned. A precision-pulser gain-stabilization system is being developed for these experiments.

6. Lifetime Measurements of Excited Levels in ^{39}Ca (W. Kessel, E. C. Hagen, N. R. Roberson, R. Bass, C. R. Gould, D. R. Tilley)

A preliminary report on this work was presented at a meeting in Heidleberg by W. Kessel. The abstract is reproduced below:

> "Über die Reaktion $^{36}Ar(\alpha,n)^{39}Ca$ wurden mit dem Tandem-Beschleuniger der Duke University bei Einschussenergien von 15,8 und 17,0 MeV Niveaus in ^{39}Ca angeregt, und ihr γ-Zerfall in Koinzidenz mit Neutronen nachgewiesen. Mit der Dopplerverschiebungsmethode (DSAM) und der Abbremsung der Rückstosskerne im Targetgas wurden die Lebensdauern der Zustände bei 2,80 und 3,64 MeV gemessen. Die konkurrierende

* Now at National Bureau of Standards, Gaithersburg, Maryland.

Reaktion $^{36}Ar(\alpha,p)^{39}K$ wurde bei der Analyse der Messdaten zur Eichung mitverwendet. Dabei konnten die Lebensdauern zweier weiterer langlebiger Zustände in ^{39}K (3,94 und 5,16 MeV) bestimmt werden. Die errechneten Übergangsstärken der Spiegelkerne werden mit Modellaus-sagen verglichen und diskutiert."

More recently a D.S.A.M. measurement on the 3.639 MeV $(9/2^-) \rightarrow$ 2.796 MeV $(7/2^-)$ transition was made. The result was $F(\tau) = (86 \pm 3)\%$ corresponding to a mean life of $\tau = 22.8$ picoseconds for the 2.796 MeV level.

7. The Application of Polarized Deuterons in (d,pγ) Angular Correlation Measurements (C. R. Gould, R. O. Nelson, J. R. Williams, D. R. Tilley, J. D. Hutton, N. R. Roberson, C. E. Busch, T. B. Clegg)

The application and use of tensor polarized beams of deuterons in (d,pγ) angular correlation experiments with spin zero targets has been investigated in connection with the measurement of mixing ratios of decays from spin 3/2 states in ^{13}C and ^{31}Si. By combining angular correlation data at two different values of the incident beam polarization,[1] the results can be analyzed without involving any unknown population parameter in the fitting procedure. The work has been published in Physical Review Letters 30 (1973) 298.

8. Lifetimes of Levels in ^{26}Al (C. R. Gould, D. R. Tilley, N. R. Roberson)

This work has been published in Phys. Rev. C7, 1068 (1973).

9. A Study of Low-Lying Levels in ^{59}Ni (J. D. Hutton, N. R. Roberson, C. R. Gould, D. R. Tilley)

Electromagnetic transition strengths for decays between low-lying levels in ^{59}Ni have been studied with the $^{56}Fe(\alpha,n)^{59}Ni$ reaction. Mean lifetimes of levels have been measured by the Doppler shift attenuation method and the recoil distance method. Level spins, mixing ratios and branching ratios have been investigated with the method of particle-γ-ray angular correlations. The following lifetimes are reported (level energy in keV, lifetime in ps): 340(120 ± 20), 465(29 ± 5), 878(0.62 ± 0.12), 1189(0.44 ± 0.07), 1302(0.18 ± 0.02), 1339(1.28 ± 0.46), 1680(0.42 ± 0.23), 1735(0.18 ± 0.04), 1948(0.20 ± 0.06). Elec-

[1] J. D. McCullen and R. G. Seyler, Nucl. Phys. A139, 203 (1969).

tromagnetic transition strengths are extracted and compared with two recent shell-model calculations. This work has been accepted for publication in Nuclear Physics.

10. The Decay Properties of Low Lying Levels of ^{53}Fe (R. O. Nelson, N. R. Roberson, C. R. Gould, D. R. Tilley)

A paper entitled "Study of Low-Lying Levels of ^{53}Fe" has been submitted for publication in Nuclear Physics. The abstract is given below:

> "Spins, parities, spectroscopic factors and decay properties were examined for 11 states of ^{53}Fe. Angular distributions were measured for the ^{54}Fe(p,d)^{53}Fe reaction at 29 MeV to determine ℓ-values and spectroscopic factors. The ^{50}Cr(α,nγ)^{53}Fe reaction was used to determine spins, mixing ratios and lifetimes. The combined results allow J^{π} assignments of $3/2^-$, $5/2^-$, $7/2^-$ and $3/2^-$ for levels at 741, 1423, 1696 and 2043 keV, respectively. Spectroscopic amplitudes and γ-ray transition rates for low-lying $7/2^-$, $9/2^-$ and $11/2^-$ states are compared with the predictions of $(f7/2)^{-3}$ shell-model calculations."

11. The Polarization of ^{3}He Particles Scattered from ^{27}Al and ^{28}Si (E. J. Ludwig, T. B. Clegg, R. L. Walter)

A paper describing this work has been submitted to Nuclear Physics.

12. Elastic Deuteron Scattering at 15 MeV (C. E. Busch, T. B. Clegg, S. Datta, E. J. Ludwig)

In addition to the cross-section and polarization angular distributions for vector polarized deuterons on ^{10}B, ^{13}C and ^{14}N reported in the last USNDC Report, similar data have been obtained for ^{12}C and ^{16}O targets. Optical-model analyses for all the targets have been completed and parameters extracted that vary in a regular manner between the various target nuclei. The work is being submitted to Nuclear Physics for publication.

13. Polarization Transfer in The D($\vec{d}$,$\vec{p}$)T Reaction at $\theta = 0°$ (T. B. Clegg, with R. A. Hardekopf, D. D. Armstrong, and P. W. Keaton, Jr., Los Alamos Scientific Laboratory)

The analysis of these data is complete and a paper has been prepared to be submitted to Physical Review. A report of this work was also made at the

Seattle American Physical Society meeting.

14. The $^{54}Fe(p,d)^{53}Fe$ Reaction (R. O. Nelson, N. R. Roberson)

A paper entitled "Evidence for Two-Step Processes in Reactions with Spherical Nuclei" has been accepted for publication in Physics Letters. The abstract is given below.

> "Experimental evidence for two-step processes in reactions with spherical nuclei is obtained from a study of $^{54}Fe(p,d)^{53}Fe$ angular distributions for low-lying $9/2^-$ and $11/2^-$ states. Predictions of the coupled-channel Born approximation give excellent agreement with the data."

15. Inelastic Effects in The Study of ^{23}Na and ^{23}Mg (R. O. Nelson, N. R. Roberson)

A paper entitled "Inelastic Effects in The Study of ^{23}Na and ^{23}Mg" has been published in The Physical Review C6 (1973) 2153.

16. Inelastic Deuteron Scattering from ^{28}Si and ^{30}Si (R. A. Hilko, R. O. Nelson, T. G. Dzubay, N. R. Roberson)

Inelastic deuteron data on ^{30}Si have been collected from 20° to 150° in the laboratory with a 23.0 MeV deuteron beam. The ^{28}Si data is best fit by the rotator-vibrator model, but for ^{30}Si the analysis slightly favors a vibrational picture over a rotational one. Coupled-channel analysis is continuing.

17. The (d,t) and (d,^{3}He) Reaction on ^{28}Si and ^{30}Si (R. A. Hilko, R. O. Nelson, C. R. Gould, N. R. Roberson)

Triton and Helion spectra were taken from 15° to 95° in the laboratory with enriched targets. Coupled-channel Born-approximation calculations have been performed for ^{29}Si and ^{29}Al with some success in testing a recent shell model calculation. Currently a bandmixing calculation is being performed to secure direct and indirect amplitudes to test this approach. A contributed paper on this work is being presented at the April American Physical Society meeting in Washington.

18. Search for The Lowest T = 3/2 Level in ^{41}Sc (T. A. Trainor, T. B. Clegg, W. J. Thompson)

The current assignment for the lowest T = 3/2 level in ^{41}Sc is an $\ell = 2$, $\Gamma = 2.5$ keV resonance seen in $^{40}Ca(p,p)^{40}Ca$ elastic scattering at $E_p = 4.899$ MeV ($E_x = 5.865$ MeV). Polarization excitation curves over this resonance indicate that it has spin J = 5/2, in disagreement with spin J = 3/2 for the parent ^{41}K(g·s). A recent β^+-delayed proton experiment in the A = 41 isobar indicates that the lowest T = 3/2 level in ^{41}Sc should lie at $E_x = 5.935$ MeV. Both of these results indicate that a reassignment of the lowest T = 3/2 level is in order.

High resolution and polarization excitation curve data were taken in the neighborhood of the energy suggested by the β^+-delayed proton experiment. A previously unobserved, narrow resonance was seen at $E_p = 4.978 \pm .005$ MeV ($E_x = 5.941$ MeV) with spin J = 3/2 and $\Gamma_p \sim \Gamma = 100$ eV. The resonance is isolated and appears to be an excellent candidate for the lowest T = 3/2 assignment.

The reduction of the total width by a factor of 25 for the lowest T = 3/2 level has considerable significance with regard to the systematics of isospin impurities in 4n + 1 nuclei. The relocation of the level by some 70 keV will require an adjustment of the coefficients in the isobaric mass equation for the A = 41 isobar.

19. $^{208}Pb(p,p')$, $^{208}Pb(p,d)$ and $^{208}Pb(p,t)$ Reactions from 16.7 to 27.3 MeV (E. J. Ludwig, P. Nettles, C. Busch, E. Klema)

Analysis of these data is continuing.

20. Isobaric Analog Resonances in ^{71}Ga (P. G. Ikossi, C. E. Busch, T. B. Clegg, E. J. Ludwig, W. J. Thompson)

Isobaric analog resonances in ^{71}Ga have been investigated by the reaction $^{70}Zn(\vec{p},p)^{70}Zn$. Two angular distributions at 3.56 and 3.94 MeV, differential cross-section excitation functions at 90°, 155° and polarization excitation functions at 115°, 155° from 3.66 to 4.90 MeV have been analyzed by the computer code ANSPEC. The results of this analysis were presented at the Southeastern Section meeting of the American Physical Society in Birmingham. In summary these results are:

J^π	E_p(MeV)	E_x(MeV)	σ(keV)	σ_p(keV)	S
$1/2^-$	3.723	22	4.2	.30± .03	0.000
$3/2^-$	4.407	23	1.8	.04± .01	0.684
$5/2^+$	4.586	14	1.3	.10± .02	0.863

Two more angular distributions were taken at 9.0 and 2.5 MeV. The differential cross section and polarization excitation functions were extended at 90° and 130° from 4.7 to 6.4 MeV and at 115° and 155° up to 5.6 MeV. Several resonances* corresponding to excitation energies in ^{71}Ga up to 2.18 MeV have been observed and are now being analyzed to extract resonance parameters and spectroscopic factors. Characteristic X-rays from proton bombardment of the target were taken to identify contaminants in the target.

21. Study of Isospin-Dependence in (d,t), (d,^{3}He) Transfer Reactions and Investigation of WBP Model As Applied to (d,d) Elastic Scattering and (d,t) or (d,^{3}He) Reactions (S. Datta, C. E. Busch, E. Ludwig, T. B. Clegg, W. J. Thompson)

The reactions ^{30}Si(d,t)^{29}Si, ^{30}Si(d,^{3}He)Al have been studied with a polarized beam of deuterons at an energy of 15 MeV. The cross-sections and the vector analyzing powers in the reactions have been measured within the angular range 25° to 90°. Comparison of these quantities in the (d,t) and (d,^{3}He) reaction (along with the comparison of similar quantities obtained in our past experiments on ^{10}B, ^{14}N and ^{32}S) forms the basis of our study in the isospin dependence in nuclear transfer reaction. During the last six months additional ^{10}B(d,t) data have been taken in the same angular range with polarized deuterons at 15 MeV.

The ^{30}Si(d,d)^{30}Si elastic scattering reaction has been studied with polarized deuterons of the same energy over the same range of angles. The comparison of the product of cross-section and the vector analyzing power in the elastic scattering and the $\ell = 0$ transfer reactions leads to an extension of the WBP (Weakly-Bound-Projectile) model for the description of (d,t) reactions. The ^{14}N(d,t$_1$)^{13}N* ($\ell = 0$ transfer) and ^{14}N(d,d)^{14}N reactions have also been studied under the same conditions and the results conform to our proposed extension of the model.

Vector analyzing powers have been measured for $\ell = 1$ transfers ($J^\pi = 3/2^-$ or $1/2^-$) occuring with targets of ^{10}B, ^{13}C, ^{14}N and ^{16}O are bombarded by 15 MeV vector polarized deuterons. The analyzing power distributions for $J^\pi = 1/2^-$ transfers were inverted from those for $J^\pi = 3/2^-$ transfers over the forward angular region when the Q-values for the reactions were similar. Calculations made with DWBA code DWUCK could predict the shift in angle between the distributions when the Q values were markedly different. A J-dependence for $\ell = 1$ transfers can therefore be inferred from our analyses of pickup reactions on 1-p shell nuclei.

---

* G. P. Couchel et al., Phys. Rev. 161 (1969) 1142.

22. Compound Elastic Scattering Experiments (R. J. Eastgate, R. Haglund, W. J. Thompson, T. B. Clegg)

Experiments are planned to investigate compound nuclear effects, especially for vector and tensor polarized deuterons on 4n nuclei.

Some preliminary studies of the excitation function for $^{32}S(\vec{d},d)^{32}S$ at $\sim$ 5 MeV and $\sim$ 8 MeV using an H_2S gas target have been made. The target must be thick ($\gtrsim$ 0.5 MeV) enough to average over compound nuclear fluctuations; to this end a new gas cell has been designed. A C.P.S. program GASSY, key RJEE, resident in the TUCC CPS Library UNCP2, has been written to calculate gas cell geometric effects, yields, cross sections, kinematic effects and energy losses (using a corrected version of the program ELOSS).

23. Cross-Section and Polarization Produced in The $^{13}C(^3He,^3He)$Reaction (T. C. Rhea, R. L. Walter, E. J. Ludwig)

Elastic scattering cross-section and polarization data for the $^{13}C(^3He,^3He)$ reaction has been obtained at 20 MeV in order to obtain optical model parameters to utilize in the DWBA calculations for our $^{13}C(^3He,n)$ study. The polarization data differed from that for ^{12}C at the larger angles $\theta > 50°$ and optical model fitting was not as successful as for $^{12}C(^3He,^3He)$ obtained earlier at our lab. The ^3He spin-orbit depth was not well-determined because the fits were poor.

24. Polarization Produced in D(d,p) Reaction and Comparison to the D(d,n) Reaction (R. A. Hardekopf, P. W. Lisowski, T. C. Rhea, R. L. Walter, T. B. Clegg)

Studies of the $D(d,\vec{p})$ reaction were performed by measuring the asymmetry produced in the inverse reaction $^3H(\vec{p},d)$. This work has appeared in Nuclear Physics A191 (1972) 468. Comparison to the $D(d,\vec{n})$ polarization is also given here.

25. Analyzing Power in The Elastic Scattering of Protons from Tritium (R. A. Hardekopf, P. W. Lisowski, T. C. Rhea, R. L. Walter, T. B. Clegg)

The analysing power of $^3H(\vec{p},p)$ elastic scattering reaction from 7 to 15 MeV and a phase shift analysis have been reported in Nuclear Physics A191 (1972) 481.

26. Capture Gamma Ray Studies (S. M. Shafroth, T. A. White)

There has been no progress on this work since the last report.

27. X-Ray Studies (A. B. Baskin, G. A. Bissinger,* C. E. Busch, P. H. Nettles,** J. T. May, A. W. Waltner, S. M. Shafroth, T. A. White+)

a. Ag K and L and Au L x-rays Produced by 12-50 MeV ^{16}O Ion Bombardment

This work has now been published in the proceedings of the International Conference on Inner Shell Ionization Phenomena, Atlanta, April 17-21, 1972. (Appendix II) Additional theoretical work is being done and it is being prepared for journal publication.

b. Yields of K and L x-rays Produced by 2-30 MeV Proton Bombardment of Ag

This work has now been published in the International Conference on Inner Shell Ionization Phenomena, Atlanta, April 17-21, 1972.

c. Relativistic Effects in Au L x-ray Production by 0.5-3.0 MeV Protons

This work has now been published in the proceedings of the International Conference on Inner Shell Ionization Phenomena, Atlanta, April 17-21, 1972.

d. Au L x-ray Production by 0.5-30 MeV Protons

This work has been published in Phys. Rev. A7, (1973) 566.

e. Au K X-rays Excited by Protons (2-14 MeV) and $^{16}O^{+}$ Ions (18-42 MeV)

This work was reported orally at the Birmingham meeting of the Southeastern Section of the American Physical Society in November 1972 (Appen-

* Present address: Rutgers University
** Present address: Scientific Atlanta
\+ Summer visitor from Furman University, Greenville, S. C.

dix III) and is being prepared for publication. Ratios of $K\alpha_2/K\alpha_1$ peaks as well as $K\beta_1/K\alpha_1$ and $K\beta_2/K\alpha_1$ vs incident projectile energy were determined using a Ge(Li) detector. The $K\alpha_2/K\alpha_1$ ratio is independent of projectile energy and charge and is 0.59 in good agreement with the value 0.59 obtained with photon excitation compiled by Nelson, Saunders and Salem.

f. The L and M-x-rays Yields of L and M x-rays arising from proton bombardment of Bi and U from E_p = 0.5 - 15 MeV and 2 - 15 MeV respectively were reported on at the New York American Physical Society meeting January 1973. (Appendix III) The uranium spectra were especially interesting because the $L\beta$ peak was aplit into $L\beta_{2,15}$ and $L\beta_{1,3,5}$ and the ratio of these peaks depended markedly on how the L shell was excited, i.e., for 3 MeV proton bombardment it was 0.74 while for 22 keV photon bombardment it was 0.41 and when excited by α decay of ^{238}Pu it was 0.21. Data have been taken for L and M x-ray yields for Hg from E_p = 2 - 14 MeV and are being analyzed.

g. Pb L and M x-rays

A paper entitled "Study of the L and M- Shell x-rays of Pb Produced by 0.5-14.0 MeV Proton Beams", C. E. Busch, A. B. Baskin, P. H. Nettles, S. M. Shafroth and A. W. Waltner, is scheduled for publication in the May issue of Phys. Rev. A. The abstract of this paper follows:

> "The L and M x-rays of Pb were observed with a Si(Li) detector of 190-eV resolution for a 6-keV x-ray line. Absolute shell-ionization cross sections were derived and compared to P.W.B.A. and B.E.A. predictions. The agreement between theory and experiment was generally good for both cross sections and x-ray ratio predictions. For proton energies less than 3 MeV the $L\alpha/L\beta$ and $L\alpha/L\gamma$ ratios display deviations that are qualitatively predicted by both theories but only absolutely reproduced by the P.W.B.A. result for $L\alpha/L\beta$. The $L\alpha/L\ell$ ratio exhibits a minimum in the proton energy range 0.5-3.0 MeV that is not predicted by a single ionization state process."

h. Ratios of L Subshell Cross Sections

This work has constituted the M.S. thesis of Mr. A. B. Baskin. It was reported on at the New York American Physical Society meeting (Appendix III).

A journal article is nearing completion. The abstract of Mr. Baskin's thesis follows:

> "The basic considerations of the study of proton induced L shell x-rays with a Si(Li) detector are reviewed. Ionization cross section ratios for the L subshells are extracted from experimentally measured pulse-height spectra of lead and bismuth for the first time. A computer program has been written which is capable of fitting up to four gaussians and a linear background to a region of data such as the $L\gamma$ structure. A pronounced maximum in the $\sigma_{L_2}/\sigma_{L_1}$ ratio is found at a proton energy of 2.0 MeV in agreement with PWBA theory and in disagreement with BEA theory. Total x-ray production cross sections and ratios of peak intensities are compared to both PWBA and BEA. Observed energy shifts of major lines are explained and compared to theory.

28. Tests of The Suitability of a 3 MeV Proton Beam for Trace Element Studies (R. L. Walter, R. D. Willis, W. Gutknecht, C. Lochmuller, J. M. Joyce)

Progress has been made in developing, calibrating, and optimizing an energy-dispersive system for proton-induced X-ray emission studies. A wide range of targets have been irradiated and comparison of various methods for elemental analyses in the parts per thousand to the parts per billion is underway. Major support for this work will come from the Environmental Protection Agency. Papers related to the work, which was initiated only ten months ago, have been delivered at the Fittsburgh Symposium on Analytical Chemistry and Applied Spectroscopy, Southeastern Regional Meeting of the American Chemical Society at Birmingham, Workshop on X-Ray Fluorescence Analysis at Seattle, and Symposium on Heavy Metals in the Environment at Research Triangle Park, N. C. A paper has appeared in Analysis Letters and one is underway for Analytical Chemistry.

C. DEVELOPMENT

1. Accelerator Improvements (F. O. Purser, J. R. Boyce, H. W. Newson, E. G. Bilpuch, R. L. Rummel, M. T. Smith, J. D. Moses, D. E. Epperson, G. E. Mitchell, R. O. Nelson)

a. Tandem Accelerator

The tandem has run routinely during the current report period. No major additions or alterations have been made.

b. Injector Cyclotron

A water leak in the cooling manifold of the lower magnet coil precipitated intermittent spark breakdown of the lower coil to ground. The cyclotron and coil have been disassembled and a new cooling manifold ordered from the Cyclotron Corporation. Damage to the coil has been repaired and, on receipt of the new cooling manifold, the accelerator will be reassembled with one improvement. A remotely adjustable magnetic channel is being designed and will be installed to allow small adjustments in steering of extracted beams without loss of beam intensity or quality.

c. Improved Beam Energy Resolution for The Tandem Accelerator

New measurements of attainable resolution with the neutral beam homogenizer used in conjunction with the direct extraction source indicate an attainable experimental energy resolution of 400 eV at 5 MeV. The high resolution system is in routine operation and a paper on the fine structure of the analogue resonance in ^{90}Mo at 5.2 MeV is being prepared.

2. Pulsed Beams (F. O. Purser, H. W. Newson, N. R. Roberson, R. O. Nelson, T. B. Clegg, D. E. Epperson, R. A. Hilko, J. Clement)

a. Mass Identification of Charged Particles by Time-of-Flight

This program has been inactive for this report period.

b. Neutron Time-of-Flight Program

A large neutron spectrometer and pulser-buncher system is being acquired from the Air Force for installation on our tandem. The pulser-buncher will be used with our direct extraction source to allow pulsed beam experiments at par-

ticle energies below the Cyclo-Graaff energy range ($16 < E_p < 32$ MeV). Beam transport studies are underway to determine optimal location of the pulser-buncher system so that it will provide a significant increase in the capability of our polarized ion source as well as allow implementation of our planned neutron time-of-flight program.

The neutron spectrometer will completely occupy target area 5, a 40' x 40' experimental area served by our double 90° magnetic analyzing system. Normal time-of-flight paths of 4 meters are possible with a reaction angular range of 270°. Extended flight paths will be possible at selected angles. As planned the neutron spectrometer area will provide a capability for measuring elastic and inelastic angular distributions, (n,n'γ) correlations, (p,n) and (p,xn) production cross sections, and other neutron-induced reactions for a wide range of neutron energies. The program should be underway by the end of the summer.

3. Polarized Source Improvements (T. B. Clegg, T. A. Trainor, C. E. Busch, P. W. Lisowski)

The TUNL Lamb-shift polarized source has continued to be used extensively within the last six months. Experiments requiring use of the source have used between 30 and 50% of the scheduled tandem accelerator time and have involved nearly half of the staff of the laboratory. The polarized ion source performance has been quite reliable with one period of eight days of continuous operation completed without difficulty. Polarized beam intensities are approximately the same for protons and deuterons and have been very reproduceable during the period. Beams of 70 μA have been obtained through the accelerator on several occasions for periods of several days. Beam polarizations are typically 75-80% of the theoretical maximum for deuterons, and 85-90% to the theoretical maximum for protons.

Significant contributions to and improvements in the polarized source operation in the last six months are as follows:

1) The addition of hardware to allow remote control of both transverse and longitudinal positioning of the extraction electrode for the duoplasmatron has improved the magnitude and reproduceability of the beam currents.

2) A thorough investigation has been made of the "quench ratio" technique for measuring beam polarizations and has shown that proton polarizations can be determined to within ± 1% and deuteron polarizations to within ± 2% at this time using this method.

3) A new power supply for the first spin rotation solenoid has much better current regulation than the one previously used. This allows experimental determination of the angle through which the spin axis is precessed to within ± 1 degree.

4. Hardware and Software for Tensor Polarization Experiments (R. F. Haglund, Jr., T. B. Clegg)

The scattering chamber rotation system described in the previous report is now approximately 60% complete. The mounting ring for the photodiode position sensors has been installed, and the switching logic and other control circuitry will be ready for installation and testing in May.

A method of data-taking for tensor polarization experiments has been chosen, and a data-acquisition program for the Honeywell DDP-224 on-line computer has been written and tested. At present, the program can handle only deuteron elastic and inelastic scattering. However, with the recent increase in the core storage size of the DDP-224, it will be possible to include a particle identification routine in the program, thus greatly enhancing its usefulness.

5. High Intensity Duoplasmatron for a Polarized Ion Source (T. B. Trainor, T. B. Clegg)

The high intensity, multiaperture duoplasmatron was operated for a brief period on the polarized source. Although arc current was limited to half the rated value for the high intensity ion source, beam currents of 1-2 μA were observed at the low energy end of the tandem. This beam was considered to be unusable because of low (10-20%) beam polarization. It was felt that the poor polarization was due to a large emittance of the beam extracted from the duoplasmatron which made it impossible to separate electrostatically the unpolarized double charge exchange component from the metastable component in the spin filter.

Efforts were made to discover the source of the emittance problem. Photographs were made of the extraction section while the extraction voltage was varied. The behavior of the beam plasma under these conditions indicated a strong non-uniformity in the plasma current density as a function of radius across the expansion cup. It is clear from the Child-Langmuir-Schottky law that a non-uniformity of this sort can produce severe divergence problems. A report on this work has been made at the meeting of the Southeastern Section of the American Physical Society.

As a result of these observations it was decided to convert the ion

source to a single aperture geometry. Work is currently underway to complete this conversion.

6. New γ-ray Scattering Chamber (F. Wimpey, D. Outlaw, T. Dittrich, G. E. Mitchell, E. G. Bilpuch)

The new γ-ray scattering chamber for the 3 MeV Van de Graaff accelerator was installed and aligned in March, 1973. Accessory equipment to the chamber includes beam collimator, vacuum system, Ge(Li) support table (permitting target centered Ge(Li) detector rotation), chamber support, and a freon cooling system. With the freon cooled baffle operating, and LN_2 in the chamber cold trap, the vacuum system achieved a vacuum of 5×10^{-7} mmHg, after about two hours pumping time. The chamber is gold plated on its inner walls to reduce background radiation. A cold finger from the liquid nitrogen trap, placed coaxial to the target rod, improves the chamber vacuum and therefore should extend target exposure life.

7. Design of a Lamb-Shift Polarized Source for Tritons (T. B. Clegg, with R. A. Hardekopf and J. L. McKibben, Los Alamos Scientific Laboratory)

This work is continuing at Los Alamos, with actual construction of some components now in progress. An abstract describing this work has been submitted for the Washington American Physical Society meeting.

8. Gamma Ray Polarimeter (J. R. Williams, C. R. Gould, R. O. Nelson, D. R. Tilley)

A five-crystal NaI polarimeter similar to that of Taras and Matas* has been assembled. Calibration tests utilizing inelastic-scattering γ-rays of known linear polarization are underway.

9. Development of a High Resolution System for The 4 MeV Van de Graaff Accelerator (D. Flynn, F. O. Purser, E. G. Bilpuch, H. W. Newson, G. E. Mitchell, L. W. Seagondollar)

This program has been inactive for this report period.

---

* P. Taras and J. Matas, Can. J. Phys. 47 (1969) 1605.

10. Program to Calculate The Energy Loss of Charged Particles in Matter (P. G. Ikossi, W. J. Thompson)

The program BABEL calculates the energy loss of a charged particle in a target consisting of up to 3 layers, each layer being a compound consisting of up to 10 components. The program has built in data for the composition of the commonly used compounds for target backings or gas cells, i.e., Mylar, Havar, Kapton, polyethelene, stainless steel, and air.

D. THEORY

1. $^9Be(p,p_0)$ and $^9Be(p,p_2)^9Be$ and The Structure of ^9Be (H. J. Votava, W. J. Thompson)

Analyses of all available cross section and polarization data has been completed and an abstract was submitted to Birmingham SESAPS meeting. A paper summarizing the results from Votava's Ph.D. thesis has been accepted for publication in Nuclear Physics.

2. Excited-State-Threshold Resonance Effects in $^9Be(p,p_0)^9Be$ and $^9Be(p,n)^9B$ (H. J. Votava, W. J. Thompson)

A paper describing and analyzing the first observation of excited-state-threshold effects on a resonance has been published in Physics Letters.

3. Proton Optical-Model Potential Near The Coulomb Barrier (J. S. Eck ((Kansas State University)), W. J. Thompson)

A paper describing the results of the analysis of cross section and polarization data near the Coulomb barrier has been accepted for publication in Physical Review C. The optical-model potential is found to have an anomalously-rapid energy dependence near the Coulomb barrier, which is related to the non-locality of the nucleon-nucleus potential.

4. Compound Elastic Scattering and Tensor Polarizations (R. J. Eastgate, W. J. Thompson)

Compound-elastic (d,d) tensor polarization analyzing powers for low energies on s-d shell nuclei have been calculated and are predicted to be very large, especially at backward angles. Design of experiments is in progress.

5. Comparison of (d,t) or (d,^{3}He) Vector Analyzing Powers with Those for (d,d) (S. K. Datta, W. J. Thompson)

A prediction of the Weakly Bound Projectile Model (WBPM) is that in direct nucleon transfer reactions in which the nucleon is transferred between s states the transfer reaction analyzing powers should be similar to those for elastic scattering of the transferer (here d). Experimental data from TUNL are being examined to test this relation, which is not predicted by conventional DWBA.

6. Reaction Mechanism Studies in ^{24}Mg(α,$\alpha'\gamma$)^{24}Mg (G. S. McNeilly, W. I. van Rij, N. P. Heydenberg ((Florida State University)), W. J. Thompson)

A report on this study, made at 16.65 ^{4}He energy, has been accepted for publication in Nuclear Physics.

7. Cluster Effects in Elastic α Scattering Using a New α-α Interaction (W. J. Thompson)

Alpha-cluster effects on ^{40}Ca(α,α) ^{40}Ca near 29 MeV have been recalculated using a new α-α interaction. The results are even more negligible than those calculated previously. This work has been reported in Particles and Nuclei.

8. Nuclear Theory Computer Programs (S. K. Datta, R. J. Eastgate, R. A. Hardekopf, W. J. Thompson)

A write-up and the computer program for the interactive optical-model computer code OPTICS has been accepted for publication in Computer Physics Communications. Its flexibility has been increased by incorporating more options for the display of polarization quantities.

A test package for the fast, high-accuracy, angular-momentum-coupling coefficient subroutines (in Fortran) is nearly completed.

The DWBA code for the TUNL computers is in progress. A major subroutine, BSEF, which calculates the bound-state wave functions, is complete. Final checks are being run on an interactive version of BSEF used for teaching purposes in the spectroscopy of nuclear bound states.

9. Computer Codes for Analysis of Fission Data (J. R. Boyce, R. Bass, F. O. Purser)

Two computer codes, developed at TUNL, are being used to analyze proton-induced fission cross section data taken at TUNL. However, both programs have been written so that neutron-induced fission cross sections can also be analyzed. The first, MERLIN, utilizes mass- and energy-dependent optical model parameters to calculate total reaction cross sections for incident protons or neutrons over an energy range 0.125 MeV $\leq E_p \leq$ 40.0 MeV. Preliminary results indicate that for proton energies below the Coulomb barrier the reaction cross section calculated by using conventional optical-model parameters does not properly describe the compound nucleus formation cross section. The reaction cross section is empirically modified to obtain the compound nucleus cross section used in obtaining "experimental" fission probabilities, $\sigma_F(\text{exp.})/\sigma_c(\text{o.m.})$.

The second code, PHROG, is based on a statistical decay model which assumes either fission or neutron emission as primary decay channels. Contributions to the total fission probability from first through third chance fission are calculated for a compound nucleus with initial excitation energy E.* Recent modifications have made it possible to utilize any one of three level density prescriptions (Fermi gas, constant temperature, or Gilbert and Cameron[1]) in the calculations of the channel decay widths Γ_n and Γ_f. Parameters for the two level densities used can be varied independently thus introducing a flexibility not present in the original version. The results of this code are compared to the results of MERLIN to obtain a self consistent set of fission thresholds and Γ_n/Γ_f curves for the isotopes studied and over the energy range $0 \leq E^* \leq 30$ MeV.

10. Proton 2p-1h and Particle-Vibration Doorways (M. Divadeenam, W. P. Beres, E. G. Bilpuch, H. W. Newson, K. Ramavataram)

The ^{41}Sc compound nucleus will be considered for predicting 2p-1h and Particle-Vibration doorway escape widths to compare with the experimentally observed resonance structure in ^{40}Ca proton scattering experiments. (See Section B.) The shell model (2p-1h) can only predict positive parity states for ^{41}Sc however the Particle-Vibration Model can predict both positive and negative parity states. The latter model has been applied to the ^{208}Pb-plus-proton case to calculate the spreading widths of the antianalog states ($2g_{9/2}$, $1i_{11/2}$, $1j_{15/2}$, $3d_{5/2}$, $4s_{1/2}$, $2g_{7/2}$ and $3d_{3/2}$) which are in the continuum region. A paper giving details of the calculation and comparison with the available experimental results will be

[1]A. Gilbert and A. G. W. Cameron, Can. J. Phys. 43 144 (1965).

written for publication.

The ^{28}Si + proton case is being considered for calculating 2p-1h doorway energies and their elastic escape widths. The predicted results will be compared to the published experimental data and also with the results obtained by Ramavataram's group at Laval University.

11. A Core-Plus-Particle Model and Shell Model Investigation of Ni Isotopes (M. Divadeenam, C. R. Gould and K. Ramavataram)

True and Thankappan's Model has been previously applied to the study of negative parity levels in ^{51}Ti. We are extending the application of this model to study ^{57}Ni and ^{59}Ni levels. These nuclei have been investigated in this laboratory. (See Section B-9) Both positive and negative parity states will be considered to study their gamma decay properties. In addition the Rochester-Oak Ridge Shell-Model code (running at Laval University) will be used for theoretical investigation of the ^{59}Ni levels. Kuo-Brown and other available matrix elements for the f-p shells will be used.

12. Methods for High Accuracy Calculations of Shell Model States (R. Y. Cusson, H. W. Meldner ((U.C.S.D.)), M. S. Weiss ((Livermore)), H. P. Trivedi)

Further refinements to the Duke-Meldner code (see D-13, previous report) have been developed so that an improved fit to the single particle energies of the shell model can be obtained. Many nuclei from ^{4}He to $^{286}(114)$ (superheavy) have been computed and compared with experiment and other calculations. The article describing these results is nearing completion.

13. Computer Codes for High Accuracy Single Particle States (R. Y. Cusson, E. G. Bilpuch, H. P. Trivedi, D. Kolb)

Starting from unpublished notes from B. Buck, a fast and accurate method has been devised[1] to find the self consistent eigenvalues and eigenfunctions of the realistic, non-local, density dependent, single particle Meldmer reaction matrix. This code is now being used in Livermore, Berkeley and Los Alamos to obtain single particle states of spherical nuclei. It is presently being modified, by adding a pairing interaction term, to include nuclei near closed shells. In particular the resonances near threshold of the region $28 \leq A \leq 60$ are expected to be readily obtained.[2]

[1] "Fast and Accurate Solutions for Meldmer's Realistic Single-Particle Hamiltonian", by R. Y. Cusson, H. Trivedi and K. Kolb, Phys. Rev. C5 (1972) 2120

[2] H. Trivedi, Ph.D. thesis topic

14. Single Particle Wavefunctions and Energies for Stripping and Pickup Reaction (R. Y. Cusson)

It has been found that stripping and pickup reactions are sensitive mainly to the exponential tail of the wavefunctions and therefore can not distinguish between fine differences in single particle states in the nuclear interior. However for states far from the Fermi sea there is considerable uncertainty in the energy due to their width so that even a knowledge of only the tail of the wf is difficult to obtain. A paper by R. Y. Cusson, D. Kolb and H. P. Trivedi discussing the influence of the removal time on the single-particle wavefunctions and energies has been submitted to Physics Letters and should bear on this question.

15. Realistic Single Particle Hamiltonian for Fission Calculation (D. Kolb, R. Y. Cusson, H. W. Newson, H. W. Schmitt ((Oak Ridge)))

Referring to item D-16 of the last report, more detailed calculations of light nuclei fission have been performed and a paper has been submitted to Zeitschrift für Physik. A calculation of the ground state and first minimum of ^{236}U has also been performed and an excitation energy of 3 MeV for the first minimum has been obtained. This is the first time to our knowledge that such a prediction has been obtained without the use of the Strutinski prescription. A summary publication of this new result is planned.

16. Light Nuclei Systematics in The Projected Hartree-Fock Scheme (R.Y. Cusson, H. C. Lee ((Chalk River)))

Following an extensive study by the authors (Annals of Physics 72 ((1972)) 353) of the deformed intrinsic states of some 56 light nuclei in the p- and s-d shell, a detailed article is under preparation (Nuclear Physics, to be published), where rotational excitations and transitions (M1, E2, M3, E4, E0) are being systematically compared with experiment. In particular, excellent agreement with experiment has been found for ^{20}Ne, ^{22}Na, ^{24}Mg, as reported in an invited paper at the Gordon Conference on Nuclear Structure, 1972, by one of us (R.Y.C.).

17. Coriolis Anti-Stretching in ^{20}Ne and α Widths (H. C. Lee and R. Y. Cusson)

An interesting correlation between the decrease in B(E2) values as one goes up the ^{20}Ne ground state band, and the decrease in α emission width has been found (Phys. Rev. Lett. 29 (1972) 1525). Both the B(E2) and the α-width are found to decrease for the same reason, namely: the radius of ^{20}Ne is calculated to decrease as J increases, due mainly to the s-d to p-f shell gap. This effect has been

confirmed by Dr. J. McGrory (private communication) in the Oak Ridge shell model calculation.

18. Applications of Group Theory to Rotational Bands in Nuclei (L. C. Biedenharn, R. Y. Cusson, O. L. Weaver ((Kansas State University)))

A contracted version of the $SL(3_1R)$ algebra proposed by Dothan Gell-Mann and Neiman, namely $T_5 \otimes SU(2)$ has been used to classify all the nuclear rotational bands (Annals of Physics), including those with half-integral spin, without having recourse to the ad hoc assumption of recoupling of an odd nucleon. The full algebra of $SL(3_1R)$ has been found to yield parameter free predictions for ratios of cross-band E2 transitions (Nuclear Physics, 1972) and has recently been found to yield a generalization of rotational-vibrational motion in which the presence of the odd particle is accounted for by introducing quantized amount of vorticity (in preparation).

19. Do Protons and Neutrons Have Internal Rotational Vibrational Excitations? (L. C. Biedenharn, R. Y. Cusson, O. L. Staunton)

For completeness in any theoretical program of nuclear studies it would not be wise to neglect the possible influence of nucleon structure on nuclear structure. The expertise required in dealing with the group theoretical foundations of nuclear collective motion is of use in discussing the possibility of such internal structure for the nucleons themselves. Thus a model involving the algebra of $SL(3_1R)$ and a "deformable" nucleon has been put forward (Physics Letters, November, 1972) and studies have shown that rotational excitations of the nucleon are quite consistent with the requirement of relativity (in preparation).

20. Cross Section for M-Shell Ionization in Heavy Atoms by Collision of Simple Heavy Charged Particles (Byung-Ho Choi)

This work will be published in Phys. Rev. A (June, 1973). The abstract follows:

"The cross sections for M electron ionization by direct Coulomb excitation of heavy target atoms by incident heavy charged particles are evaluated. Incident particles are described in the plane wave Born approximation, and screened hydrogenic wave functions are used for the atomic electrons. Numerical results are given for Au, U and No, and the theory is compared with experimental data for Ho as an illustration. Explicit expressions for the absolute values of the M subshell

form factors of bound-free transitions are presented as functions of momentum and energy transfers. The results are discussed."

21. Tables for Born Approximation Calculations of L-Subshell Ionization by Simple Heavy Charged Particles (B.-H. Choi, E. Merzbacher, G.S. Khandelwal)

This work will be published in Atomic Data (1973). The abstract follows:

"Tables are presented for the calculation of the Born cross sections for ionization of individual L-subshells by simple heavy charged particle impact. The tables cover a wide range of proton energies above a few tenths of an MeV and many values of the atomic number, specified by dimensionless energy and screening parameters. Explicit expressions for the absolute values of the L-subshell form factors of bound-free transitions are presented as functions of momentum and energy transfer. Errors in an earlier paper are corrected."

UNIVERSITY OF COLORADO NUCLEAR PHYSICS LABORATORY

A. (p,n) REACTION DATA

1. Microscopic Analysis (R. F. Bentley and C. D. Zafiratos)

A microscopic theory of the (p,n) reaction has been compared to a) all of our analog transition data, b) all of the cases where we saw a strong 2+ excited analog state and c) data for a few low-lying states which were chosen on the basis of their presumably simple structure. Our microscopic model employed an effective interaction with a Yukawa radial dependence. Central, $\vec{\sigma}\cdot\vec{\sigma}$, and tensor terms were included in the projectile-target nucleon interaction. Exchange was not included in our calculations nor were $\vec{\ell}\cdot\vec{s}$ terms included in the effective interaction.

For isobaric analog transitions only the central force operates. Calculations made with a Yukawa range of 1.0 fm are shown in Fig. A-1. Similar calculations for the 2+ analog state are shown in Fig. A-2.

The sensitivity of the microscopic calculations to configuration is illustrated for the $^{58}Fe(p,n)^{58}Co$ analog transition in Fig. A-3. The effects of varying the choice of configurations are quite small. This is not due to a lack of sensitivity to the nuclear interior.

Though the over-all agreement with data shown in Fig. A-1 is qualitatively good, much better agreement would be required if this data were to be useful in detecting configuration mixing. Since the rather successful macroscopic analysis of the analog data employed a complex form factor, we attempted to obtain better agreement with data by including an imaginary component in the effective interaction. The improvement in the case of ^{56}Fe with the use of a complex form factor was not consistently found in other cases, however.

We then investigated the contributions of a two-step process involving sequential pick-up and stripping processes: (p,d) (d,n). Coupled channels calculations were made with the code CHUCK to include both the one-step charge exchange contribution and the above two-step process. Some results are shown in Fig. A-4.

The magnitude of the two-step reaction is large enough to significantly change the shape of the calculated angular distributions. Our conclusion then, is that detailed agreement between theory and experiment is unlikely unless the two-step mechanism is included in those calculations. It seems likely that a complex form factor can, in part, mock-up the two-step effects. However, the prescription for the imaginary portion of such a form factor may well vary widely as the shells involved in the pick-up and stripping steps are varied.

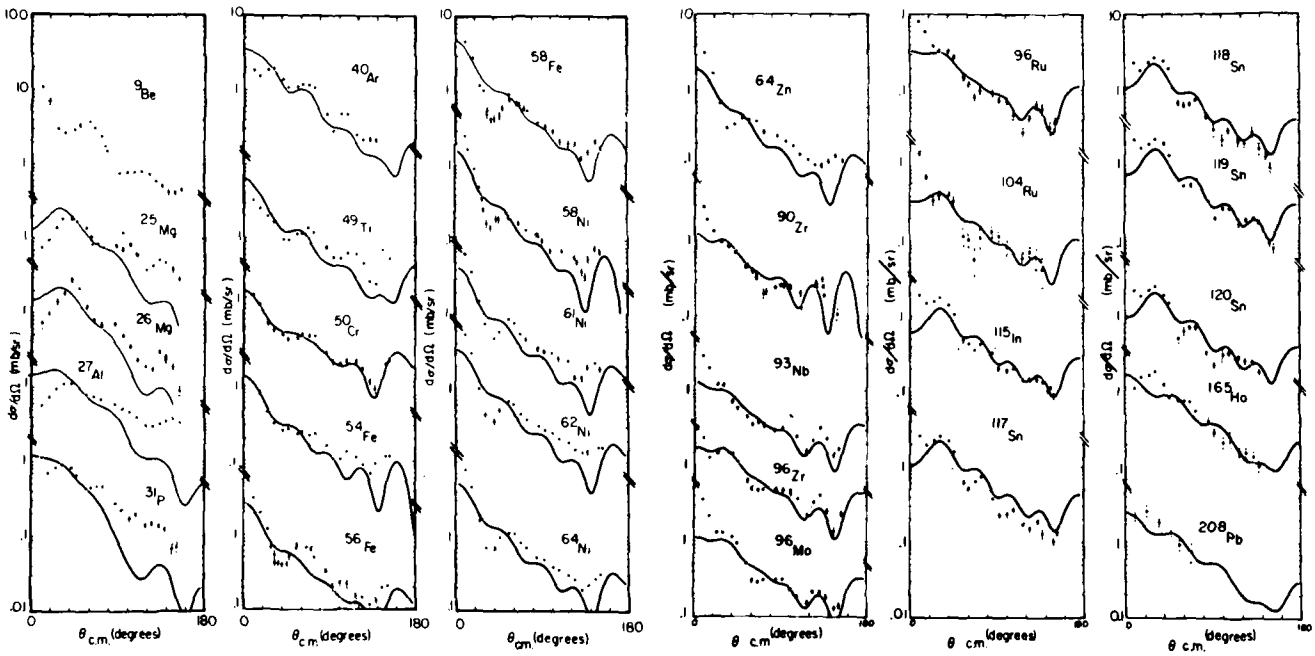

Fig. A-1 Fits of the (p,n) reaction to isobaric analog ground state transitions by a microscopic analysis for 22.8 MeV data.

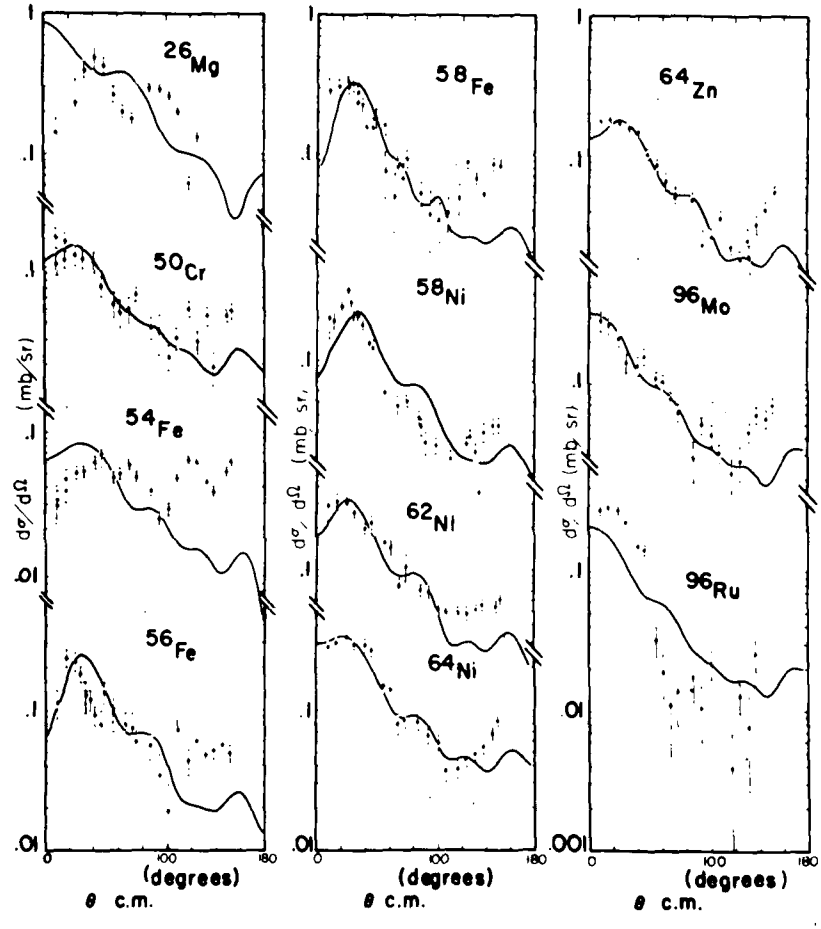

Fig. A-2 Fits of the (p,n) reaction to isobaric analog excited 2+ state transitions by a microscopic analysis for 22.8 MeV data.

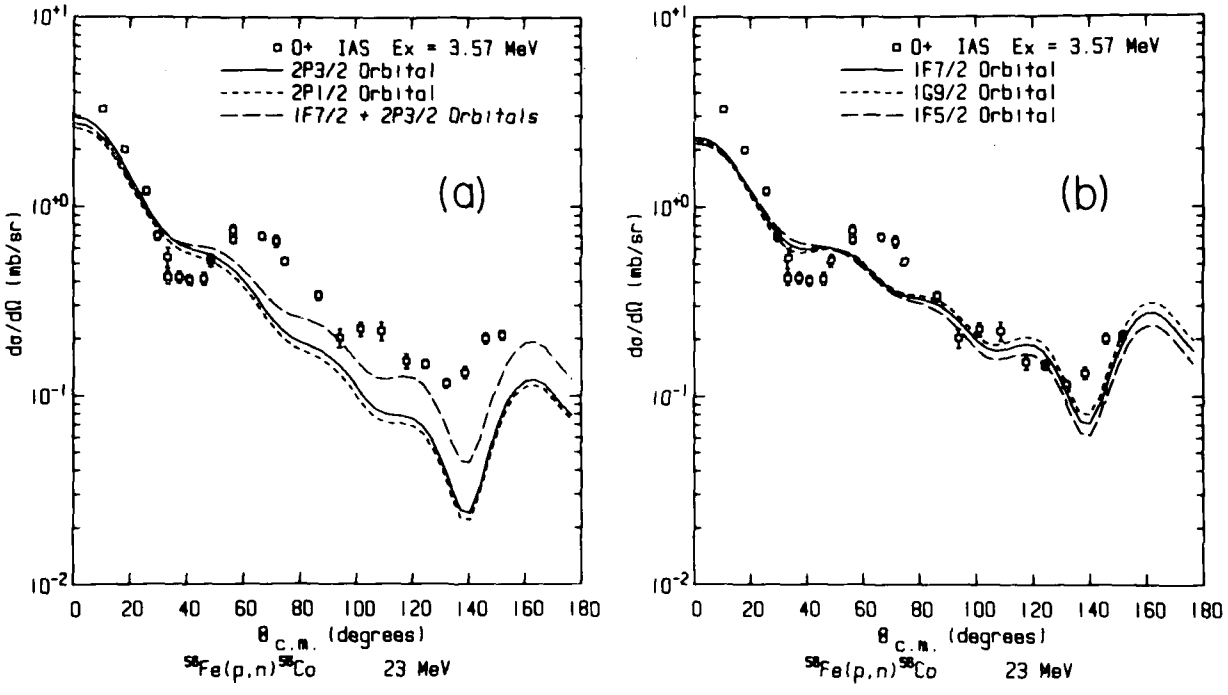

Fig. A-3 Effect of configuration on microscopic analysis of the (p,n) reaction on ^{58}Fe.

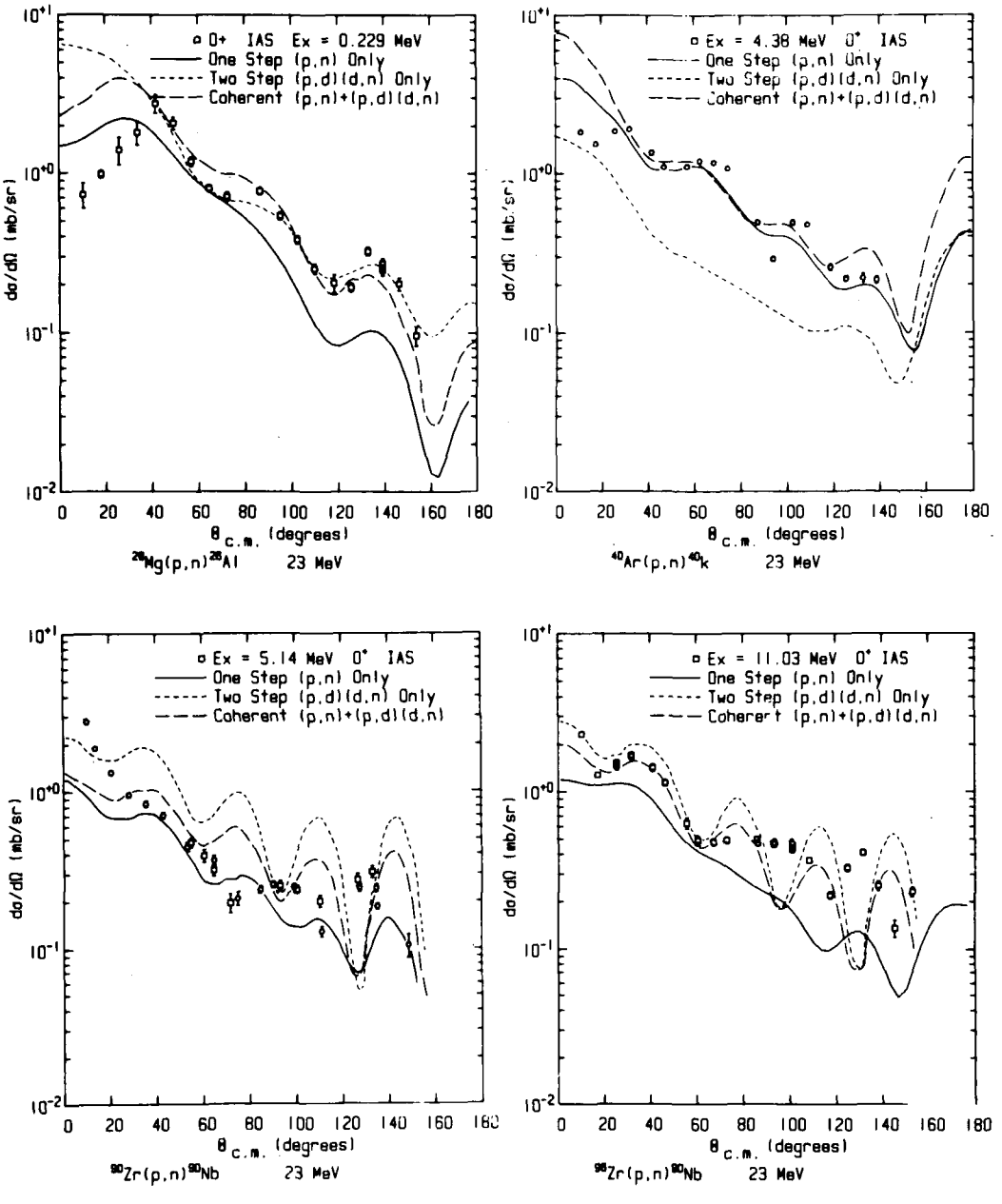

Fig. A-4 Coupled channels analysis with one step (p,n) and two step (p,d)(d,n) processes.

2. Studies on Heavy Elements (H. Fielding, C. D. Goodman, D. A. Lind, L. D. Rickertsen, S. D. Schery, C. D. Zafiratos)

Experimental measurements of the (p,n) reaction for the isobaric analog ground state have been made for selected high Z nuclei at a proton energy of 25.8 MeV. The targets were ^{197}Au, ^{206}Pb, ^{207}Pb, ^{208}Pb, ^{209}Bi, ^{232}Th and the angular distributions are shown in Fig. A-5.

Preliminary attempts to fit the angular distributions using macroscopic DWBA calculations have been moderately successful. It is possible to fit the data with both real and complex form factors. The real form factor required a strong surface contribution for best fit. A complex form factor consisting of real volume plus imaginary surface terms also provided an adequate fit. Attempts to predict neutron elastic scattering using (p,p) and (p,n) data have not been as successful as reported by Carlson et al. for lower Z elements.[1] However, the resultant elastic scattering predictions were still better than, for example, the predictions of Becchetti-Greenlees' global neutron parameters.[2]

It is possible to get a good fit to the ^{208}Pb (p,n) data using a coupled channels microscopic calculation that includes the effects of a two-step process to an intermediate deuteron state. This result is very promising and further investigation is under way.

---

[1] J. D. Carlson, D. A. Lind, C. D. Zafiratos, Phys. Rev. Lett. 30, 99 (1973).

[2] F. D. Becchetti, Jr., and G. W. Greenlees, Phys. Rev. 182, 1190 (1969).

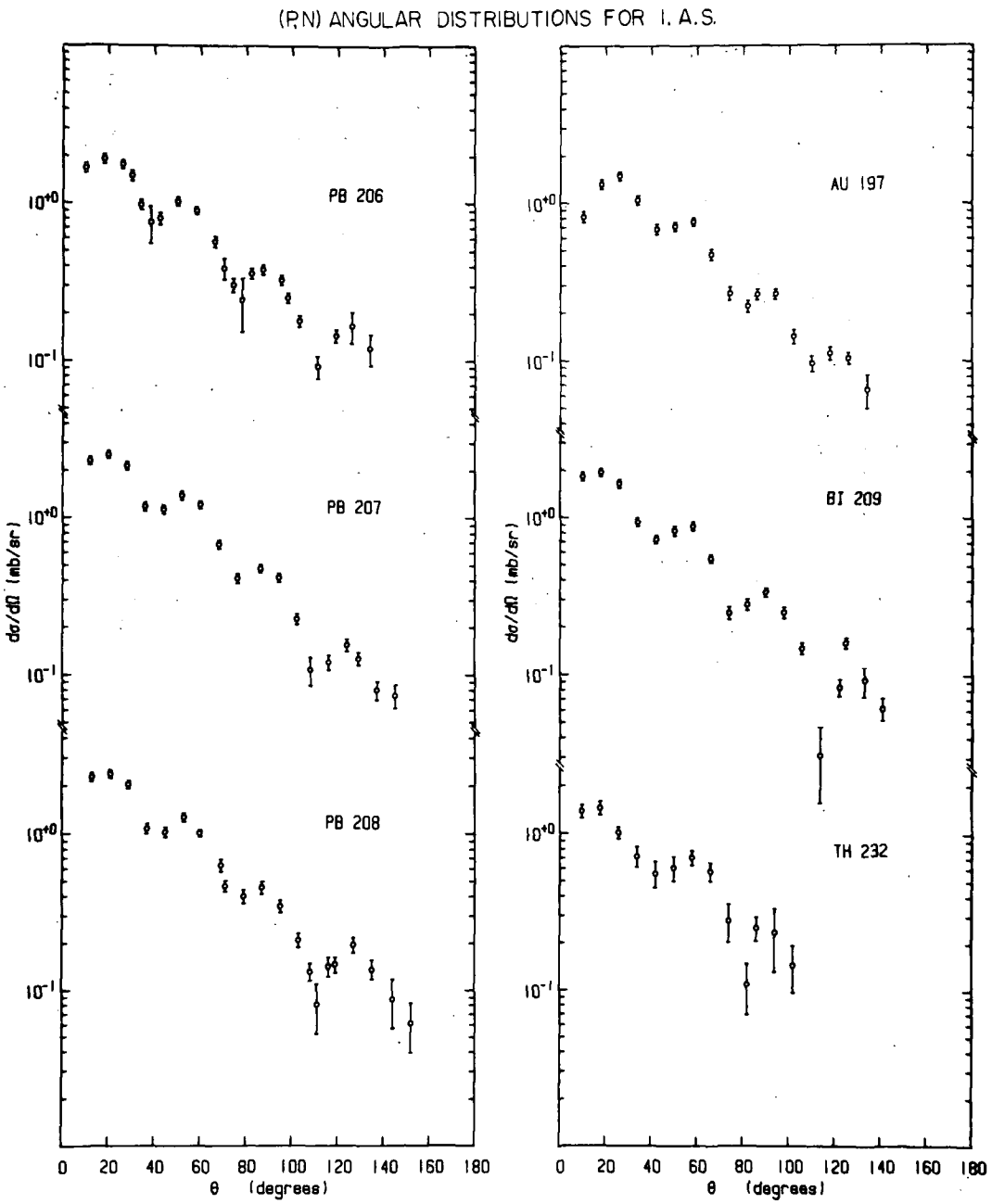

Fig. A-5 (p,n) reaction cross sections to the isobaric analog ground state for several heavy elements.

B. APPARATUS AND FACILITY DEVELOPMENT

1. Neutron Time-of-Flight Facilities (D. A. Lind, C. D. Zafiratos, S. Schery, H. Fielding, and D. Komonytsky)

Starting in September, 1971, installation of the beam swinger facility was initiated; hence the program of (p,n) studies described in the 1971 Progress Report[1] was terminated. During the past year equipment for a neutron time-of-flight facility geared to the swinger has been constructed. The efforts were directed toward 1) beam optics properties, 2) detector improvements, and 3) scattering chamber design.

In Fig. B-1 a general layout of the time-of-flight geometry is shown. The beam swinger carries the primary beam through bends of +45° and -135° so that it intersects the primary beam direction at 90°. The system then rotates about the primary beam direction as an axis. Three channels for neutron drift are arranged at 90° to the axis of rotation and separated by 8° in angle. The primary beam, target chamber and beam stop are fixed to the swinger and rotate with it.

a) Beam preparation

Measurements of the cyclotron output beam indicated that up to several microamps of protons are available with phase space for x and y motions of 3 mm mrad. However, the sources for x and y motions are located at different points. The beam presented to the entrance of the swinger had to be in the form of a circular waist about 1.6 cm in diameter so that as the swinger rotates it will be presented with a beam of uniform phase space properties. An additional requirement is that a double focus is desired inside a shield wall to dispose of unwanted beam. These requirements have made the problem of proper focussing quite difficult. The optimum beam at the swinger entrance is essentially a parallel beam which is more difficult to prepare than a beam with a sharp focus.

The specific properties of the incoming beam to the swinger determine not only the isochronism but also the focal properties of the beam at the target chamber. Specific observation of the time spread of the beam at the entrance of the swinger and at the target showed no observable time broadening indicating that the time spread introduced by the swinger (<0.2 ns) is quite acceptable.

A second problem concerns the momentum spread in the beam and the magnet stability. No clean-up slits are used to define the beam at

---

[1] Technical Progress Report, U. of Colorado Nuclear Physics Laboratory, COO-535-653, Nov., 1971.

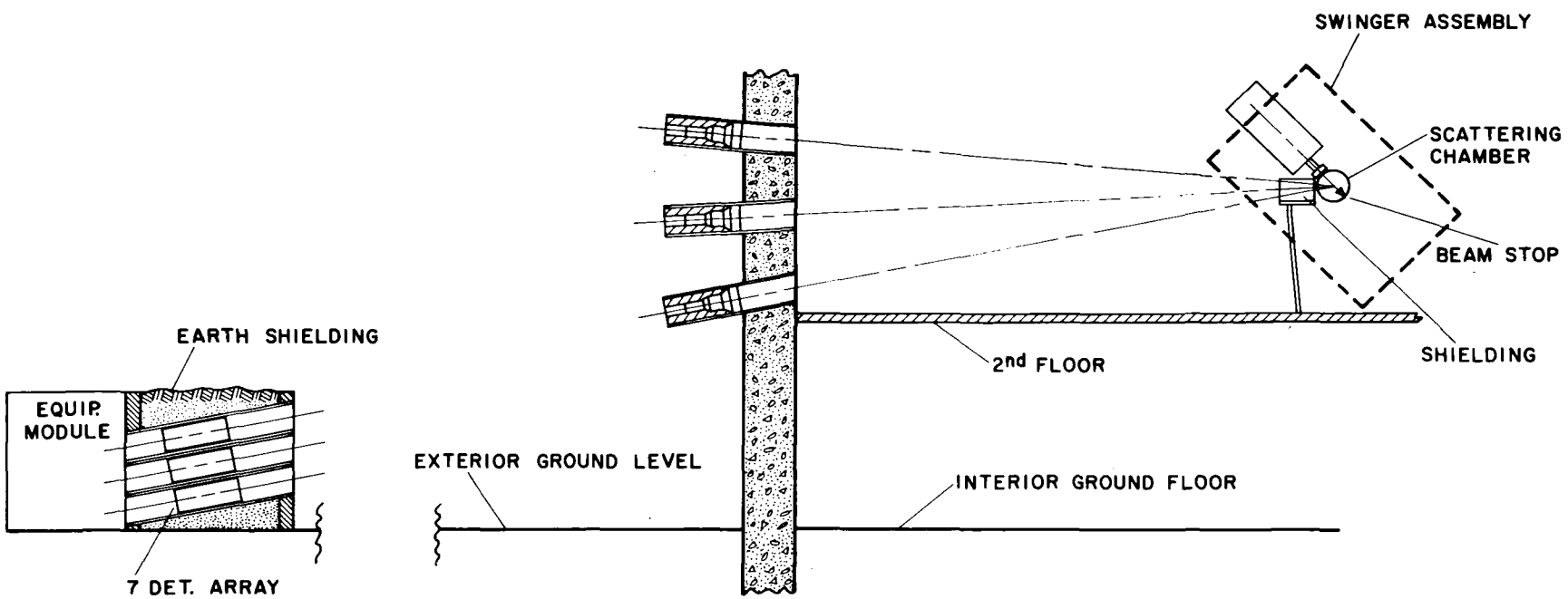

Fig. B-1 Schematic of the TOF layout using the beam swinger.

the target. Momentum spread in the primary beam must remain constant and small so the entire beam envelope is suitably confined on the target (≈1 cm diameter) since for isochronism a radial focus exists about 40 cm upstream from the target. There are about 20 magnets (focussing as well as steering) in the line; regulation of many of them has had to be improved to maintain suitably acceptable beam properties.

b) Detector Improvements

To improve sensitivity, detectors 8 in. (20 cm) in diameter have been made, similar to those described in the 1971 Progress Report.[1] The time resolution measured by coincidence observations with a ^{60}Co source and a small plastic scintillator was 0.75 ns. The n-γ discrimination seemed to remain unchanged indicating that light collection from the larger cell is equally good to that of the 6 in. cell used previously.

Three detectors feed fast discriminators for timing and n-γ discrimination while integrated signals feed linear amplifiers and discriminators for threshold and crossover timing information. The basic electronics system is unchanged from that described previously.[1]

For monitoring purposes a cooled Si(Li) particle detector mounted in the scattering chamber and biased to look at the elastic scattered group was fed to a separate time-to-amplitude converter. Thus the time structure of scattered protons could be determined and a direct comparison could be made for each angle of the (p,n) cross section with the elastic scattering cross section at a fixed angle. Using crossover timing on the integrated output pulse, a time resolution of 4 ns was obtained, so good discrimination between beam bursts was achieved.

A collimator 24 in. long formed of steel plate was used adjacent to the scattering chamber to define the beams to the three detectors. The detectors are placed behind at least 2 ft. of concrete shielding. General detector background seems to be significantly better than in the former experimental set-up.

c) Scattering Chamber

A new 60 cm diameter scattering chamber was designed and constructed to provide for an internal Faraday cup and a solid state detector with an angle drive. Thus the angular distribution of protons scattered from the targets can be measured for the same targets

---

[1] Technical Progress Report, U. of Colorado Nuclear Physics Laboratory, COO-535-653, Nov., 1971.

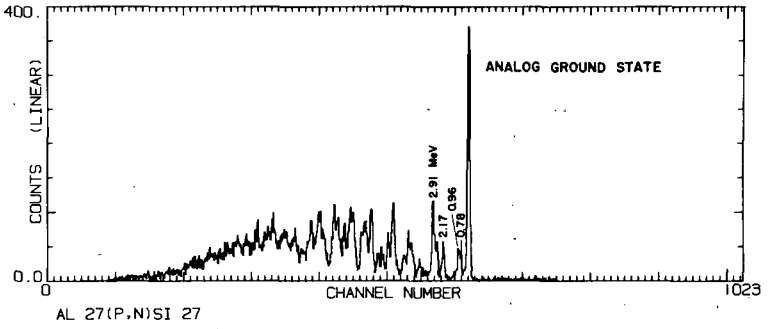

Fig B-2 TOF neutron spectrum from ^{27}Al for 23 MeV protons.

used for (p,n) work. A 0.050 in. thick aluminum wall on the chamber provides for little or no attenuation of the neutrons.

Because the beam is not focussed at the target but is diverging to a spot size of 1 cm square, targets at least 1.5 cm square must be used. Accommodation for gas cells is more difficult.

Overall operation of the system has been checked out. Beams of 200 to 500 na of 23 MeV protons at the target with 0.8 ns full width for the observed neutron peak at a flight distance of 9 meters was observed. Fig. B-2 shows a spectrum for the $^{27}Al(p,n)^{27}Si$ reaction obtained with the system. Final data acquisition awaits improvements in magnet stabilization since the ion optic tuning is extremely sensitive to magnet drift. It is relatively easy to make the minor beam tuning adjustments needed to obtain maximum transmission through the swinger for all angular positions.

Since our next program of work involves (^{3}He,n) studies, we have investigated the application of pulse height-flight time correlation[1] to unscramble the overlap of successive beam bursts. Thus far the ion source gate has not been successful when used with helium arcs. Rather than install external beam switching hardware, we propose the correlation technique for use with the (^{3}He,n) reaction because the reaction Q-values are large and positive so the neutrons are energetic while the RF repetition frequency is about 10 MHz. Thus there is a large ratio between energy of neutrons arriving at the detector from the first and second previous initiating beam pulses. Furthermore, since the flight times for the most energetic neutrons over a 10-meter path are of the order of 100 ns, the energy of overlap neutrons will be about 0.25 that of the non-overlap group. By using appropriate threshold discrimination and the pulse height information, it seems quite possible to achieve unfolding of the contributions of the first two beam bursts. Earlier beam bursts will contribute little because the pulse amplitude discrimination will eliminate them.

---

[1] L. C. Northcliffe, C. W. Lewis, and D. P. Saylor, Nucl. Inst. and Meth. 83, 93 (1970).

US ARMY BALLISTIC RESEARCH LABORATORIES
RADIATION LABORATORY

A. NEUTRON PHYSICS

1. Small-angle Elastic Scattering Cross Sections for C, N, and O.

(W. P. Bucher, C. E. Hollandsworth, A. Niiler) Relevant to NCSAC-35, Requests 31, 33, 38, 39, 43.

Construction and assembly of the new collimator for small-angle scattering measurements has been completed. Measurements for C, N, and O in the neutron energy range from 10 to 14 MeV are in progress. Additional measurements will be made for nitrogen near the structure in the total cross section around 7.9 MeV.

A paper describing the technique used in these measurements has been accepted for publication in Nuclear Instruments and Methods.

2. Small-angle Elastic Scattering of 7.55-MeV Neutrons: A Survey.

(W. P. Bucher, C. E. Hollandsworth, D. McNatt, A. Niiler) Relevant to NCSAC-35, Requests 22, 31, 33, 60, 97.

Absolute cross sections for the scattering of 7.55-MeV neutrons from Be, C, Al, Fe, Cu, Sn, and W at laboratory scattering angles of 2.67, 4.78, 6.83, 8.50, 10.80, and 14.09 degrees have been determined. These data will be compared with the predictions of various "global parameter" sets for the optical model and with "best-fit" parameters for particular elements where complete angular data sets exist.

3. Forward-angle Elastic Scattering Cross Sections for Pb.

(W. P. Bucher, C. E. Hollandsworth, A. Niiler)

Our data on the scattering of 8.0-MeV neutrons from Pb have been extended to both larger and smaller angles by new measurements at scattering angles of 20° and 1.4°. The 20° measurement was done in ring geometry; the 1.4° measurement was carried out using the small-angle collimator described previously. In the latter measurement the cross section for scattering at 1.4° was determined relative to the cross section at 4.5°. Normalization is provided by a previous ring geometry measurement at 4.5°.

The scattering measurements for C, N, and O described in Section 1 are made relative to the scattering from a Pb sample. To establish the cross section scale, absolute scattering cross sections for Pb are measured in ring geometry. Ring geometry measurements have been made for the scattering of 11.0, 12.5, and 14.0-MeV neutrons. These data are currently being processed.

4. Breakup Nucleons from the D + d Reaction.
(A. Niiler and Y. S. Park)

The D + d breakup reaction is being investigated in the energy range 10-16 MeV and laboratory angle range 0° - 80°. Proton spectra have been measured with two E - ΔE silicon surface barrier detector telescopes in the angular range 10° to 80°. Deuterated polyethylene foils, $(CD_2)_x$, are used as targets with the carbon and hydrogen backgrounds determined from separate runs with ^{12}C and CH_2 targets. Neutron spectra have been measured with a recoil-proton telescope at 0° over an energy range of 12 to 16 MeV using a gaseous deuterium target.

Preliminary results show that the total breakup cross section measured at 0° via the D(d,n)pd reaction is in generally good agreement with results from the D(d,p)nd measurement when the latter are extrapolated to 0°. The shape of the breakup spectra exclude the possibility that this breakup reaction can be described simply by three-body phase space. However, if the final state consists of several substates of non-zero relative angular momenta, the fits to the data are markedly improved.

B. CHARGED PARTICLE PHYSICS

1. Gamma Decay of Low-Lying Levels in ^{93}Nb.
(R. M. Tapphorn* and R. Shnidman)

A paper with the above title has been accepted for publication in the Physical Review. The abstract follows: Mean lifetimes for four levels in ^{93}Nb have been measured by the Doppler-shift-attenuation method. Gamma-ray angular distributions have been measured for the gamma decay of excited levels in ^{93}Nb up to 1127 keV in excitation. The levels were excited by the $^{90}Zr(\alpha,p\gamma)^{93}Nb$ reaction at a bombarding energy of 14.77 MeV. Spectra of gamma rays in coincidence with protons were obtained with a 55-cm^3 Ge(Li) detector. Spin assignments obtained from the present results for the low-lying positive-parity levels in ^{93}Nb are in agreement with previous assignments. A J^π of $3/2^-$ has been assigned to a level at 685 keV in excitation and a J^π of $5/2^-$ $(3/2^-)$ has been assigned to an 809-keV negative-parity level. Gamma-ray mixing ratios measured for the gamma decay of excited low-lying levels in ^{93}Nb have been combined with lifetime measurements to calculate the electromagnetic transition strengths. The experimental E2 transition strengths are shown to be consistent with those predicted by a weak-coupling model.

---

* National Research Council Resident Research Associate.

2. Study of ^{93}Nb Levels with the ^{96}Mo(p,α)^{93}Nb Reaction.
(Y. S. Park, H. D. Jones, D. E. Bainum)

The results of this investigation have been published under the above title in Phys. Rev. C 7, 445 (1973).

C. CHANNELING STUDIES
(H. B. Dietrich* and T. J. Rock)

We have made detailed studies of the scintillation response of NaI(Tℓ) to channeled heavy ions. Early results have been published and the reader is referred to this work[1] for a discussion of the basic results and terminology. We have recently refined and extended these measurements. We have obtained < 100 > axial data for previously unstudied ^{32}S, ^{12}C, ^{7}Li, and ^{4}He ions and we have observed two previously unresolved facets of the response to channeled ions. The axial data is shown in Fig. C-1. The newly-observed structure consists of an anomalous reduction in the scintillation response to particles incident near the < 100 > axis and a clearly resolved "third peak" of intermediate pulse height in the channeled spectra. The reduction has a broad angular extent. The half-angle is much greater than the critical angle for channeling. It cannot be accounted for by a traditional blocking picture. The reduction increases with both Z_1 and E. The exact origin of the "third peak" is still unresolved. However, it is presently believed to result from a two-step axial dechanneling process where the particles first feed from the axis to the most open planes and subsequently dechannel into random trajectories.

---

* National Research Council Resident Research Associate

[1] Phys. Rev. B 7, 1743 (1973).

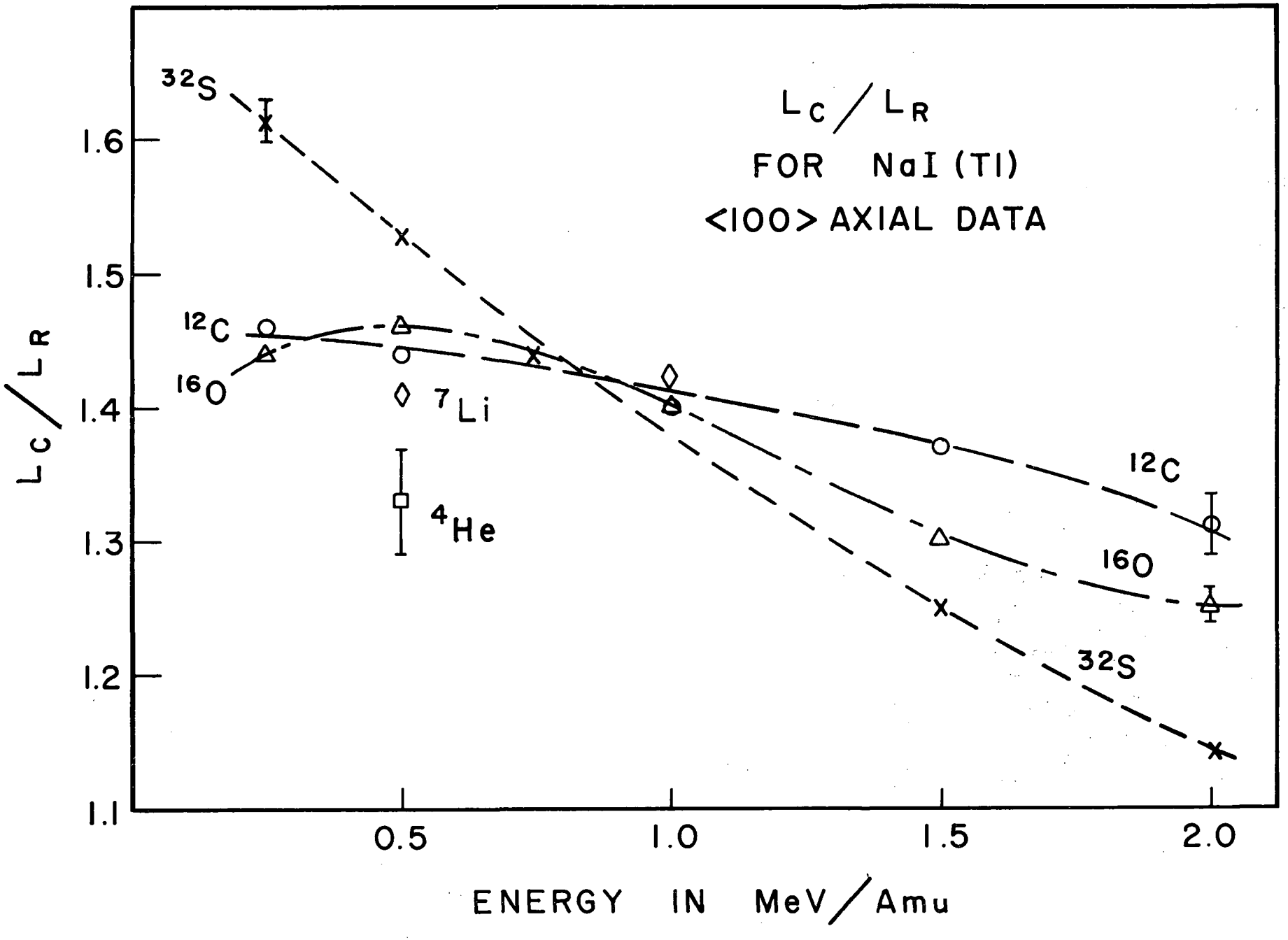
L_C / L_R
FOR NaI (Tl)
<100> AXIAL DATA
^{32}S
^{12}C
^{16}O
^{7}Li
^{4}He
^{12}C
^{16}O
^{32}S
1.6
1.5
1.4
1.3
1.2
1.1
0.5
1.0
1.5
2.0
L_C / L_R
ENERGY IN MeV/Amu

Fig. C-1.

YALE UNIVERSITY

A. FAST NEUTRON POLARIZATION STUDIES (F. W. K. Firk, G. T. Hickey, R. J. Holt, R. Nath and H. L. Schultz)

1. Polarization of neutrons in n-^{16}O scattering

The absolutely calibrated source of polarized neutrons from the reaction $^{12}C(n,\vec{n})^{12}C$[1] has been used in a study of the differential polarization of neutrons elastically scattered from a liquid oxygen target. The analyzing power of ^{16}O has been measured at eight angles between 20° and 150° as a continuous function of energy from 1 to 4 MeV. The energy resolution of the time-of-flight spectrometer was 0.75 ns. m^{-1} (equivalent to 50 keV at 2 MeV). A high-field spin precession solenoid was used in order to reduce the systematic errors to negligible amounts[2]. The results are being analyzed using a general R-function reaction theory in order to obtain the parameters of both local and distant levels. Examples of the measured differential polarizations in the region of 3 MeV are shown in Fig. A-1.

2. Polarization of neutrons in n-^{9}Be scattering.

The differential polarization of neutrons elastically scattered from ^{9}Be has been measured at energies between 1.5 and 4 MeV using the technique outlined above. The measurements have been completed and the data are being analyzed. Although this is a more complex problem than encountered in our previous studies on spin-zero nuclei, it is hoped that a

[1] R. J. Holt, F. W. K. Firk, R. Nath and H. L. Schultz, Phys. Rev. Lett. 28 (1972)114

[2] R. Nath, F. W. K. Firk, R. J. Holt and H. L. Schultz, Nucl. Instr. and Meth. 98 (1972)385

relatively small number of channels will dominate the reaction at these energies thereby permitting a satisfactory R-matrix analysis.

3. Polarizations of ground-state photoneutrons from the reactions $^{12}C(\gamma,\vec{n}_0)^{11}C$ and $^{16}O(\gamma,\vec{n}_0)^{15}O$.

The polarizations of photoneutrons from the reactions $^{12}C(\gamma,\vec{n}_0)^{15}$ and $^{16}O(\gamma,\vec{n}_0)^{15}O$ have been measured at 45° and 90° in the photon energy range covering the giant dipole states in these nuclei. The polarimeter associated with the Yale Linac used either a liquid He or a carbon analyzer. The effects of non-ground state transitions were evaluated by comparing the product of the photoneutron polarization, p, and the analyzing power, A, for two values of the incident electron energy, namely 64 and 30 MeV (see Fig. A-2). At the lower value, the effective photon end-point energy is ~ 28.5 MeV so that, in ^{16}O, photoneutrons with energies between 6 and 13 MeV are due to ground-state transitions. The results for $^{16}O(\gamma,\vec{n}_0)^{15}O$ are shown in Fig. A-2; the data at 45° are compared with recent results from Stanford on the $^{16}O(\gamma,\vec{p})^{15}N$ reaction (measured by the inverse reaction of radiative capture of polarized protons). The agreement between the magnitudes of the photoneutron and photoproton polarizations is generally good. There is clearer evidence, however, of structure in the higher resolution photoneutron data throughout the resonance region. These new results are being combined with recent photoneutron angular distribution measurements to yield the amplitudes and phases of the s- and d-wave components of the dipole states.

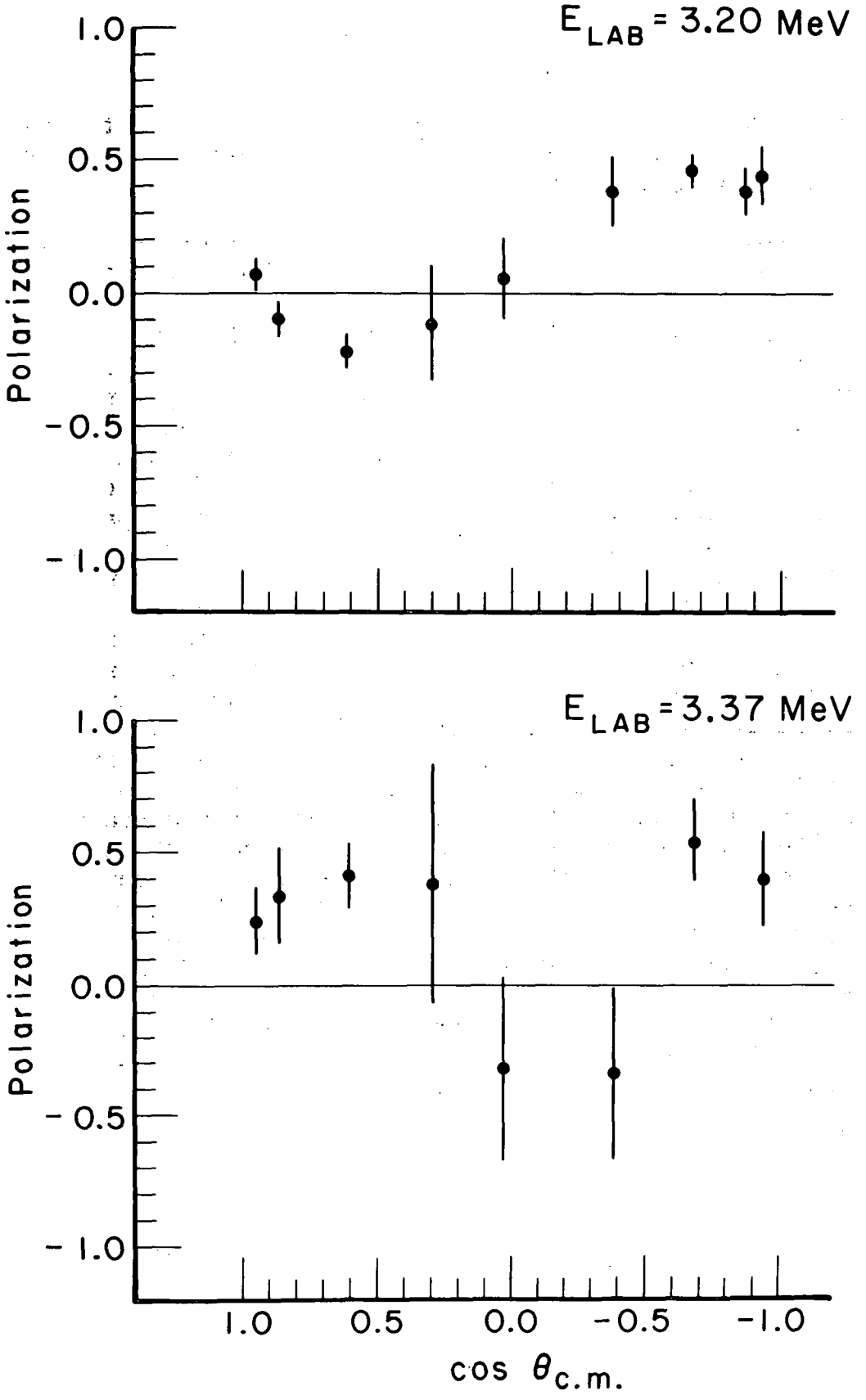
E_{LAB} = 3.20 MeV
1.0
0.5
0.0
-0.5
-1.0
Polarization
E_{LAB} = 3.37 MeV
1.0
0.5
0.0
-0.5
-1.0
Polarization
1.0
0.5
0.0
-0.5
-1.0
cos $\theta_{c.m.}$

Fig. A-1

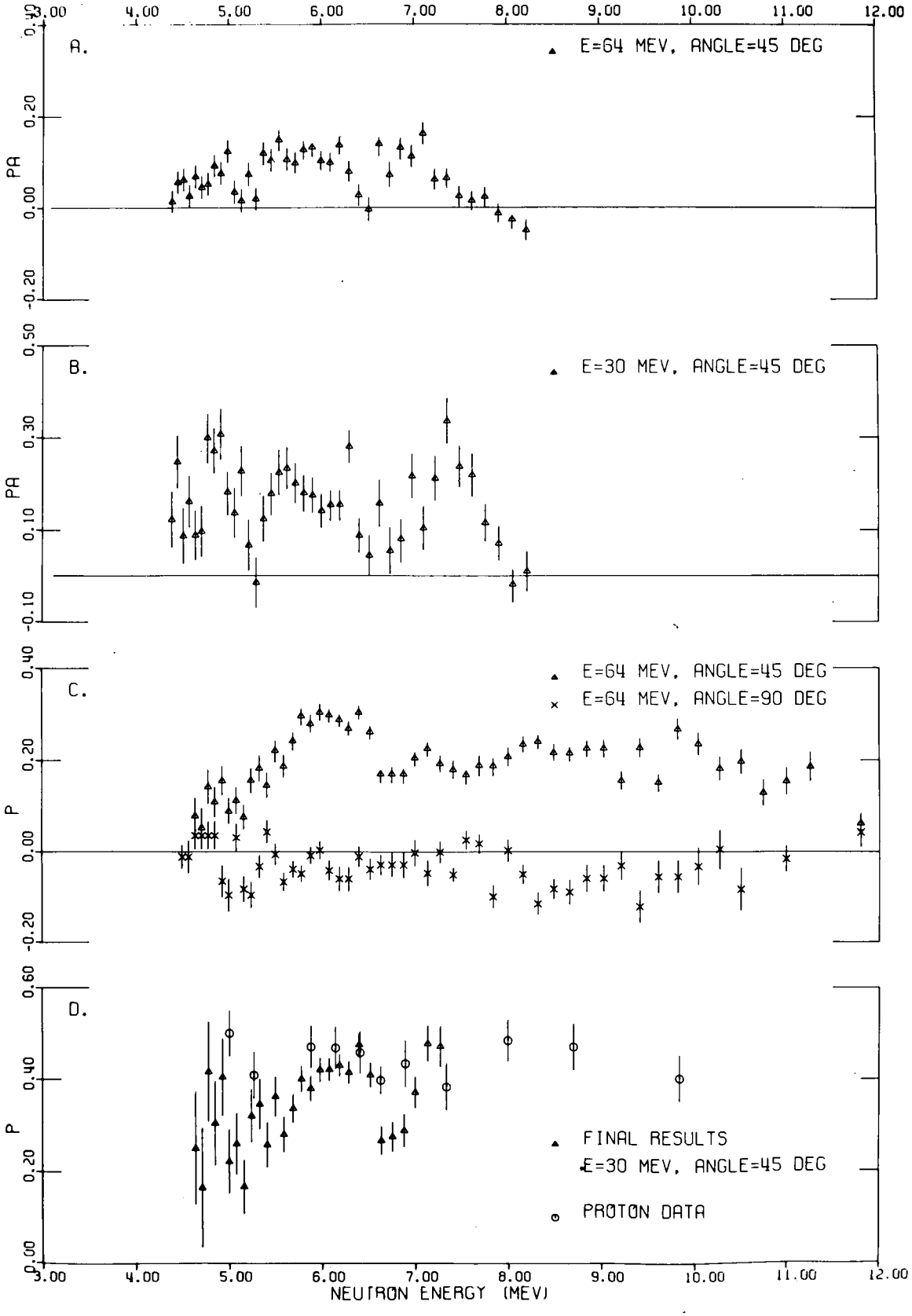

Fig. A-2. $^{16}O(\gamma,\vec{n}_0)^{15}$